Characterization of trafficking factors involved in Ebola virus entry

Shirley Qiu

Thesis submitted to the University of Ottawa
in partial fulfillment of the requirements for the degree of
Doctor of Philosophy, with specialization in Microbiology and Immunology

Department of Biochemistry, Microbiology, and Immunology
Faculty of Medicine
University of Ottawa

Abstract

Ebola virus (EBOV) and other members of the *Filoviridae* family are enveloped RNA viruses that are the causative agents of sporadic outbreaks of highly lethal disease in humans and non-human primates. EBOV entry into host cells requires attachment, internalization, and subsequent trafficking to the late endosomal/lysosomal compartment in order to reach the filovirus entry receptor, Niemann-Pick C1 (NPC1) and other triggering factors required for EBOV glycoprotein (GP)-mediated fusion between the viral and host membranes.

The highly regulated nature of endosomal trafficking coupled with the dependence of EBOV on accurate endolysosomal trafficking for entry led us to hypothesize that the virus depends on—and potentially actively regulates—a consortium of specific host trafficking factors. In this thesis, we investigated the role of two trafficking complexes involved in endosomal maturation and trafficking, the Homotypic Fusion and Vacuole Protein Sorting (HOPS) complex and the PIKfyve-ArPIKfyve-Sac3 (PAS) complex, in EBOV entry. Furthermore, in order to further dissect how the PAS complex is regulated and performs its effector functions, we performed a protein-protein interaction screen using BioID in order to define the PAS cellular interactome.

Using an inducible CRISPR/Cas9 system, we found that depletion of each HOPS subunit, as well as depletion of a positive regulator of the HOPS complex, UVRAG, impaired EBOV entry. Furthermore, we mapped a region of UVRAG spanning residues 269-442 to be key for binding to the HOPS complex and mediating EBOV entry, indicating that expression of and coordination between the HOPS complex and UVRAG are required for EBOV entry.

Similarly, knockout of each subunit of the PAS complex was found to impair EBOV entry. Further molecular dissection using small molecule inhibitors and enzymatic mutants of PIKfyve and Sac3 demonstrated that PIKfyve kinase activity is required for EBOV entry, while Sac3 phosphatase activity is dispensable. Using a fluorescent probe for phosphatidylinositol(3,5)bisphosphate, the lipid product generated by PIKfyve, we also found evidence that stimulation of cells by EBOV virus-like-particles enhances PIKfyve activity, suggesting that the virus can promote its entry by activating the PAS complex.

Finally, using BioID to screen for interacting proteins of the PAS complex, we identified candidate interactors involved in endosomal trafficking as well as other cell processes including mitochondrial function and cell cycle regulation. Further characterization of one candidate interactor, the coatomer complex I (COPI), using proximity ligation assays validated the interaction between ArPIKfyve and COPI subunit COPB1, and provides further evidence for a role of COPI in endosomal trafficking.

Taken together, these results highlight the importance of cellular trafficking factors involved in diverse facets of endosomal dynamics, from lipid metabolism to membrane tethering, for the entry of EBOV and other filoviruses, and further shed light on how EBOV can actively modulate host trafficking networks to promote successful viral entry and infection. Further molecular dissection of how the virus hijacks cell trafficking will facilitate the development of antiviral therapeutics as well as elucidate how these fundamental cellular processes are regulated.

But, sure, the sky is big, I said;
Miles and miles above my head;
So here upon my back I'll lie
And look my fill into the sky.
And so I looked, and, after all,
The sky was not so very tall.
The sky, I said, must somewhere stop,
And—sure enough!—I see the top!
The sky, I thought, is not so grand;
I 'most could touch it with my hand!
And reaching up my hand to try,
I screamed to feel it touch the sky.

-Edna St. Vincent Millay, Renascence (1912)

Acknowledgements

I owe the completion of this PhD to the mentors, colleagues, friends and family who have supported me and helped me grow as a student, a scientist, and a person. Though I have undoubtedly made many mistakes and questioned myself more times than I can count, these struggles taught me not only the importance of diligence, critical thinking, and hard work, but equally the importance of compassion, humility, and honesty. We are often told that as scientists we owe much to the shoulders of giants we stand on, and this is true. However, I also truly believe that moving forward as a scientific community will depend on nurturing and cultivating the seeds of curiosity found in every child. Whoever became a giant started as a child curious about nature and our place in it. I hope I can become a mentor and a leader in building a world free of obstacles and full of possibilities for the next generation of scientists.

First and foremost, I owe much of my growth to Dr. Marceline Côté. Simply put, I have never met a scientist as passionate and devoted to research as she is. So much of a PhD depends on mentors, and I am fortunate to have had one with the intelligence of a true scientific thinker, the compassion of a true leader, and the perseverance of a true fighter. The challenges in the future that I will face will be made easier knowing that Marceline too has faced them, and succeeded.

I would also like to acknowledge my TAC members Drs. Tommy Alain, Ryan Russell, Vanessa D'Costa, and Marc-Andre Langlois for their guidance and insights throughout my PhD, which have undoubtedly improved the quality of my research and given me much-needed outside perspective whenever I was stuck in my PhD bubble.

I would like to specially acknowledge Corina Stewart, who started as my colleague when we both began grad school years ago, and through our many trials, tribulations, frustrations and joys, became a true friend. It would be a blessing to ever find someone again with whom I work so well.

Thank you to members of the Côté lab past and present for all the good times in and outside the lab, which I will always remember. I would like to specially acknowledge Yuxia Bo as the backbone of our lab from the very beginning, and someone we could always count on.

Suresh, you were always a breath of fresh air with your no-nonsense, BS-free takes on anything and everything. I would also like to thank Sai Priya Anand, Fabiola Salambanga, and Kathy Fu as the first students who I supervised, and as such bore the burden of me learning how to be a mentor. I hope you know that I learned as much as you did.

I would like to thank the many friends and colleagues I have had the privilege to know at RGN. From coming in clutch with reagents, offering commiseration through grad student struggles, and making me laugh countless times. A special shoutout to my office mates Skye, Dave, Chantal, and Shannon for some truly memorable conversations that took place in our office which I dearly hope was sound proof.

I would like to thank Dominique. You are truly a rare gem. You treat everyone with kindness and dignity, regardless of what they have to offer to you. With unconditional love and support you encourage me to be the best version of myself I can be. I would also like to thank Claire, Christian, and the Giguère Samson family for figuratively and literally inviting me into your home. Words cannot express my gratitude.

Finally, I wish to thank my family: my brothers Shaw and Sherman and especially my parents Lian Qiu and Yi-Shan Wu, to whom I dedicate this thesis. I will never be able to fully comprehend the odds you overcame and the hard and at times thankless work you put in to give your children a bright future. All that you have sacrificed and struggled for has, and will always be, the foundation for every success I have.

Work in this thesis was supported by NSERC CGS M and PGS D scholarships.

Table of Contents

List of Abbreviations

ΔM: Mucin-like domain deletion

APPL: Adaptor protein, phosphotyrosine interacting with PH domain and leucine zipper 1

Arf1: ADP-ribosylation factor 1

ARL1: ADP ribosylation factor like GTPase 1

ArPIKfyve: Associated regulator of PIKfyve

ATCC: American Type Culture Collection

BCA: Bicinchoninic acid assay

BDBV: Bundibugyo virus

BIG1: Brefeldin A-inhibited guanine nucleotide-exchange protein 1

βlam: β-lactamase

BLOC: Biogenesis of lysosome-related organelles complex

BOMV: Bombali virus

Ca^{2+}: Calcium ion

CatB: Cathepsin B

CatL: Cathepsin L

cDNA: Complementary DNA

CFR: Case fatality rate

CHMP3: Charged multivesicular body protein 3

CLR: C-type lectin receptor

COPI: Coatomer complex I

COPII: Coatomer complex II

CORVET: Class C core vacuole/endosome tethering

COVID-19: Coronavirus disease 2019

CRISPR: Clustered regularly interspaced short palindromic repeats

DC: Dendritic cell

DC-SIGN: Dendritic cell-specific ICAM-3-grabbing non-integrin

DMEM: Dulbecco's Modified Eagle Medium

DMSO: Dimethyl sulfoxide

Dox: Doxycycline

DRC: Democratic Republic of the Congo

EBOV: Ebola virus

ECL: Enhanced chemiluminescence

EE: Early endosome

EGF: Epidermal growth factor

EGFR: Epidermal growth factor receptor

EIPA: Ethyl-isopropyl amiloride

EMA: European Medicines Agency

ER: Endoplasmic reticulum

ESCRT: Endosomal sorting complexes required for transport

FDA: Food and Drug Administration

FRET: Fluorescence resonance energy transfer

FYVE: Fab1, YOTB, Vac1, EEA1

G: Glycoprotein

GAG: Glycosaminoglycan

GAP: GTPase-activating protein

GAPVD1: GTPase-activating protein and VPS9 domain-containing protein 1

GEF: Guanine nucleotide exchange factor

GFP: Green fluorescent protein

GLUE: GRAM-like ubiquitin-binding in EAP45

GO: Gene ontology

GP: Glycoprotein

GP_{CL}: Cleaved glycoprotein

gRNA: Guide RNA

HA: Hemagglutinin

HEK293T: Human embryonic kidney 293 cells

HER2: Human epidermal growth factor receptor 2

hMGL: Human macrophage galactose- and acetylgalactosamine-specific C-type lectin

HOPS: Homotypic fusion and vacuole protein sorting

HPV16: Human Papillomavirus Type 16

HR: Heptad repeat

HRP: Horseradish peroxidase

HT1080: Human fibrosarcoma cells

IAV: Influenza A virus

IFL: Internal fusion loop

IFN: Interferon

IGF1R: Insulin like growth factor 1 receptor

IL: Interleukin

ILV: Intraluminal vesicle

JUNV: Junín virus

Kb: Kilobase

KO: Knockout

LC3: Microtubule associated protein 1 light chain 3

LC-MS/MS: Liquid chromatography-tandem mass spectrometry

LE: Late endosome

LLOV: Lloviu virus

LSECTin: Lymph node sinusoidal endothelial cell C-type lectin

L-SIGN: Liver/lymph node-specific intracellular adhesion molecules-3 grabbing non-integrin

LY: Lysosome

MARV: Marburg virus

MLAV: Měnglà virus

MLD: Mucin-like domain

MLV: Murine leukemia virus

MT: Microtubule

MVB: Multivesicular body

NK: Natural killer cell

NP: Nucleoprotein

NPC1: Niemann-Pick C1

NPC1-C: Niemann-Pick C1 C luminal domain

NSF: N-ethylmaleimide sensitive factor

PAM: Protospacer adjacent motif

PAS: PIKfyve-ArPIKfyve-Sac3

PBS: Phosphate buffered saline

PCR: Polymerase chain reaction

PCSF: Prize-collecting Steiner Forest

PHAC: Public Health Agency of Canada

PI: Phosphoinositide

PIKfyve: Phosphatidylinositol 3-Phosphate 5-Kinase, FYVE domain containing

PLA: Proximity ligation assay

PLEKHM1: Pleckstrin homology and Run domain containing M1

PMA: Phorbol 12-myristate 13-acetate

PPE: Personal protective equipment

PPI: Protein-protein interaction

PS: Phosphatidylserine

PtdIns(3,5)P_2: Phosphatidylinositol (3,5) bisphosphate

PtdIns(4,5)P_2: Phosphatidylinositol (4,5) bisphosphate

PtdIns3P: Phosphatidylinositol (3) phosphate

PX/PH: Phox homology

RAVV: Ravn virus

RBD: Receptor binding domain

RdRp: RNA-dependent RNA polymerase

RESTV: Reston virus

RFP: Red fluorescent protein

RIG-I: Retinoic acid-inducible gene I

RILP: Rab-interacting lysosomal protein

RNP: Ribonucleoprotein

RUBICON: Run domain Beclin-1-interacting and cysteine-rich domain-containing protein

rVSV: Recombinant Vesicular stomatitis virus

Sac3: SAC Domain-Containing Protein 3

SAINT: Significance Analysis of INTeractome

SARS-CoV-1/SARS-CoV-2: Severe acute respiratory syndrome coronavirus 1/2

SDS-PAGE: Sodium dodecyl sulphate–polyacrylamide gel electrophoresis

sGP: Soluble glycoprotein

SNARE: Soluble N-ethylmaleimide-sensitive factor attachment protein receptors

SNX: Sorting nexin

ssGP: Small soluble glycoprotein

STAT: Signal transducer and activator of transcription

SUDV: Sudan virus

SV40: Simian virus 40

TAFV: Taï Forest virus

TAM: Tyro3, Axl, Mer

TBC1D15: TBC1 domain family member 15

TBC-2: TBC1 domain family member 2

TfR: Transferrin receptor

THP-1: Human monocytic cells

TIM: T-cell immunoglobulin and mucin

TLR: Toll-like receptor

TPC: Two-pore channel

TRPML: Transient receptor potential mucolipin

USO1: General vesicular transport factor p115

UVRAG: UV radiation resistance-associated gene

V-ATPase: Vacuolar-type ATPase

Vero: African green monkey kidney epithelial cells

VLP: Virus like particle

VP: Viral protein

VPS: Vacuolar protein sorting

VSV: Vesicular stomatitis virus

WDR91: WD repeat-containing protein 91

WHO: World Health Organization

Xkr8: XK-related protein 8

List of Figures

List of Tables

Chapter 1: General Introduction

They can't run, they can't walk, they can't swim, they can't crawl. They ride.

-David Quammen, Spillover

1.1 Filovirus biology and epidemiology

1.1.1 The Filoviridae family

The *Filoviridae* family of viruses comprises of six known genera: *Ebolavirus*, *Marburgvirus*, *Cuevavirus*, *Dianlovirus*, *Striavirus*, and *Thamnovirus* (Figure 1.1) (1). *Ebolavirus* and *Marburgvirus* species are associated with highly lethal viral hemorrhagic fever diseases in humans and non-human primates, with case fatality rates ranging from 20% to over 90% (2). The *Cuevavirus* and *Dianlovirus* genera each contain a single virus, Lloviu virus (LLOV) and Měnglà virus (MLAV), respectively, both of which have only been sequenced in bat species and are not known to infect humans (3,4) . The *Striavirus* and *Thamnovirus* genera likewise each contain a single virus, whose sequences were identified from high throughput sequencing of fish samples from the South China Sea (5).

The *Ebolavirus* genus contains six identified species to date: Ebola virus (EBOV, formerly Zaire Ebola virus), Sudan virus (SUDV), Bundibugyo virus (BDBV), Taï Forest virus (TAFV, formerly Côté D'Ivoire Ebola virus), Reston virus (RESTV), and the recently identified Bombali virus (BOMV) (1,6). EBOV, SUDV, and BDBV have been the sources of sporadic outbreaks of Ebola virus disease (EVD) since 1976, with EBOV being the causative agent of the majority of outbreaks. Until the large scale 2013-2016 west Africa outbreak of EVD, the majority of EVD outbreaks were restricted to the Democratic Republic of the Congo (DRC,

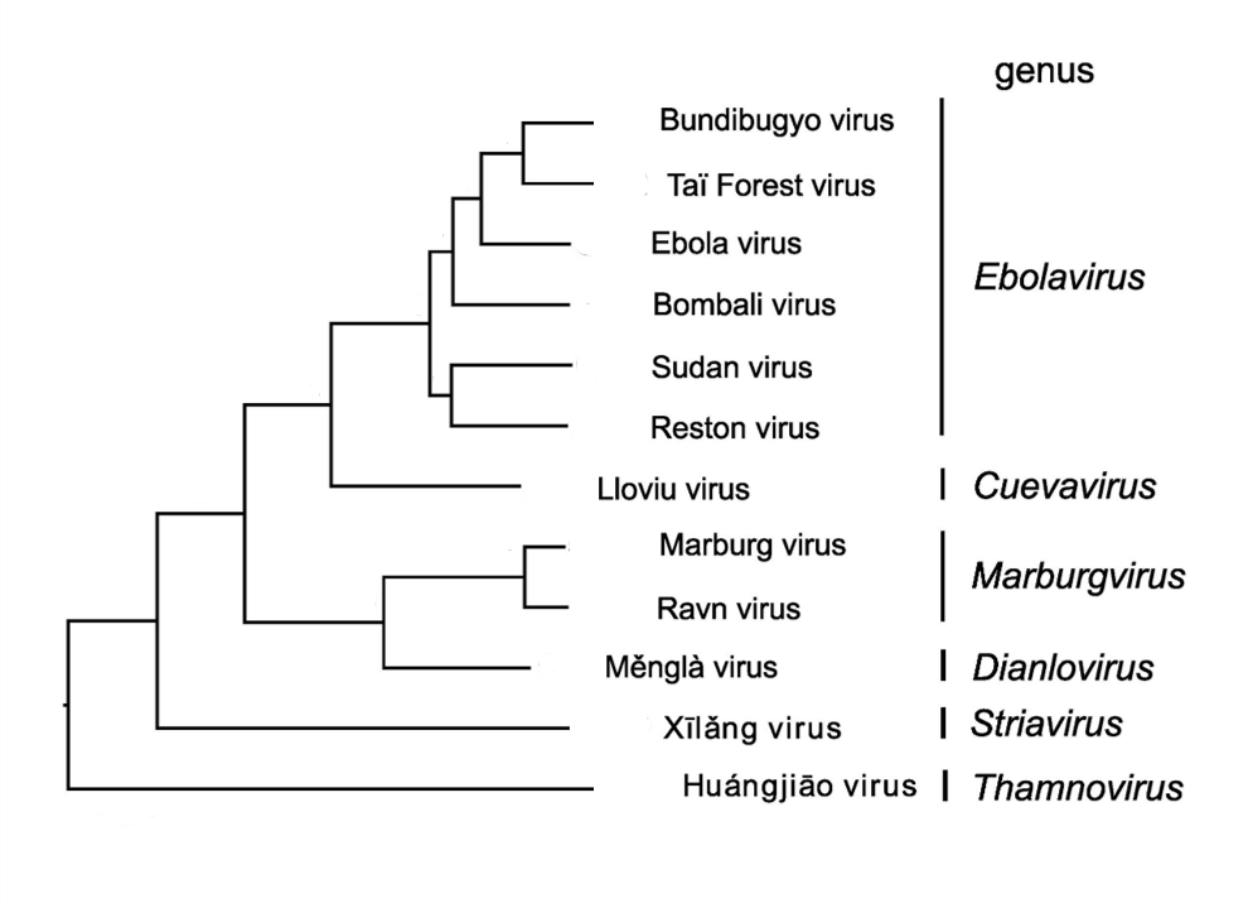

Figure 1.1. The Filoviridae family

A phylogenetic tree showing genera and species of known viruses within *Filoviridae*. Modified from Kuhn et al. (2020) with permission in accordance with the Creative Commons Attribution License BY-SA 4.0 (https://creativecommons.org/licenses/by-sa/4.0/) (1).

formerly Zaire), Sudan, and Uganda (2). Only one case of a human TAFV infection has been recorded, in a scientist who performed an autopsy on an infected chimpanzee in Taï national park, Côté D'Ivoire in 1994; she later recovered (7). RESTV, which was first identified in cynomolgus macaques imported from the Philippines to a research facility in Reston, Virginia in 1989, is highly pathogenic in non-human primates but not known to cause disease in humans (8).

The *Marburgvirus* genus contains a single species, *Marburg marburgvirus*, which is further subclassified into two closely related viruses, Marburg virus (MARV) and Ravn virus (RAVV), both of which are pathogenic to humans and nonhuman primates (9).

We are only just beginning to understand the full diversity of filoviruses. Analysis of mammalian genomes, particularly bat genomes, has uncovered numerous endogenous filoviral-like elements, suggesting that filoviruses may have been circulating in mammalian hosts as long as 40 million years ago (10–12).

1.1.2 Filovirus structure

The name *Filoviridae* is derived from the latin word *filum*, meaning "thread", in reference to their filamentous morphology. Filovirus virions are pleomorphic, with a uniform diameter of 80 nm and varying lengths of up to 14000 nm, with a median length of 1000 nm for EBOV virions (Figure 1.2A) (13). Virions are enveloped in a lipid membrane derived from the host cell plasma membrane during viral budding and egress. Each virion contains a single copy of a single stranded, negative sense RNA genome, which is approximately 19kb in size (Figure 1.2B). The filovirus genome encodes seven major gene products, all of which are structural protein incorporated into nascent virions: the nucleoprotein (NP), viral protein 35 (VP35), VP40, VP24, the viral glycoprotein (GP), VP30, and the RNA-dependent RNA polymerase (L) (14–17).

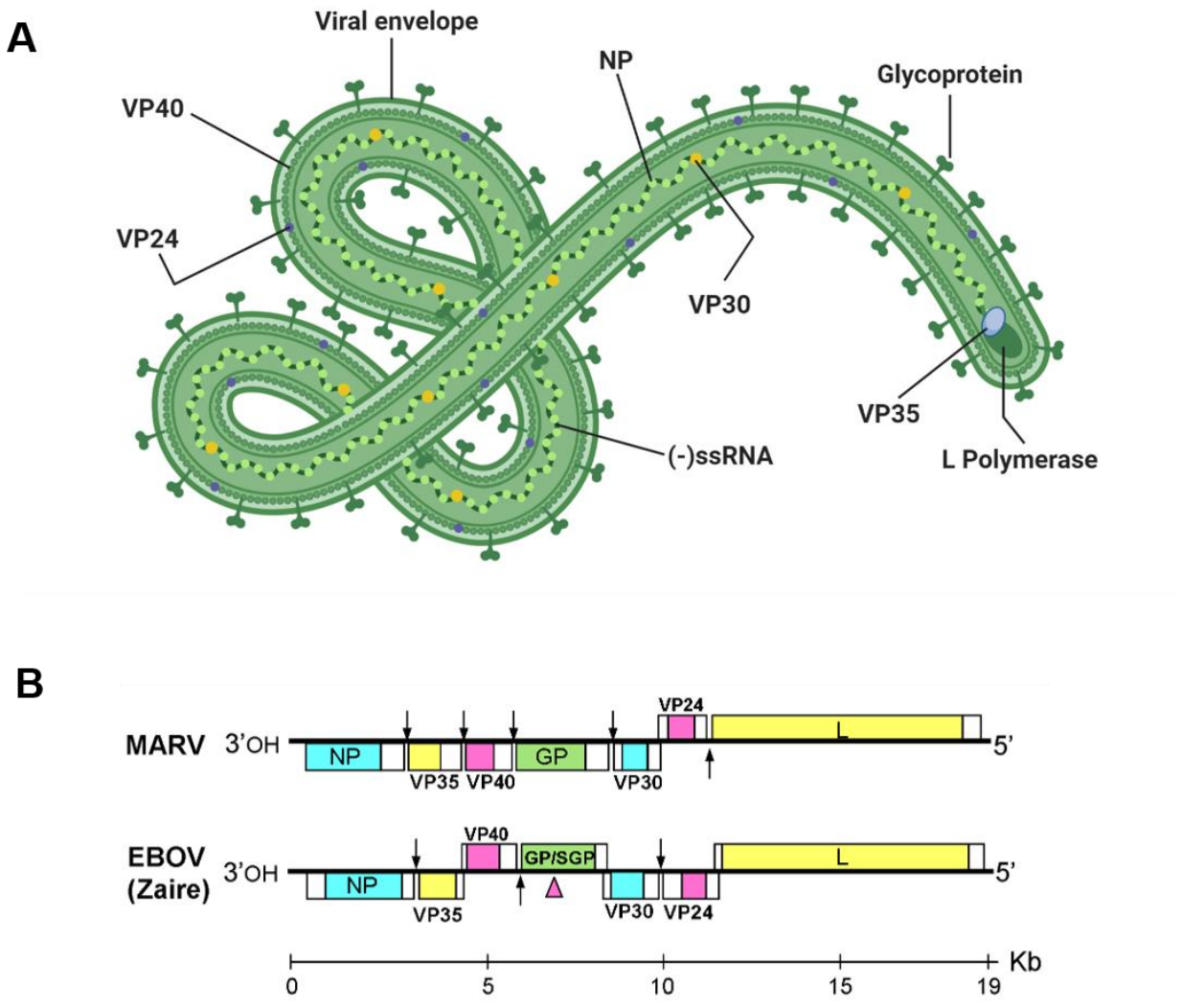

Figure 1.2. Filovirus structure and genome organization

(A) Schematic of the general structure of a filovirus virion. Created with BioRender.com. (B) Genome organization of Marburg virus (MARV) and Ebola virus (EBOV). Open reading frames are labeled and indicated by colored boxes, non-coding regions by empty boxes. Vertical arrows indicate transcription initiation and termination sites, except for regions of overlap, where these sites are not marked. The pink arrowhead points to the location of an editing site in the GP gene of EBOV. Reprinted from Belyi et al. (2010) with permission in accordance with the Creative Commons Attribution License BY 4.0 (https://creativecommons.org/licenses/by/4.0/) (12).

The viral genome is complexed with NP, VP30, VP35, and L to form the ribonucleoprotein complex (RNP) (18,19). The RNP in turn is further complexed with the major and minor matrix proteins (VP40 and VP24), and the entire viral particle is surrounded by a lipid membrane studded with the trimeric GP, which is the only viral protein expressed on the surface of the virion and plays a critical role in viral entry (17,20).

The major matrix protein VP40 is the primary determinant of viral morphogenesis and plays a key role in viral budding (21–23). Filovirus-like-particles (VLPs), structurally indistinguishable from the native virus, can be produced simply through expressing VP40 in cells (24,25). For the purposes of studying viral entry, VLPs are typically generated by co-expressing VP40, NP, and the GP of the filovirus of interest, which can then be used to recapitulate the filovirus entry pathway in target cells (24,26,27).

A feature unique to members of the *Ebolavirus* genus is the production of two GP variants from the GP open reading frame due to transcriptional editing: soluble GP (sGP) and small soluble GP (ssGP) (28,29). sGP and ssGP share a common N-terminal sequence with the full length viral membrane associated GP, but contain unique C-terminal sequences. In addition, both sGP and ssGP form homodimers, in contrast to the trimeric form of virus associated GP (30). Furin cleavage of the sGP precursor protein also results in the production of an additional peptide, delta-peptide (31). While these GP variants are not incorporated into virions, they still can be shed from cells and have been shown to have roles in immunoregulation and pathogenesis during EBOV infection (32,33). sGP is known to compete for binding with host antibodies directed against virus associated GP, acting as a decoy for the immune system (34), while delta-peptide has been shown to act as a viroporin, able to induce membrane permeabilization and cytotoxicity in cells (35–37).

1.1.3 Filovirus epidemiology and zoonosis

The severe virulence and at times sensationalized media depictions of filovirus disease outbreaks has engendered this virus family with a fearsome image that has inspired an unusual degree of public attention not normally garnered by so-called neglected tropical pathogens.

As zoonotic pathogens, filoviruses circulate and persist in non-human animal reservoirs and are sporadically transmitted to humans during spillover events, either directly from the reservoir animal or through an intermediate or amplifying host. Various species of bats have long been suspected or confirmed to be the wild reservoir for currently known filoviruses (38–41). Live MARV has been isolated from Egyptian fruit bats (*Rousettus aegyptiacus*) found in Kitaka Cave, Uganda, which were the likely source of a small outbreak of Marburg virus disease (MVD) in miners working in the cave (42). No live ebolavirus has been isolated from bats, while indirect evidence in the form of viral RNA and ebolavirus-specific antibodies has been detected in a number of bat species in multiple geographic locations, including the DRC, Spain, China and the Philippines (4,43–48). Nonhuman primates and domesticated pigs have been implicated as intermediate hosts for filoviruses (49,50).

The first recorded filovirus-associated outbreak was a small outbreak of MVD amongst laboratory workers in Germany and Yugoslavia in 1967, acquired from infected African green monkeys imported from Uganda (51). A total of 31 cases was reported, with 7 deaths (case fatality rate (CFR) of 23%). The etiological agent was named Marburg virus, after the German city which was the site of one of the outbreaks. Since this initial MVD outbreak, 12 others have been recorded, all of which (aside from laboratory acquired infections) have occurred in Africa (52). The largest MVD outbreak occurred in Angola in 2004-2005, with 227 deaths amongst 252 recorded cases (CFR 90%) (53).

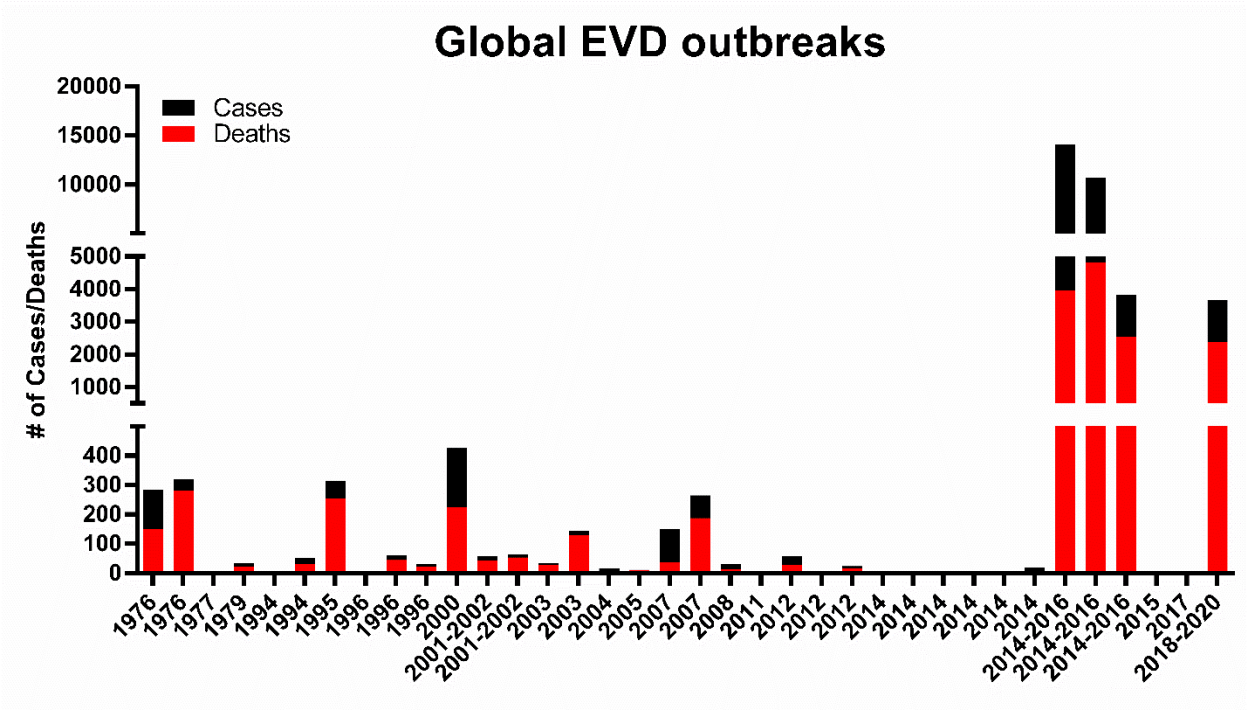

Figure 1.3. Global Ebola virus disease (EVD) outbreaks

Recorded cases and deaths from EVD since the discovery of EBOV in 1976 and as of November 18, 2020. Repeated years indicate outbreaks in different locations within the same year. Data obtained from the Centers for Disease Control and Prevention (2).

The first recorded incidences of EVD occurred simultaneously in the Yambuku region of Zaire (now the DRC) and in Sudan in 1976. They were later determined to have been caused by separate ebolavirus species, which were named Zaire ebolavirus (now renamed Ebola virus) and Sudan ebolavirus, and in both cases were spread primarily within hospitals where infected patients were treated (54). The Zaire outbreak resulted in 318 cases (280 deaths, CFR 88%) and the Sudan outbreak resulted in 284 cases (151 deaths, CFR 53%). EBOV and SUDV have been responsible for the majority of EVD outbreaks to date, with EBOV being responsible for over 70% of outbreaks (Figure 1.3). Until the 2013-2016 West African epidemic, most EVD outbreaks were limited to under 500 cases and contained to mainly rural areas of the DRC, Republic of the Congo, Sudan, Gabon and Uganda (2). The West African epidemic, also known as the Makona outbreak, after the strain of EBOV responsible, was by far the largest in magnitude to date with 28,646 recorded cases (11,323 recorded deaths, CFR 40%), which is likely an underestimate due to the large number of unrecorded cases (55–57). The Makona outbreak was unique from other EVD outbreaks in numerous ways, including its epicentre in three countries it previously had not affected (Guinea, Sierra Leone, and Liberia), its uncontrolled and exponential spread in urban areas, and the international export of several cases, heightening fears of its pandemic potential. It was this epidemic that brought the Ebola virus spectre to global public attention, galvanizing research efforts towards the production of vaccines and therapeutics, including a live attenuated vaccine based on recombinant VSV (rVSV-ZEBOV), developed by the Public Health Agency of Canada (PHAC) and deployed in Guinea in a phase III clinical trial in 2015 (58). Results of this and subsequent trials showed the vaccine to be protective and effective at containing transmission; it was later approved for use by the WHO, European Medicines Agency (EMA) and the FDA (59,60).

Since the end of the West African epidemic and as of this writing, three more outbreaks of EVD have occurred in the DRC and Uganda (61), with the most recent outbreak declared over on November 18, 2020 by the DRC Ministry of Health and WHO. These outbreaks recorded 3654 cases and 2375 deaths. The administration of the rVSV-ZEBOV vaccine under Compassionate Use protocols during these outbreaks appeared to be effective in reducing transmission according to an interim WHO report, although vaccine deployment was hampered by military conflict and civil unrest in the affected regions (62).

1.1.4 Clinical presentation of filovirus disease

EVD and MVD present similar clinical symptoms as other viral hemorrhagic fever diseases such as Lassa fever or yellow fever, as well common comorbidities such as malaria, complicating diagnosis in regions where multiple diseases are present. The incubation period is between 2 and 21 days, with 5-10 days being the average (63). Transmission occurs through direct contact and mucous membrane exposure to infected bodily fluids, including through handling of infected corpses (64). Transmission during outbreaks frequently occurs through funeral practices that involve close contact with the body, as well as to caregivers and health care workers not adequately protected by PPE. Only symptomatic patients appear to be infectious (64,65).

Initial symptoms are nonspecific and commonly include fever, myalgia, headache and abdominal discomfort. Other commonly reported symptoms include a maculopapular rash and conjunctivitis (66). In patients with severe disease, symptoms such as dehydration, leukopenia, and bradycardia present 7-14 days after initial illness onset, and are associated with high viremia (67). Despite being known as a hemorrhagic fever disease, internal or external hemorrhage is not a universal symptom and typically occurs in fewer than 50% of clinical cases (68). In fatal cases,

death occurs from multiple organ failure and shock, generally 6-9 days from initial illness onset. While in some cases experimental therapeutics have been administered to infected patients, care is primarily supportive, involving rehydration and pain management (69).

Survivors may experience a constellation of symptoms known as "post-Ebola syndrome," these include prolonged muscle and joint pain, vision impairment, and neurological issues such as headache and memory loss (70–72). Profound mental effects, including post traumatic stress, are also common among EVD survivors. Viral persistence in immune privileged sites such as the eye or urogenital tract has been reported, and virus shedding in semen and subsequent sexual transmission has been reported in two studies (73,74). However, the incidence, effects, and risk of transmission from Ebola virus persistence are still largely unknown (75).

1.1.5 Host immune response to filovirus infection

Filoviruses display a broad cell tropism and can infect diverse cell types, with the exception of lymphocytes (76,77). *In vivo*, macrophages and dendritic cells (DC) are major early and sustained targets of infection, and contribute to dissemination of the virus to other organs and tissues (78,79). Viral replication can occur in all organs, with the liver, spleen and other lymphoid tissues known to be the primary sites for virus production (63).

The high virulence and mortality rate of filovirus disease is associated with multiple mechanisms of both innate and adaptive immune dysfunction induced by the virus, including suppression of type I interferon (IFN) response, impairment of DC maturation, induction of lymphocyte and NK cell apoptosis and stimulation of a massive release of pro-inflammatory cytokines ("cytokine storm") (77,80–89). Multiple viral proteins have been shown to interfere with cellular immune responses in addition to their functions in viral replication. For example, VP35 has been shown to antagonize IFN I signalling by impairing signalling through RIG-I-like

receptors (90–98), while VP24 blocks the transcription factor STAT1 from entering the nucleus (99–103). Viral evasion and dysregulation of the host immune response is an important marker of disease severity and survival outcomes in patients, with an early and robust induction of inflammatory mediators and antibodies correlated with better survival outcomes (104–110).

1.1.6 Filovirus replication and budding

Filoviruses share the same general mechanisms of replication as other viruses within the *Mononegavirales* order (111). The filoviral RNA dependent RNA polymerase (RdRp) L mediates transcription and replication of the genome. Following viral entry and release of the nucleocapsid into the cytoplasm, L works in concert with NP, VP35, and VP30 to transcribe RNA using the incoming viral genome as a template. The polymerase complex initiates transcription at a single promotor site at the 3' end of the genome, generating monocistronic mRNAs in decreasing abundance based on distance from the 3' end, due to polymerase stuttering. Therefore NP is produced in the most abundance and L is produced in the least abundance (112).

Genome replication proceeds through the synthesis of a positive sense RNA intermediate (the antigenome), which serves as a template for the synthesis of new negative sense viral genomes. Mature nucleocapsids assemble with GP and VP40 at the plasma membrane for budding of nascent virions (24,25,113). Positively charged lysine residues exposed on VP40 dimers facilitate their initial recruitment to the plasma membrane by interacting with anionic membrane lipids (23,114,115). Following initial association with the plasma membrane, VP40 dimers have been shown to oligomerize further to form the viral matrix (116–118). Both phosphatidylinositol-4,5-bisphosphate (PtdIns(4,5)P_2) and phosphatidylserine (PS), which are abundant on the inner leaflet of the plasma membrane, have been shown to interact with VP40 to

promote oligomer stability and budding (119–123). The role of PS in the filovirus life cycle is of particular interest as it seems to play important roles in both budding and entry (for its involvement in entry see section 1.2.2). EBOV and MARV budding are dependent on interactions between VP40 and PS, while incorporation of PS in the filoviral envelope enhances attachment and internalization via binding to PS receptors on target cells (120,121,124). It has been demonstrated that EBOV co-opts a host scramblase, Xkr8, to externalize PS on the surface of budding virions (125).

1.2 Ebola virus entry

1.2.1 Ebola virus glycoprotein structure and function

As an enveloped virus, EBOV entry is contingent upon fusion of the viral envelope with the cellular membrane, in order to release the viral nucleocapsid into the cytoplasm to initiate replication. This fusion event is catalyzed by the viral envelope protein, GP, the only viral protein to be expressed on the surface of virions and the primary determinant of viral entry (126).

The EBOV GP is synthesized as a single polypeptide precursor, GP_0 (160kDa), which is cleaved into two subunits, the amino terminal GP_1 (140 kDa) and the carboxyl terminal GP_2 (26 kDa) by the enzyme furin in the golgi (127). $GP_{1,2}$ heterodimers remain associated through disulfide bonds, and further associate into trimers via non-covalent interactions to form the mature virion-associated GP (Figure 1.4) (29,128,129). GP_1 is the subunit responsible for cellular attachment and contains the receptor binding domain (RBD) required to trigger membrane fusion, while GP_2 contains the fusion peptide responsible for mediating the fusion event itself (20).

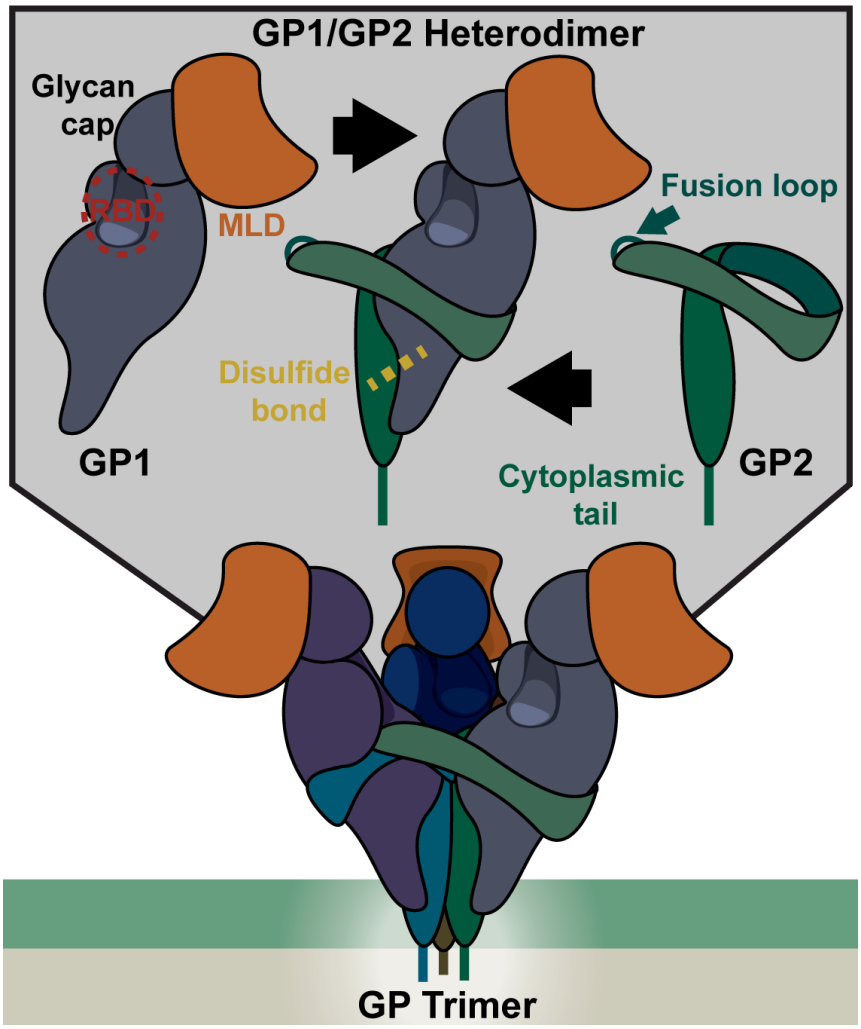

Figure 1.4. Ebola virus glycoprotein (GP) structure

Schematic of the membrane associated EBOV glycoprotein, composed of a trimer of GP_1-GP_2 heterodimers. The receptor binding domain (RBD) on GP_1 is shielded by the highly glycosylated glycan cap and mucin-like domain (MLD). Reprinted from Moller-Tank and Maury (2015) with permission in accordance with the Creative Commons Attribution License BY 4.0 (https://creativecommons.org/licenses/by/4.0/) (130).

Trimeric GP exists as a metastable structure in its prefusion form, undergoing a cascade of conformational changes upon encountering the required triggering factors within target cells in order to reach its final stable conformation upon membrane fusion. These conformational changes are irreversible, therefore premature triggering of GP results in inactivation of the virus (131). EBOV has evolved mechanisms in order to exquisitely control the sequence of events during viral entry to ensure proper GP triggering and viral fusion in the appropriate cellular compartment.

GP_1 can be divided into four subdomains: the base, the RBD, the glycan cap and the mucin-like domain (MLD). The base domain forms a hydrophobic, semicircular surface that acts as a clamp to stabilize the fusion loop within GP_2 (132). The glycan cap and MLD are heavily glycosylated with both N- and O-linked glycans present. These glycans shield the highly conserved RBD from immune detection and can enhance cellular attachment by binding to cell surface lectins (128,133–136). A recent study has suggested that the glycan cap may play an additional role in stabilizing the prefusion conformation of GP by preventing premature triggering (137). Deletion of the MLD from GP (ΔM mutation) does not impair infectivity of the virus and in fact enhances GP incorporation onto virions and reduces cytotoxicity in virus producing cells (128,138), therefore ΔM GP variants are commonly used for *in vitro* EBOV entry assays.

GP_2 contains a fusion peptide, transmembrane domain, and a short cytoplasmic tail, and is categorized as a class I viral fusion protein on the basis of its α-helical two heptad repeats that associate during fusion to form a six helix bundle (139,140). The fusion peptide resides in an internal loop and contains a series of hydrophobic residues bounded by an antiparallel, disulfide-linked β-scaffold. In the prefusion state, the internal fusion loop wraps around the outside of the

GP trimer. Its hydrophobic side chains are sequestered from solvent by packing into a neighboring GP_1 monomer (132,141). Fusion requires extrication of the fusion loop and extension into the apposing host cell membrane.

1.2.2 Attachment and internalization

EBOV entry begins with attachment of virions to the cell surface and triggering of internalization. Viral attachment is mediated by non-specific interactions between EBOV and cell surface proteins. Two types of nonspecific attachment have been described for EBOV: interaction between GP and various carbohydrate binding receptors, and interactions between PS embedded in the viral envelope and cell surface PS receptors.

Glycosylated residues on GP have been shown to mediate binding to numerous C-type lectin receptors (CLRs), including dendritic cell-specific ICAM-3-grabbing non-integrin (DC-SIGN), liver/lymph node-specific SIGN (L-SIGN), lymph node sinusoidal endothelial cell C-type lectin (LSECTin), and human macrophage galactose- and acetylgalactosamine-specific C-type lectin (hMGL) (133,142–148). The glycosaminoglycans (GAGs) heparin and heparan sulfate have also been shown to bind to GP and act as potential attachment factors (149). The wide distribution of CLRs and other carbohydrate receptors among different cell types may contribute to the broad cellular tropism of EBOV, however, more work is required to understand the role of these attachment factors *in vivo* during EBOV infection and pathogenesis.

In addition to GP-dependent cell attachment, PS expressed on the EBOV envelope has been shown to facilitate attachment by interacting with TIM (T-cell immunoglobulin and mucin) and TAM (Tyro3, Axl, Mer) families of PS receptors. Normally retained on the inner leaflet of the plasma membrane, PS is externalized to the outer leaflet during apoptosis and acts as a marker for apoptotic bodies (150). Recognition by PS receptors on phagocytes and other immune

cells facilitates the engulfment and clearance of apoptotic bodies, and expression of PS on viral envelopes to enhance their uptake by phagocytes is known as apoptotic mimicry (151). Two of the TIM family receptors in humans (TIM-1 and TIM-4) have been shown to enhance EBOV entry by directly binding to virion associated PS (152–155), while the TAM receptors interact with PS via an intermediate protein (Gas6 or Protein S) (156,157). Unlike carbohydrate receptors which appear to mediate attachment only, PS receptors may function in both attachment and internalization of EBOV by enhancing macropinocytosis (152,153,157,158), however it is still unclear whether these receptors are sufficient to activate viral internalization or work in concert with other internalization triggers.

Due to the large size of filovirus particles (>1μm in length), macropinocytosis is considered the predominant mechanism of viral internalization. Macropinocytosis involves the nonselective uptake of fluid, solutes, ligands and other particles into large endocytic vesicles called macropinosomes, and is driven by actin rearrangements at the plasma membrane that form protrusions that engulf extracellular contents (159). Unlike clathrin- or caveolin-mediated endocytosis, which generate vesicles smaller than 100nm in diameter, macropinosomes can range from 0.2-5 μm in diameter (160). Internalization of EBOV displays several hallmarks of macropinocytosis, including induction of actin ruffling at the plasma membrane, a concomitant transient elevation in fluid uptake, and sensitivity to macropinocytosis inhibitors such as EIPA (an inhibitor of Na^+/H^+ exchange) and staurosporine (an inhibitor of protein kinase C) (157,161–165). The requirement for Dynamin-2 (a GTPase involved in the scission of newly formed macropinosomes) in EBOV internalization is unclear, and appears to be cell-type dependent (157,161–163,165).

In most cell types macropinocytosis is not a constitutive process and must instead be triggered, typically through engagement of cell surface receptors by ligands such as growth factors or PS, which induces a cell signalling cascade that results in actin mobilization. A key remaining question is how EBOV triggers its macropinocytic uptake. In addition to activation of the TIM and TAM family of PS receptors, recent studies have also suggested that EBOV can activate other receptor tyrosine kinases such as epidermal growth factor receptor-2 (HER2) and insulin like growth factor 1 receptor (IGF1R) (166,167), which results in the activation of the PI3K/Akt pathway known to be important for macropinocytosis. Further work is required to elucidate the exact mechanisms by which EBOV triggers macropinocytosis in multiple cell types.

1.2.3 Endosomal trafficking of virions and proteolytic priming of EBOV GP

Following internalization, EBOV particles enclosed in nascent endosomes must undergo trafficking to the late endosome/lysosome (LE/LY) compartment, which contains triggering factors required for GP-mediated membrane fusion. To date two triggering factors for EBOV have been well characterized: proteolytic cleavage of GP by pH-dependent cellular cathepsin proteases, and GP binding to the filoviral entry receptor, Niemann-Pick C1 (NPC1).

Multiple lines of evidence support the key importance of endolysosomal trafficking for EBOV entry. Experiments examining the kinetics of EBOV entry have observed that while VLPs or VSV pseudotypes bearing EBOV GP are internalized relatively quickly, they experience a lag in cytoplasmic entry compared to particles bearing the envelope proteins of other viruses such as VSV G, Influenza HA and LCMV GP, with delivery to NPC1+ endolysosomes acting as the rate limiting step (168). This is further supported by studies tracking real time EBOV trafficking and fusion in live cells, which have demonstrated that the slower trafficking kinetics of virus

particles bearing EBOV GP is a due to the requirement for the virus to reach Rab7+ and NPC1+ LE/LY compartments (169,170). Furthermore, EBOV GP-mediated entry is impaired in cells expressing dominant negative forms of Rab5 and Rab7, GTPases that are required for maturation of early endosomes (EEs) to LE/LYs (163). Finally, a genetic screen for cellular proteins important for EBOV GP-mediated entry using mutagenized haploid cells found that regulators of endolysosomal architecture and trafficking predominated the top candidate hits. In addition to the now well characterized EBOV entry factors cathepsin B and NPC1, the screen also identified all members of the homotypic fusion and vacuole protein sorting (HOPS) complex, a tethering complex involved in LE/LY fusion, as well as PIKfyve and Sac3 (also known as Fig4), regulators of phosphoinositide lipids required for endosomal maturation. Follow-up characterization of EBOV GP-mediated entry into cells deficient in the HOPS subunit VPS33a revealed a defect in a later, post-internalization step of viral entry, consistent with the localization and function of the HOPS complex in the LE/LY compartment (171).

Endosomal pH plays a key role in EBOV entry. Firstly, EBOV must reach low pH (<5.5) endosomal compartments containing activated cathepsins B and L (CatB and CatL). These low pH-dependent cysteine proteases proteolytically prime GP for receptor interaction by cleaving GP_1 to remove the glycan cap and MLD (172–174). This exposes the RBD, and appears to additionally prime GP for fusion by removing the β13-β14 loop in GP_1, which overlays the GP_2 internal fusion loop (IFL), forming part of the GP_1 clamp (132,175,176). Furthermore, Rab7+/NPC1+ LE/LYs have higher CatL activity than early endosomes lacking these markers, likely a function of their lower pH (168). Low pH has also been found to stabilize GP both pre- and post cathepsin cleavage, which may prevent premature fusion triggering (177). Finally, a low pH environment appears to be required for conformational changes in the IFL required for

insertion into the target membrane, as well as stabilization of the six helix bundle during fusion (141,178,179). These findings indicate that a low pH is required for the fusion event itself as well as for optimal activity of cathepsin proteases.

While it is well established that cathepsin cleavage is essential for EBOV GP-mediated fusion, the specific dependence on CatB and/or CatL appears to be both virus-specific and cell-type dependent. For example, while CatB is required for EBOV, BDBV, and TAFV entry, it is dispensable for RESTV, LLOV, and MARV, while SUDV has intermediate sensitivity to CatB inhibition (180,181). EBOV entry in Vero cells is dependent on both CatB and CatL, while CatL is dispensable for EBOV entry into DCs (182). Finally, an additional role for cathepsins beyond unmasking of the RBD of GP has been suggested, as evidenced by the surprising finding that pre-cleaved EBOV GP remains sensitive to inhibition with E64d, a pan cysteine protease inhibitor (173,174,183). Specifically, while pre-cleaved EBOV GP can mediate at least partial fusion in the presence of E64d, full fusion and genome release is impaired (169). This implies an additional role for cathepsins for full fusion pore formation and expansion.

1.2.4 NPC1 binding and fusion

The LE/LY resident protein NPC1 was identified to be the receptor for EBOV in two independent studies in 2011 (171,184), and has been found to be the cellular receptor for all known filoviruses (181,185–188). NPC1 is a large, ubiquitously expressed 13-pass transmembrane cholesterol transporter localized to the limiting membrane of LE/LYs. In concert with the soluble cholesterol binding protein NPC2, it functions in the efflux of cholesterol from LE/LYs to the ER and other sites (189). Mutations resulting in loss of function of either gene underlie the lysosome storage disease Niemann Pick disease type C (190). NPC1 contains three major luminal domains, A, C and I. Structural characterization of EBOV GP bound to NPC1

along with mutagenesis studies have identified key residues on both proteins that participate in binding. The RBD on GP has been mapped to residues 54-201 (191–193), with the receptor binding site on cleaved GP (GP_{CL}) forming a wave-like contour, with a basic/polar crest and a hydrophobic trough previously occupied by the glycan cap (176,194). On NPC1, the GP binding site has been mapped to residues 372-640, which comprise the C luminal domain (NPC1-C) (176). NPC1-C forms two protruding loops, both of which engage with the hydrophobic cavity on GP_{CL} (175,176,195,196). These hydrophobic interactions appear to form the primary basis of GP_{CL}-NPC1-C binding, while the hydrophilic residues in the polar crest participate in more nonspecific electrostatic interactions with one NPC1-C loop (191,194). Mutations in GP that result in the occlusion of the hydrophobic trough or disrupt the overall basic charge of the polar crest impair binding to NPC1-C; similarly, mutating residues in the NPC1-C loops that form contacts with the GP_{CL} hydrophobic cavity abrogate binding (175,176,194).

The specificity of the interaction between NPC1 and EBOV GP and the use of NPC1 as the receptor by all known filoviruses strongly implies that NPC1 is a highly conserved host factor for filoviruses and is a major determinant of host range and zoonotic transmission, as mutations in the NPC1-C domain have been found to confer resistance to EBOV infection in other vertebrates such as reptiles (186,197,198).

Following proteolytic priming and NPC1 binding, EBOV GP-mediated membrane fusion proceeds through a sequence of conformational changes shared by class I viral fusion proteins; namely: (1) release of the fusion loop and insertion into the endosomal membrane, forming an extended intermediate structure connecting the viral and host membrane, and (2) folding back of the α-helical heptad repeats to form a final, stable six helix bundle conformation of the trimeric GP. These conformational changes bring the viral and cell membranes in close apposition,

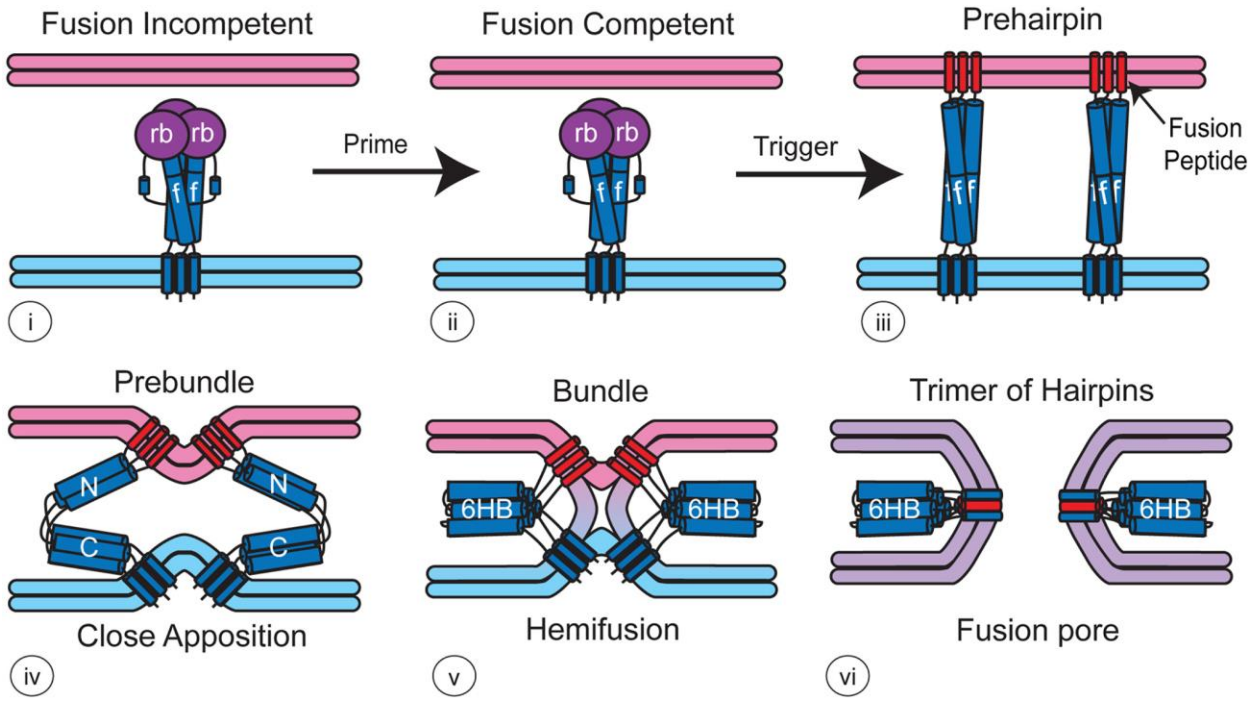

Figure 1.5. Schematic of membrane fusion mediated by a class I viral fusion protein

Fusion between viral and cell membranes catalyzed by a generic class I viral fusion protein. Prior to triggering, the receptor binding (rb) subunit of the viral envelope protein forms a clamp over the fusion subunit (f). Upon encountering the appropriate triggering factor(s), the fusion peptide is released and able to insert into the target membrane, forming an extended intermediate structure (also called the prehairpin) connecting the viral (light blue) and host cell (light pink) membranes (iii). The fusion protein then folds back, causing the N- and C-terminal heptad repeats to form the final, stable six helix bundle (6HB) conformation. This brings the two membranes into close apposition, hemifusion, and full fusion, allowing the formation of a fusion pore. The final post fusion conformation of the viral fusion protein is termed a trimer of hairpins. Reprinted from White and Whittaker (2016) with permission (199).

followed by hemi-fusion of the outer leaflets, full fusion of the inner leaflets forming a fusion pore, then expansion of the pore, allowing release of the viral nucleocapsid (131) (Figure 1.5).

The direct fusion trigger that initiates this sequence of conformational changes in GP is still unresolved. There remains debate on whether GP_{CL}:NPC1 binding is sufficient to initiate full fusion. Protein crystallography analysis comparing uncleaved GP to GP_{CL} bound to NPC1 has revealed several conformational changes, namely an upward movement of the β3-α1 loop that may facilitate the release of the IFL, initiating fusion (176). However, incubation of viral particles bearing GP_{CL} with cells ectopically expressing NPC1-C on the plasma membrane does not permit viral fusion and entry, even under low pH conditions (185). Similarly, the requirement for cathepsins post-fusion but pre nucleocapsid release discussed in section 1.2.3 suggests an additional role for cathepsins in GP-mediated fusion. Similar to other membrane fusion events, GP-mediated fusion is dependent on Ca^{2+} (200,201), however, whether Ca^{2+} is a direct fusion trigger has not been determined. A potential role for the endosomal calcium two-pore channels (TPCs) in fusion triggering has been proposed, however it remains unclear whether TPCs are directly involved in fusion triggering or whether they play a role in endosomal trafficking of virions (170,202,203). Further investigation is required to delineate the exact mechanism by which GP mediates fusion. A schematic of the EBOV entry pathway is summarized in Figure 1.6.

1.3 Endosomal trafficking

1.3.1 Overview of endosomal trafficking pathways

Endocytosis is a complex and tightly regulated process involving the uptake of extracellular fluids, solutes, ligands, and other particles into membrane-bound vesicles called

endosomes. Endocytosed contents enter a highly dynamic and heterogeneous endosomal labyrinth that feeds into multiple trafficking pathways functionally connecting all cellular compartments. Broadly speaking, endocytosed cargos are funnelled into three trafficking routes: the recycling pathway leading back to the plasma membrane (either directly from early endosomes or through intermediate recycling endosomes), the degradation pathway culminating in the lysosomal compartment, and a bidirectional pathway from endosomes to the golgi network (Figure 1.7). The sorting of cargo to specific pathways, the motility of endosomes, and the maintenance of organelle and endosome identity and morphology is regulated by an extensive and interconnected signalling network consisting of phosphoinositide signalling lipids and the cytosolic proteins they recruit in a dynamic spatiotemporal manner (204).

Pathogens that utilize the endosomal system for infection also depend on this signalling network, and it is becoming increasingly evident that they frequently hijack regulators of cell trafficking to their advantage (205–209). An overview of the degradative endosomal pathway utilized by EBOV and other late-penetrating viruses which enter the cytoplasm through the LE/LY compartment is presented below.

1.3.2 Regulation of endosome maturation

While there exist various cell-type dependent intricacies in endosomal dynamics, endosome maturation follows a set of broadly conserved mechanisms and hallmarks. All endocytic pathways (i.e., clathrin/caveolin-mediated endocytosis, macropinocytosis, phagocytosis, etc) converge at the early endosome (EE) compartment. EEs are a mosaic heterogenous structures, containing both tubular and vacuolar domains, and are recognized as the primary sorting centre of the endosomal system. EEs destined for maturation into LEs/LYs as part of the degradation pathway undergo a sequence of specific changes. These include a

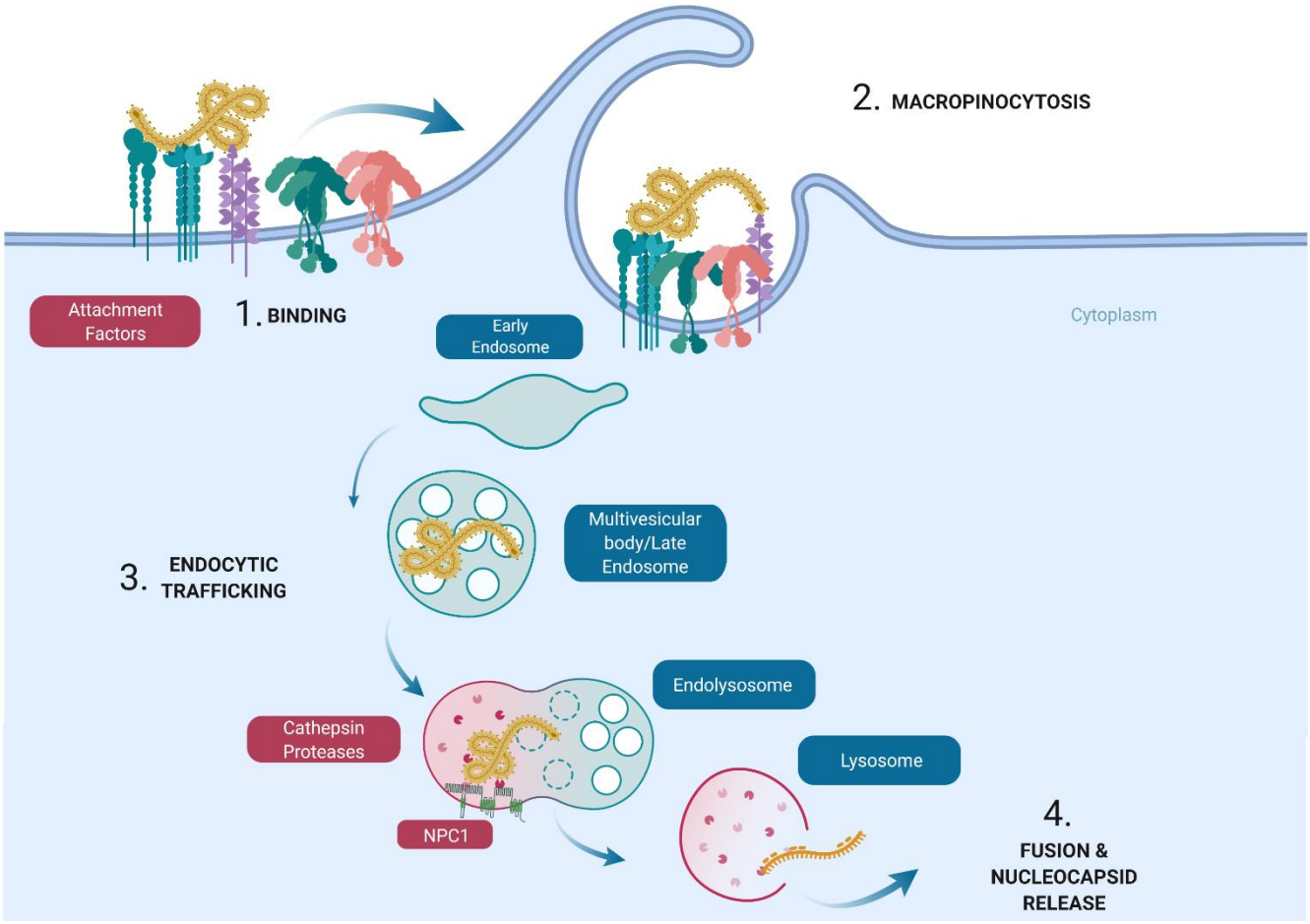

Figure 1.6. Overview of the Ebola virus entry pathway

Created using Biorender.com

decrease in the luminal pH and acquisition of LE/LY hydrolases, a change in overall morphology including the formation of intraluminal vesicles (ILVs), and a net movement towards the cell centre mediated by specific microtubule (MT) motor proteins. Two molecular switching events central to endosome maturation are (1) the switch from the EE-associated Rab5 GTPase to the LE/LY-associated Rab7 GTPase and (2) the conversion of phosphoinositide lipids on endosomal membranes (PtdIns3P→PtdIns(3,5)P_2). PtdIns3P and PtdIns(3,5)P_2 regulators and effectors work in concert and often in feedback loops with Rab5 and Rab7 effectors to sequentially recruit cytosolic effectors such as tethering complexes, SNARE proteins, MT motor proteins and their adaptors that together facilitate endosome maturation (204).

A well-recognized marker of endosome maturation is the switch from Rab5 to Rab7, which are considered master regulators of endosome maturation based on their recruitment of EE- and LE/LY-specific cytosolic effectors (209–212). Rab5 is activated on EEs by Rabex-5, a guanine nucleotide exchange factor (GEF) which further forms a complex with the Rab5 effector Rabaptin-5 (213–218). Rabaptin-5 further stimulates Rabex-5 GEF activity, generating a feedback loop enhancing Rab5 activation and resulting in the rapid recruitment of numerous Rab5 effectors (213). These include EE-specific tethering factors such as the CORVET complex, Rabenosyn-5, and EEA1, as well as the phosphoinositide 3-kinase (PI3K) Vps34, which generates PtdIns3P on EE membranes (219–227). The displacement of Rab5 for Rab7 is mediated in part by the inactivation of Rab5 by GTPase activating proteins (GAPs) such as Rab GAP-5 and TBC-2, which activate Rab5-mediated hydrolysis of GTP to GDP (228–230). The switch from Rab5 to Rab7 is also mediated by the Ccz1-Mon1 GEF complex, which can bind to both PtdIns3P and GTP-bound Rab5, and activates Rab7 activity (231–235). Ccz1-Mon1 has also been shown to displace Rabex-5 from the membrane, thereby providing a possible

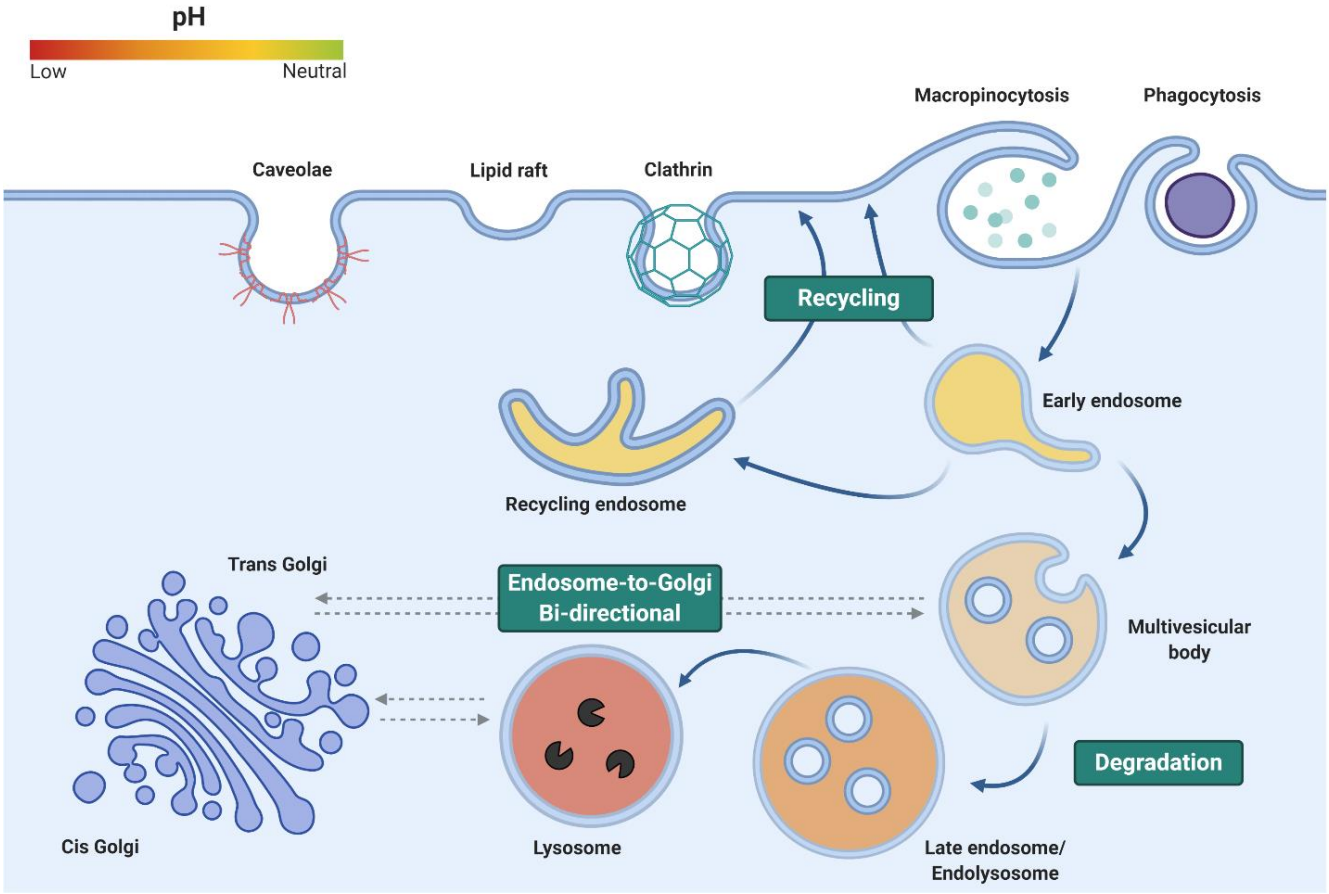

Figure 1.7. Overview of endocytic trafficking pathways

Created using Biorender.com

mechanism by which Rab7 recruitment in turn releases Rab5 from endosomal membranes (212). Rab7 effector proteins include the LE/LY-specific HOPS tethering complex and its adaptors PLEKHM1 and Arl8b (236–238), adaptor proteins that link endosomes to MT motor proteins such as RILP (239,240), and phosphoinositide regulators that downregulate PtdIns3P such as WDR91 (241). Rab7 activation further promotes activity of the HOPS complex by releasing UVRAG, a positive regulator of the HOPS complex, from Rubicon, which normally sequesters UVRAG away from the HOPS complex (242,243). Together these effectors promote movement of LEs towards the cell centre as well as fusion between LEs and LYs.

Similar to the Rab switch, the switch from PtdIns3P to PtdIns(3,5)P_2 on endosomal membranes is another key mediator of endosome maturation. PtdIns3P and PtdIns(3,5)P_2 belong to a class of seven phospholipids called phosphoinositides (PIs), which are differentially localized on membranes throughout the cell and act as finely tuned molecular switches through their ability to be rapidly interconverted via (de)phosphorylation by various PI kinases and phosphatases. This in turn allows the dynamic recruitment of PI-specific effectors to regulate a diverse array of cellular processes such as trafficking, signalling, and cytoskeletal dynamics (244).

PtdIns3P is generated on EE membranes by the PI3-kinase Vps34, which forms a complex with p150 and Beclin-1 (245). Vps34 is initially recruited to EE membranes via a direct interaction between p150 and Rab5-GTP (219,246). PtdIns3p effectors, some of which are also Rab5 effectors (ex. EEA1 and Rabenosyn-5) contain PtdIns3P binding domains such as FYVE, PX and GLUE (220,223,247,248). Among these effectors are several components of the Endosomal Sorting Complexes Required for Transport (ESCRTs), including Hrs (ESCRT-0) and EAP45 (ESCRT-II) (249). ESCRT proteins play a key role in the sorting of ubiquitinated

proteins on the limiting membrane of endosomes into ILVs, generating intermediate endosomes known as multivesicular bodies (MVBs) (250). ILV formation can also occur through ESCRT-independent mechanisms, such as through the lipids lysobisphosphatidic acid (LBPA) and ceramide, which are enriched in ILVs (251–253). ILVs serve multiple functions in both degradation and secretion: facilitating the sequestration and delivery of biomolecules to the lysosome, serving as transport vesicles for delivering contents back to the plasma membrane, or are even released into the extracellular milieu as exosomes (254,255). The mechanisms regulating these differential functions of ILVs are complex and under active investigation.

Another key PtdIns3P effector is PIKfyve, recruited via its FYVE domain (256). PIKfyve (Fab1 in yeast) is a lipid kinase that specifically phosphorylates the D5 position of the PI inositol head group to generate PtdIns(3,5)P_2 from PtdIns3P as well as PtdIns5P from PtdIns. It associates in a ternary complex with the opposing phosphatase Sac3 (Fig4 in yeast, which specifically dephosphorylates PtdIns(3,5)P_2 to PtdIns3P) and the scaffolding protein ArPIKfyve (Vac14 in yeast) (257–266). PIKfyve is the sole enzyme known to generate PtdIns(3,5)P_2, therefore is a crucial regulator of endosome maturation (267,268). Furthermore, the activity of both PIKfyve and Sac3 is tightly coordinated within the PIKfyve-ArPIKfyve-Sac3 (PAS) complex, as numerous studies have demonstrated that integrity of the complex is necessary for enzymatic activity of both proteins (259,260,262,264,266,269–272). Indeed, recent structural and biochemical characterization of the PAS complex has revealed that PIKfyve and Sac3 mutually regulate each other's function via their protein phosphorylation and dephosphorylation activities, respectively. PIKfyve autophosphorylation represses its lipid kinase activity and stimulates Sac3 lipid phosphatase activity, while Sac3 can directly dephosphorylate PIKfyve to stimulate its lipid

kinase activity (262). However, how this protein (de)phosphorylation activity within the PAS complex is regulated remains uncharacterized.

Generation of PtdIns(3,5)P_2 is crucial for endosome maturation as well as endosomal membrane homeostasis. Impairment of PtdIns(3,5)P_2 production via inhibition of PIKfyve or perturbation of PAS complex formation results in impairment of cargo delivery to lysosomes as well as abnormally enlarged vacuole-like endosomal compartments (258,263,273–279). The origins and mechanisms governing PAS-dependent vacuole formation remain unclear and appear to be cell-type dependent, although a recent report has suggested that vacuole formation occurs through an imbalance in fission-fusion cycles within the endolysosomal system, resulting in lysosome coalescence (277). Despite the importance of PtdIns(3,5)P_2 for cell trafficking, relatively few PtdIns(3,5)P_2 effectors have been identified compared to PtdIns3P effectors, particularly in mammalian cells. The low abundance of PtdIns(3,5)P_2, accounting for approximately 0.05 - 0.1% of total PIs in quiescent cells, presents technical challenges in its measurement as well as the identification of effectors (280). Proposed PtdIns(3,5)P_2 effectors in mammalian cells include ESCRT-III component CHMP3 (Vps24p) (281), as well as transient receptor potential mucolipin 1 (TRPML1) and the two-pore channels (TPCs) TPC-1 and TPC-2, which are endosomal cation channels permeable to Ca^{2+} (282,283). The TPCs and TRPML1 have been the most well characterized PtdIns(3,5)P_2 effectors to date, and the ML1N probe, derived from the PtdIns(3,5)P_2-binding N-terminus of TRPML1, has been used *in vitro* to visualize PtdIns(3,5)P_2 dynamics in cells (284). Ca^{2+} flux plays a central role in membrane fusion, and these Ca^{2+} permeable channels are themselves key trafficking regulators (285–290). The mechanisms regulating the interaction between the PAS complex and Ca^{2+} channels remain unclear. One hypothesis is that activation of PIKfyve and resulting PtdIns(3,5)P_2 production

occurs in localized microdomains on endosomal membranes, perhaps at docking sites for membrane fusion. These domains also contain other tethering and fusion factors, including TRPML1/TPCs and SNARE proteins, thereby localizing transient PtdIns(3,5)P_2 and Ca^{2+} flux to facilitate membrane tethering and SNARE-mediated fusion (282,289,291). However, it is likely that there are other PtdIns(3,5)P_2/PIKfyve effectors that work in concert with these Ca^{2+} channels, as attempts to rescue phenotypes associated with PIKfyve disruption such as enlarged vacuoles or impaired endolysosomal trafficking using TRPML agonists (MLSA1) or Ca^{2+} ionophores (ionomycin) have resulted in complete, partial, or no rescue depending on the cell type and assay used (282,289,291–297). Therefore further molecular dissection of the interplay between PtdIns(3,5)P_2 and Ca^{2+} channels as well as identification of other PtdIns(3,5)P_2 effectors are required to fully understand how this PI regulates endosome maturation and fusion.

Finally, progressive acidification of the endosomal lumen from EEs (pH ~ 6.5) to LYs (pH ~ 4.5) is another key marker of endosomal maturation. Endosome acidification proceeds primarily through the activity of vacuolar H^+ ATPases (V-ATPases), as well as ion channels and pumps that counter the positive charge generated in the lumen by V-ATPases, such as Na^+/K^+-ATPase, chloride channels, and Ca^{2+} channels (298,299). The decrease in luminal pH serves multiple functions in the degradation pathway, including cargo sorting and the activation of low-pH dependent hydrolases such as cathepsin proteases. Numerous viruses also depend on low pH for activation and conformational changes during entry (207). Common agents used to perturb endosomal pH include lysosomotropic weak bases such as ammonium chloride (NH_4Cl) and V-ATPase inhibitors such as bafilomycin (300,301).

1.4 Rationale, hypothesis and objectives

EBOV entry into target cells requires internalization and intracellular trafficking of virions to the late endosomal/lysosomal compartment, which contains triggering factors required for viral membrane fusion, including the filovirus receptor, NPC1. Because of the importance of accurate endolysosomal trafficking for EBOV to reach entry-conducive cellular compartments, we hypothesize that the virus relies on—and potentially actively regulates—a consortium of specific host trafficking factors, which represent potential targets for antivirals. The overarching objective of this thesis is to characterize how these trafficking factors are involved in EBOV entry.

The specific aims of each chapter are outlined below:

Chapter 2: Characterize the role of UVRAG and the HOPS tethering complex in EBOV entry

a) Assess the importance of expression of each HOPS subunit and UVRAG for viral entry
b) Characterize how the HOPS complex and UVRAG interact during viral entry

Chapter 3: Characterize the role of PIKfyve-ArPIKfyve-Sac3 (PAS) phosphoinositide regulating complex in EBOV entry

a) Assess the importance of expression of each subunit for viral entry
b) Determine the role of PIKfyve and Sac3 enzymatic activity for viral entry
c) Visualize PtdIns3P and PtdIns(3,5)P_2 dynamics during viral entry

Chapter 4: Investigate the PAS cellular interactome

a) Screen for the PAS proximal interactome using BioID
b) Perform network and gene ontology analysis on high confidence BioID screen hits
c) Assess the interaction between the PAS complex and the COPI complex

Chapter 2: Filoviruses use the HOPS Complex and UVRAG to traffic to Niemann-Pick C1 compartments during viral entry

Yuxia Bo[1,2,3]*, Shirley Qiu[1,2,3]*, Rory P. Mulloy[1,2,3], Marceline Côté[1,2,3]

[1] Department of Biochemistry, Microbiology and Immunology, University of Ottawa, Ottawa, Canada

[2] Ottawa Institute of Systems Biology, University of Ottawa, Ottawa, Canada

[3] Centre for Infection, Immunity, and Inflammation, University of Ottawa, Ottawa, Canada

* contributed equally to this work. Author order was determined alphabetically.

This chapter has been previously published in the Journal of Virology.

Filoviruses use the HOPS complex and UVRAG to traffic to Niemann-Pick C1 compartments during viral entry

Yuxia Bo*, Shirley Qiu*, Rory P. Mulloy, Marceline Côté. Journal of Virology (2020) 94(16) e01002-20

*Contributed equally, author order determined alphabetically

Author contributions: YB and SQ contributed to CRISPR experiments and infection assays. Surveyor endonuclease assays were performed by YB. UVRAG deletion constructs were generated and validated by SQ. Microscopy experiments were performed by SQ. RPM contributed to qPCR experiments for manuscript revisions (data not incorporated). Figures were produced by SQ. Manuscript was written and edited by SQ and MC.

2.1 Abstract

Ebola virus (EBOV) entry requires internalization into host cells and extensive trafficking through the endolysosomal network in order to reach late endosomal/lysosomal compartments that contain triggering factors for viral membrane fusion. These triggering factors include low-pH activated cellular cathepsin proteases, which cleave the EBOV glycoprotein (GP) to expose the binding domain of the filoviral receptor, Niemann-Pick C1 (NPC1). Here, we report that trafficking of EBOV to NPC1 requires expression of the homotypic fusion and protein sorting (HOPS) tethering complex as well as its regulator, UV radiation resistance associated gene (UVRAG). Using an inducible CRISPR/Cas9 system, we demonstrate that depletion of HOPS subunits as well as UVRAG impairs entry by all pathogenic filoviruses. UVRAG depletion resulted in reduced delivery of EBOV virions to NPC1+ cellular compartments. Furthermore, we show that deletion of a domain on UVRAG known to be required for interaction with the HOPS complex results in impaired EBOV entry. Taken together, our studies demonstrate that EBOV requires both expression and coordination between the HOPS complex and UVRAG in order to mediate efficient viral entry.

2.2 Introduction

Ebola virus (EBOV) and other members of the *Filoviridae* family are highly pathogenic enveloped RNA viruses and are the causative agents of multiple outbreaks of hemorrhagic fever diseases in humans and non-human primates, primarily in central and east Africa (55). Recent outbreaks of Ebola virus disease, including the 2013-2016 outbreak in West Africa that resulted in nearly 29,000 reported cases and over 11,000 deaths, have spurred the development of antibody-based therapeutics and vaccines currently under clinical review (302–305).

Filovirus virions harbor a characteristic filamentous morphology and are enclosed by a host cell derived lipid envelope studded with the trimeric viral glycoprotein (GP). The EBOV GP is classified as a class I viral fusion protein, comprised of heterodimers of subunits GP1 and GP2. GP1 contains a receptor binding domain shielded by a glycan cap, while GP2 contains a hydrophobic fusion loop, heptad repeat regions and a transmembrane domain (20,132,176). GP-mediated fusion requires triggering factors within the host cell, including cleavage of the GP1 glycan cap by host low pH-dependent cathepsin proteases, and interaction with the filoviral receptor, the cholesterol transporter Niemann Pick-C1 (NPC1), localized in late endosomes/lysosomes (171,173,174,180,184,185). Due to the late endosomal localization of these triggering factors, EBOV entry is not only dependent on internalization in host cells, but also trafficking to the entry-conducive intracellular compartments (168–170).

Previous work has shown that EBOV entry requires the activity of cellular trafficking factors, such as the PIKfyve-ArPIKfyve-Sac3 phosphoinositide regulating complex and the homotypic fusion and protein sorting (HOPS) complex, both involved in maturation and fusion of late endocytic compartments (171,227,260,296,306). Many of these trafficking factors were identified in a loss-of-function haploid (HAP) genetic screen performed by Carette et al., including all members of the HOPS complex (171). Using cells deficient in a component of the HOPS complex, VPS33A, they demonstrated accumulation of VSV pseudotypes bearing EBOV GP in endosomal compartments, indicating a defect in viral fusion and cytoplasmic escape in these cells. However, whether the class C core vacuole/endosome tethering (CORVET) complex, which shares 4 core subunits (C-Vps core) with the HOPS complex (227), is also required for filoviral entry has yet to be determined. In addition, how the HOPS complex is regulated during viral entry is uncharacterized. Interestingly, studies have demonstrated that UV radiation

resistance associated gene (UVRAG) positively regulates endocytic trafficking by directly binding to members of the HOPS complex (243,307). Furthermore, Pirooz et al. demonstrated that UVRAG is required for endocytic transport of vesicular stomatitis virus (VSV) and influenza A viruses (IAV) through interactions with core components of the HOPS complex and SNAREs (308). Whether filoviruses also require UVRAG for entry remains to be determined.

Using an inducible Clustered Regularly Interspaced Short Palindromic Repeats (CRISPR)/Cas9 system, we demonstrate that members of the C-Vps core and HOPS-specific, but not CORVET-specific, subunits are required for entry mediated by all pathogenic filoviral GPs. Furthermore, we show that UVRAG expression is required for filovirus entry, with evidence that its ability to bind to the HOPS complex is key to its role in viral entry. Taken together, our studies suggest that filoviruses require coordination of the HOPS complex and UVRAG for delivery to NPC1+ compartments and efficient viral entry.

2.3 Results

2.3.1 An inducible CRISPR/Cas9 system to investigate host trafficking factors required for viral entry

One potential confounding factor with studying vesicular trafficking proteins by generating knockout (KO) cell lines is the development and selection of compensatory mechanisms over several cellular divisions (309). Therefore, to mitigate this problem and investigate the roles of trafficking host factors in viral entry, we designed a CRISPR/Cas9 system by which KOs can be rapidly induced and tested. In this approach, cell lines are engineered to encode Cas9 under the control of a doxycycline (Dox) inducible promoter and two guide RNAs (gRNAs) targeting the gene of interest (Fig. 2.1A).

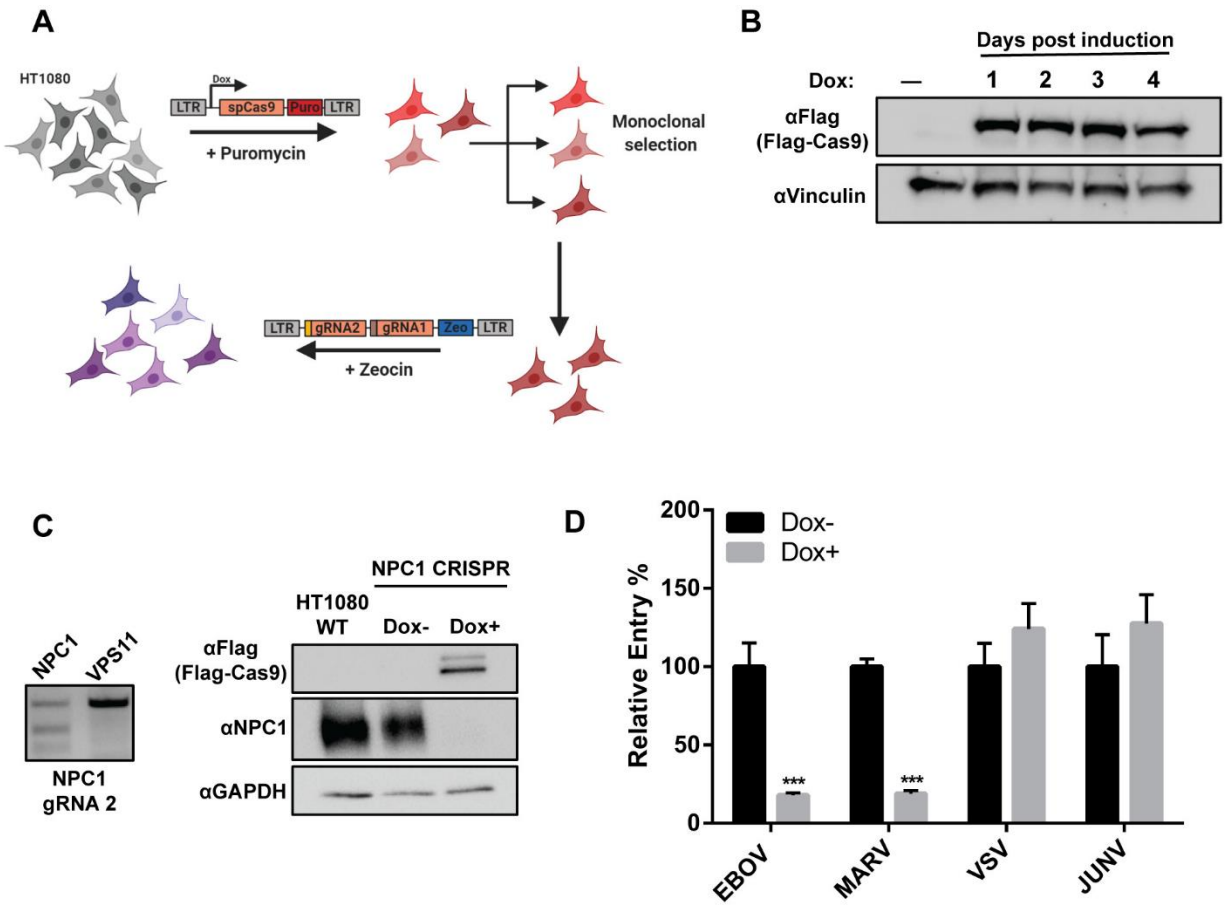

Figure 2.1. An inducible CRISPR/Cas9 system to investigate host trafficking factors required for viral entry

(A) Schematic of doxycycline (Dox)-inducible CRISPR/Cas9 system using dual gRNAs in HT1080 cells. (B) Time course of Flag-Cas9 expression in CRISPR cells after Dox induction. (C) Left: Surveyor nuclease assay showing region of NPC1 targeted by one of the dual gRNAs. Right: Expression of Flag-Cas9 and NPC1 in NPC1 CRISPR cells after 4 days of Dox induction. (D) NPC1 CRISPR cells were induced for 4 days in Dox, followed by infection with βlam-VLPs harboring EBOV GP, MARV GP, VSV G or JUNV GPC. Entry was detected by measuring the percentage of cells with cleaved CCF2, normalized to uninduced cells. Results are representative of 3 independent experiments. Asterisks indicate significant difference in entry compared to uninduced cells. *** $p<0.001$.

For this study, the human fibrosarcoma cell line, HT1080, was chosen as: 1) it is susceptible to filoviral GP-mediated entry and that of other viral glycoproteins, 2) its flat morphology allows for easy visualization and tracking of viral particles by microscopy (296,310), and 3) it is pseudodiploid and more karyotypically stable then U2-OS cells, which are also used for microscopy analysis of EBOV trafficking due to their advantageous morphology (169). We first created monoclonal HT1080 cell lines by transduction of a lentiviral vector encoding a Dox-inducible Cas9 and selection with puromycin (311) (Fig. 2.1A). Following characterization of the clones, one cell line was selected based on its lack of leakiness and high and sustained levels of Cas9 expression following Dox treatment (Fig. 2.1B). This HT1080 Cas9 monoclonal cell line can then be transduced with lentiviral vectors encoding gRNAs for the gene of interest. To increase the likelihood of KO generation, we generated lentiviral vectors containing two guide RNAs for each gene of interest (312) (Fig. 2.1A). This strategy allows the targeting of different exons, which is valuable when splicing variants are reported, and alleviates the impact of one guide RNA with low targeting efficiency. The lentiviral vector also encodes a zeocin resistance gene allowing the selection of a polyclonal cell line (Fig. 2.1A).

As a proof of concept, we targeted NPC1, the filovirus receptor (171,184,185), and generated an HT1080 NPC1 CRISPR cell line (Fig. 2.1 A,C,D). Cas9 expression was induced with Dox and cells were incubated for four days to allow efficient gene editing. To confirm that the gene was edited, we performed a surveyor endonuclease assay. For this, the region of interest was amplified by PCR using primers flanking the gRNA-targeted site and genomic DNA extracted from the induced or non-induced cell populations. The PCR products are then denatured at high temperature and slowly cooled down to allow DNA homo and heteroduplexes to form. Heteroduplexes, which indicate that targeting of the gene resulted in indels, are then

digested with T7 endonuclease I. Analysis of the NPC1 genomic DNA regions around the gRNAs using the endonuclease assay revealed that the region was modified for the HT1080 NPC1 CRISPR cells (presence of a cleaved band in addition to the uncleaved band), but not for another CRISPR cell line (Fig. 2.1C, left panel, gRNA 2 shown). While this method indicates that the targeting was successful, it does not allow quantitative assessment of knockdown. Therefore, we measured NPC1 expression by immunoblot and found it to be undetectable following four days of Dox stimulation (Fig. 2.1C, right panel).

Finally, to assess the potential of this strategy to investigate viral entry host factors, we used viral-like particles (VLPs) which can be generated by the co-expression of the EBOV nucleoprotein and matrix protein (VP40) (24). These VLPs have the characteristic filamentous morphology of filoviruses and can enter cells when viral GPs are co-expressed during production. In addition, using a VP40 construct fused with Beta-lactamase (βlam), viral entry and delivery of VP40 into the target cell cytoplasm can be measured after loading the target cells with the βlam fluorescence resonance energy transfer (FRET) substrate, CCF2. Dox induced or non-induced NPC1 CRISPR cells were incubated with VLPs harboring EBOV or MARV GPs, or the rhabdovirus vesicular stomatitis virus (VSV) glycoprotein (G), or the arenavirus Junin virus (JUNV) glycoprotein precursor (GPC) as controls. As expected, we found that entry was abrogated specifically for EBOV and MARV VLPs upon NPC1 targeting, while entry mediated by VSV G or JUNV GPC was not affected (Fig. 2.1D). Taken together, these experiments validate our CRISPR/Cas9 strategy for the rapid and efficient generation of KO cell lines to test the importance and roles of host factors in viral entry.

2.3.2 HOPS, but not CORVET, is required for efficient EBOV GP-mediated entry

To further test our system, we first sought to investigate the HOPS complex as it was previously identified in a screen for EBOV host factors using haploid cells (171). The HOPS complex shares 4 subunits (C-Vps core, composed of Vps11, Vps16, Vps18, and Vps33a) with the CORVET complex (227). In addition, each contains 2 specific subunits (HOPS, Vps39 and Vps41; CORVET, Vps3 and Vps8). In order to investigate the importance of the C-Vps core as well the HOPS- and CORVET-specific subunits in filovirus entry, we generated HT1080 CRISPR cell lines targeting the C-Vps core (Fig. 2.2), as well as a Vps39, as a representative for the HOPS complex and Vps3 and Vps8, the two accessory subunits of the CORVET complex (Fig. 2.3). Following four days of Dox induction of Cas9 expression, genomic DNA targeting was assessed by endonuclease assays (Figs. 2.2, 2.3, inserts) and viral entry was assessed using VLPs harboring the glycoproteins of EBOV, MARV, VSV, or JUNV. We found that the genetic targeting of all of the C-Vps subunits reduced viral entry mediated by both EBOV and MARV GP, but had no effect on that by VSV G or JUNV GPC (Fig. 2.2). These results indicated that efficient filovirus entry into cells requires an intact C-Vps core and suggest dependence on the CORVET and/or HOPS complex(es) for entry (Fig. 2.2, A-D).

Therefore, we next investigated subunits exclusive to CORVET (Vps3 and Vps8) or HOPS (Vps39) (Fig. 2.3A-C). Again, targeting of the genes was confirmed by endonuclease assay (Fig. 2.3, inserts). Using VLPs, we found that targeting the CORVET-specific subunits, Vps3 and Vps8, had no effect on viral entry by any of the EBOV- or MARV-GP VLPs (Fig. 2.3A,B). In contrast, targeting of the HOPS-specific subunit, Vps39, specifically reduced EBOV and MARV GP-mediated entry (Fig. 2.3C). Collectively, these data suggest that viral entry in the

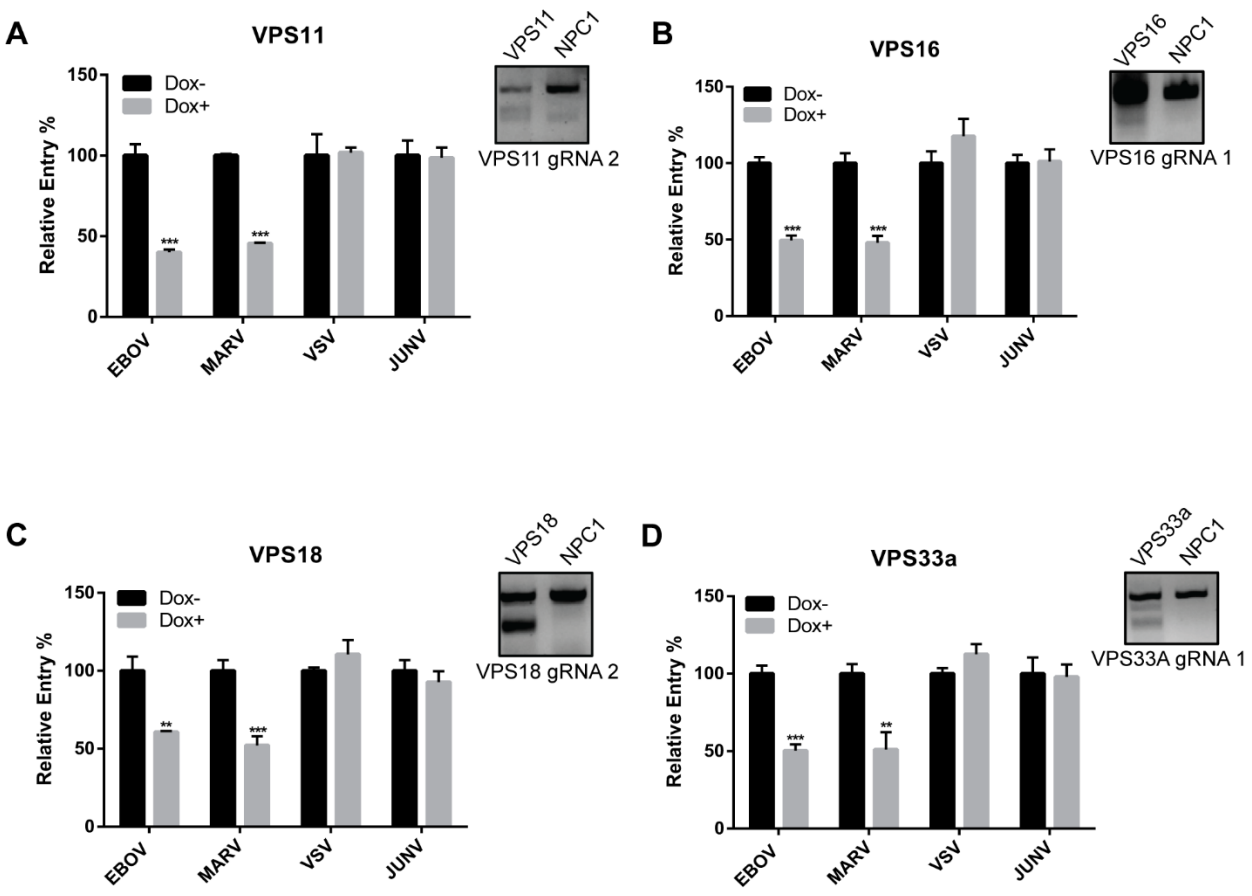

Figure 2.2. The C-Vps core is required for filovirus entry

Infection by a panel of βlam-VLPs harboring EBOV GP, MARV GP, VSV G or JUNV GPC in: (A) VPS11, (B) VPS16, (C) VPS18, and (D) VPS33a CRISPR cells following 4 days of Dox induction. Entry was detected by measuring the percentage of cells with cleaved CCF2, normalized to uninduced cells. Results are representative of 3 independent experiments. Asterisks indicate significant difference in entry compared to uninduced cells. Surveyor nuclease assay results for one gRNA of each targeted gene are shown on the right. ** $p<0.01$, *** $p<0.001$.

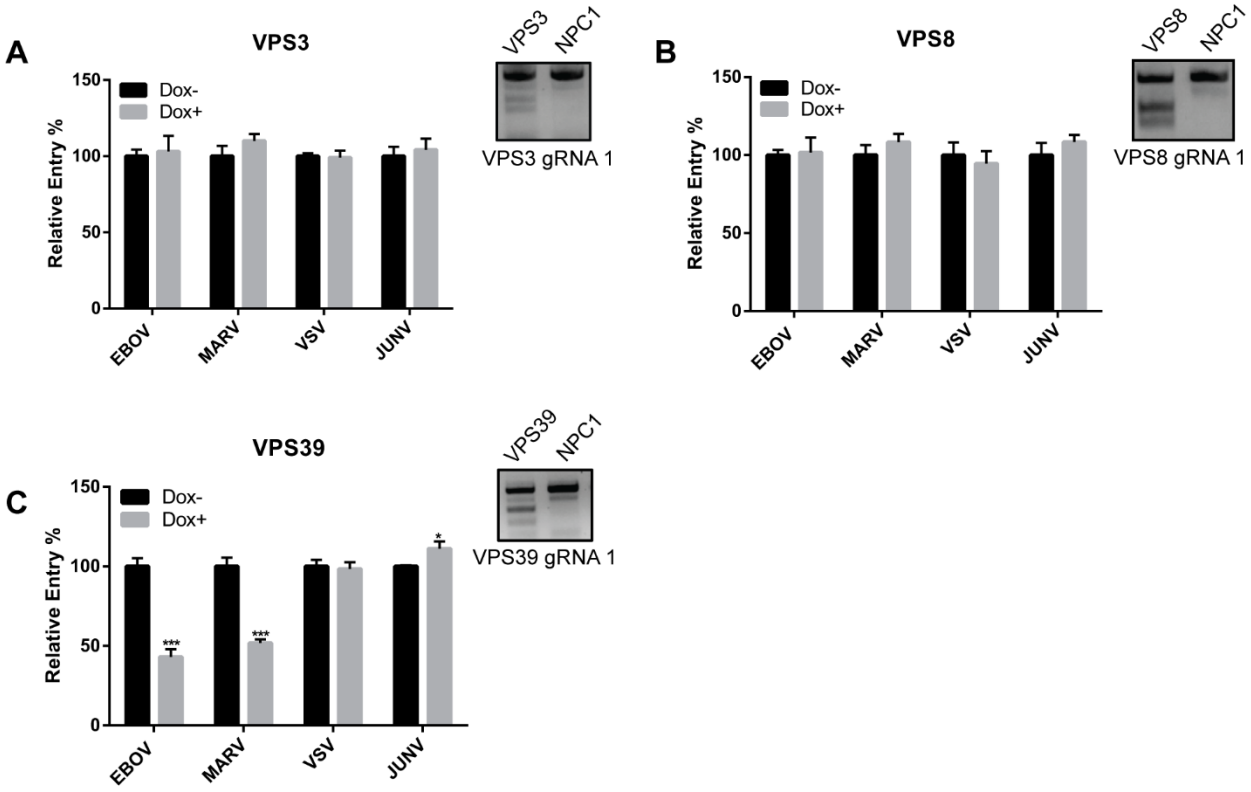

Figure 2.3. A HOPS-specific, but not CORVET-specific subunit is required for filovirus entry

Infection by a panel of βlam-VLPs harboring EBOV GP, MARV GP, VSV G or JUNV GPC in: (A) VPS3, (B) VPS8, and (C) VPS39 CRISPR cells following 4 days of Dox induction. Entry was detected by measuring the percentage of cells with cleaved CCF2, normalized to uninduced cells. Results are representative of 3 independent experiments. Asterisks indicate significant difference in entry compared to uninduced cells. Surveyor nuclease results for one gRNA of each targeted gene are shown on the right. *$p<0.05$, *** $p<0.001$.

CRISPR cells targeting C-Vps and a HOPS-specific subunit was consistently reduced for VLPs harboring the GPs of EBOV or MARV, suggesting that the HOPS complex plays an important role in filoviral entry, while the CORVET complex is dispensable. In addition, these experiments indicate that our inducible CRISPR/Cas9 system can be broadly used to study the importance of host trafficking factors in viral entry.

2.3.3 UVRAG is required for EBOV GP-mediated entry

Previous studies have shown that UVRAG positively regulates the C-Vps core complex during autophagosome and endosomal maturation, and can pull-down the HOPS-specific subunit Vps39, indicating that UVRAG plays a role in HOPS activity (307). To investigate whether UVRAG is also required for EBOV GP-mediated entry, we used our inducible CRISPR/Cas9 system and engineered HT1080 UVRAG CRISPR cells (Fig. 2.4A). Targeting of the UVRAG gene was confirmed by an endonuclease assay (Fig. 2.4A, insert). Interestingly, we noticed that UVRAG depletion resulted in decreased cell growth (data not shown).

Using VLPs harboring the EBOV GP or VSV G, we tested the effect of UVRAG depletion on viral entry. We found that Dox stimulation of the UVRAG CRISPR cells reduced EBOV GP-mediated entry, but had no effect on entry of VLPs harboring VSV G (Fig. 2.4A). To confirm that the decrease in viral entry was specifically due to UVRAG depletion, we engineered the UVRAG CRISPR cells to stably express UVRAG cDNA with silent mutations at the protospacer adjacent motif (PAM) sequences of both gRNA-targeted sequences. Because the PAM sequences are required for Cas9 binding (313), this UVRAG cDNA is not targeted and can be expressed following Dox treatment. As expected, entry mediated by both EBOV GP and VSV

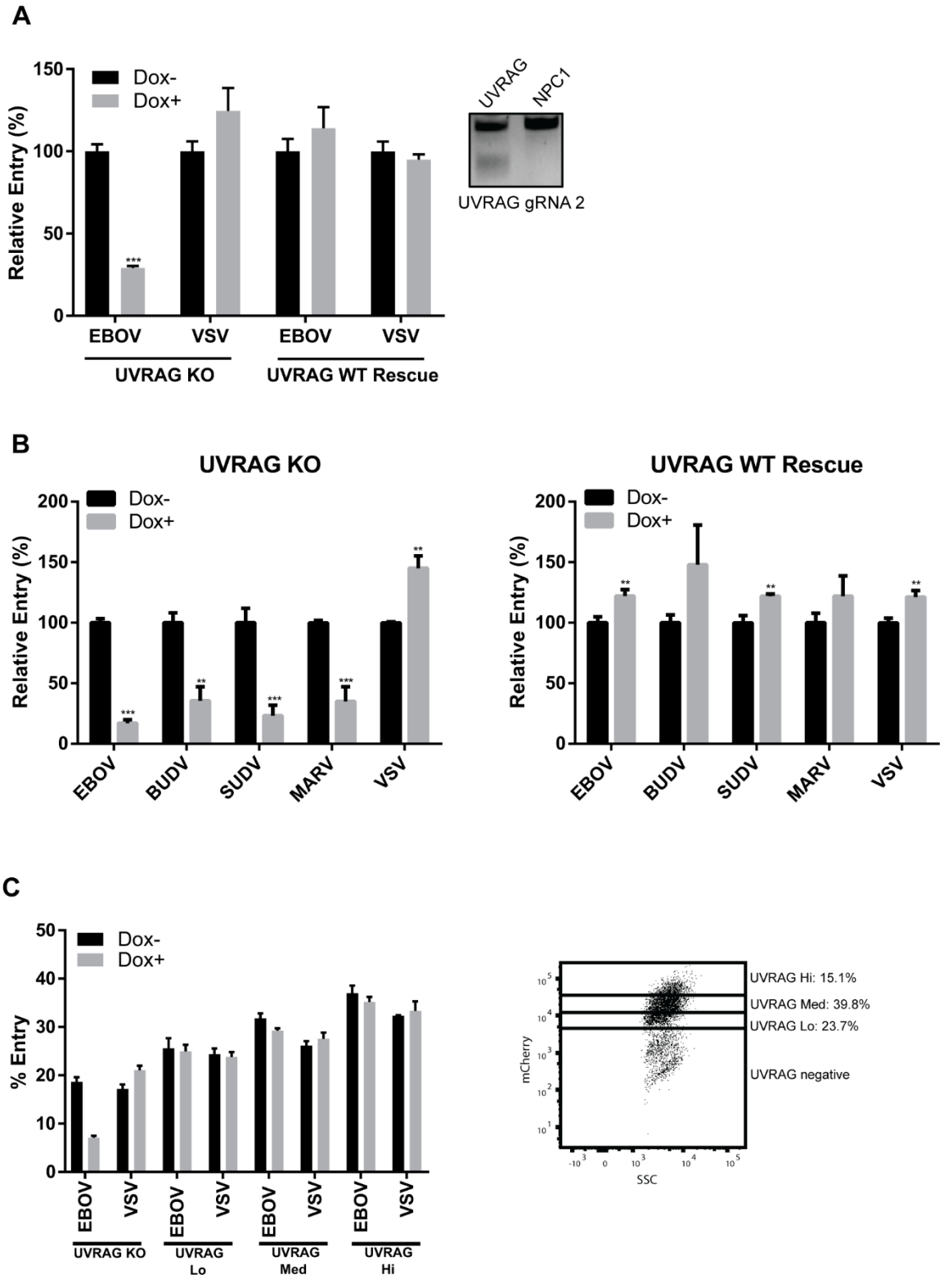
A
Relative Entry (%)
150
100
50
0
Dox-
Dox+
***
EBOV
VSV
EBOV
VSV
UVRAG KO
UVRAG WT Rescue
UVRAG
NPC1
UVRAG gRNA 2
B
UVRAG KO
UVRAG WT Rescue
Relative Entry (%)
200
150
100
50
0
Dox-
Dox+
**
***
EBOV
BUDV
SUDV
MARV
VSV
C
% Entry
50
40
30
20
10
0
Dox-
Dox+
EBOV
VSV
UVRAG KO
UVRAG Lo
UVRAG Med
UVRAG Hi
mCherry
SSC
UVRAG Hi: 15.1%
UVRAG Med: 39.8%
UVRAG Lo: 23.7%
UVRAG negative

Figure 2.4. UVRAG expression is required for filovirus entry

(A) UVRAG KO and WT-addback CRISPR cells were induced in Dox for 4 days, followed by infection with βlam-VLPs harboring EBOV GP or VSV G. Entry was detected by measuring the percentage of cells with cleaved CCF2, normalized to uninduced cells. Results are representative of 3 independent experiments. Asterisks indicate significant difference in entry compared to uninduced cells. Surveyor nuclease results for UVRAG gRNA2 is shown on the right (B) Infection of UVRAG KO or WT-addback CRISPR cells by a panel of VLPs bearing different filoviral glycoproteins or VSV G following 4 days of Dox induction. Asterisks indicate significant difference in infection compared to uninduced cells. Results are representative of 3 independent experiments. (C) UVRAG KO and WT-addback CRISPR cells were induced and infected with VLPs as in (A). Entry in the low (lo), medium (med) and high (hi) mCherry-UVRAG expressing cells was determined by mCherry expression (dot plot, inset). Percent entry was significantly increased for both EBOV and VSV with increasing mCherry expression (One-way ANOVA, Tukey's test. $p<0.05$). ** $p<0.01$, *** $p<0.001$.

G was unaffected by Dox treatment in the rescued UVRAG CRISPR cells (Fig. 2.4A), indicating that the specific reduction in entry for EBOV VLPs was due to UVRAG depletion. To test whether UVRAG is required for entry by multiple filoviruses, we generated VLPs harboring the GPs of the other pathogenic ebolavirus species: BUDV and SUDV, and MARV. Using those VLPs, we found that entry by all filoviruses tested was decreased in the Dox-induced UVRAG CRISPR cells, yet was rescued when UVRAG cDNA was added back (Fig. 2.4B). These results indicate that UVRAG is required for a filovirus-specific entry step.

Because the UVRAG construct is fused with mCherry, the effect of the UVRAG expression level on viral entry can be analyzed. The UVRAG-mCherry positive population was separated into three groups: the low, medium and high expressors (Fig. 2.4C). Viral entry in each of these groups was then determined. We found an increase in the percentage of cells with cleaved CCF2 with increasing expression of UVRAG (Fig. 2.4C), indicating enhanced viral entry when UVRAG is overexpressed. This increase was not specific to EBOV GP-mediated entry as it was also observed for VLPs harboring VSV G (Fig. 2.4C). Taken together, these results suggest that UVRAG is a nonspecific positive regulator of viral entry, yet is specifically required for filovirus entry.

2.3.4 EBOV trafficking to NPC1+ compartments requires UVRAG

UVRAG is involved in multiple cellular roles, such as autophagosome formation and maturation, and endosomal maturation (307,314). Because all filoviruses require trafficking to compartments containing NPC1 for entry, a simple hypothesis is that UVRAG depletion leads to accumulation of viral particles in early compartments lacking NPC1 due to a failure in endosome maturation. To test this hypothesis, we produced fluorescent EBOV VLPs using VP40 fused to green fluorescent protein (GFP) and fusion defective EBOV GP^{F535R} to allow viral accumulation

in compartments containing NPC1 (172,296). Following four days of Dox induction, UVRAG CRISPR cells were incubated with fluorescent EBOV VLPs at 4°C to allow virus binding to the cell surface, before switching to 37°C to allow internalization and trafficking of viral particles in cells. After 3 hours, cells were fixed, stained for NPC1, and visualized by confocal microscopy (Fig. 2.5A). While we did not observe differences in the number of internalized EBOV VLPs in the UVRAG CRISPR cells following Dox stimulation (Fig. 2.5A, B), we found that colocalization with NPC1 was drastically decreased (Fig. 2.5A,C). Interestingly, we noticed a slight increase in internalized VLPs in the rescued UVRAG cells, irrespective of Dox treatment (Fig. 2.5B). Importantly, in the rescued cells, colocalization of VLPs with NPC1 remained unchanged upon Dox stimulation (Fig. 2.5A,C). Taken together, these data suggest that UVRAG is required for EBOV trafficking to NPC1.

2.3.5 Deletion of UVRAG domains required for HOPS association impairs EBOV entry

Using an inducible CRISPR strategy, our results suggest that the C-Vps core and the HOPS complex, but not the CORVET complex, are required for filovirus entry (Figs. 2.2, 2.3). In addition, using the same strategy, we showed that UVRAG is required for filovirus entry (Fig. 2.4), more specifically for delivery of viral particles to NPC1 compartments (Fig. 2.5). Because previous studies have shown that endosome fusion and autophagosome-lysosome fusion are mediated by a C-Vps-UVRAG complex (307), it is likely that the function of these proteins is also linked during filovirus-GP mediated entry. Two regions of UVRAG have been shown to interact with the C-Vps core subunit Vps16: the Ca^{2+}-dependent phospholipid binding C2 domain and a region that encompasses amino acids 269-442 located in a domain of unknown function (307). To investigate whether expression of these regions is required for UVRAG

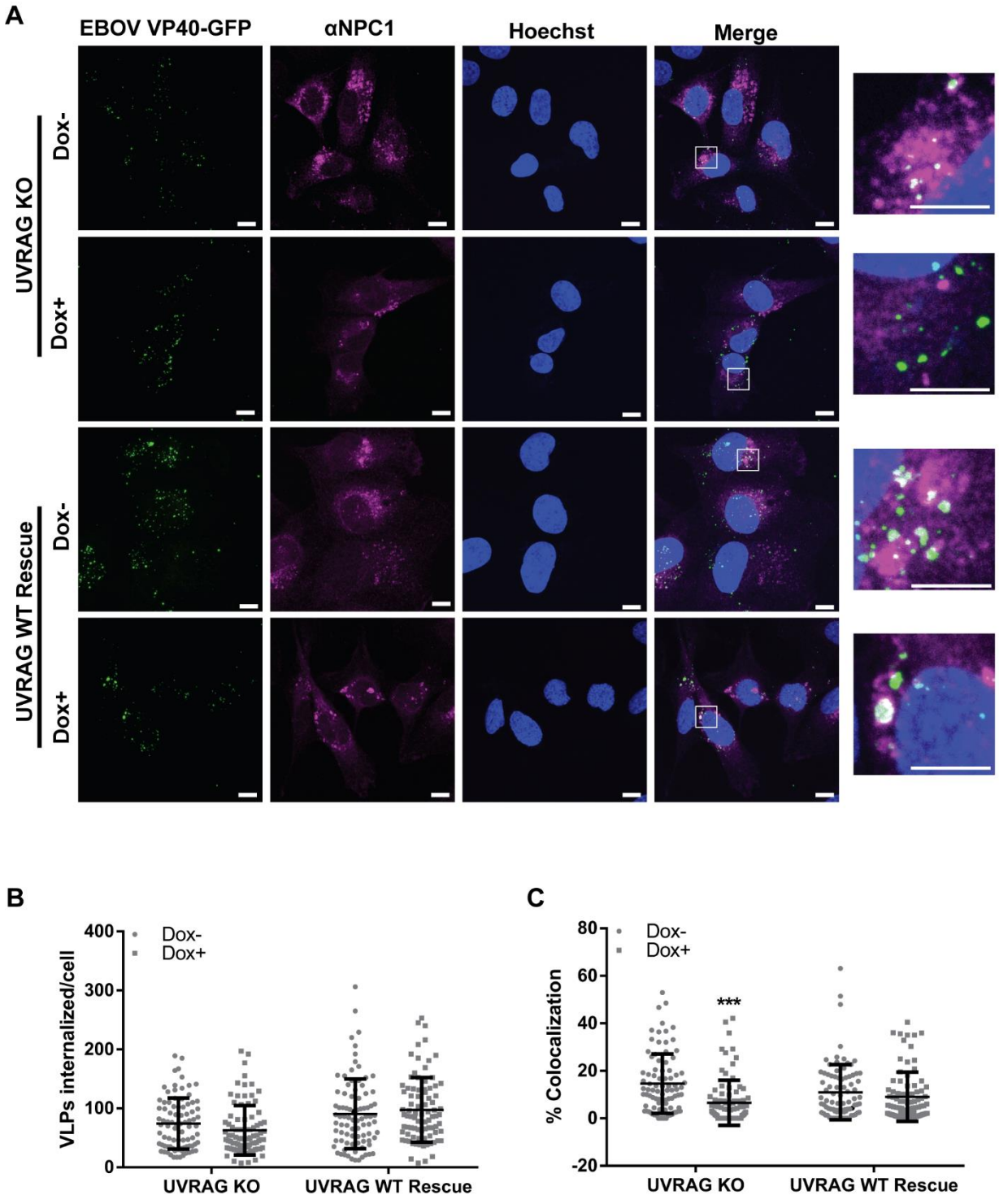
A
EBOV VP40-GFP
αNPC1
Hoechst
Merge
UVRAG KO
Dox-
Dox+
UVRAG WT Rescue
Dox-
Dox+
B
VLPs internalized/cell
400
300
200
100
0
Dox-
Dox+
UVRAG KO
UVRAG WT Rescue
C
% Colocalization
80
60
40
20
0
-20
Dox-
Dox+
***
UVRAG KO
UVRAG WT Rescue

Figure 2.5. EBOV trafficking to NPC1+ compartments is impaired in UVRAG deficient cells

(A) UVRAG CRISPR KO and WT-addback cells were induced in Dox for 4 days, followed by reseeding onto coverslips. Cells were then infected with GFP-VLPs harboring fusion deficient EBOV ΔM GPF535R for 3 hours. Cells were fixed, permeabilized, and stained with a NPC1 antibody and Hoechst. Cells were imaged on an LSM800 confocal microscope (Zeiss). (B) Number of internalized VLPs and (C) colocalization between VLPs and NPC1 was analyzed using Imaris software (Bitplane). Results shown are combined normalized data from 3 experiments. Asterisks indicate significant difference in colocalization compared to uninduced cells, as determined by unpaired t-test with Welch's correction, and statistical significance determined using the Holm-Šídák method. *** $p<0.001$.

function and viral entry, we deleted the C2 domain (ΔC2), the middle region (Δ269-442), or both regions (ΔC2/Δ269-442) in the UVRAG PAM mutated cDNA (Fig. 2.6A). Using lentiviral vectors, these constructs were transduced in the UVRAG CRISPR cells. All deletion mutants were expressed at similar levels, suggesting that the deletions had no effect on protein stability (Fig. 2.6B).

UVRAG interacts with C-Vps to perform at least two functions: endosome and autophagosome maturation (307). This latter process involves the fusion of autophagosomes with late endosomes/lysosomes for degradation of autophagosome contents. A block in autophagosome maturation can be detected by the accumulation of the lipidated form of LC3 (LC3-II) which would be otherwise degraded in the lysosomes (315). To characterize the effect of the UVRAG deletions mutants on this C-Vps-dependent function, we treated the UVRAG CRISPR cells with Dox to deplete endogenous UVRAG and tested for the ability of UVRAG WT, ΔC2, Δ269-442, or ΔC2/Δ269-442 to rescue autophagosome maturation by blotting for LC3. As expected, an increase in LC3-II was observed in the UVRAG-depleted cells, which was rescued when UVRAG WT was expressed (Fig. 2.6C). Similarly, expression of UVRAG ΔC2 was also able to rescue autophagosome maturation, suggesting that the C2 domain is not required for UVRAG-mediated autophagosome maturation (Fig. 2.6C). Interestingly, the UVRAG deletion mutants Δ269-442 and ΔC2/Δ269-442 were both unable to rescue autophagosome maturation (Fig. 2.6C). These results suggest that Δ269-442 is required for UVRAG's ability to mediate autophagosome maturation in HT1080 cells, while C2 is dispensable for this function.

Next, we sought to investigate whether the UVRAG deletion mutants could rescue EBOV GP-mediated entry. The UVRAG CRISPR cells were treated with Dox and exposed to

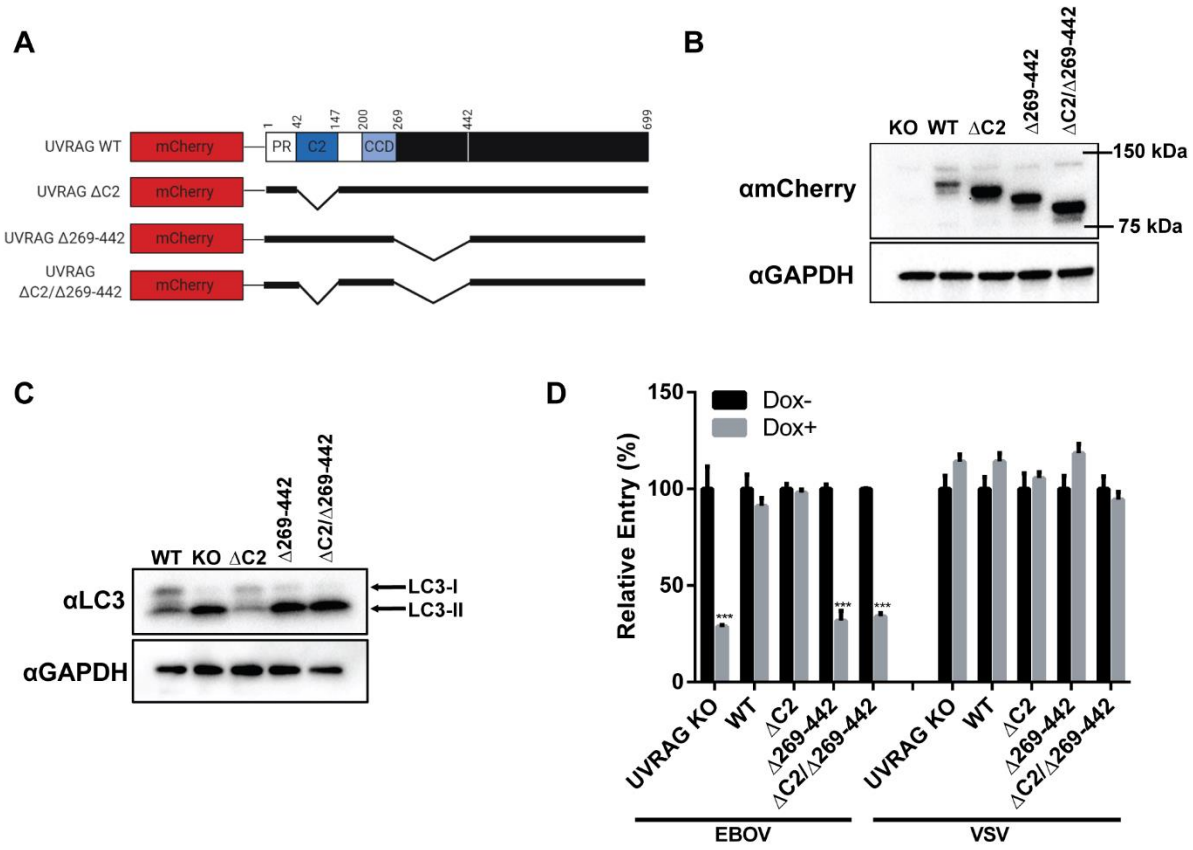

Figure 2.6. Deletion of UVRAG domains required for HOPS association impairs EBOV entry

(A) Schematic of mCherry tagged UVRAG deletion constructs. (B) Immunoblot of mCherry-UVRAG in UVRAG CRISPR cells transduced with the deletion constructs. (C) Expression of LC3 in UVRAG CRISPR cells transduced with the deletion constructs was detected by immunoblot following 4 days of induction in Dox. (D) UVRAG CRISPR KO, WT-addback, or deletion construct-addback cells were induced in Dox for 4 days, followed by infection with βlam-VLPs harboring EBOV GP or VSV G. Entry was detected by measuring the percentage of cells with cleaved CCF2, normalized to uninduced cells. Asterisks indicate significant difference in entry compared to uninduced cells. Results are representative of 3 independent experiments. *** $p<0.001$.

VLPs harboring EBOV GP or VSV G. As previously shown, the expression of UVRAG WT rescued the inhibition in EBOV VLP entry, while entry mediated by VSV G remained unaffected (Fig. 2.6D). Similar to its ability to restore autophagosome maturation (Fig. 2.6C), we found that UVRAG ΔC2 was also able to compensate for endogenous UVRAG depletion in the context of EBOV entry (Fig. 2.6D). In contrast, UVRAG Δ269-442 and the double deletion, which could not restore autophagosome maturation (Fig. 2.6C), did not rescue EBOV VLP entry (Fig. 2.6D). These data suggest that there are functional similarities in the interactions between UVRAG and C-Vps to perform autophagosome or endosomal maturation. Taken together, these results provide further evidence suggesting that UVRAG is required for EBOV GP-mediated entry.

2.4 Discussion

To infect cells, filoviruses are internalized via macropinocytosis and trafficked to endosomal/lysosomal compartments containing triggering factors required for viral membrane fusion and subsequent delivery of the viral genome into the host cell cytoplasm. In this study, we present an inducible dual-gRNA CRISPR/Cas9 strategy to investigate the roles of host factors in viral entry. We demonstrate that filoviruses require the HOPS, but not the CORVET, complex for entry. In addition, we show that UVRAG is required for filovirus entry, more specifically, for delivery of EBOV particles to intracellular vesicles containing the entry receptor, NPC1. Finally, the ability of UVRAG to mediate EBOV GP-mediated entry depends on a domain known for interacting with the HOPS complex, suggesting that its role in viral entry involves coordination with the HOPS complex. Our findings strengthen the notion that a specific trafficking pathway is required for efficient filovirus entry, more specifically one that involves the HOPS complex and UVRAG.

Multiple genetic strategies have been used to identify host factors required in viral entry, including RNAi screens and more recently, screens based on mutagenized haploid cells and CRISPR/Cas9 (171,316–318). One main advantage of these methods is the non-biased discovery of novel genes. However, because of the requirement for multiple days of selection and expansion of initial cell populations, genes required for cell proliferation and survival are generally negatively selected, preventing investigation of their potential roles in viral entry. Here, we used an inducible Cas9 system combined with a dual-gRNA strategy for the specific investigation of the roles of proteins involved in endosomal/lysosomal cargo trafficking. The rapid testing of viral entry after inducing expression of Cas9 and knocking out specific genes makes the study of essential cellular genes possible. For instance, this system allowed us to study the role of UVRAG in filovirus entry. UVRAG's role in autophagy is very well characterized, yet autophagy-independent functions have also been described (307,314). While its role in vesicular trafficking was the focus of this study, UVRAG is also involved in cell proliferation and homeostasis (314,319). The negative effect of UVRAG knockout on cellular proliferation could explain why UVRAG was not identified in the HAP screen for EBOV host factors (171). While the dual guide strategy is not easily amenable for non-biased screens, using the inducible Cas9 with a single gRNA could allow such screens.

Previous studies have shown that, following internalization, EBOV particles traffic from a Rab5+ early compartment to a Rab7+ late compartment (163). The passage through a Rab5+ vesicle could imply a role for the CORVET complex, a Rab5 effector, which has been implicated in early endosome fusion (225). In addition, transition to late compartments implies the use of the HOPS complex. Using the inducible CRISPR/Cas9 strategy, we targeted all members of the C-Vps core which have been found to be localized to both early and late endosomal

compartments (227). Interestingly, we found that targeting the subunits of the C-Vps core and those of the HOPS complex specifically reduced entry by the GPs of EBOV and MARV but had no effect on that by VSV G and JUNV GPC, which is in agreement with results from Carette *et al* (171). In contrast, targeting Vps3 or Vps8 did not affect entry by any of the VLPs, suggesting that filovirus entry does not depend on the CORVET complex (Fig. 2.3A,B). Previous studies have shown that while the depletion of CORVET-specific subunits has no effect on late endosomal compartments, it alters early endosomal subpopulations differentially (320). These endosomal populations are characterized by the presence of Rab5 with either the early endosome antigen 1 (EEA1), the adaptor protein, phosphotyrosine interacting with PH domain and leucine zipper 1 (APPL1), or both (321). Interestingly, Vps3 depletion seemed to mostly affect APPL1 positive endosomal population causing its fragmentation (321). While more work is needed to characterize our CORVET CRISPR cell lines, it is possible that if filoviral VLPs, or even those harboring VSV G and JUNV GPC, transit through early endosomal compartments, those early compartments are among the subpopulations that are not coordinated by CORVET. Another possibility is that Vps3 or Vps8 targeting only slows viral trafficking to entry-conducive compartments and kinetic experiments may be necessary to reveal a role for the CORVET complex in filoviral entry.

Recent studies have shown that UVRAG can coordinate C-Vps and HOPS functions (307). Here we show that depletion of UVRAG specifically leads to reduced filovirus GP-mediated entry (Figs. 2.5, 2.6). In a previous study, Pirooz et al. showed an increase in VSV and influenza A entry when UVRAG was overexpressed and an inhibition when UVRAG, Vps16, or Vps18 were depleted (308). While we also observed increase entry upon UVRAG overexpression (Fig. 2.4C), our results suggest that UVRAG and the C-Vps are not required for

VSV G-mediated entry (Figs. 2.2, 2.4). The C-Vps and HOPS complex were also showed to be dispensable for VSV infection by Carette *et al* (171). Since VSV G-mediated membrane fusion in the endosome is triggered by low pH, it is possible that the need for VSV to traffic deeper in the endosomal pathway, which is mediated by the HOPS and UVRAG, depends on the pH of early endosomes which is likely cell-type specific and can also be modulated by cell-extrinsic factors such as extracellular pH (322). This could explain differences in the observed dependence on UVRAG and endosomal maturation for VSV entry. In addition to a role in endosome/lysosome fusion, UVRAG is known to be important for both the initiation and maturation of autophagosomes (307,314). Initiation of autophagosomes requires UVRAG interaction with Beclin and maturation is dependent on interaction with the C-Vps complex. While a defect in autophagy initiation was not observed in our HT1080 UVRAG CRISPR cells, autophagosome fusion with lysosomes seemed impaired as an accumulation of LC3-II was apparent in the Dox-treated cells (Fig. 2.6C). An absence of an effect on autophagy initiation in UVRAG KO cells was also reported in lymphocytes (319), suggesting that a role for UVRAG in autophagosome formation may be cell type specific. A recent study reported a role for autophagy-associated proteins, such as Beclin and LC3, in EBOV internalization (323). While we did not observe a reduction in VLP internalization in UVRAG-depleted cells, more work needs to be done to assess the autophagy-dependent functions of UVRAG in EBOV entry. Interaction of UVRAG with C-Vps and the HOPS complex has been previously shown to map to the C2 (42-147) and 269-442 regions of UVRAG (307,308). Interestingly, we found that UVRAG function in viral entry requires the domain comprising of amino acids 269-442, while the C2 deleted UVRAG was able to both rescue infection and autophagosome clearance (Fig. 2.6C,D), suggesting that this region is not involved in C-Vps and HOPS complex function in

HT1080 cells. Instead, in our system, region 269-442 was critical for UVRAG-mediated autophagosome maturation and virus trafficking (Fig. 2.6C,D). More work is required to analyze the contribution of this region for UVRAG functions in autophagosome/endosome maturation and viral entry.

In conclusion, our study describes a dual gRNA and inducible CRISPR/Cas9 system to study host factors involved in viral entry. Using this strategy, our data support a model by which filovirus entry requires a specific set of host trafficking proteins for virus delivery to the intracellular entry receptor, NPC1. Better molecular characterization of this conserved trafficking pathway and the identification of additional host proteins involved in its regulation could pave the way to the development of panfiloviral therapeutic strategies.

2.5 Materials and Methods

Cell lines and antibodies

HEK293T and HT1080 cells (ATCC) were cultured in Dulbecco's Modified Eagle Medium (DMEM, Wisent) supplemented with 10% Fetal Bovine Serum (Sigma), 1U/mL penicillin, 1µg/mL streptomycin, 3µg/mL glutamine (Corning) at 37°C and 5% CO_2. Antibodies used were NPC1 (Abcam), Flag (Sigma), mCherry (Abcam), LC3 (Novus Biologicals), GAPDH (Abcam), and vinculin (Abcam).

CRISPR cloning and cell lines

HT1080 cells expressing doxycycline (Dox)-inducible Cas9 were generated by first producing lentiviral vectors via co-transfection of HEK293T cells with pCW-Cas9 (gift from Eric Lander & David Sabatini, addgene #50661) (311), packaging vector psPAX2 (gift from Didier Trono, addgene #12260) and a plasmid encoding VSV G (pMDG, gift from James

Cunningham, Brigham and Women's Hospital, Boston) in a 4:3:1 ratio using JetPRIME transfection reagent (Polyplus). Lentiviruses were harvested 48h post transfection, filtered with a 0.45 μm filter, then used to infect HT1080 cells in the presence of 8μg/mL polybrene. Following puromycin selection, monoclonal cell populations were isolated via ring cloning and expanded. Several clones were induced in 1μg/mL Dox over 4 days and were assessed for Flag-Cas9 expression by immunoblot. Uninduced clones were also assessed for leaky expression of Flag-Cas9 by immunofluorescence and immunoblot. One clone with strong expression of Flag-Cas9 upon Dox induction and no detectable expression in the absence of Dox was ultimately chosen for further experimentation.

Paired gRNA constructs were generated as described previously (312). Briefly, two gRNAs targeting the gene of interest were cloned into the lenti sgRNA(MS2)_zeo backbone (gift from Feng Zhang, Addgene #61427) using pDonor sU6 (gift from Andrea Ventura, Addgene #69351) (324). The gRNA sequences were as follows: NPC1 (ACGCCTGTAATGCCACCAAC, CACAAGCAAAAACGCCATGT), VPS11 (GCGCTTCGTTTTCTTCGACA, GTGTGTCACCCGTAGTTTGT), VPS16 (GCAGAGTATATATCGAGCAC, GATGGTGCTGTACTGGTTTA), VPS18 (GTCCTCTACGTGAACCGAAA, GGACATGAACCGCTTCGATC), VPS33A (GAACCTAAACGTGTTGCGCG, GAATACCTAACTGGACCCTT), VPS3 (GTGGTAGACGAAGCAGTCGT, CATGAGGAAGCGTTTGCACT), VPS8 (GTTGGAGGAGTATCAACTTG, GGAAGCGCTCATTGTACATA), VPS39 (TATAGATCCCACCCATGTGA, GTCAAGCACCTCACCGCTCA), and UVRAG (ATCTTCGGAACATTGCTGCC, GATATCTGAGGGGCACTTGT).

Lentiviruses expressing dual gRNAs were produced by co-transfecting HEK293T cells with the lentiviral vector containing the dual gRNAs, psPAX2, and pMDG in a 4:3:1 ratio, as described above. Lentiviruses were then used to infect the monoclonal Cas9-inducible HT1080 cells in the presence of 8μg/mL polybrene, followed by zeocin selection. Cas9 expression was induced by seeding the CRISPR cell lines in 6-well plates to approximately 30% confluence in the presence of 1μg/mL Dox. Untreated cells were kept as controls. Cells were allowed to proliferate for 96h, at which point they were reseeded for further experimentation in the absence of Dox.

Genomic DNA extraction was performed by lysing cell pellets in 50mM NaOH at 95°C for 20 min, followed by neutralization with 1M Tris pH 7.0 to a final concentration of 0.8 M, pH 8.3. Samples were centrifuged at 17,000g for 5 min, and supernatant transferred to new tubes. Amplicons containing gRNA target regions were generated by PCR using Herculase II fusion DNA polymerase (Agilent). Surveyor endonuclease assays were performed by incubating PCR products in 1X NEBuffer2 with the following thermocycler conditions: 95°C (10 min), 95-85°C (ramp rate -2°C/sec), 85-25°C (ramp rate -0.3°C/sec) to allow DNA duplexes to form. Due to the heterogeneity of the cell population from which DNA was extracted, both homoduplexes and heteroduplexes of DNA may form. Heteroduplexes, which indicate that targeting of the gene resulted in indels, were then digested with T7 endonuclease I (NEB) at 37°C for 1h. Digested products were resolved by agarose gel electrophoresis and visualized under UV light.

UVRAG cloning and generation of polyclonal cell line expressing gRNA insensitive UVRAG

Synonymous mutations of PAM sequences on mCherry-UVRAG cDNA (gift from Do-Hyung Kim, Addgene #86743) (243) were performed using overlapping PCR and confirmed by Sanger sequencing. Further cloning was done using this PAM-mutated UVRAG construct. C2

and 269-442 deletions were generated using overlapping PCR, and confirmed by Sanger sequencing and immunoblot. All mCherry-UVRAG constructs were cloned into the pLV-EF1a-IRES-Blast (gift from Tobias Meyer, Addgene # 85133) (325) lentiviral vector.

UVRAG rescue cell lines with addback of WT or mutant UVRAG were generated by transducing UVRAG CRISPR cells with the mCherry-UVRAG constructs. Lentiviruses were generated as described above, and used to infect UVRAG CRISPR cells in the presence of 8μg/mL polybrene, followed by selection in blasticidin. Expression of mCherry-UVRAG in the cell lines was validated by microscopy, flow cytometry and immunoblot.

Viral-like-particle production and viral entry assays

EBOV virus-like-particles (VLPs) were produced by co-transfecting HEK293T cells with plasmids encoding EBOV NP, EBOV VP40 fused to β-lactamase or GFP (kind gifts of Dr. Lijun Rong, University of Illinois), and the viral envelope protein (mucin deleted EBOV GP or EBOV/ Bundibugyo ebolavirus (BUDV)/ Sudan ebolavirus (SUDV)/ Taï Forest ebolavirus (TAFV)/ Reston ebolavirus (RESTV) GP, or the glycoproteins of Marburg virus (MARV), VSV, Junin (JUNV)) (all plasmids were kind gifts of Dr. James Cunningham, Brigham and Women's Hospital) using JetPRIME transfection reagent at a 1:1:1.15 ratio. Virus containing supernatants were collected and concentrated by ultracentrifugation (20,000 RPM, 1.5h, 4°C, Beckman Coulter Optima XPN-100, SW32Ti rotor) through a 20% (w/v) sucrose cushion. Viruses were resuspended in PBS and stored at -80°C.

Entry assays were performed by seeding HT1080 cells in 48-well plates at approximately 90% confluence. VLPs were added and plates were centrifuged at 200g for 30 min at 4°C, then incubated at 37°C for 3 h. Cells were washed with serum-free DMEM and loaded with CCF2-

AM (Invitrogen) according to kit instructions for 1h at room temperature. The staining solution was supplemented with 15 mM NH_4Cl and 250µM probenecid (Sigma). Following staining, cells were washed once in PBS, trypsinized, and cleavage of CCF2 analyzed using a FACSCelesta flow cytometer (BD Biosciences). Stained cells were defined as cells positively shifted compared to unstained cells (emission in 525/50 filter), and β-lactamase+ (successful reporter release post-VLP fusion) cells defined as cells shifted positively (emission in 450/50 filter) compared to stained, uninfected cells.

Immunofluorescence and microscopy

HT1080 cells were seeded onto 18 mm coverslips and grown to approximately 60% confluence. Fusion deficient (GP^{F535R}) ΔMuc EBOV VLPs containing VP40-GFP were spinoculated onto cells (200g, 30 min, 4°C) to allow cell surface binding but not internalization. Cells were shifted to 37°C for 3h to allow infection to proceed, followed by fixation in formalin, permeabilization with 0.5% triton X-100, and block in 20% FBS for 30 min. Cells were then incubated in an NPC1 antibody (5µg/mL concentration) for 1h, followed by incubation with an Alexafluor 647-conjugated secondary antibody (Thermo) for 1 hour, Hoechst staining (1µg/mL, Thermo) and mounting in PermaFluor Aqueous Mounting medium (Thermo). Immunofluorescence images were captured on an LSM800 Zeiss confocal microscope using a 63X/1.4 Oil Plan-Apochromat objective. Fifteen to twenty Z-stacks were acquired per image.

Immunoblots

Cells were washed in PBS, then lysed in buffer containing 1% Triton X-100, 0.1% NP40, 150mM NaCl, 10mM Tris-HCl pH 7.4 supplemented with a protease inhibitor cocktail (Cell signaling). Protein concentration was determined using a BCA assay following manufacturer protocol (Thermo). Equal amounts of protein were resolved by SDS-PAGE and transferred on

PVDF membranes. Proteins were detected using the indicated primary antibodies (1µg/mL concentration), HRP-conjugated secondary antibodies and visualized using chemiluminescence according to manufacturer protocol (Biorad Clarity ECL substrate).

Image and Statistical Analysis

Image analysis was performed using Imaris software (Bitplane) as described previously (296). Briefly, VLPs were modeled as GFP+ puncta with a diameter of 0.3 µm or greater. For determination of colocalization with NPC1, VLPs were assigned colocalization values based on intensity correlation to the Alexafluor647 channel (NPC1), and colocalization threshold manually determined for each experiment. The same threshold was used for both induced and noninduced cells in each experiment. Percentage of VLPs colocalized to NPC1 was then determined by dividing the number of VLPs above the colocalization threshold by the total VLP count per cell. For determination of number of internalized VLPs per cell, cell boundaries were modeled using cell fluorescence background intensity (647nm), and VLPs were modeled as described above.

Data are presented as mean ± S.D. Statistical analysis was performed by unpaired t-test with Welch's correction, and statistical significance determined using the Holm-Šídák method, unless otherwise indicated. *$p<0.05$, ** $p<0.01$, *** $p<0.001$.

2.6 Acknowledgements

We would like to acknowledge technical support from the uOttawa CBIA core staff, Chloë van Oostende and Skye Green and technical assistance of Jessie Duong for initial characterization of cell lines. We also acknowledge Corina Stewart for her contribution to editing this manuscript. This research was funded by the Canadian Institutes of Health Research: grant

number ER1-143489352509 and PJT155984390487 to M.C.; S.Q. was supported by a graduate scholarship from the Natural Sciences and Engineering Research Council of Canada. M.C. is a Canada Research Chair in Molecular Virology and Antiviral Therapeutics and is a recipient of an Ontario Ministry of Research, Innovation and Science Early Researcher Award.

Chapter 3: Ebola virus requires phosphatidylinositol (3,5) bisphosphate production for efficient viral entry

Shirley Qiu[1,2], Anders Leung[3], Yuxia Bo[1,2], Robert Kozak[3], Sai Priya Anand[1,2], Corina Warkentin[1,2], Fabiola D. R. Salambanga[1,2], Jennifer Cui[1,2], Gary Kobinger[3], Darwyn Kobasa[3,4], Marceline Côté[1,2]

1 Department of Biochemistry, Microbiology and Immunology, University of Ottawa, Ottawa, Canada

2 Ottawa Institute of Systems Biology, University of Ottawa, Ottawa, Canada

3 Special Pathogens Program, National Microbiology Laboratory, Public Health Agency of Canada, Winnipeg, Canada

4 Department of Medical Microbiology, University of Manitoba, Winnipeg, Canada

This chapter has been previously published in Virology.

Ebola virus requires phosphatidylinositol (3,5) bisphosphate production for efficient viral entry

Shirley Qiu, Anders Leung, Yuxia Bo, Robert Kozak, Sai Priya Anand, Corina Warkentin, Fabiola D.R. Salambanga, Jennifer Cui, Gary Kobinger, Darwyn Kobasa, Marceline Côté
Virology 513 (2018) 17-28

Author contributions: SQ, YB, and SA contributed to CRISPR experiments and infection assays. SQ, CW, and FS contributed to microscopy experiments. CL-4 experiments were performed by AL, RK, GK, and DK. All other experiments were performed by SQ. Figures were produced by SQ. Manuscript was written by SQ and MC, and edited by SQ, MC, JC, GB, RK, and DK.

3.1 Abstract

For entry, Ebola virus (EBOV) requires the interaction of its viral glycoprotein with the cellular protein Niemann-Pick C1 (NPC1) which resides in late endosomes and lysosomes. How EBOV is trafficked and delivered to NPC1 and whether this is positively regulated during entry remain unclear. Here we show that the PIKfyve-ArPIKfyve-Sac3 cellular complex, which is involved in the metabolism of phosphatidylinositol (3,5) bisphosphate (PtdIns(3,5)P_2), is critical for EBOV infection. Although the expression of all subunits of the complex was required for efficient entry, PIKfyve kinase activity was specifically critical for entry by all pathogenic filoviruses. Inhibition of PIKfyve prevented colocalization of EBOV with NPC1 and led to virus accumulation in intracellular vesicles with characteristics of early endosomes. Importantly, genetically-encoded phosphoinositide probes revealed an increase in PtdIns(3,5)P_2-positive vesicles in cells during EBOV entry. Taken together, our studies suggest that EBOV requires PtdIns(3,5)P_2 production in cells to promote efficient delivery to NPC1.

3.2 Introduction

Ebola virus (EBOV) is a highly pathogenic zoonotic virus belonging to the *Filoviridae* family and the causative agent of severe hemorrhagic fever disease in humans and non-human primates. Currently, there are no FDA-approved therapeutics for the treatment of Ebola virus disease. Virions harbour the characteristic filoviral filamentous morphology and are surrounded by a host-derived lipid envelope which is acquired during budding from cells. Studded on the viral envelope is the metastable trimeric EBOV glycoprotein (GP), which is the primary determinant of viral entry (20). GP is composed of heterodimers of the subunits GP_1, which contains the receptor binding domain shielded by a glycan cap (132), and GP_2, which contains a hydrophobic fusion loop and heptad repeat regions (140). Viral fusion requires a number of

triggering factors, including cleavage of the glycan cap on GP_1 by low-pH dependent cysteine proteases, and interaction with a host receptor (173,174,184,185).

Identification of Niemann-Pick C1 (NPC1), a late endosomal/lysosomal resident protein, as the filovirus receptor indicated that viral particles require not only initial internalization but also trafficking through the endosomal system for delivery to intracellular compartments containing NPC1 (171,184). In support of this, recent studies have shown that EBOV displays late entry kinetics due to the need to traffic deep into the endocytic pathway (168). Using live cell imaging to visualize viral-host membrane lipid mixing, Spence et al. and Simmons et al. found that EBOV GP-mediated viral membrane fusion occurs primarily in NPC1+ and Rab7+ compartments (169,170). However, which cellular proteins are involved in viral trafficking and whether EBOV actively regulates its delivery to NPC1+ compartments remains largely unexplored.

A previous genetic screen for EBOV entry host factors uncovered a number of genes encoding trafficking factors in addition to genes encoding the triggering factors, cathepsin B and NPC1. Among others, genes of the subunits that form the Homotypic Fusion and Protein Sorting (HOPS) complex, as well as those of PIKfyve and Sac3 were found to be enriched for gene-trap insertions in a cell population resistant to vesicular stomatitis virus expressing EBOV GP compared to unselected control cells (171). Interestingly, PIKfyve and Sac3 are found in the same ternary complex, which is scaffolded by the adaptor protein ArPIKfyve (259,264,266). The PIKfyve-ArPIKfyve-Sac3 (PAS) complex is recruited to phosphatidylinositol (3) phosphate (PtdIns3P)-enriched endosomal membranes via a FYVE domain located at the N-terminal of PIKfyve and plays an essential role in regulating vesicular trafficking (256). PIKfyve, a lipid kinase, is the sole known enzyme capable of producing phosphatidylinositol (3,5) bisphosphate

(PtdIns(3,5)P_2) in mammalian cells, while the phosphatase function of Sac3 hydrolyzes PtdIns(3,5)P_2 to regenerate PtdIns3P (263). Biochemical characterization of the complex has shown that integrity of the entire complex is critical for maintaining PIKfyve kinase activity, while Sac3 stability depends primarily on association with ArPIKfyve (264,269,270,326,327).

PtdIns(3,5)P_2 is a member of a family of phospholipids collectively called phosphoinositides (PIs), whose precise spatiotemporal localization on membranes throughout the cell allows them to dynamically regulate signalling events by recruiting and activating various effectors (Balla, 2013). PtdIns(3,5)P_2, despite composing less than 1% of the total PI pool, is known to be a critical regulator of endosomal membrane homeostasis and progression of cargo through the endosolysosomal trafficking system (328,329). Cells with reduced PtdIns(3,5)P_2 levels display profoundly enlarged endosomes as well as defective autophagy, endosomal maturation and trafficking of endocytosed cargoes (278,330–333). Knock-out of any member of the PAS complex is embryonic or perinatal lethal in mice and dysfunction of the complex has been implicated in a number of neurological and motor diseases, including Charcot-Marie Tooth Disease Type 4J and Amyotrophic Lateral Sclerosis (265,334–338).

Despite its critical role in development and cell homeostasis, little is known about the PAS complex's mechanisms of action and activation. Furthermore, the role of this complex in host-pathogen interactions in the context of virus entry is largely uncharacterized. In this study, we determined that all three subunits of the PAS complex are required for EBOV entry. Specifically, the presence of all subunits is required for PIKfyve kinase activity and PtdIns(3,5)P_2 production, which is critical for EBOV entry, while Sac3 phosphatase activity appears to be dispensable. Loss of PIKfyve activity reduced EBOV colocalization with its receptor NPC1 and resulted in viral particle accumulation in predominantly early endocytic compartments. Importantly, we

observed increased PtdIns(3,5)P_2 onto vesicular membranes during viral entry, raising the possibility that EBOV both requires and upregulates PtdIns(3,5)P_2 to promote its delivery to NPC1.

3.3 Results

3.3.1 Expression of Sac3 and ArPIKfyve is required for efficient EBOV GP-mediated entry in cells

To investigate a role for the PAS complex in EBOV entry, we first sought to generate cell lines deficient in the expression of each subunit of the complex using CRISPR/Cas9. Human fibrosarcoma cells, HT1080, were infected with lentiviral vectors encoding Cas9 and specific gRNAs for the Sac3, ArPIKfyve, and PIKfyve genes. Following puromycin selection of the transduced cells, we subcloned the polyclonal populations to obtain monoclonal cell lines. This strategy allowed us to isolate knockout (KO) clones for ArPIKfyve and Sac3, but not PIKfyve. Immunoblot analysis confirmed loss of expression of the proteins and genotyping indicated the presence of frame-shift mutations in the KO cells (Fig. 3.1A, data not shown). In agreement with previous studies, Sac3 levels were also reduced in ArPIKfyve KO cells, presumably due to the requirement of ArPIKfyve to stabilize Sac3 within cells (269). Importantly, both ArPIKfyve and Sac3 KO cell lines exhibited the enlarged vacuole phenotype indicative of reduced cellular PtdIns(3,5)P_2 (Fig. S3.1A) (264).

Using these cells, we tested whether loss of ArPIKfyve or Sac3 influenced entry by virus-like-particles (VLPs) harbouring EBOV GP or Junin virus (JUNV) GP. These VLPs, which harbour the native filovirus morphology, were produced by co-transfection of plasmids encoding the EBOV nucleoprotein (NP), the matrix protein VP40 fused to Beta-lactamase (βlam), as well as either EBOV GP or JUNV GP (24). Viral entry following fusion of the viral membrane with

the cellular membrane can be detected in cells loaded with the cytoplasmic CCF4-AM β-lactamase cleavable dye (24,27,339). Because the mucin domain of EBOV GP causes toxicity in GP-expressing cells but has been shown to be dispensable for viral entry, we used EBOV GP with the mucin domain deleted (ΔM) for our studies (128). Using this assay, we found that while entry of JUNV VLPs was similar in all cell lines, EBOV VLP entry was defective in cells knocked-out for Sac3 or ArPIKfyve (Fig. 3.1B). In addition, when compared side-by-side, entry of EBOV VLPs was always more reduced in ArPIKfyve KO than in Sac3 KO cells. We also tested infection of murine leukemia virus (MLV) pseudotypes bearing EBOV GP or vesicular stomatitis virus (VSV) G, and observed similar results (Fig. S3.1B). Because JUNV GP- and VSV G-mediated entry also require internalization and the low pH in early or late endosomes (340–343), our data indicate that the loss of Sac3 or ArPIKfyve expression does not lead to a generalized block of viral entry in the endosomes but specifically inhibits EBOV GP-mediated entry.

To confirm that the inhibition of entry was specific to the loss of Sac3 or ArPIKfyve expression and not due to potential off-targets of our CRISPR/Cas9 strategy, we expressed the proteins *in trans* in the KO cells. Because of the stable expression of Cas9 and gRNA in our monoclonal cell lines, we modified the cDNA of WT ArPIKfyve and Sac3 by the introduction of synonymous mutations generating 2 mismatches in the target sequence of the gRNA. Transfection of plasmids encoding the modified cDNAs into the KO cell lines led to expression of the proteins and rescue of the enlarged vacuole phenotype indicating that the PtdIns(3,5)P_2 levels were restored (Fig. 3.1C,E, Fig. S3.1C). Entry of EBOV VLPs was partially or completely restored to WT cell levels when the WT proteins were re-introduced in the KO cells

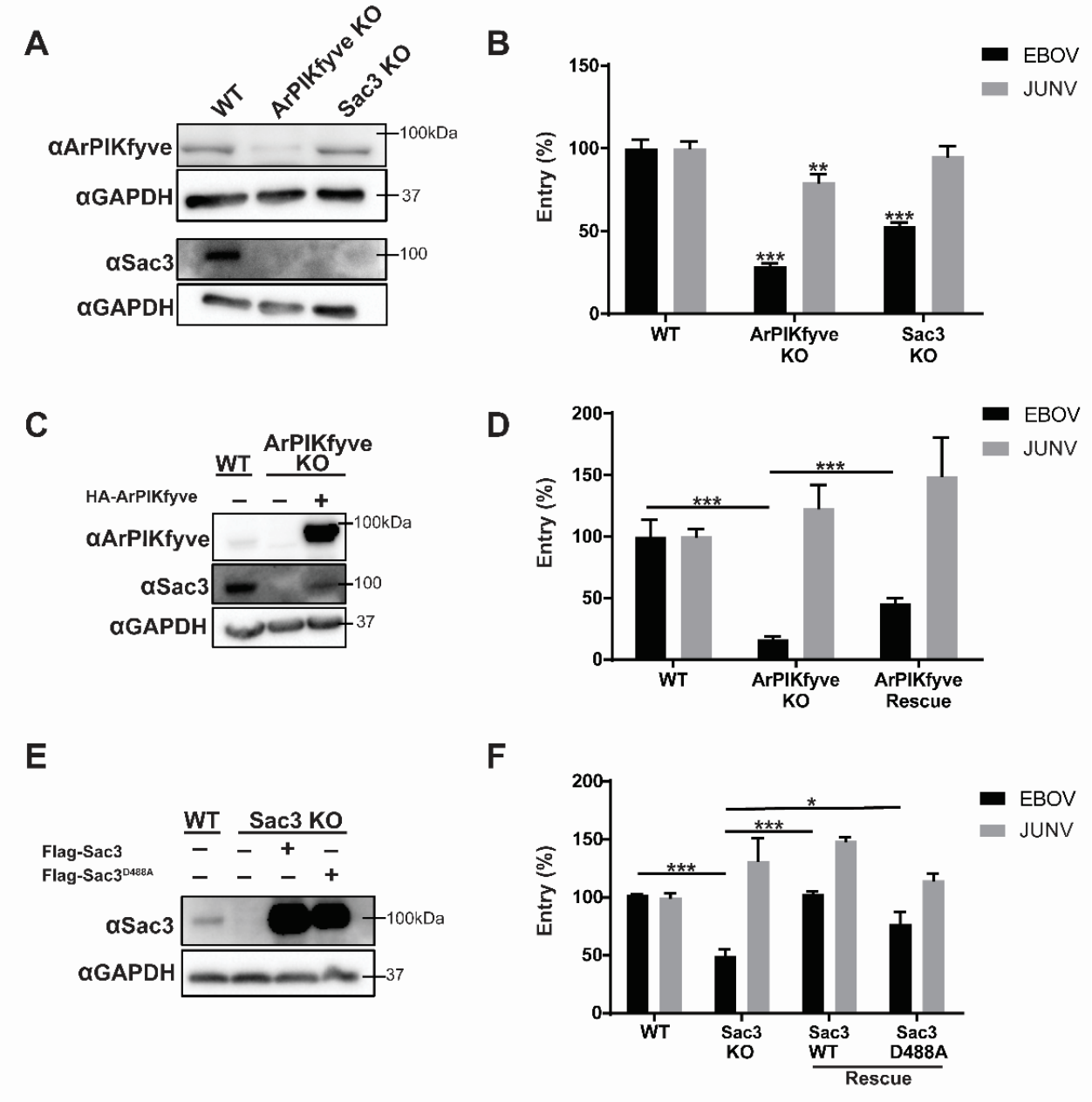
A
WT
ArPIKfyve KO
Sac3 KO
αArPIKfyve
αGAPDH
αSac3
αGAPDH
100kDa
37
100
B
EBOV
JUNV
Entry (%)
150
100
50
0
***
**
***
WT
ArPIKfyve KO
Sac3 KO
C
WT
ArPIKfyve KO
HA-ArPIKfyve
– – +
αArPIKfyve
αSac3
αGAPDH
100kDa
100
37
D
EBOV
JUNV
Entry (%)
200
150
100
50
0
***
***
WT
ArPIKfyve KO
ArPIKfyve Rescue
E
WT
Sac3 KO
Flag-Sac3
Flag-Sac3D488A
– – + –
– – – +
αSac3
αGAPDH
100kDa
37
F
EBOV
JUNV
Entry (%)
200
150
100
50
0
*
***
***
WT
Sac3 KO
Sac3 WT
Sac3 D488A
Rescue

Figure 3.1. EBOV GP-mediated entry requires ArPIKfyve and Sac3 expression, but not Sac3 phosphatase activity

(A) Expression of ArPIKfyve and Sac3 in the HT1080 CRISPR/Cas9 monoclonal KO cells. (B) Entry of βlam-VLPs harbouring EBOV ΔM GP or JUNV GP in Sac3 and ArPIKfyve KO cells was detected by measuring the percentage of cells with cleaved CCF4, normalized to WT cells. Asterisks indicate significant difference in entry compared to WT cells. (C,D) ArPIKfyve KO cells were transfected with plasmids encoding LacZ (mock) or gRNA-insensitive ArPIKfyve^{WT} and infected with βlam-VLPs. Protein expression (C) and viral entry (D) were assessed 48 hours post-transfection. (E,F) Sac3 KO cells were transfected with plasmids encoding LacZ (mock) or gRNA-insensitive Sac3^{WT} or phosphatase-deficient Sac3^{D488A} and infected with βlam-VLPs. Protein expression (E) and viral entry (F) were assessed 48 hours post-transfection. *$p<0.05$, ** $p<0.01$, *** $p<0.001$.

(Fig. 3.1D,F). The partial rescue of EBOV VLP entry in the ArPIKfyve-transfected KO cells may be a result of the incomplete restoration of endogenous Sac3 upon ArPIKfyve transfection (Fig. 3.1C). Interestingly, we also noticed that the level of infection by JUNV VLPs was slightly increased in the rescued cells compared to the mock transfected cells.

3.3.2 The phosphatase activity of Sac3 is dispensable for efficient EBOV GP-mediated entry

To tease out the role of the catalytic activity of Sac3 in EBOV entry, we introduced a D488A mutation in the Sac3 cDNA modified to be insensitive to the gRNA. This mutation was previously shown to abrogate Sac3 phosphatase activity (344) while still allowing its interaction with ArPIKfyve and PIKfyve for full complex formation (260,345). Therefore, a PAS complex containing $Sac3^{D488A}$ would be able to synthesize PtdIns(3,5)P_2 but be incapable of hydrolyzing it to PtdIns3P. As expected, expression of $Sac3^{D488A}$ in the KO cells rescued the enlarged vacuole phenotype, indicating that PIKfyve activity is restored following PAS complex formation (Fig. S3.1C). Interestingly, we found that expression of $Sac3^{D488A}$ rescued EBOV VLP entry in cells to a similar extent as $Sac3^{WT}$ (Fig. 3.1E,F), suggesting that EBOV GP-mediated entry requires formation of the PAS complex but not Sac3 phosphatase activity.

3.3.3 PIKfyve is required for efficient EBOV GP-mediated entry

As we were not successful in generating a PIKfyve deficient cell line using the above single gRNA strategy, we engineered an expression system that allows dual expression of gRNAs targeting two different exons of the gene (Fig. 3.2A) (312). For this, we first generated an HT1080 monoclonal cell line expressing a doxycycline-inducible Cas9 gene (311). This cell line was then transduced with a lentiviral vector encoding two different gRNAs targeting PIKfyve and a zeocin resistance gene. Following selection, cells were induced with doxycycline,

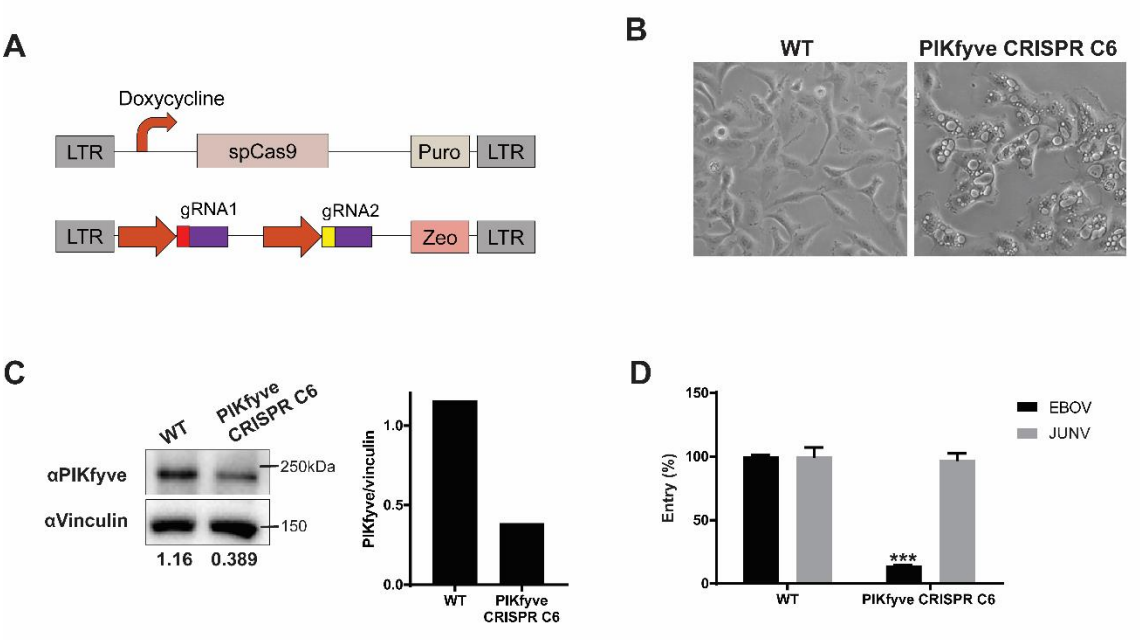

Figure 3.2. EBOV GP-mediated entry requires PIKfyve

(A) Schematic of the inducible and dual gRNA CRISPR strategy. spCas9 = *S. pyogenes* Cas9, Puro = puromycin, LTR = Long Terminal Repeat, Zeo = zeocin. (B) Phase-contrast images of PIKfyve WT and PIKfyve CRISPR clone 6 (C6) cells (C) PIKfyve CRISPR C6 cells were lysed and PIKfyve protein expression was examined by immunoblot and densitometry. (D) Entry of βlam-VLPs harbouring EBOV ΔM GP or JUNV GP in the PIKfyve WT and PIKfyve CRISPR C6 cell lines was detected by measuring the percentage of cells with cleaved CCF4, normalized to WT cells. Asterisks indicate significant difference in entry compared to WT cells. *** $p<0.001$.

monoclonal cells were obtained, and one clone exhibiting enlarged vacuoles without displaying an obvious growth defect was selected and characterized (Fig. 3.2B,C). Analysis of the genomic target regions in PIKfyve revealed that the selected clone had one allele with a partial deletion of exons 10 and 11, and another with a nucleotide insertion in exon 11, both causing frameshifts (data not shown). Surprisingly, immunoblot analysis revealed that PIKfyve was still expressed, albeit at a lower level compared to WT cells (Fig. 3.2C). The protein detected in the CRISPR cells could be PIKfyve splicing variant(s) of similar molecular weight to the PIKfyve detected in the WT cells, as splicing variants have been observed and predicted for the PIKfyve gene (346), or it could be a non-functional protein of similar molecular weight to the WT protein generated by the frameshift introduced by CRISPR/Cas9. Nevertheless, the presence of enlarged vacuoles indicates that the residual expression of PIKfyve in these cells leads to insufficient levels of PtdIns(3,5)P_2 (Fig. 3.2B). We therefore sought to test if EBOV entry is impacted in these PIKfyve deficient cells. As observed with the ArPIKfyve and Sac3 KO cells, EBOV VLP entry was reduced in the PIKfyve deficient cells while entry of VLPs harbouring JUNV GP was unaffected (Fig. 3.2D). Taken together, our data indicate that the expression of PIKfyve, ArPIKfyve, and Sac3 is required for efficient EBOV GP-mediated viral entry.

3.3.4 PIKfyve kinase activity is required for EBOV GP-mediated entry

Previous studies have shown that the kinase activity of PIKfyve is dependent on its association within an intact complex composed of Sac3 and an ArPIKfyve homodimer (264,347). Our data demonstrating that formation of the PAS complex is required for EBOV entry while Sac3 phosphatase activity is dispensable strongly suggest that it is PIKfyve kinase activity that is critical for viral entry. To further validate the importance of PIKfyve kinase activity, we first examined the effect of specific small molecule inhibitors of PIKfyve activity,

YM-201636 and apilimod, on EBOV entry (258,348). Vero cells were treated with increasing concentrations of YM-201636 or apilimod and exposed to MLV pseudotypes encoding LacZ and bearing EBOV GP or VSV G. We found that the PIKfyve kinase inhibitors specifically blocked EBOV GP-mediated infection, but not that of VSV G (Fig. 3.3A). The IC90 was lower for apilimod than YM-201636, 25 nM and 1.5 μM respectively, which correlates with the respective potency of both inhibitors to target PIKfyve activity (258,348). Neither inhibitor was cytotoxic at the concentrations and durations tested, as measured using Cell Titer-Glo, a metabolic activity assay (data not shown). Because lower concentrations of apilimod were needed to block PIKfyve activity and EBOV-GP mediated entry, we further tested apilimod on VLP entry. As expected, entry by VLPs bearing EBOV GP was reduced (88% reduction) while entry by VLPs bearing VSV G was largely unaffected (8% reduction) (Fig. 3.3B).

As a complementary approach, we overexpressed PIKfyve^{WT} or the characterized kinase-dead mutant PIKfyve^{K1877E} in 293T cells (261,263). 293T cells were selected for these experiments as the large size of the PIKfyve open reading frame rendered transfection of Vero cells and HT1080 cells inefficient. When overexpressed, the kinase-dead mutant acts as a dominant negative form as it replaces endogenous PIKfyve in the PAS complex. In addition, we fused the proteins to RFP to enable analysis of viral entry exclusively in the transfected RFP-positive cells by flow cytometry. As expected, cells expressing PIKfyve^{K1877E} exhibited the enlarged vacuole phenotype indicative of reduced PtdIns(3,5)P_2 levels (data not shown) (261,263). Furthermore, entry by EBOV VLPs was reduced in cells expressing PIKfyve^{K1877E} compared to cells expressing PIKfyve^{WT} (78% reduction), while entry by JUNV VLPs was mostly unaffected (24% reduction) (Fig. 3.3C). Collectively, these studies indicate that PIKfyve activity is critical for EBOV entry in cells.

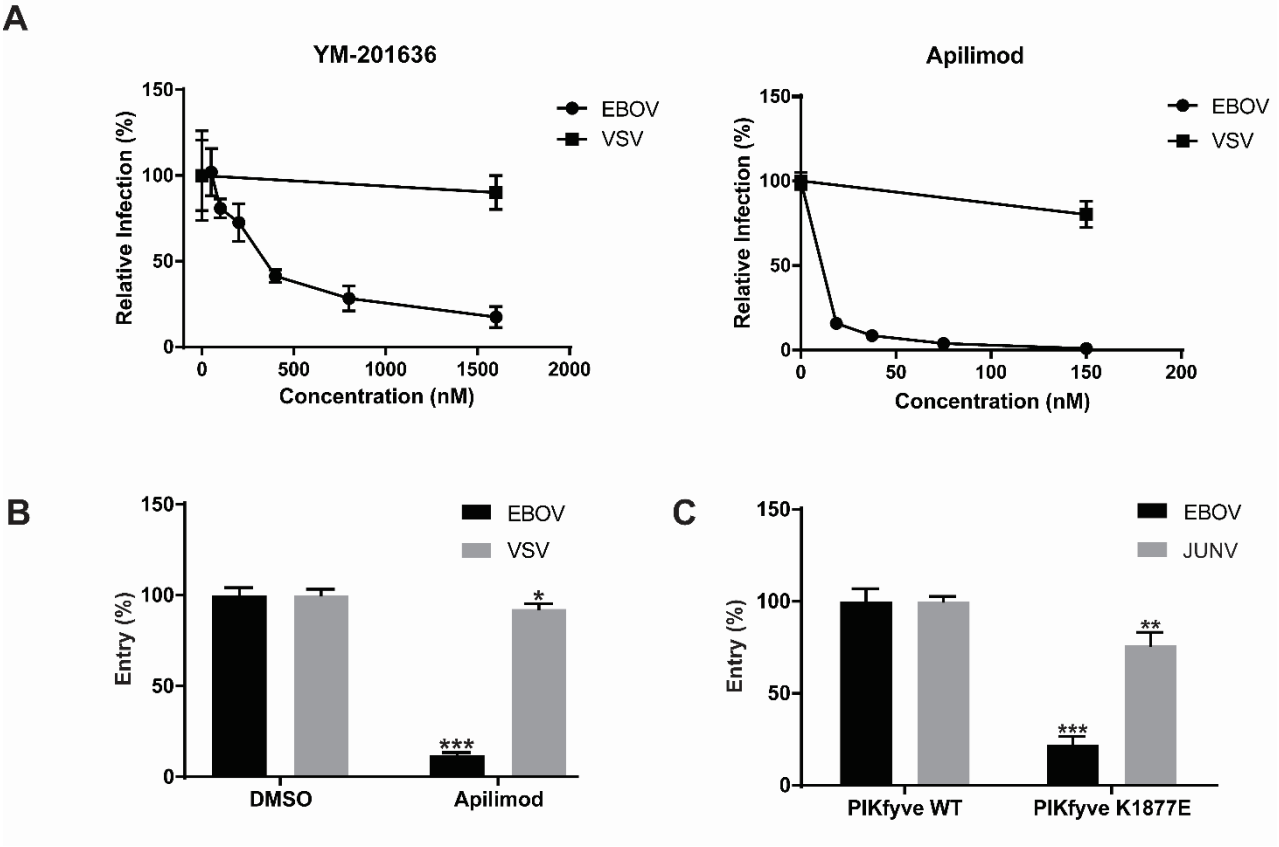

Figure 3.3. EBOV GP-mediated entry requires PIKfyve kinase activity

(A) Infection by MLV pseudotypes harbouring EBOV ΔM GP or VSV G in Vero cells treated with increasing concentrations of YM-201636 or apilimod was measured by quantitation of LacZ+ foci. (B) Entry of βlam-VLPs harbouring EBOV ΔM GP or VSV G in Vero cells treated with DMSO or 50nM apilimod was detected by measuring the percentage of cells with cleaved CCF4, normalized to DMSO treated cells. Asterisks indicate significant difference in infection compared to DMSO-treated cells. (C) 293T cells transfected with plasmids encoding PIKfyveWT or kinase-dead PIKfyveK1877E both fused to RFP were exposed to βlam-VLPs harbouring EBOV ΔM GP or JUNV GP. Entry of the VLPs in cells was detected by measuring the percentage of RFP+ cells with cleaved CCF4, normalized to PIKfyveWT-transfected cells. Asterisks indicate significant difference in infection compared to PIKfyveWT-transfected cells. *p<0.05, ** p<0.01, *** p<0.001.

3.3.5 *PIKfyve activity is required by all pathogenic filoviruses, for EBOV GP-mediated entry in a differentiated monocytic cell line, and for replication of infectious EBOV*

We next determined whether PIKfyve activity is required for entry of other filoviruses by examining the effect of apilimod on entry by MLV pseudotypes harbouring the GPs of the pathogenic EBOV species as well as Marburg GP. We found that apilimod efficiently blocked entry of all filoviruses tested (Fig. 3.4A), suggesting that PIKfyve activity is required by all pathogenic filoviruses.

Based on previous studies in nonhuman primates and in infected patients suggesting that mononuclear phagocytes are the initial targets of EBOV (349), we sought to test apilimod on VLP entry in a human monocytic cell line. THP-1 cells were differentiated with phorbol myristate acetate (PMA) and incubated with apilimod before exposure to VLPs bearing EBOV GP or VSV G. Again, EBOV GP-mediated entry of VLPs was reduced by apilimod (63% reduction), albeit requiring a higher concentration than in Vero cells, while VSV G-mediated entry was mostly unaffected (15% reduction) (Fig. 3.4B). This result suggests that PIKfyve kinase activity is important for EBOV entry in multiple cell types. Finally, to confirm that PIKfyve is important for replicative EBOV, we tested the effect of apilimod on replication of infectious EBOV in Vero cells. As expected, EBOV replication was dramatically impaired in the presence of apilimod compared to untreated cells (Fig. 3.4C).

3.3.6 *PIKfyve inhibition does not influence NPC1 expression and blocks entry of precleaved EBOV VLPs*

Previous studies have shown that the PAS complex is important for endosomal/lysosomal homeostasis and that PIKfyve inhibition can lead to a decreased degradative capacity of lysosomes and altered abundance of lysosomal proteins in some cell types (276,278). Since EBOV entry requires the lysosomal proteins cathepsin B and NPC1, we sought to determine if

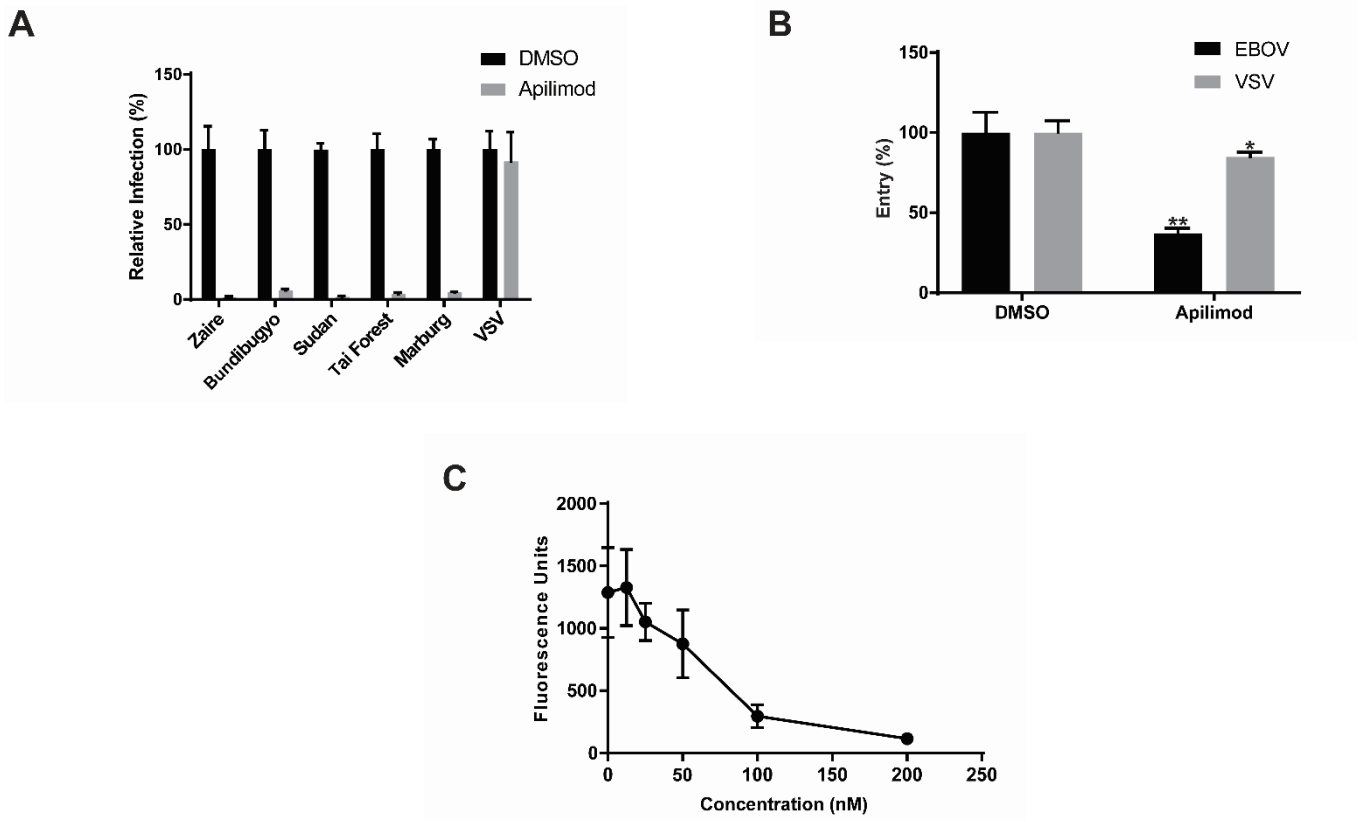

Figure 3.4. PIKfyve activity is required by all pathogenic filoviruses, for EBOV GP-mediated entry in a differentiated monocytic cell line and for replication of infectious EBOV

(A) Infection by MLV pseudotypes harbouring filoviral GPs or VSV G in Vero cells treated with 25 nM apilimod was measured by quantitation of LacZ+ foci. Infection by all MLVs bearing filoviral GPs was significantly reduced ($p<0.001$). (B) Entry of βlam-VLPs harbouring EBOV ΔM GP or VSV G in PMA-differentiated THP-1 macrophages treated with DMSO or 1μM apilimod was detected by measuring the percentage of cells with cleaved CCF4, normalized to DMSO treated cells. Asterisks indicate significant difference in infection compared to DMSO treated cells. (C) Replication of recombinant infectious EBOV expressing GFP was measured 6 days post-infection in Vero cells treated with the indicated concentrations of apilimod. *$p<0.05$, ** $p<0.01$.

the anti-EBOV effect of apilimod and YM-201636 is due solely to a block at the GP cleavage step or an effect on NPC1 expression. To examine whether PIKfyve inhibition affects a different step than the cathepsin cleavage step, we tested the effect of apilimod on thermolysin-cleaved virions. As previously shown, treatment of viruses with thermolysin mimics cathepsin B cleavage of GP and renders the cleaved virions insensitive to CA-074, a specific cathepsin B inhibitor (173). Using EBOV VLPs bearing thermolysin-cleaved GP, we found that although these virions were not blocked by CA-074, their entry was still inhibited by apilimod (Fig. 3.5A). This indicates that, while PIKfyve inhibition may or may not have an effect on the cathepsin cleavage of GP, PIKfyve activity is required for a step other than GP cleavage by cathepsin B. Next, we looked at the expression of NPC1 in cells treated with increasing concentrations of apilimod and did not observe any significant change in the expression (Fig. 3.5B). Taken together, our data suggest that the PIKfyve inhibitors block at a step distinct than that of cathepsin B cleavage and do not alter NPC1 expression in cells.

3.3.7 PIKfyve activity is required for trafficking of virions to NPC1+ endolysosomes

To examine the fate of VLPs in cells treated with PIKfyve inhibitors, we used EBOV VLPs containing VP40 fused to the green fluorescent protein (GFP), NP, and fusion deficient EBOV GP (F535R) (172). This modification on GP still allows viral particles to undergo endocytosis and trafficking, including cleavage by cathepsin proteases and binding to NPC1. However, complete membrane fusion is inhibited, potentially at the hemifusion step (Spence et al., 2016). Therefore, we used these particles to monitor VLP accumulation at the site of fusion. HT1080 cells were incubated with the fusion-deficient GFP VLPs for 3 hours in the presence or absence of apilimod, fixed, and stained for NPC1 (Fig. 3.6A). We found that cells treated with apilimod internalized similar levels of VLPs compared to the DMSO treated cells (Fig. 3.6B).

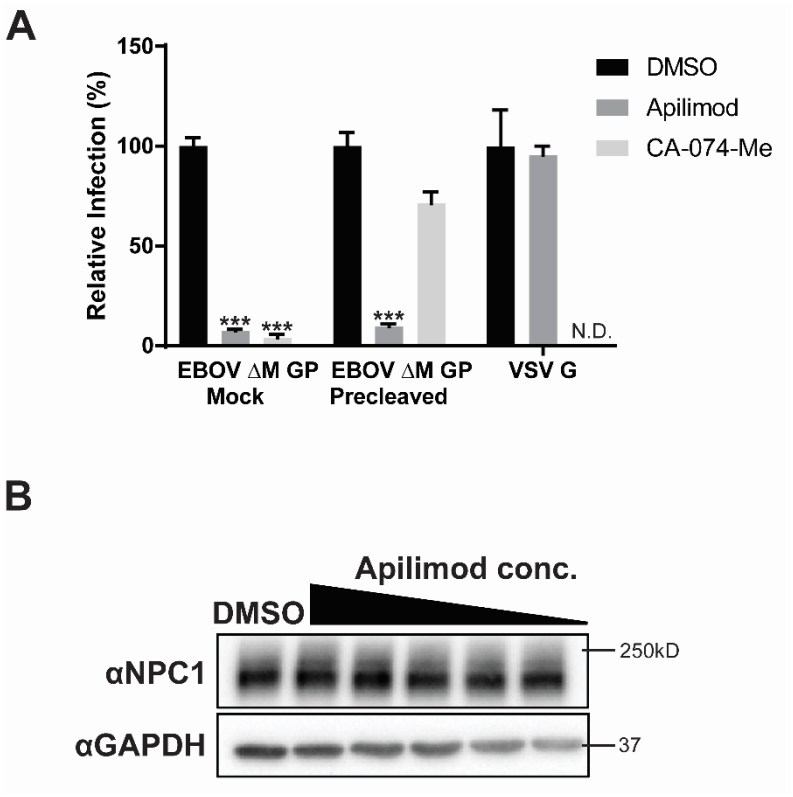

Figure 3.5. Apilimod block of infection cannot be bypassed by precleavage of EBOV GP and does not affect viral receptor expression

(A) βlam-VLPs harbouring EBOV ΔM GP were precleaved using thermolysin. Vero cells treated with DMSO, apilimod (50nM) or cathepsin B inhibitor CA-074-Me (80 μM) were exposed to precleaved or mock treated VLPs, or to VLPs harbouring VSV G, and entry was detected by measuring the percentage of cells with cleaved CCF4, normalized to DMSO treated cells. Asterisks indicate significant difference in infection compared to DMSO treated cells. N.D. = Not Done. *** $p<0.001$ (B) HT1080 cells were treated with two-fold dilutions of apilimod starting at 100nM for 4 hours, followed by cell lysis and detection of NPC1 expression by immunoblot.

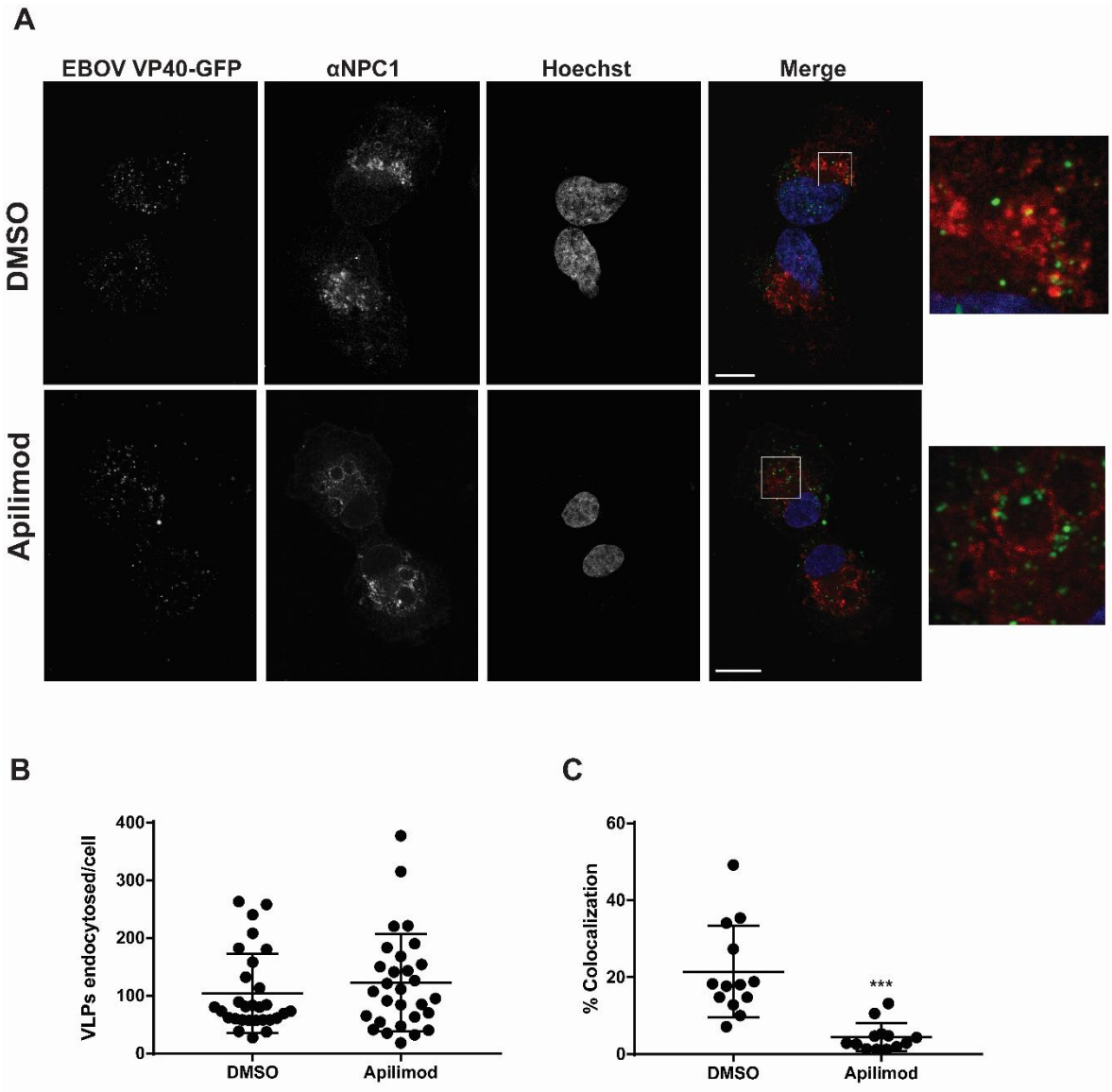

Figure 3.6. Inhibition of PIKfyve activity leads to reduced co-localization of EBOV VLPs with NPC1 but does not affect endocytosis of VLPs

(A) Coverslip-bound HT1080 cells treated with apilimod (50nM) were infected with GFP-expressing VLPs harbouring fusion deficient EBOV ΔM GP^{F535R} for 3 hours. Cells were then fixed, permeabilized, and stained with an NPC1 antibody and Hoechst. Cells were imaged on an LSM800 confocal microscope (Zeiss). Pixel size = 0.05µm. Bar = 10 µm (B) Endocytosed VLPs (n=29) and (C) Colocalization between VLPs and NPC1 (n=13) were analyzed using Imaris software (Bitplane). *** $p<0.001$.

However, when we examined NPC1 stained by immunofluorescence, we observed decreased colocalization of the EBOV VLPs with NPC1 in the apilimod treated cells (Fig. 3.6A,C). We then sought to characterize the site of VLP accumulation in these cells. Upon staining with Rab7 and EEA1, we observed that the apilimod-induced vacuoles were either exclusively Rab7+ or EEA1+ (Fig. 3.7). In addition, when cells were exposed to VLPs and treated with apilimod, an accumulation of the VLPs within EEA1+ vacuoles was noticeable, while a majority of VLPs were closely associated with Rab7+ vesicles in the DMSO treated cells, suggesting that the VLPs were trapped in compartments characteristic of early endosomes upon apilimod treatment (Fig. 3.7). Taken together, these data suggest that PIKfyve activity is required for trafficking and delivery of EBOV particles to late endosomal or lysosomal NPC1+ compartments.

3.3.8 EBOV induces relocalization of a PtdIns(3,5)P2 probe to intracellular vesicles

While basal levels of PIKfyve activity could be sufficient for EBOV entry, it is also possible that, during entry, EBOV induces PIKfyve activation. To monitor PtdIns(3,5)P_2 in cells, we transfected Vero cells with a previously described genetically-encoded tandem PtdIns(3,5)P_2 probe, 2XML1N, that allows visualization of the dynamics of this phospholipid in cells (284). This probe is derived from the N-terminus of the endosomal transient receptor potential cation channel, mucolipin-1 (TRPML1) which binds to PtdIns(3,5)P_2 in the nanomolar range. Previous characterization of the probe revealed that it binds to PtdIns(3,5)P_2 with high specificity *in vitro* and that its expression in cells allows detection of changes in PtdIns(3,5)P_2 levels, with cytoplasmic localization when PtdIns(3,5)P_2 levels are low and vesicular localization when levels are high (284). We also monitored PtdIns3P expression by co-transfecting the FYVE-RFP probe. Cells were serum-starved, exposed to the Epidermal Growth Factor (EGF), which is known to activate the PI3K/Akt pathway and PIKfyve (330), or exposed to EBOV

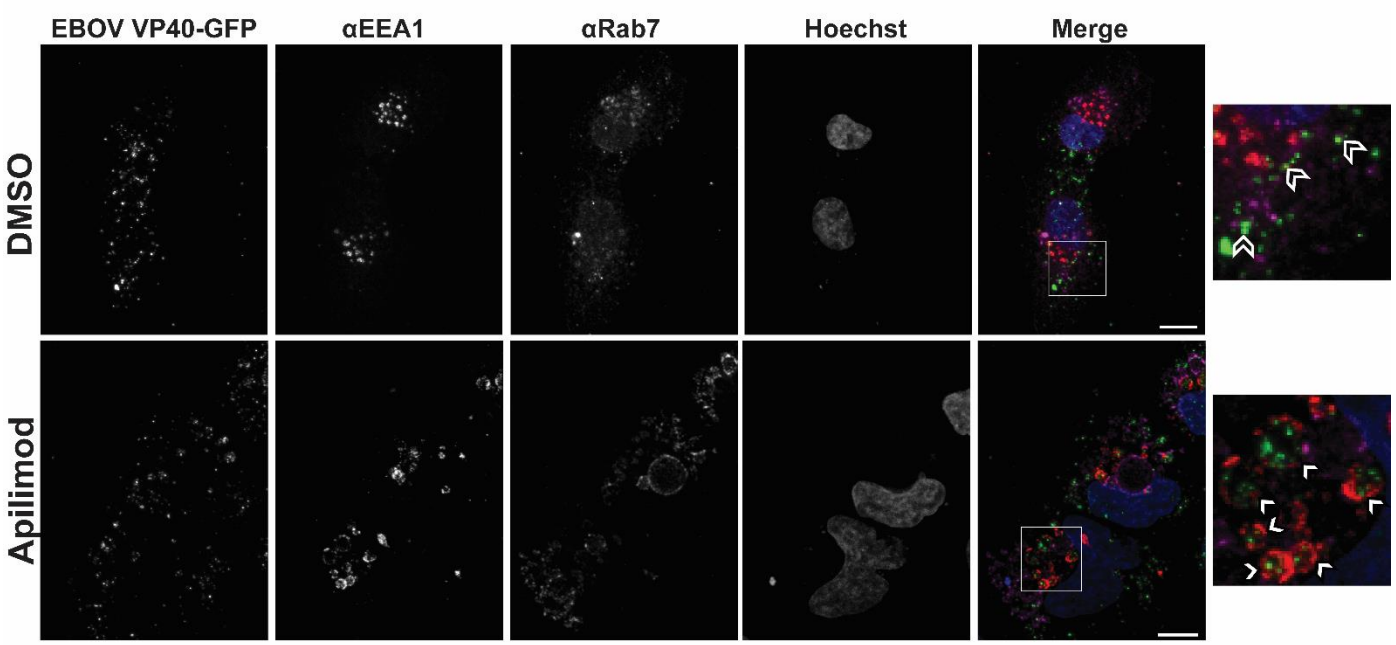

Figure 3.7. Inhibition of PIKfyve activity leads to EBOV VLP accumulation in primarily EEA1+ vacuoles

Coverslip-bound HT1080 cells treated with apilimod (50nM) were infected with GFP-expressing VLPs (green) harbouring fusion deficient EBOV ΔM GPF535R for 3 hours. Cells were then fixed, permeabilized, and stained with EEA1 (red) and Rab7 (purple) antibodies and Hoechst. Cells were imaged on an LSM800 confocal microscope (Zeiss). Images are representative of 3 independent experiments. Pixel size = 0.22µm. Filled arrowheads indicate VLPs within EEA1+ vacuoles, and open arrowheads indicate VLPs associated with Rab7. Bar = 10 µm.

VLPs, both in the presence or absence of apilimod. Using this assay, we found that, as expected, EGF treatment induced a change in the expression pattern of the 2XML1N probe from diffuse to punctate, suggesting increased production of PtdIns(3,5)P_2 on vesicular membranes (Fig. 3.8A,B). Interestingly, cells exposed to EBOV VLPs also displayed vesicular relocalization of the 2XML1N probe, indicating that EBOV triggers increased vesicular PtdIns(3,5)P_2 in the host cell during entry. The upregulation of 2XML1N puncta by EGF or VLPs was specifically abolished by apilimod treatment, validating the specificity of the probe for PtdIns(3,5)P_2 in our assay. As expected, in contrast, apilimod treatment did not reduce the FYVE-RFP vesicular localization. Instead, a slight increase in vesicular localization of FYVE-RFP could be observed, especially when apilimod-treated cells were stimulated with EGF, suggesting an increase in PtdIns3P on vesicular membranes. Further validation of the PtdIns(3,5)P_2 probe was performed by transfection of a mutated 2XML1N probe (7Q-2XML1N) with modifications of the PtdIns(3,5)P_2 binding domain, which rendered the probe cytoplasmic in distribution in all conditions tested (Fig. 3.8C, data not shown) (284). In addition, incubation of cells with an unrelated cargo, dextran, did not result in increased 2XML1N puncta compared to serum starved-cells (Fig. S3.2). Taken together, our data suggest that, as measured by the 2XML1N probe localization, EBOV actively regulates vesicular PtdIns(3,5)P_2 in the host cell during viral entry.

3.4 Discussion

EBOV entry is a multi-step process involving binding to the cell surface, internalization via macropinocytosis and trafficking through the endolysosomal system for delivery to compartments containing the priming and triggering factors for viral fusion, cathepsin proteases

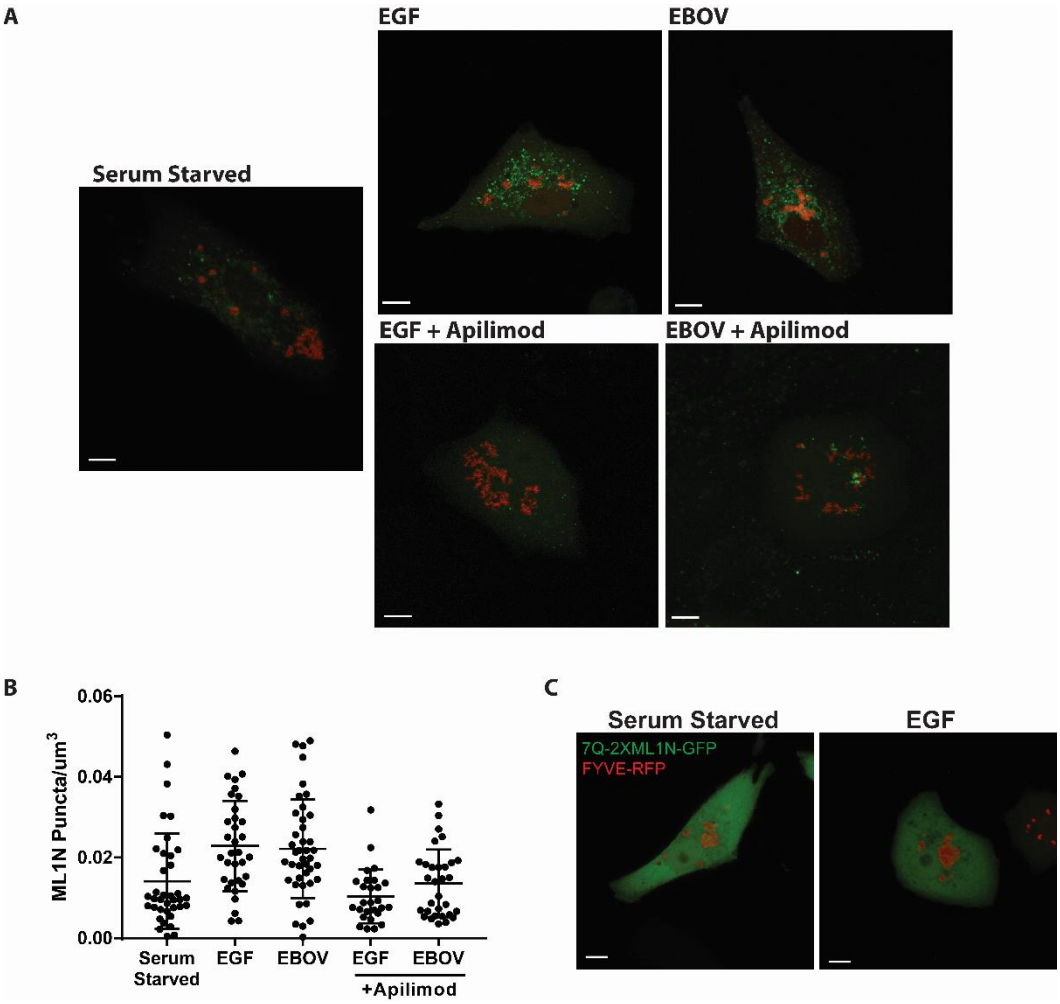

Figure 3.8. EBOV induces relocalization of a PtdIns(3,5)P2 probe to intracellular vesicles

(A) Serum-starved Vero cells transfected with FYVE-RFP and 2XML1N-GFP probes were seeded in 8 well chamber slides and treated with EGF (100ng/mL), EGF + apilimod (50nM), VLPs harbouring EBOV ΔM GP (MOI~100), or VLPs + apilimod for 30 minutes. Live cells were imaged on an LSM800 confocal microscope (Zeiss). Pixel size = 0.19µm (B) ML1N+ puncta were quantitated using Imaris software (Bitplane) n≥22. Number of puncta was significantly increased in EGF- and EBOV ΔM-treated cells compared to serum starved cells ($p<0.01$) and number of puncta was significantly reduced with apilimod treatment ($p<0.001$). (C) Serum-starved Vero cells transfected with FYVE-RFP and 7Q-2XML1N-GFP probes were seeded in 8 well chamber slides and incubated in the presence or absence of EGF (100ng/mL) for 30 minutes. Cells were imaged as in (A). Bar = 10 µm.

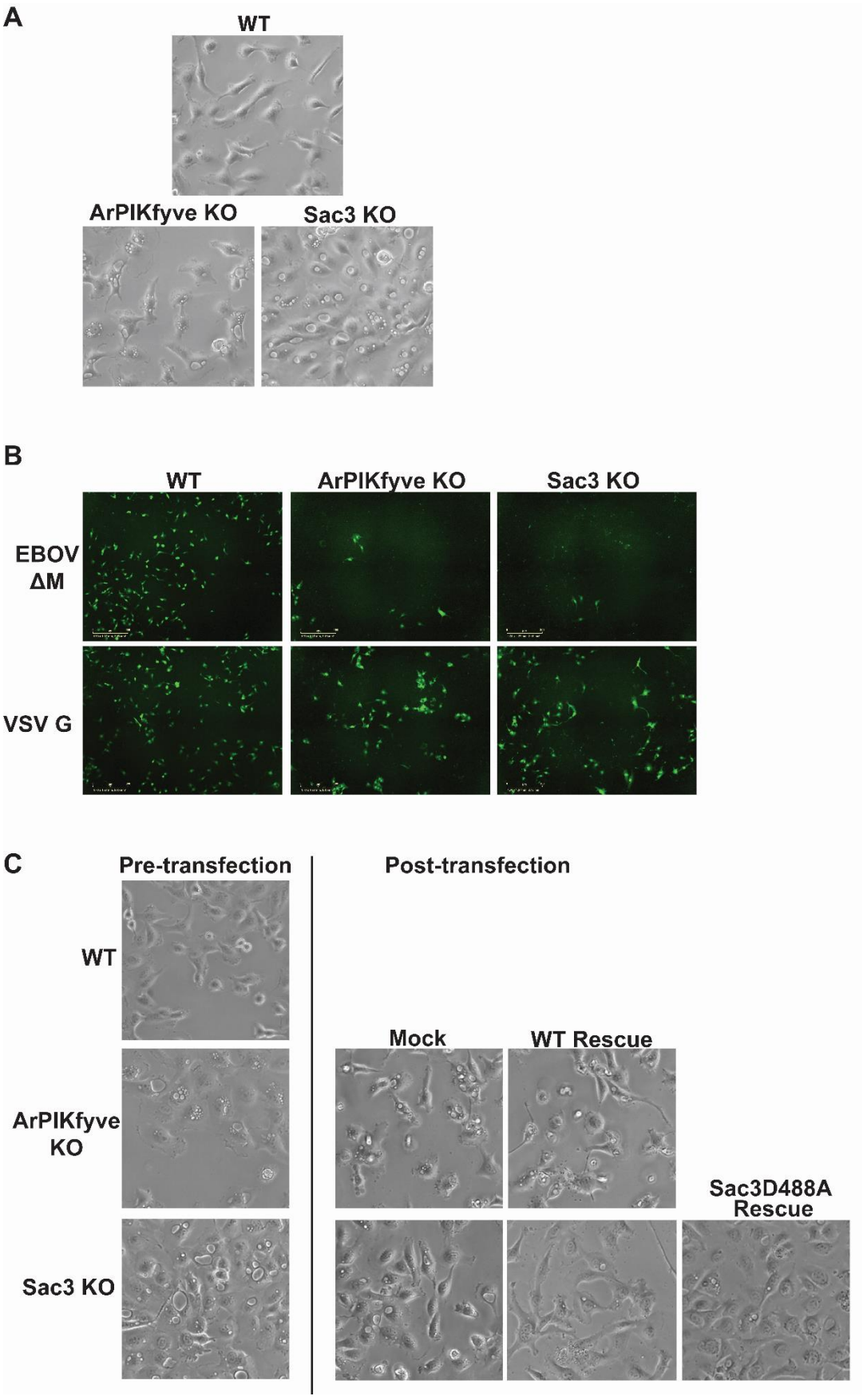
A
WT
ArPIKfyve KO
Sac3 KO
B
WT
ArPIKfyve KO
Sac3 KO
EBOV ΔM
VSV G
C
Pre-transfection
Post-transfection
WT
ArPIKfyve KO
Sac3 KO
Mock
WT Rescue
Sac3D488A Rescue

Figure S3.1. Phenotype of ArPIKfyve and Sac3 CRISPR/Cas9 HT1080 cells

(A) Phase-contrast microscopy images of the ArPIKfyve and Sac3 KO cells. (B) Entry of GFP-expressing MLV pseudotypes harbouring EBOV ΔM GP or VSV G in ArPIKfyve and Sac3 KO cells was measured by visualization of GFP+ foci on an Incucyte ZOOM Cell Analysis system (Essen Biosciences). Images are representative of 2 independent experiments. (C) Phase-contrast images of ArPIKfyve and Sac3 KO cells transfected with gRNA-insensitive plasmids encoding WT cDNA. Images were taken 24 hours post-transfection.

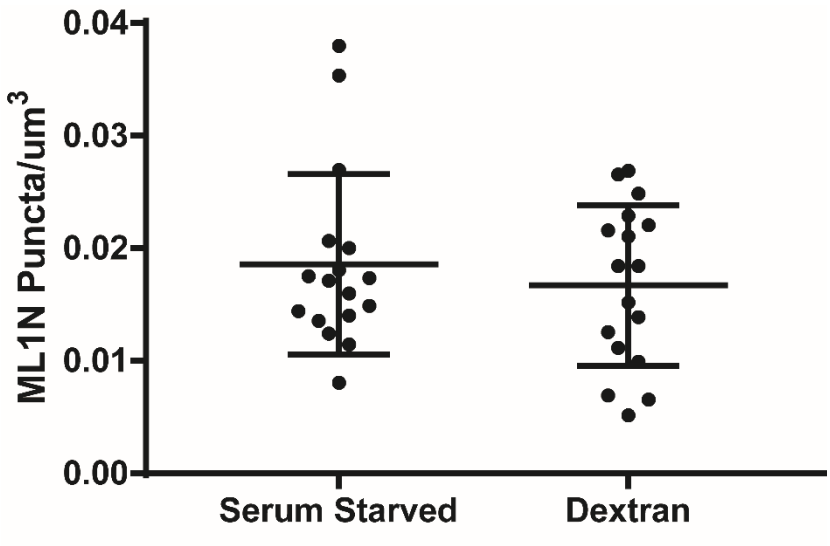

Figure S3.2. Incubation of cells with dextran does not increase vesicular localization of a PtdIns(3,5)P_2 probe

Serum-starved Vero cells transfected with 2XML1N-GFP were seeded in 8 well chamber slides and treated with or without red dextran (10 µg/mL) for 30 minutes. Live cells were imaged on an LSM800 confocal microscope (Zeiss). ML1N+ puncta were quantitated using Imaris software (Bitplane) n=17.

and NPC1 (155,163,165,169,170,174). The requirement for interaction with proteins localized in specific intracellular vesicles suggests that EBOV depends on specific host trafficking proteins for viral entry. However, the host factors involved in viral trafficking are largely uncharacterized. A previous genetic screen hinted into the requirement of a specific set of host trafficking factors, including the HOPS tethering complex, lysosomal biogenesis regulator BLOC1, and the phosphoinositide regulators PIKfyve and Sac3. Interestingly, PIKfyve and Sac3 associate in a ternary complex along with scaffolding protein ArPIKfyve, which, although not identified in the screen, is critical for regulating the enzymatic activity of PIKfyve and Sac3. Here we characterized the role of the PIKfyve-ArPIKfyve-Sac3 complex in EBOV entry.

In our study, we found that expression of all subunits of the PAS complex is required for EBOV infection, and loss of expression of any member of the complex led to inhibition of EBOV GP-mediated but not JUNV GP- or VSV G-mediated entry. Further studies using enzymatically-dead mutants revealed that the lipid kinase activity of PIKfyve is required for EBOV entry, whereas the lipid phosphatase activity of Sac3 is dispensable. Pharmacological inhibition of PIKfyve activity using two distinct PIKfyve inhibitors, YM-201636 and apilimod, also led to a block of EBOV pseudotype and VLP entry in Vero, HT1080, and differentiated THP-1 cells. In addition, PIKfyve activity was required for entry by all known pathogenic Ebola viruses and Marburg virus as well as replication of infectious EBOV. Our studies suggest that PIKfyve is a critical filovirus entry factor in multiple cell types. The inhibition of EBOV entry and replication by apilimod was also reported by Nelson et al. while the current article was in preparation (306). Using pseudotypes and VLPs, they determined that apilimod blocked viral entry in Huh 7, Vero, and primary macrophages. Interestingly, they observed that the concentration of apilimod required to inhibit EBOV was higher in Huh7 cells than in Vero cells

and primary macrophages. In our study, a higher concentration of apilimod was required to block viral entry in differentiated THP-1 than in Vero cells. This could possibly be due to higher endogenous levels of PIKfyve in differentiated THP-1 cells, active drug efflux mechanisms, or the existence of a minor PIKfyve-independent entry pathway in THP-1 cells. Interestingly, in an earlier study in which the target of apilimod was identified, Cai et al. also reported that higher concentrations of apilimod were required to inhibit TLR signaling in THP-1 cells compared to human peripheral blood mononuclear cells (348). Nevertheless, our study and that of Nelson et al. demonstrate that apilimod blocks EBOV entry in multiple cell lines and in primary cells, indicating that the requirement for PIKfyve activity during EBOV entry is robust among multiple cell types. Nelson et al. also found that VLPs failed to reach NPC1+ compartments, and reported viral accumulation in EEA1+ compartments. Similarly, we found that apilimod reduced colocalization between EBOV VLPs and NPC1 and caused the accumulation of the viral particles in EEA1+ and Rab7- vesicles. Although the precise cellular compartment in which VLPs accumulate remains to be elucidated, our studies suggest that EBOV requires a functional PAS complex for entry and that inactivation of PIKfyve results in sequestration of EBOV particles in early endocytic compartments which are not conducive to full fusion and nucleocapsid release (169,170).

EBOV-specific dependence on PIKfyve kinase activity suggests that the production of PtdIns(3,5)P_2 is required for viral entry. In support of this, our data indicate an increase in PtdIns(3,5)P_2-containing vesicles during EBOV entry as visualized using a specific fluorescent probe. It is tempting to speculate that PIKfyve activity is altered during viral entry to promote EBOV delivery to NPC1. A previous study has indicated that EBOV can activate the PI3K pathway, in part by inducing the phosphorylation of Akt (350). Interestingly, it has been shown

that PIKfyve can be activated directly by Akt upon EGF stimulation (330). An additional study has suggested that EBOV requires AMP-activated Protein Kinase during viral internalization (164), which has also been shown to activate PIKfyve directly (351). If and how the virus activates and regulates the PAS complex remains to be determined.

In addition, the role of PtdIns(3,5)P_2 effectors during viral entry remains uncharacterized. Investigation of PtdIns(3,5)P_2 effectors remains technically challenging due to the paucity of effectors identified to date. The best characterized effectors thus far are TRPML1 and the two-pore channels (TPC), TPC-1 and TPC-2, all of which are cation channels permeable to Ca^{2+} (282,283). Interestingly, Sakurai et al. reported that TPCs are required for EBOV entry, and infection is reduced via TPC knock-out or small-molecule inhibition (202). Simmons et al. have also reported that EBOV particles fuse in both NPC1+ and TPC+ endosomal compartments, further suggesting that Ca^{2+} channels may play a role in EBOV trafficking (170). In an attempt to investigate the involvement of TRPML1 during EBOV entry, we examined whether MLSA1, a TRPML1 agonist, could restore infection by MLV pseudotypes bearing EBOV GP in apilimod-treated cells. We did not observe a rescue in EBOV infection in the presence of increasing concentration of MLSA1 (up to 80 μM) even with concentrations of apilimod as low as 5 nM (data not shown). While this result indicates that TRPML1 activation is not sufficient to rescue EBOV infection in apilimod treated cells, TRPML1 activation by PtdIns(3,5)P_2 could still be essential for EBOV entry in addition to the activation of one or more other effectors all working cooperatively.

In this study, we have demonstrated that an intact PAS complex and PIKfyve kinase activity is required for EBOV GP-mediated entry, but not VSV G- and JUNV GP-mediated entry, indicating that these viruses have differential requirements for host trafficking machinery

during entry. VSV entry has been shown to require the LDL receptor, endocytosis and low pH-dependent viral membrane fusion in early endosomes (342,352,353). JUNV entry is known to require the transferrin receptor (TfR) and endocytosis (340). If viral entry follows the usual cellular trafficking of TfR, this would indicate that the virus-receptor complex would be targeted to recycling endosomes, where TfR is sorted to be recycled back to the cell surface (354). Whether recycling endosomes are the site of fusion for JUNV remains to be determined, but the fact that JUNV entry is largely insensitive to PIKfyve inhibitors indicates that, similarly to VSV, JUNV does not require extensive endolysosomal trafficking for entry. Interestingly, Rizopoulos et al. recently demonstrated that PIKfyve is required for vaccinia virus infection (355), and two groups found that *Salmonella enterica* requires PIKfyve for infection and actively modulates PtdIns(3,5)P_2 levels through secretion of a bacterial phosphatase (356,357). Collectively, these and our studies indicate that the PAS complex and its product PtdIns(3,5)P_2 are critical for infection by a number of pathogens.

Finally, given that the PAS complex is important for EBOV entry in multiple cell types, including macrophages, and given that it is required for replication of infectious EBOV, our study suggests that the complex is a potential therapeutic target. Additionally, since all pathogenic filoviruses were sensitive to PIKfyve inhibition, this complex could represent a target for pan-filoviral therapy.

3.5 Materials and Methods

Cells, antibodies, and inhibitors

HEK293T, Vero E6, and HT1080 cells (ATCC) were cultured in Dulbecco's Modified Eagle Medium (DMEM, Lonza) supplemented with 10% Fetal Bovine Serum (Sigma), 100U/mL penicillin and 100µg/mL streptomycin (Wisent). THP-1 cells (ATCC) were cultured in Roswell

Park Memorial Institute medium (RPMI, Wisent), supplemented with 10% FBS (Wisent), 100U/mL penicillin and 100µg/mL streptomycin (Wisent), 50µM β-mercaptoethanol (MP Biomedical), 1 mM sodium pyruvate (Gibco), and 4.5 g/L glucose (Gibco). Cells were maintained at 37°C in 5% CO_2. Three days prior to infection, THP-1 cells were differentiated with 100nM phorbol 12-myristate 13-acetate (PMA, Sigma) in RMPI supplemented with 10% FBS and penicillin/streptomycin.

Stock solutions of YM-201636 (Cayman), apilimod (Ark Pharm, Inc), MLSA1 (Tocris), and CA-074-Me (Sigma) were prepared in DMSO and stored at -20°C. Antibodies used were NPC1 (Abcam), EEA1 (Thermo), Rab7 (Abcam), PIKfyve (Millipore), VAC14/ArPIKfyve (Ptglabs), FIG4/Sac3 (Millipore), and GAPDH (Cell Signalling).

Plasmids and cloning

The Sac3 cDNA (OriGene Technologies) was cloned into the pCaggs vector. The D488A mutation and nucleotide changes in the gRNA target sequence were performed by overlapping PCR. The HA-ArPIKfyve construct was a kind gift from Dr. Assia Shisheva, Wayne State University. HA-ArPIKfyve was subcloned in pCaggs and mutations were performed by overlapping PCR. The HA-PIKfyve and citrine-PIKfyve constructs were kind gifts of Dr. Lois Weisman, University of Michigan. The citrine at the N-terminus of PIKfyve was replaced by RFP using Gibson assembly. Mutations were also introduced using Gibson assembly. All mutations were confirmed by Sanger sequencing.

Generation of PIKfyve, ArPIKfyve and Sac3 deficient cells

ArPIKfyve and Sac3 knock-out cells were generated using a lentiviral CRISPR/Cas9 system. Briefly, gRNA were cloned into lentiCRISPR v2 (gift from Feng Zhang, Addgene

plasmid # 52961) (358). The gRNA sequences used are the following: CGCACGATGTTAGGCGTGAG for ArPIKfyve, TTCTGGACCGAGCTGATGAT for Sac3, and CTGACTGATGTGCGCTTGCT for PIKfyve. Lentiviral vectors were produced in 293T cells by co-transfection of the lentiCRISPR v2 with packaging vector psPAX2 (gift from Didier Trono, Addgene plasmid # 12260) and a plasmid encoding VSV G (gift from James Cunningham, Brigham and Women's Hospital) in a 4:3:1 ratio. Lentiviruses were used to infect HT1080 cells in the presence of 5μg/mL polybrene and transduced cells were selected in puromycin 72 hours post-infection. Cells exhibiting a vacuolar phenotype indicative of PtdIns(3,5)P_2 reduction were ring-cloned and further analyzed by immunoblot and genotyping.

The PIKfyve deficient cells were generated by first producing lentiviral vectors via transfection of 293T with plasmids encoding pCW-Cas9 (gift from Eric Lander & David Sabatini, Addgene plasmid # 50661) (311), psPAX2 and VSV G in a 4:3:1 ratio. Lentiviral vectors were then used to infect HT1080 cells, followed by puromycin selection, to obtain a doxycycline-inducible Cas9 population. Two gRNAs targeting PIKfyve were cloned into the lenti sgRNA(MS2)_zeo backbone (gift from Feng Zhang, Addgene plasmid # 61427) (324) using pDonor_sU6 (gift from Andrea Ventura, Addgene plasmid # 69351) using a previously published method (312). The two gRNA sequences used were AGTTTCAGGATCACCGCTAC and AATGGTTGATGGACGTTGGC. Lentiviruses encoding dual gRNAs were produced in 293T cells as above and used to infect the dox-inducible Cas9 HT1080 cells. Following zeocin selection, Cas9 expression was induced for four days using doxycycline and cells exhibiting a vacuolar phenotype indicative of reduced PtdIns(3,5)P_2 were ring-cloned and further analyzed for PIKfyve expression by immunoblot and genotyping.

Genotyping was performed by extracting genomic DNA from cells using the QuickExtract solution (Epicenter) following the manufacturer protocol. A 500-600 base pair region surrounding the gRNA target site was amplified by PCR using primers containing restriction sites for cloning into pCAGGS. Five to twelve clones per cell line were sequenced by Sanger sequencing.

Viral pseudotype and virus-like-particle production

Murine leukemia virus (MLV) pseudotypes were produced in 293T cells by cotransfecting an MLV retroviral vector encoding LacZ or GFP, the packaging plasmid MLV gag/pol, and a plasmid encoding the viral envelope protein (EBOV Δmucin GP, other Ebola species (all Δmucin), MARV GP, VSV G or JUNV GP) (all plasmids were kind gifts of Dr. James Cunningham, Brigham and Women's Hospital) using Lipofectamine 2000 at a 1:1:1.15 ratio. Virus-containing cell supernatants were harvested at 48, 72, and 96 hours post-transfection. Viruses were concentrated via ultracentrifugation (20,000 RPM, 1.5 hours, 4°C, Beckman Coulter Optima XPN-100, SW32Ti rotor) through a 20% (w/v) sucrose cushion. Viruses were resuspended in PBS and stored at -80°C.

EBOV virus-like-particles (VLPs) were produced in 293T cells by cotransfecting plasmids encoding the EBOV NP, EBOV VP40 fused to β-lactamase or GFP (kind gifts of Dr. Lijun Rong, University of Illinois), and the viral envelope protein at a 1:1:1.15 ratio. Virus containing supernatants were collected and concentrated as described above.

Cleavage of EBOV GP on VLPs was performed by incubating concentrated VLP preparations in 250 μg/mL thermolysin (Sigma) for 1 hour at 37°C. Thermolysin activity was quenched by incubation in 10mM EDTA on ice for 10 minutes, and VLPs were stored at -80°C.

Infection and entry assays

For the VLP entry assays, cells were seeded in 48-well plates and grown to approximately 90% confluence. VLPs were added and plates were centrifuged at 250xg for 1 hour at 4°C before incubation at 37°C for 3 hours. Cells were washed with serum-free DMEM and loaded with CCF4-AM (Invitrogen) according to kit instructions for one hour at room temperature. The staining solution was supplemented with 15mM NH_4Cl and 250µM probenecid (Sigma). Following staining, cells were washed once in PBS, trypsinized, and fluorescence analysed using a FACSCelesta flow cytometer (BD Biosciences). Stained cells were defined as cells positively shifted compared to unstained cells (emission in 525/50 filter), and β-lactamase+ (successful reporter release post VLP fusion) cells defined as cells shifted positively (emission in 450/50 filter) compared to stained, uninfected cells. VLP titres were calculated to obtain 20-40% entry in the control cells (WT or DMSO-treated) for each experiment.

For infections by MLVs encoding LacZ, Vero cells were seeded in 24-well plates and grown to approximately 50% confluence. Cells were preincubated with inhibitors for one hour and then incubated with virus for 4-6 hours in the presence of 5µg/mL polybrene. Cells were then placed in fresh medium supplemented with 15mM NH_4Cl overnight, washed, then incubated for 72 hours, at which point they were fixed in formalin and stained with 100µM X-Gal in staining buffer (5mM potassium ferricyanide, 5mM potassium ferrocyanide, 2mM magnesium chloride in PBS). Positive foci were counted visually using a light microscope. For the apilimod/MLSA1 matrix assay using LacZ MLVs, HT1080 cells were seeded in white bottom 96-well plates (Thermo) and grown to approximately 50% confluence. Cells were incubated with inhibitors and infected with viruses as above. LacZ+ cells were quantitated 72 hours post-infection using the Beta-glo Assay System (Promega) according to manufacturer

protocol. For infections by MLVs encoding GFP, HT1080 cells were seeded in 96-well plates and grown to approximately 50% confluence. Cells were incubated in inhibitors and virus as above and wells were imaged for GFP-expressing cells using an incucyte ZOOM cell analysis system (Essen Biosciences). Cytotoxicity of the drugs was measured using the metabolic activity assay Cell Titer-Glo (Promega), following the manufacturer protocol.

For infection with replication-competent EBOV, black 96-well plates with glass bottom wells (Matrix) were coated with poly-lysine prior to seeding with Vero cells. After 48 hours, the culture medium was removed and cells were pretreated with inhibitors in DMEM with 1% FBS for 1 hour. Ebola virus (strain Mayinga) expressing GFP was added to each inhibitor and virus-inhibitor mixtures were incubated for 15 minutes at room temperature. Virus-inhibitor mixtures were then added to cells to provide a final MOI of 1. Control wells contained virus diluted in DMEM with 1% FBS or medium only. GFP expression was read daily after infection using a BioTek Synergy/HTX plate reader. All experiments with EBOV were performed in the Biosafety Level 4 facility at the National Microbiology Laboratory of the Public Health Agency of Canada in Winnipeg.

Fluorescence microscopy

For immunofluorescence experiments, HT1080 cells were seeded onto 18 mm coverslips and grown to approximately 60% confluence. Cells were pre-incubated in DMSO or 50nM apilimod for 1 hour prior to infection. Fusion deficient (GP^{F535R}) ΔM EBOV VLPs expressing GFP were spinoculated onto cells (250xg, 1 hour) at 4°C to allow binding but not endocytosis. Cells were then immediately incubated in pre-warmed (37°C) media with inhibitors for 3 hours, at which point cells were fixed in formalin, permeabilized with 0.5% triton X-100, and blocked in 20% FBS for 30 minutes. Cells were then incubated in an NPC1 antibody, or EEA1 and Rab7

antibodies for 1 hour followed by incubation with the appropriate secondary antibodies (Thermo) for 1 hour, Hoechst staining and mounting in PermaFluor Aqueous Mounting medium (Thermo). Immunofluorescence images were captured on an LSM800 Zeiss confocal microscope using a 63X/1.4 Oil Plan-Apochromat objective. Ten to fifteen Z-stacks were acquired per image, with a pixel size of 0.05µm for NPC1 stained images and 0.22µm for EEA1/Rab7 stained images.

The 2XML1N WT and mutant probes were kind gifts of Dr. Rob Parton, University of Queensland (Addgene plasmids # 67796 and 67797) (359). Vero cells were seeded to approximately 80% confluence and transfected with the 2XML1N-GFP and FYVE-RFP probes at a 1:1 ratio using Lipofectamine 2000 according to manufacturer protocol. For experiments including red dextran (MW 10 000, Thermo), cells were only transfected with the 2XML1N-GFP probe. Twenty-four hours post-transfection, cells were seeded into coverglass bottom 8-chamber slides (Thermo) and grown to approximately 60% confluence, and incubated with EGF, apilimod, VLPs, or red dextran (10 µg/mL) in phenol red- and serum-free medium for 30 minutes. Cells were imaged live on an LSM800 Zeiss confocal microscope equipped with an environmental chamber to maintain a humidified environment of 37°C, 5% CO_2. Images were captured using a 63X/1.4 Oil Plan-Apochromat objective, and ten to fifteen Z-stacks were acquired per image, with a pixel size of 0.19µm.

Image and statistical analyses

Image analysis was performed using Imaris software (Bitplane). For quantitation of VLPs, VLPs were modeled as GFP+ puncta with a diameter of 0.35 µm or greater. For determination of colocalization with NPC1, VLPs were assigned colocalization values based on intensity correlation to NPC1, and colocalization threshold manually determined for each

experiment. The same threshold was used for both DMSO and inhibitor-treated cells in each experiment. Percentage of VLPs colocalized to NPC1 was then determined by dividing the number of VLPs above the colocalization threshold by the total VLP count per image. For determination of number of internalized VLPs per cell, cell boundaries were modeled using cell fluorescence background intensity (647nm), and VLPs were modeled as described above. For quantitation of 2XML1N-GFP labelled puncta, GFP+ puncta were modeled as objects with a diameter of 1–1.5 µm, and cell volume was determined using cell fluorescence background intensity (510nm).

Data are presented as mean ± S.D. and are representative of three independent experiments unless stated otherwise. Statistical analysis was performed by unpaired t-test with Welch's correction, and statistical significance determined using the Holm-Šídák method. *$p<0.05$, ** $p<0.01$, *** $p<0.001$.

3.6 Acknowledgements

We would like to thank Chloë van Oostende, Skye McBride and the uOttawa Cell Biology & Image Acquisition Core Facility for assistance with imaging, Dr. Ryan Russell for assistance with the PI probes and Dr. Assia Shisheva for critical reading of this manuscript. S.Q. is supported by a scholarship from the Natural Sciences and Engineering Research Council of Canada (NSERC). M.C. is a Canada Research Chair in Molecular Virology and Antiviral Therapeutics. This work was supported by a grant to M.C. by NSERC. Work performed by R.K. and G.K. was supported by CIHR (grant # 143521) and the Public Health Agency of Canada, and work performed by D.K. and A.L. was supported by the Public Health Agency of Canada.

Chapter 4: Investigation of the PIKfyve-ArPIKfyve-Sac3 cellular interactome

Shirley Qiu[1,2,3], Mathieu Lavallée-Adam[1,2,3], Marceline Côté[1,2,3]

[1] Department of Biochemistry, Microbiology and Immunology, University of Ottawa, Ottawa, Canada

[2] Ottawa Institute of Systems Biology, University of Ottawa, Ottawa, Canada

[3] Centre for Infection, Immunity, and Inflammation, University of Ottawa, Ottawa, Canada

Author contributions: Experiments were designed by MC and SQ. Liquid chromatography–tandem mass spectrometry (LC-MS/MS) and MaxQuant analysis were performed by Dr. Lawrence Puente at the OHRI Proteomics Core Facility. All other experiments and analysis were performed by SQ. Figures were produced by SQ. Manuscript was written by SQ and edited by SQ, MLA and MC.

4.1 Abstract

Conversion between phosphatidylinositol-3-phosphate and phosphatidylinositol-3,5-bisphosphate on endosomal membranes is critical for maturation of early endosomes to late endosomes/lysosomes, and is regulated by the PIKfyve-ArPIKfyve-Sac3 (PAS) complex. Despite the importance of the PAS complex for endosomal homeostasis and cell survival, there is still little known about how PAS activity is regulated or how it coordinates its activity with other cellular proteins. In this study, we screened for the cellular interactome of the PAS complex using proximity-dependent biotin labelling (BioID). After independently screening the interactomes of ArPIKfyve and Sac3, we identified 89 high confidence protein hits shared by both proteins. Network and functional enrichment analysis of these hits revealed pathways with known involvement of the PAS complex, including vesicular organization and PI3K/Akt signalling, as well as potentially novel pathways, such as cell cycle and mitochondrial regulation. Interestingly, we also identified two subunits of the coatomer complex I (COPI), a golgi-associated complex with an emerging role in endosomal dynamics. We validated the specific interaction between ArPIKfyve and COPI subunit COPB1 via immunofluorescence and proximity ligation assays. Furthermore, this interaction was insensitive to treatment with brefeldin A or the PIKfyve inhibitor apilimod, suggesting that the COPI-PAS interaction is not dependant on PIKfyve mediated PtdIns(3,5)P_2 production or a Brefeldin A sensitive guanine nucleotide exchange factor (GEF). Taken together, these results provide insight into the PAS complex interactome, including the first known interactome study of Sac3, and provide preliminary evidence of interaction between the PAS and COPI complexes.

4.2 Introduction

Endosomal trafficking is a dynamically regulated process dependent on precise coordination between membrane-associated proteins and lipids embedded in endosomal membranes. Phosphoinositide lipids (PIs) are a group of seven signalling lipids, each of which possesses a unique subcellular distribution and entourage of effector proteins. Each PI contains an inositol head group which can be phosphorylated or dephosphorylated on its D3, D4, and/or D5 positions. The interconversion between the seven PI species, catalyzed by specific lipid kinases and phosphatases, enables dynamic recruitment of effector proteins and thus control of both organelle identity and function (244,360–363).

The conversion between phosphatidylinositol-3-phosphate (PtdIns3P) and phosphatidylinositol-3,5-bisphosphate (PtdIns(3,5)P_2) is a key event for the maturation of early endosomes to late endosomes and lysosomes. PtdIns3P and PtdIns(3,5)P_2 dynamics are regulated by the PIKfyve-ArPIKfyve-Sac3 (PAS) ternary complex, composed of the lipid kinase PIKfyve, lipid phosphatase Sac3 (also known as Fig4), and the scaffolding protein ArPIKfyve (associated regulator of PIKfyve, also known as Vac14). The PAS complex is recruited to PtdIns3P-enriched early endosomal membranes via an N-terminal FYVE domain found on PIKfyve (256). PIKfyve catalyzes the phosphorylation of PtdIns3P to PtdIns(3,5)P_2, which is reversibly dephosphorylated by Sac3 to regenerate PtdIns3P. Recent structural characterization of the PAS complex has revealed it to be composed of a pentamer of ArPIKfyve, with one copy each of PIKfyve and Sac3 (262). In addition to their lipid kinase and phosphatase activities, PIKfyve and Sac3 can also modulate each other's activity within the complex via PIKfyve autophosphorylation and dephosphorylation of PIKfyve by Sac3 (262). The mechanisms by which this is regulated are unknown.

Production of PtdIns(3,5)P_2 on endosomal membranes is a crucial precursor to endosomal maturation and eventual delivery of endocytosed cargo to endolysosomes for degradation. Cells with reduced PtdIns(3,5)P_2 levels can be characterized by the formation of aberrantly enlarged cytoplasmic vacuoles. *In vivo*, dysfunction of the PAS complex has been implicated in a number of neurological and motor diseases, including Charcot-Marie Tooth Disease Type 4J, Yunis-Varón Syndrome, and Amyotrophic Lateral Sclerosis (269,334–337,364). In addition to its central role in endosomal maturation, the PAS complex is involved in regulating diverse cellular trafficking pathways, including endosome-to-golgi retrograde transport (332,365), autophagy (331,333,366–368), and toll-like receptor (TLR) localization (348,369,370). In addition, the PAS complex plays a key role in the entry of a number of viruses dependent on trafficking to late endosomal compartments, including Ebola virus and Vaccinia virus, as well as in the persistence and replication of endosomal pathogens such as *Salmonella* (205,296,306,357).

Despite the critical role of this complex in maintaining cellular homeostasis, the mechanisms of action underlying its regulation as well as its effector functions remain elusive. In particular, the cellular interactome of the PAS complex in metazoan cells has been relatively uncharacterized. Previous reports examining ArPIKfyve have identified possible interactions with endolysosomal regulators such as Rab9, the homotypic fusion and vacuole protein sorting (HOPS) complex, and amyloid precursor protein (APP) (371–373). However, these studies relied on co-immunoprecipitation of interacting proteins, which likely represent a fraction of the true ArPIKfyve interactome due to the limited ability of co-IP techniques to capture weak and/or transient PPIs.

In this study, we used BioID, a sensitive and high throughput proximity-based labelling method, to investigate the cellular interactome of the PAS complex (374–376). Using ArPIKfyve

and Sac3 birA fusion proteins, we were able to identify 89 high confidence protein interactions shared by both proteins. Gene ontology analysis of these hits returned pathways known to involve PAS activity, such as the PI3K/Akt signalling pathway and phosphoinositide metabolism, as well as pathways not previously known to involve the PAS complex, such as cell cycle regulation. Interestingly, consistent with an ArPIKfyve interactome study performed by Schulze et al. (373), we recovered COPB1 and COPG1, members of the coatomer complex I (COPI). COPB1 was also identified in a screen for PtdIns(3,5)P_2 interacting proteins (377), providing further evidence of a possible interaction between these two membrane associated complexes. While COPI is well characterized as coat protein complex involved in retrograde golgi transport, there is evidence that at least some COPI subunits are recruited to endosomal membranes and participate in endosome function and dynamics (378,378–383). Using the highly sensitive proximity ligation assay (PLA), we confirmed an interaction between COPB1 and ArPIKfyve. This interaction was not sensitive to treatment with apilimod (an inhibitor of PIKfyve kinase activity) or Brefeldin A (an inhibitor of Arf1, a GTPase required for COPI assembly on golgi membranes), suggesting that the PAS-COPI interaction is not dependant on PtdIns(3,5)P_2 production or Arf1 in a Brefeldin A-sensitive manner. Taken together, our BioID screen has revealed a largely overlapping ArPIKfyve and Sac3 interactome, with both previously identified and novel potential protein interactions in numerous cellular pathways. In particular, we highlight the COPI complex as a potential functional interactor of the PAS complex on endosomal membranes, which may play a role in the mechanism by which COPI regulates endosome function.

4.3 Results

4.3.1 Validation of BioID fusion proteins

BioID protein-protein interaction (PPI) screening relies on the fusion of birA*, a modified promiscuous biotin ligase derived from *Escherichia coli* (R118G mutation, hereafter referred to as simply birA), and the protein of interest. Expression of this fusion protein in cells results in proximity-based biotinylation of vicinal proteins, which can then be isolated using streptavidin affinity purification and identified by mass spectrometry (Fig. 4.1A). Due to the difficulty of expressing exogenous PIKfyve in cells, we focused on generating ArPIKfyve and Sac3 birA fusion proteins, using a previously described myc-birA construct (375). BirA was fused at the N-terminus and expression was validated in 293T cells by probing lysates from transfected cells with anti-myc and antibodies recognizing ArPIKfyve and Sac3 (Fig. 4.1B). Next, in order to assess whether the fusion proteins were functional in their roles within the PAS complex, we used our previously established ArPIKfyve and Sac3 CRISPR knockout (KO) cells (296). A characteristic phenotype of depletion of any subunit of the PAS complex is the formation of enlarged cytoplasmic vacuoles, concomitant with reduced PtdIns(3,5)P_2 levels. Previous characterization of the ArPIKfyve and Sac3 CRISPR cells has shown that the vacuole phenotype can be ablated by expressing the WT protein *in trans*, which is a qualitative indication of restoration of PAS functionality (296). We found that transfection with plasmids encoding the birA fusion proteins into their respective KO cells reduced the vacuole phenotype, confirming their functionality in cells (Fig. 4.1C).

Next, we assessed biotin labelling by expressing birA-ArPIKfyve and birA-Sac3 in 293T cells (birA alone was used as a control) and performing a biotin labelling time course (15 min to 18 hrs). Cell lysates were probed with streptavidin-HRP to visualize biotinylated proteins. Consistent with previous studies on birA labelling (375,384,385), we observed an optimal

labelling time of 18 hrs for all birA constructs (Fig. 4.1D). As expected, the birA-ArPIKfyve and birA-Sac3 proteins shared some similarities in labelling patterns consistent with their close interaction and potentially overlapping interactomes, while still each displaying a unique general labelling pattern.

4.3.2 BioID screen and SAINT analysis reveal overlapping ArPIKfyve and Sac3 interactomes

To screen for the cellular interactome of each protein, birA-ArPIKfyve or birA-Sac3 were transfected into 293T cells. To retain the stoichiometry of the PAS complex, the birA fusion proteins were co-transfected with the other PAS subunits (PIKfyve and either ArPIKfyve or Sac3). Cells transfected with birA alone were used as a negative control. Twenty-four hours post transfection, cells were incubated overnight (18h) in biotin, and biotinylated proteins were subsequently isolated using streptavidin agarose beads. Following extensive washing, beads were boiled in SDS loading buffer, and proteins were resolved by SDS-polyacrylamide gel electrophoresis (SDS-PAGE), trypsin digested in-gel, and peptides were analysed by LC-MS/MS.

Maxquant analysis of three independent BioID experiments yielded a total of 930 identified prey proteins using ArPIKfyve-birA as bait, and 944 proteins using Sac3-birA as bait. Importantly, PIKfyve was captured by both ArPIKfyve and Sac3 baits as a top prey protein by spectral count, in part validating that the birA fusion proteins were expressed in the appropriate location within cells and in the same subcellular complex.

Statistical analysis of the protein hits was performed using SAINT (Significance Analysis of INTeractome), which uses label free quantitative information to score probability of specific

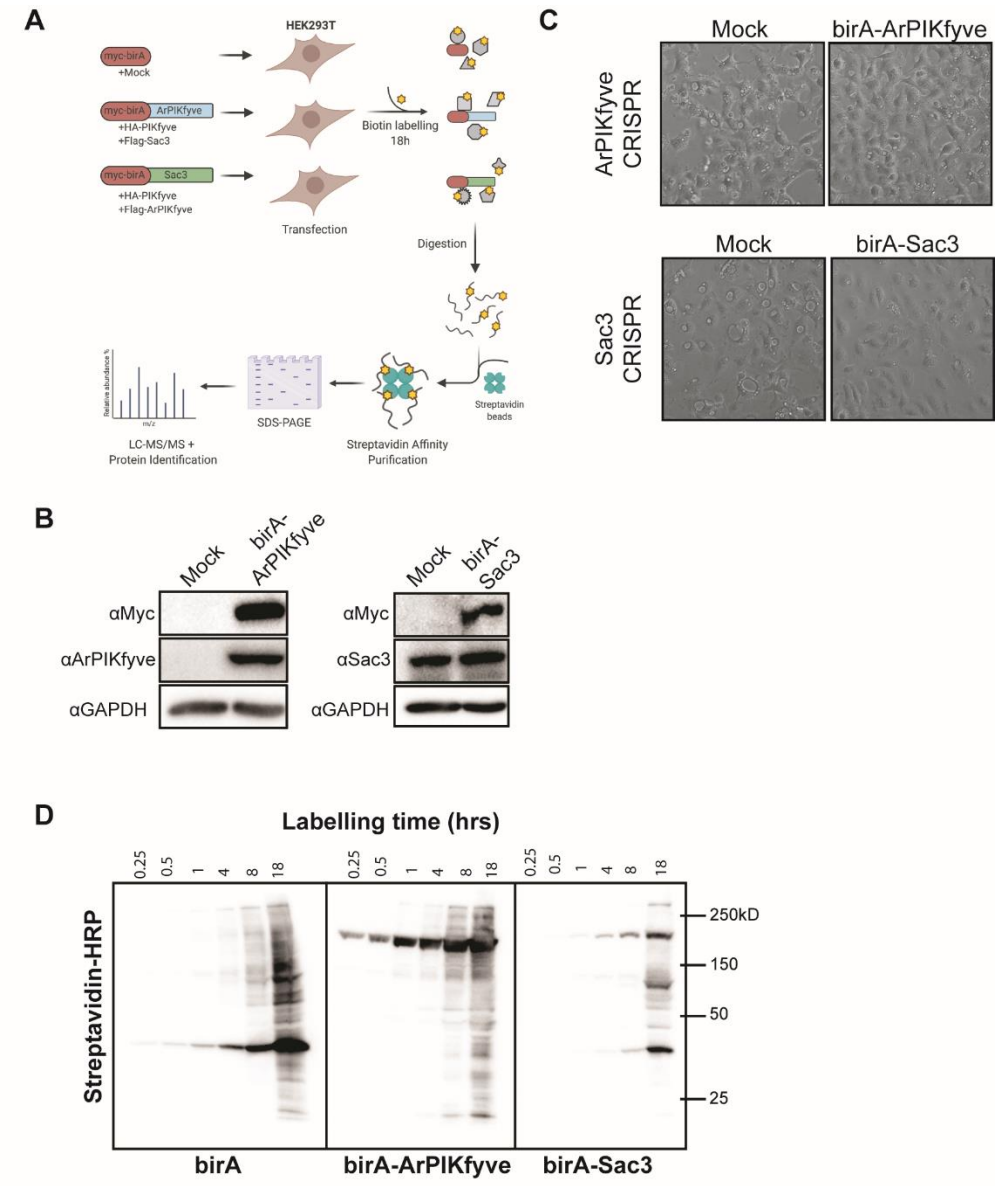

Figure 4.1. A proximity biotin labelling approach to investigate the ArPIKfyve and Sac3 cellular interactome

(A) Schematic of the BioID assay using birA-ArPIKfyve and birA-Sac3 fusion proteins. Created with Biorender.com (B) HEK293T cells were transfected with plasmids encoding birA-ArPIKfyve and birA-Sac3 fusion constructs. Cells were lysed and expression of myc-birA and ArPIKfyve/Sac3 was detected by immunoblot using specific antibodies (C) birA-ArPIKfyve, birA-Sac3 or birA alone (mock) were transfected into ArPIKfyve or Sac3 CRISPR knockout HT1080 cells. Cells were imaged pre- and post-transfection by phase contrast microscopy to visualize cytoplasmic vacuoles. (D) birA, birA-ArPIKfyve, or birA-Sac3 were transfected into HEK293T cells. Cells were incubated with biotin (50µM) for 0.25–18 hours, lysed, and biotin-labelled proteins were detected by immunoblot using streptavidin-HRP.

vs nonspecific interactions (386). Proteins captured using birA alone as bait were incorporated as a control dataset to control for background interactions. SAINT analysis yields a SAINT probability (SP) score for each protein identified in the screen, and a SP score ≥ 0.9 was used to further screen hits for both the ArPIKfyve and Sac3 baits. This yielded 146 and 190 high confidence hits for ArPIKfyve and Sac3, respectively (Fig. 4.2A,B). Of these, 89 proteins were shared by both ArPIKfyve and Sac3, indicating a substantial overlap in their respective interactomes (Fig. 4.2A). As expected, the top three SAINT hits for both proteins were the three subunits of the PAS complex, further validating the robustness of the BioID assay.

In order to gain an overview of the cellular localization of the top SAINT hits for ArPIKfyve and Sac3, we performed a Gene Ontology analysis based on cellular component for the high confidence hits for each bait. This revealed the hits for each protein to be broadly distributed throughout the cell, while being primarily associated with membranes and membrane-bound organelles, consistent with the PAS complex's known membrane-associated functions, such as endosomal maturation, autophagy regulation, and endosome-to-golgi retrograde transport (Fig. 4.2C).

We also cross-referenced our complete list of ArPIKfyve and Sac3 BioID hits with two previous studies examining the ArPIKfyve interactome (Schulze et al, (373)) and the PtdIns(3,5)P_2 interactome (Catimel et al, (377)) (Fig. 4.2D). We elected to compare all identified hits for ArPIKfyve and Sac3 instead of the top SAINT hits in order to account for different methodologies and stringency levels in screening interactome hits in the three studies. This revealed that 19% of the total BioID hits for ArPIKfyve and Sac3 were also uncovered by one or both of Schulze et al. and Catimel et al. These included selected proteins of interest highlighted by the respective authors, including NSF (Sac3 SP, 0.84; ArPIKfyve SP, 0.36), TBC1D15 (Sac3

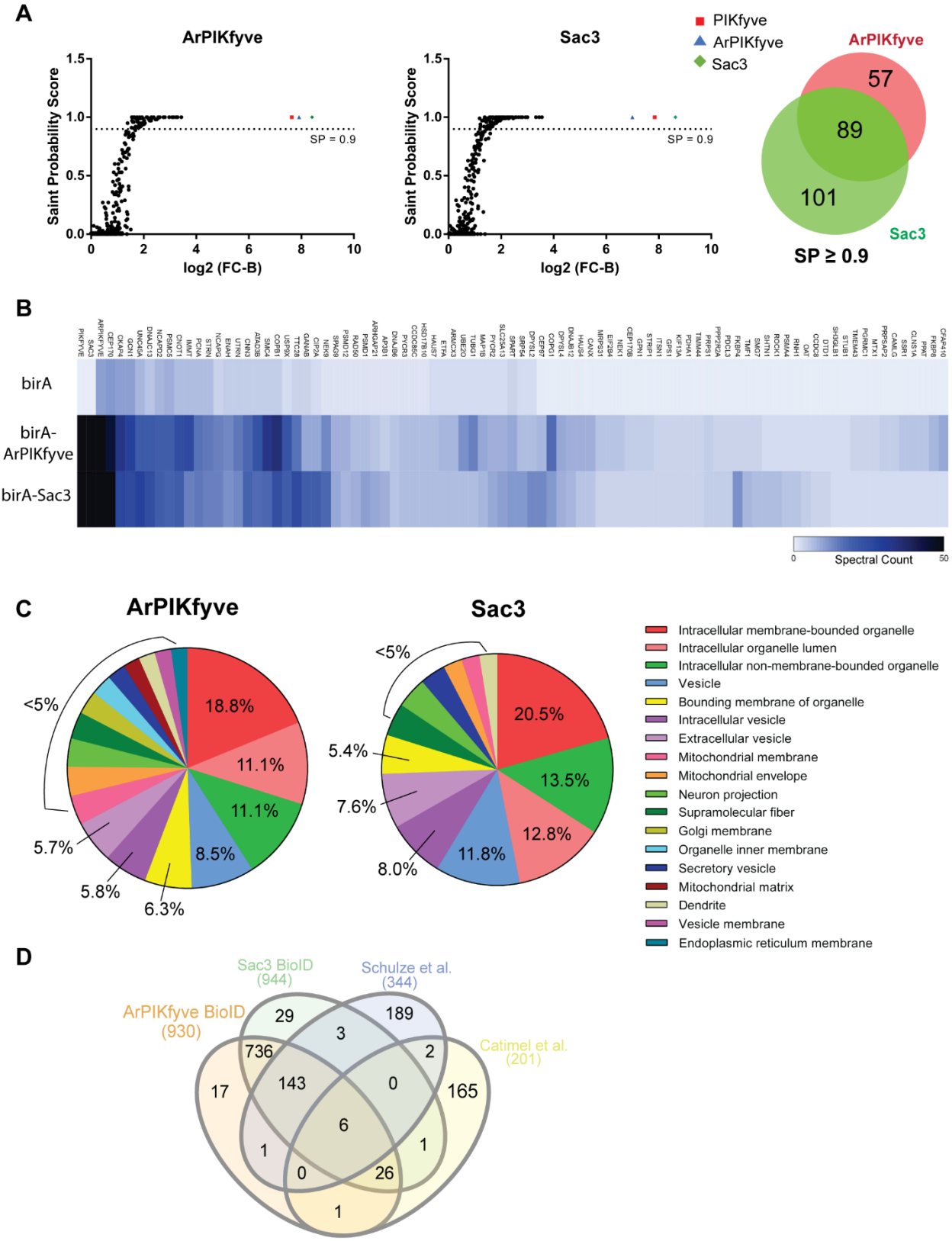
A
ArPIKfyve
Sac3
Saint Probability Score
log2 (FC-B)
SP = 0.9
PIKfyve
ArPIKfyve
Sac3
57
89
101
SP ≥ 0.9
B
birA
birA-ArPIKfyve
birA-Sac3
Spectral Count
C
ArPIKfyve
Sac3
<5%
18.8%
11.1%
11.1%
8.5%
6.3%
5.8%
5.7%
20.5%
13.5%
12.8%
11.8%
8.0%
7.6%
5.4%
Intracellular membrane-bounded organelle
Intracellular organelle lumen
Intracellular non-membrane-bounded organelle
Vesicle
Bounding membrane of organelle
Intracellular vesicle
Extracellular vesicle
Mitochondrial membrane
Mitochondrial envelope
Neuron projection
Supramolecular fiber
Golgi membrane
Organelle inner membrane
Secretory vesicle
Mitochondrial matrix
Dendrite
Vesicle membrane
Endoplasmic reticulum membrane
D
Sac3 BioID (944)
Schulze et al. (344)
ArPIKfyve BioID (930)
Catimel et al. (201)
29
189
3
736
2
17
143
0
165
6
1
1
0
26
1

Figure 4.2. SAINT analysis reveals overlapping ArPIKfyve and Sac3 interactomes

(A) Scoring of hits from the ArPIKfyve and Sac3 BioID screens was performed using SAINT (Significance Analysis of INTeractome) within the CRAPome online interface (389). Scatter plots display each hit as a function of its saint probability (SP) score vs its fold change in spectral count over the birA negative control (FC-B). Inset venn diagram displays overlapping BioID hits for ArPIKfyve and Sac3 with a SP ≥ 0.9. (B) Heat map showing spectral counts for the high confidence BioID hits (SP ≥ 0.9) for ArPIKfyve and Sac3 (compared to birA control). Generated using ProHits-viz (390). (C) Pie chart displaying the top represented cellular component Gene Ontology (GO) terms for the high confidence BioID hits for ArPIKfyve and Sac3. Percentages represent the number of genes annotated with each term over the total number of annotated genes. Charts were generated using Blast2GO (391). (D) Venn diagram displaying overlaps of ArPIKfyve and Sac3 BioID screen hits with hits from an ArPIKfyve interactome screen (Schulze et al., (373)) and a PtdIns(3,5)P_2 interactome screen (Catimel et al., (377)). Diagram generated using InteractiVenn (392).

SP, 0.72; ArPIKfyve SP, 0), GAPVD1 (Sac3 SP, 0.82; ArPIKfyve SP, 0.19) (which were identified in our BioID screen but did not meet the SAINT cut-off probability score), and members of the COPI complex: COPA (Sac3 SP, 0.12; ArPIKfyve SP, 0.81), COPB1 (Sac3 SP, 1; ArPIKfyve SP, 1), and COPB2 (Sac3 SP, 0.8; ArPIKfyve SP, 0.39). Interestingly, while we expected the greatest overlap to be between the ArPIKfyve BioID hits and the Schulze et al. ArPIKfyve interactome study hits, we found instead that the largest overlap included both ArPIKfyve and Sac3 BioID hits and hits from the Schulze et al. study (143 proteins), further signifying a largely shared ArPIKfyve and Sac3 proximal and potentially functional interactome (Fig. 4.2D).

4.3.3 Network and gene ontology analysis of BioID screen hits

In order to narrow down proteins and pathways of interest within the ArPIKfyve and Sac3 shared interactome, we used the Prize-collecting Steiner Forest (PCSF) approach to model a network using the top SAINT hits shared by both proteins (387,388). PCSF is a graph theory problem described as follows: given an undirected graph **G = (V, E)**, where the vertices are labeled with prizes p_v and the edges are labeled with costs $c_e > 0$, the goal is to identify a subnetwork **G′ = (V′, E′)** with a forest structure, minimizing the total edge costs in E′, the total node prizes left out of V′, and the number of trees in G′.

Applied to biological networks, PCSF aims to identify compact and biologically relevant subnetworks. The vertices, or nodes, represent biomolecules (such as proteins), and every edge corresponds to the cellular interaction between two biomolecules. The PCSF approach is becoming increasingly popular for the analysis of large "-omics" datasets, and is advantageous for uncovering subnetworks missed by traditional network analysis methods due to its ability to reduce bias towards pathways surrounding "hub vertices" that have a large number of reported

interactions (393,394). In addition, PCSF returns networks containing both terminal vertices (representing proteins from the experimental dataset) as well as Steiner vertices (representing proteins that link subnetworks but are not present in the experimental dataset). The number of Steiner vertices returned can be adjusted based on the desired stringency of the algorithm, and is useful for identifying proteins missed by experimental assays that may still be functionally related to the protein or pathway of interest.

For our BioID data, prizes were assigned to proteins based on their SP score. Costs were assigned based on the frequency of interaction between two proteins, using PPI data from the STRING protein interaction database (395). In order to further cluster the resulting subnetwork into functional groups, we performed functional enrichment analysis using EnrichR (396), which returned 8 clusters grouped by biological processes (Fig. 4.3). Table 4.1 outlines the genes in each cluster and a selection of the top biological process GO terms for each group.

Examining the biological processes within the 8 clusters, we recognized four broader cellular processes: intracellular trafficking (clusters 1, 2, 3, 7), cell growth and survival signalling (clusters 4, 5), neuron function (clusters 1, 5), and cell cycle/DNA regulation (clusters 1, 4, 5, 6, 8). Within these processes we identified pathways with known direct involvement of the PAS complex, such as vesicle organization (cluster 2), phosphoinositide regulation (cluster 7), and PI3K/Akt signalling (cluster 4). We also observed pathways in which PAS complex activity has been indirectly implicated, including synaptic vesicle function and NCAM signalling (371,372,397,398), and insulin receptor signalling (399–401).

Interestingly, we observed multiple pathways related to cell cycle and DNA regulation, as well as regulation of golgi trafficking. There is little known about whether and how the PAS complex is involved in these processes. We were particularly intrigued by cluster 2, which

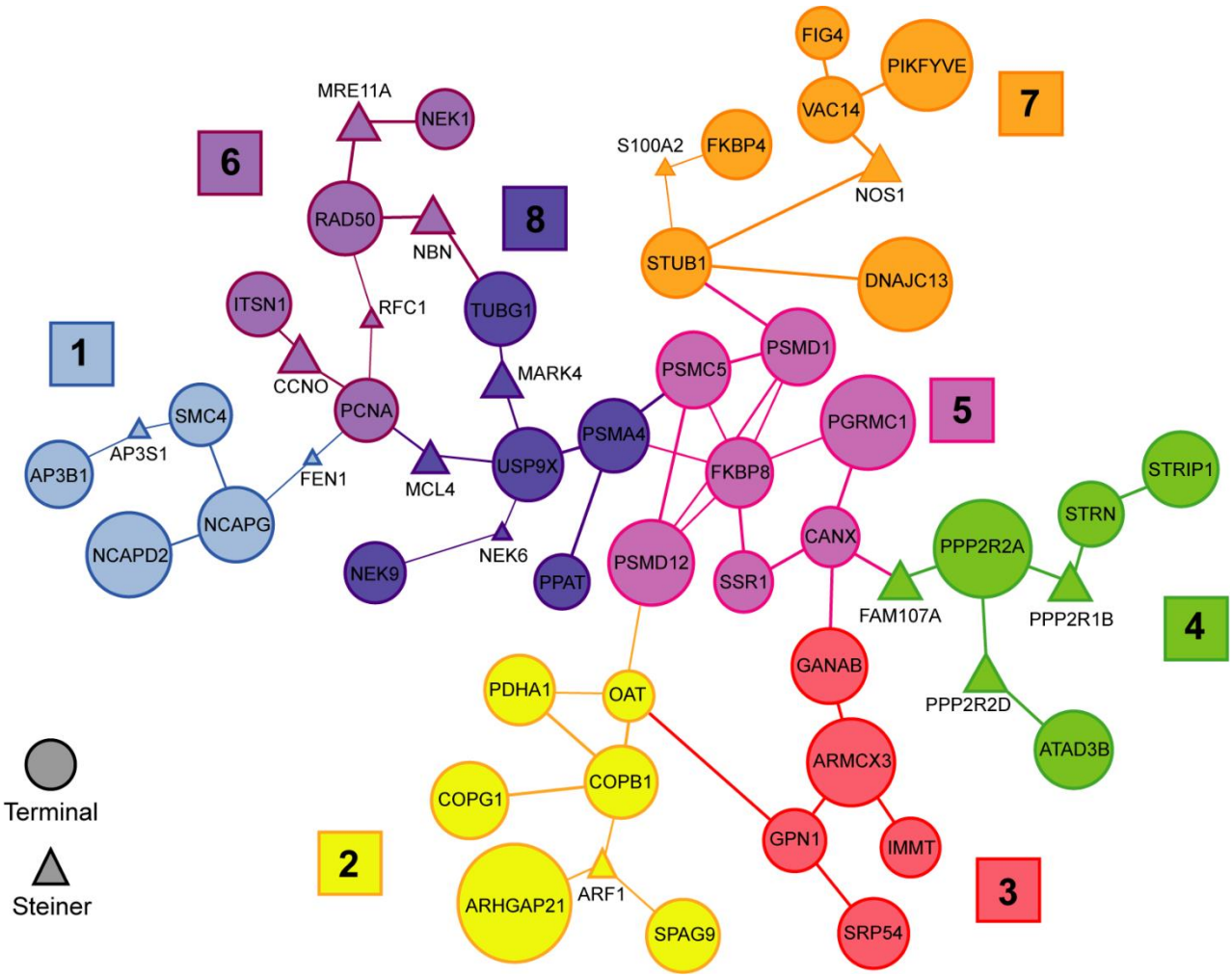

Figure 4.3. Functional network analysis of the top shared ArPIKfyve and Sac3 BioID hits using the Prize Collecting Steiner Forest (PCSF) algorithm

Final PCSF subnetwork of high confidence BioID hits shared between ArPIKfyve and Sac3 (SP ≥ 0.9), clustered by Gene Ontology (GO) biological processes using EnrichR. The vertex sizes and edge widths are proportional to the amount of times that a vertex or edge appeared in the PCSF runs. The network contains terminal vertices (representing proteins from the BioID screens) as well as Steiner vertices (representing proteins that link subnetworks but were not present in the BioID dataset). Clusters are described in Table 1.

Table 4.1. Top gene ontology (GO) biological process enrichment terms for the PCSF network

Cluster	GO Term	P-Value	Genes
1	Mitotic cell cycle	0.00206	FEN1, NCAPG, NCAPD2, SMC4, AP3S1, AP3B1
	DNA conformation change	0.00242	
	Anterograde synaptic vesicle transport	0.00666	
	Golgi Associated Vesicle Biogenesis	0.0272	
	Clathrin derived vesicle budding	0.0343	
	Trans-Golgi Network Vesicle Budding	0.0392	
2	COPI-dependent Golgi-to-ER retrograde traffic	0.00169	ARF1, ARHGAP21, COPB1, COPG1, OAT, PDHA1, SPAG9
	COPI-mediated anterograde transport	0.00302	
	Vesicle organization	0.00871	
	Asparagine N-linked glycosylation	0.0158	
3	Mitochondrial calcium ion homeostasis	1	GANAB, ARMCX3, GPN1, IMMT, SRP54
	Intracellular protein transmembrane transport	1	
	Protein transmembrane transport	1	
4	PI3K-Akt signaling pathway	0.00479	PPP2R1B, PPP2R2D, PPP2R2A, STRN, ATAD3B, FAM107A, STRIP1
	M Phase	0.0245	
	Cyclin D associated events in G1	0.0281	
5	NCAM signaling for neurite out-growth	0.00102	PSMC5, PSMD12, PSMD1, SSR1, CANX, FKBP8, PGRMC1
	M Phase	0.00104	
	MAPK family signaling cascades	0.00121	
	Insulin receptor signalling cascade	0.00124	
	Regulation of G1/S transition of mitotic cell cycle	0.00126	
	Signaling by Wnt	0.00128	
	Signal transduction by p53 class mediator	0.00128	
6	Translesion synthesis by POLK	0.001	RAD50, PCNA, RFC1, MRE11A, NBN, CCNO, NEK1, ITSN1
	PCNA-Dependent Long Patch Base Excision Repair	0.00107	
	Regulation of TP53 Activity	0.0011	
	Lagging Strand Synthesis	0.00116	
	Telomere C-strand (Lagging Strand) Synthesis	0.0013	
	Resolution of AP sites via the multiple-nucleotide patch replacement pathway	0.00133	
	Gap-filling DNA repair synthesis and ligation	0.00138	
	Cell Cycle Checkpoints	0.00154	
	Non-homologous end-joining	0.0016	
7	Phosphatidylinositol biosynthetic process	0.0183	FIG4, VAC14, PIKFYVE, NOS1, STUB1, DNAJC13, S100A2, FKBP4
	Phosphatidylinositol-3-phosphate biosynthetic process	0.019	
	Myelin assembly	0.02	
	Glycerophospholipid biosynthetic process	0.039	
8	Activation of NIMA Kinases	0.00449	NEK9, PSMA4, NEK6, TUBG1, MARK4, PPAT, USP9X, MCL1
	Cell Cycle	0.0207	
	Nuclear Pore Complex (NPC) Disassembly	0.0299	
	Nuclear Envelope Breakdown	0.0451	

contains COPB1 and COPG1, members of the COPI complex, a vesicular coat complex involved in retrograde golgi transport, as well as ADP-ribosylation factor 1 (ARF1) (a GTPase required for COPI recruitment to golgi membranes) as a Steiner node. Schulze et al. recovered COPI subunits COPA, COPB2, COPD, and COPE in their ArPIKfyve interactome screen, and Catimel et al. recovered COPB1 and COPZ1 in their PtdIns(3,5)P_2 interactome screen. These concurrent findings strongly suggest some sort of interaction between the PAS complex and the COPI complex. While the COPI complex is associated with golgi trafficking, previous studies have found additional roles for COPI in multivesicular body formation, endosomal maturation, and phagocytosis, although the mechanism of action is still poorly understood (378,378–383). Therefore we decided to further investigate the interaction between the PAS complex and the COPI complex.

4.3.4 Validation of interaction between ArPIKfyve and COPB1

Whether COPI interacts mechanistically with the PAS complex has not been investigated. In addition, little is known about what regulates its recruitment and function on endosomal membranes. To begin examining how COPI interacts with the PAS complex, we used ArPIKfyve as a representative of the PAS complex and COPB1 as a representative of the COPI complex. First, we used immunofluorescence to label endogenous COPB1 and ArPIKfyve in HT1080 cells to examine their localization patterns. As expected, COPB1 displayed a mainly perinuclear, golgi-associated localization pattern, while ArPIKfyve displayed a more diffuse cytoplasmic localization (Fig. 4.4A). While COPB1 endosomal staining was much weaker compared to its perinuclear staining, likely due to the low amount of endosome-associated COPB1 relative to golgi-associated COPB1, there appeared to be a small amount of COPB1 colocalizing with ArPIKfyve.

To gain better resolution of endosomal COPB1, we performed a proximity ligation assay (PLA), a highly sensitive immunofluorescence-based method to detect protein-protein interactions. Briefly, both COPB1 and ArPIKfyve were labelled with their respective primary antibodies, which were then labelled with oligonucleotide-conjugated secondary antibodies (PLA probes). Next, hybridizing connector oligos join the PLA probes only if they are in close proximity to each other and a ligase forms a closed, circle DNA template for rolling-circle amplification by a DNA polymerase. Lastly, labeled oligos hybridize to the complementary sequences within the amplified DNA, which are then visualized and quantified as discrete spots (PLA signals) by microscopy. Compared to the COPB1 and ArPIKfyve single antibody negative controls, adding both antibodies revealed a significant increase in PLA signals (Fig. 4.4B). Furthermore, these signals showed a diffuse localization pattern in cells, suggesting that COPB1-ArPIKfyve interactions occur throughout the cytoplasm, presumably on endosomal membranes.

4.3.5 ArPIKfyve-COPB1 interaction is not brefeldin A sensitive or affected by inhibition of PIKfyve kinase activity

Next, we sought to delineate a possible mechanism underlying the interaction between the PAS complex and COP1 using inhibitors for each complex. First, we tested whether inhibition of PIKfyve kinase activity alters ArPIKfyve-COPB1 association. In order to do so, we repeated the PLA assay after treating cells with apilimod, a potent PIKfyve inhibitor. However, we did not see a significant reduction in PLA signals between COPB1 and ArPIKfyve (Fig. 4.5). Previous reports have indicated that Arf1 GTPase activity is required for recruitment of COP1 to endosomal membranes (379,382). To test whether inhibition of Arf1 alters COPB1-ArPIKfyve interaction, we tested whether brefeldin A, which inhibits guanine nucleotide exchange factors (GEFs) required for Arf1 activation, alters PLA signals between COPB1 and ArPIKfyve. However, we did not observe a significant change with Brefeldin A treatment (Fig. 4.5),

suggesting that either Arf1 is not required for COPB1-ArPIKfyve interaction or that is uses a GEF that is brefeldin A insensitive for recruitment endosomal sites containing ArPIKfyve.

4.3.6 Dynamic detection of protein-protein interactions using TurboID

While BioID is a robust method to screen for the global cellular interactome of a protein of interest, its relatively long overnight labelling time reduces its sensitivity to detect more transient protein-protein interactions that occur during dynamic events such as viral entry or growth factor stimulation. This issue is particularly pronounced for cellular trafficking proteins such as the PAS complex that rapidly dock and release from other proteins to precisely regulate fusion and fission events between endosomal compartments. In order to address these issues, we have also cloned ArPIKfyve and Sac3 fusion constructs with TurboID, a modified biotin ligase that has a labelling time as short as ten minutes (385). When compared side-by-side with their respective BioID fusion constructs, we observed similar labelling efficiency at 15-30 minutes with the TurboID constructs as overnight labelling with the BioID constructs (Fig. 4.6). This drastically shortened labelling time will allow us to capture dynamic and short-lived protein-protein interactions that occur during cell stimulation by growth factors, small molecule inhibitors and virus particles.

4.4 Discussion

Here we present a systemic study of the cellular PAS interactome using BioID. BioID and other proximity-based labelling methods have become powerful tools for PPI screening, with BioID being advantageous for its ability to capture PPIs that are too weak and or/transient to be recovered by traditional co-immunoprecipitation methods, its applicability to both soluble and insoluble proteins, and the strength of the biotin-streptavidin interaction which allows more stringent purification conditions to reduce background contamination. Using this approach, we aimed to uncover novel protein regulators and effectors of the PAS complex.

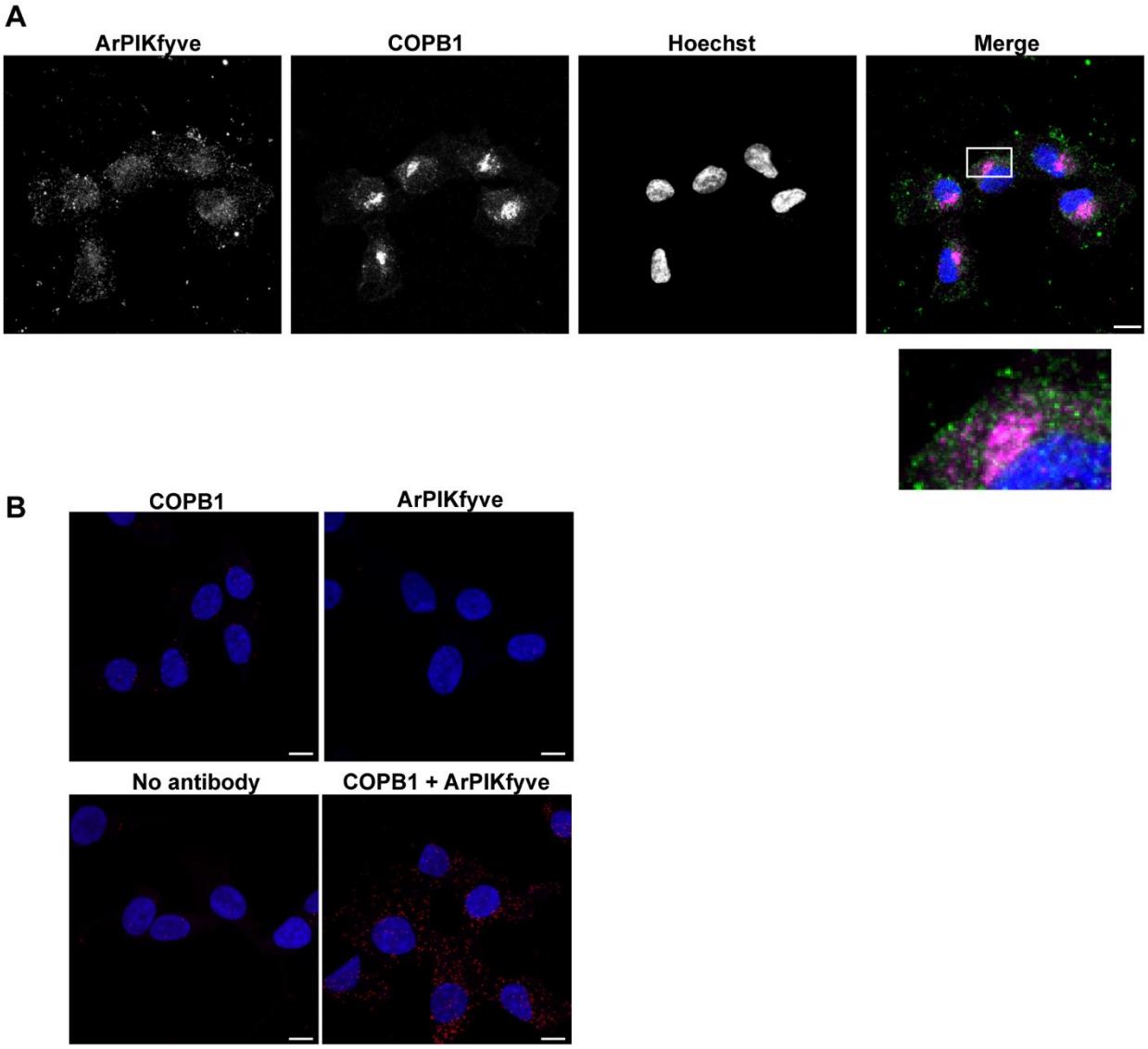

Figure 4.4. Validation of interaction between ArPIKfyve and COPB1 using immunofluorescence and proximity ligation assay (PLA)

(A) Coverslip-bound HT1080 cells were fixed, permeabilized, and stained with ArPIKfyve (green) and COPB1 (magenta) antibodies, and Hoechst. Cells were imaged on an LSM800 confocal microscope (Zeiss). Bar = 10µm. (B) HT1080 cells seeded in angiogenesis chambers were fixed, permeabilized, and PLA was performed according to manufacturer protocol (Sigma) using ArPIKfyve and COPB1 antibodies and Hoechst. Cells were imaged as above. Bar = 10µm.

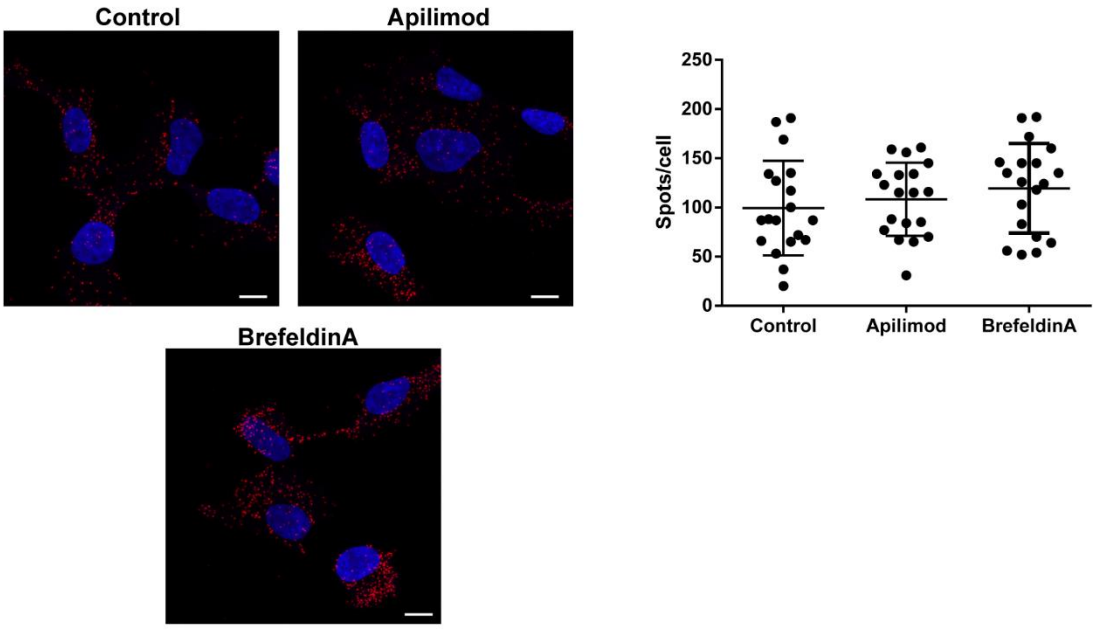

Figure 4.5. COPB1-ArPIKfyve interaction is not sensitive to brefeldin A or PIKfyve enzymatic activity

HT1080 cells seeded in angiogenesis chambers were treated with brefeldin A (50µM), apilimod (50nM) or a control (DMSO) for 1 hour, fixed, permeabilized, and PLA was performed according to manufacturer protocol (Sigma) using ArPIKfyve and COPB1 antibodies and Hoechst. Cells were imaged on an LSM800 confocal microscope (Zeiss). Bar = 10µm. PLA spots were quantitated using Imaris (Bitplane).

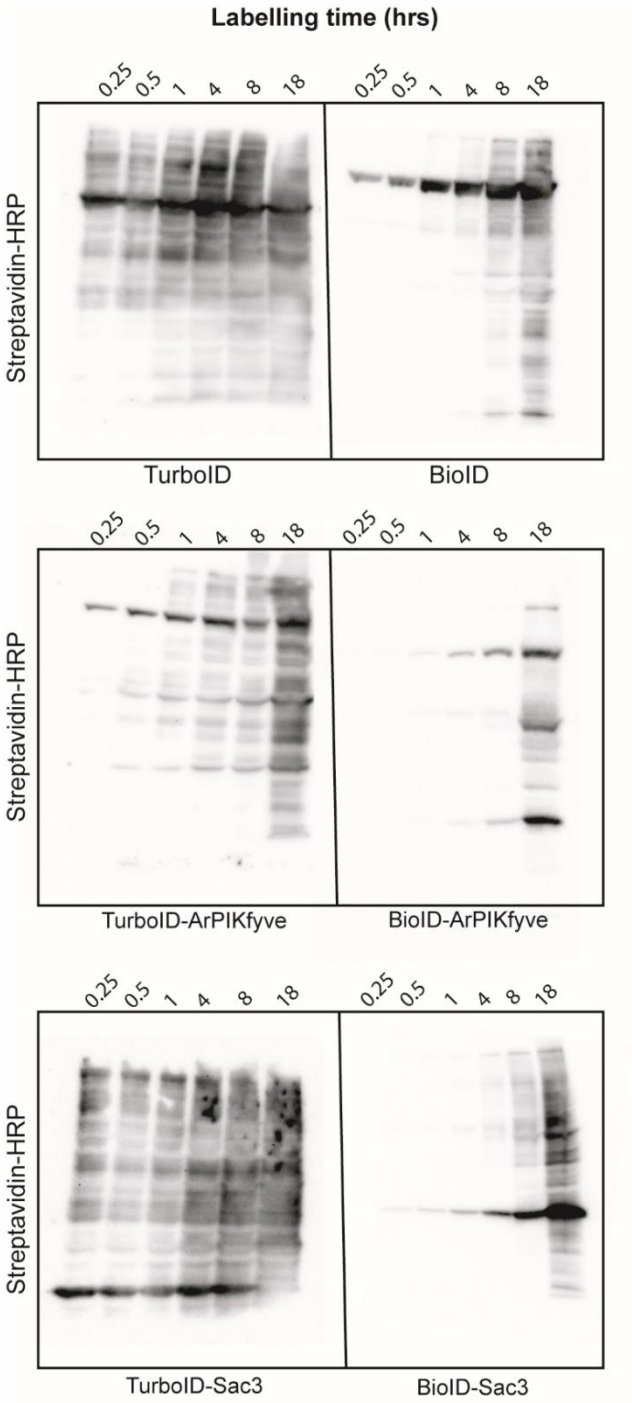

Figure 4.6. Comparison of labelling time for BioID and TurboID biotin ligases

HEK293T cells were transfected with the indicated BioID (birA) or TurboID constructs, followed by incubation in biotin (50µM) for 0.25–18 hours. Cells were then lysed and biotin-labelled proteins were detected by immunoblot using streptavidin-HRP.

In our study we generated birA fusion proteins for both ArPIKfyve and Sac3, which enabled us to screen for interactions specific to each protein, as well as common interactions shared by both. ArPIKfyve shared approximately 61% of its high confidence BioID hits with Sac3, and Sac3 shared approximately 47% of its high confidence BioID hits with ArPIKfyve, suggesting a largely shared interactome for both proteins. This is consistent with previous characterization of the complex demonstrating that association and integrity of the ternary complex is necessary for PIKfyve and Sac3 enzymatic function (262,264,269–271). Sac3 in particular is dependent on associating with ArPIKfyve for stability and protection from proteosome-dependent degradation (269). It is important to note that while the labelling radius of the birA enzyme used in this study is relatively stringent (approximately 10nm), as a purely proximity dependent labelling method, BioID cannot distinguish between direct interactions, indirect interactions, or vicinal non-interacting proteins. Nonetheless, as the first interactome study of the PAS complex to examine two of its subunits side by side, we were interested to examine the common hits of ArPIKfyve and Sac3, which could represent functional regulators or effectors of the PAS complex as a whole and are prime candidates for follow-up validation and characterization.

Two previous studies have examined the PAS complex-related interactome. Schulze et al. examined the ArPIKfyve interactome by expressing Flag-tagged ArPIKfyve in HEK293T cells and purifying co-immunoprecipitated proteins (373). Catimel et al. screened for the PtdIns(3,5)P_2 interactome by incubating cytosolic colon carcinoma cell extracts with PtdIns(3,5)P_2 liposomes and beads and purifying bound proteins, which represent potential PAS interacting proteins, particularly PIKfyve effector proteins (377). Comparison of the 344 and 201 reported hits from Schulze et al. and Catimel et al., respectively, with the 930 ArPIKfyve and 944 Sac3 BioID hits

from our study revealed a substantial overlap with Schulze et al. (143 proteins) and a smaller overlap with Catimel et al. (26 proteins). While it is expected that different methodologies will identify different sets of interactors, we recovered a number of the hits highlighted by Schulze et al. using both birA-ArPIKfyve and birA-Sac3, including TBC1D15, GAPVD1, and NSF, although these did not meet our SAINT threshold. Similarly, we also recovered a number of endosomal trafficking regulators shared with the Catimel et al. study, such as Rab5C, SNX1 and SNX2.

We were particularly interested in following up on the COPI complex, the sole multisubunit trafficking complex to be identified in all three screens. USO1 (general vesicular transport factor p115), which is involved in COPII-mediated anterograde golgi transport, was also one of the few proteins identified in all three screens. Catimel et al. also identified the COPI associated GTPase Arf1 in their screen, which was also present as a Steiner vertex in the PCSF network of our BioID hits. Schulze et al. identified the Arf1 regulators ARL1 and BIG1 in their screen, further evidence of a functional interaction between golgi trafficking factors, primarily the COPI complex, and the PAS complex.

The COPI complex consists of seven core subunits: COPA, COPB1, COPB2, COPD, COPE, COPG and COPZ. Recruitment of the COPI complex to golgi membranes requires the GTPase Arf1, which in turn is regulated by a complement of ArfGEFS and Arf GTPase activating proteins (GAPs) (402,403). Similar to other coat protein complexes such as clathrin coats, COPI facilitates vesicle formation and cargo selection, and operates in the transport of cargo from the trans golgi network to the cis golgi network, as well as from the golgi to the endoplasmic reticulum. While best characterized for its function in retrograde golgi trafficking, accumulating evidence has revealed roles for COPI in the endosomal system. For example,

inhibition of Arf1 by Brefeldin A or depletion of COPI subunits by siRNA were found to disrupt endosomal trafficking, sorting of proteins to the lysosome for degradation, and recycling of internalized cargo such as transferrin receptors and SNAREs (379,381–383,404,405). Similarly, studies using IdIf CHO cells, which harbour a temperature sensitive COPE mutant that is lost at the nonpermissive temperature have also shown that COPE loss is coupled with disruption of endocytic trafficking and endosomal structure (378,381,404).

However, how COPI recruitment to endosomal membranes is regulated is unknown, and a functional interaction between the PAS complex and COPI has been unexplored. Previous studies have reported that COPI recruitment to endosomes is dependent on Arf1, and that Arf1 recruitment to endosomes requires an acidic luminal pH, suggesting that COPI may be specifically recruited to late endosomes and lysosomes (381,382,406). Using a highly sensitive PLA assay, we validated the specific interaction between ArPIKfyve and COPB1. This interaction was not affected by inhibiting PIKfyve kinase activity or by treatment with Brefeldin A. The latter contrasts with previous reports indicating that Arf1 is required for recruitment of COPI to endosomes, however, it is possible that the COPI-PAS interaction occurs independent of Arf1, or engages with an ArfGEF or other Arf GTPase that is Brefeldin A insensitive. Furthermore, it is still unclear whether the PAS-COPI interaction occurs directly or via PtdIns(3,5)P_2, and further work is required to dissect which COPI subunits participate in the interaction. Finally, the functional consequences of PAS-COPI interaction remain to be determined. The fact COPI was captured by three independent interactome screens, as well as the fact that we performed our BioID screen in unstimulated cells suggests some level of basal interaction between the PAS complex and COPI. Whether this interaction can be upregulated or inhibited remains to be determined. A deeper molecular dissection of the PAS-COPI interaction

is warranted in order to understand both the mechanisms underlying the interaction as well as its biological consequences in cells.

BioID is a powerful approach for PPI screening, particularly for the interrogation of trafficking pathways that contain numerous membrane-associated proteins, since the covalent attachment of biotin to proteins allows the use of harsher lysis conditions in order to effectively solubilize membranes. However, there are limitations to this study, pointing to the need of multiple complementary approaches in order to gain a robust interactome map for the PAS complex. First, the relatively long labelling time of the birA enzyme precludes its use for the analysis of rapid changes in PPIs during dynamic events that occur in the time scale of minutes or hours. While this was not a major concern for this interactome study as we were interested in characterizing PAS complex interactions under basal conditions, it would be significantly less efficient at capturing changes in PAS PPIs that occur during dynamic processes such as stimulation by growth factors or pathogens. Secondly, recent structural characterization of the PAS complex has illuminated that the relative orientation of each subunit plays a key role in how PIKfyve and Sac3 access their lipid substrates on membranes and therefore how the complex functions as a whole. Although we validated functional activity of the birA-ArPIKfyve and birA-Sac3 fusion proteins prior to performing the screen, we cannot exclude the possibility that the addition of multiple birA tags within the complex could affect its interactions with other proteins. The use of modified biotin ligases like TurboID and miniTurbo, which are smaller than birA and display comparable biotin labelling in time frames as short as ten minutes could ameliorate the above issues (Fig. 4.6) (385). Finally, it will be important to examine the PAS interactome in multiple cell types, as the PAS complex is known to have distinct roles in regulating trafficking in specialized cells such as adipocytes, neurons, and melanocytes

(333,398,399,407–409). An interactome map of the PAS complex in these different cell types will allow a comprehensive understanding of PAS function in cellular homeostasis and elucidate its role in disease pathogenesis.

In conclusion, this study highlights BioID as a valuable tool to interrogate the PAS interactome, that could be easily applied to study the cellular interactomes of other trafficking complexes and regulators. We also provide additional evidence of a functional interaction between the PAS complex and the COPI complex.

4.5 Materials and Methods

Cell, inhibitors and antibodies

HEK293T and HT1080 cells (ATCC) were cultured in Dulbecco's Modified Eagle Medium (DMEM, Lonza) supplemented with 10% Fetal Bovine Serum (Sigma), 100U/mL penicillin and 100µg/mL streptomycin (Wisent).

Stock solutions of apilimod (Ark Pharm, Inc) and BrefeldinA (Cayman) were prepared in DMSO and stored at -20°C. Antibodies and HRP conjugates used were Myc (Cell Signalling), ArPIKfyve (Thermo and Santa cruz), FIG4/Sac3 (Millipore), GAPDH (Cell Signalling), Streptavidin-HRP (Cell Signalling), and COPB1 (Abcam).

Plasmids and cloning

ArPIKfyve (gift from Dr. Assia Shisheva, Wayne State University) and Sac3 (Origene) were cloned onto the C-terminal of myc-BioID (gift from Kyle Roux, Addgene plasmid # 35700) using restriction enzyme cloning. ArPIKfyve and Sac3 were cloned onto the C-terminal of V5-TurboID (gift from Alice Ting Addgene plasmid # 107169) using Gibson assembly. Sequences of all cloned constructs were confirmed by Sanger sequencing.

BioID screen, affinity purification and mass spectrometry

HEK293T cells were transfected with plasmids encoding ArPIKfyve-birA or Sac3-birA complemented with plasmids encoding the other subunits of the PAS complex (HA-PIKfyve and either myc-ArPIKfyve or Flag-Sac3) in 1:1:1 ratio, using Jetprime transfection reagent (Polyplus) following manufacturer protocol. Cells transfected with a plasmid encoding birA were used as a control. Twenty-four hours post transfection, cells were incubated overnight in the presence or absence of biotin (Sigma, 50µM), followed by cell lysis in 1% Triton X-100, 0.1% NP40, 150mM NaCl, 10mM Tris-HCl pH 7.4. Protein concentration was assessed using a bicinchoninic acid (BCA) assay (Thermo) and lysates were incubated with streptavidin-agarose beads for 1 hr. Bound proteins were eluted by boiling in SDS buffer for 10 minutes. Eluted proteins were resolved by SDS-PAGE, and gels were subsequently silver stained following manufacturer protocol (Thermo). Stained lanes were excised and stored in 1% acetic acid. Proteomics analysis was performed at the Ottawa Hospital Research Institute Proteomics Core Facility. Proteins were digested in-gel using trypsin, peptide extracts were concentrated by Vacufuge (Eppendorf) and LC-MS/MS was performed using a Dionex Ultimate 3000 RLSC nano HPLC (Thermo) and an Orbitrap Fusion Lumos mass spectrometer. This experiment was performed three independent times (one technical replicate per experiment), and all three experiments were combined into one MaxQuant analysis to identify peptides from mass spectra. The results were exported to Scaffold (Proteome Software, USA) for further validation and viewing. Protein identifications were filtered with a FDR < 1%.

SAINT and PCSF Analysis

SAINTexpress analysis was performed using combined data from 3 biological replicates of the BioID within the CRAPome interface (389). Negative controls using birA as bait were

given to SAINT to model non-specific interations. A saint probability (SP) score ≥ 0.9 was used to further screen hits for both the ArPIKfyve and Sac3 baits, and shared hits for both baits with SP ≥ 0.9 were selected for PCSF and network analysis.

PCSF analysis was implemented within R using a previously optimized package (388). Prizes were assigned to proteins based on their SP score. Costs were assigned based on the frequency of interaction between two proteins, using PPI data from the STRING protein interaction database (395). The hub penalization parameter mu was set to 0.005. To increase robustness of the final network, the PCSF analysis was run 10 times with added noise (0.1% of each edge cost) to edge costs with each run. Functional enrichment analysis on the final PCSF network was performed using EnrichR, which is included in the PCSF R package. The p-values are calculated using the Fisher test and adjusted for multiple hypotheses using the Benjamini-Hochberg method.

Immunoblots

Cells were washed in PBS, then lysed in buffer containing 1% Triton X-100, 0.1% NP40, 150mM NaCl, 10mM Tris-HCl pH 7.4 supplemented with a protease inhibitor cocktail (Cell signaling). Protein concentration was determined using a BCA assay following manufacturer protocol (Thermo). Equal amounts of protein were resolved by SDS-PAGE and transferred on PVDF membranes. Proteins were detected using primary antibodies and HRP-conjugated secondary antibodies and visualized using chemiluminescence according to manufacturer protocol (Biorad Clarity ECL substrate). For detection of biotinylated proteins, membranes were blocked in 2% BSA and biotinylated proteins were detected using streptavidin-HRP (1:10000 dilution).

PLA, immunofluorescence and microscopy

For immunofluorescence experiments, HT1080 cells were seeded onto 18 mm coverslips and grown to approximately 60% confluence. Cells were then by fixed in formalin, permeabilized with 0.5% triton X-100, and blocked in 20% FBS for 30 min. Cells were then incubated in ArPIKfyve (Thermo) and COPB1 (Abcam) primary antibodies (1:50 and 1:100 dilutions, respectively) for 1h, followed by incubation with appropriate Alexafluor-conjugated secondary antibodies (Thermo) for 1 hour, Hoechst staining (1µg/mL, Thermo) and mounting in PermaFluor Aqueous Mounting medium (Thermo). Immunofluorescence images were captured on an LSM800 Zeiss confocal microscope using a 63X/1.4 Oil Plan-Apochromat objective. Fifteen to twenty Z-stacks were acquired per image.

For PLA experiments, HT1080 cells were seeded in poly-D-lysine (Sigma) coated angiogenesis chambers (Ibidi) and grown to approximately 60% confluency. If necessary, prior to fixation cells were incubated with inhibitors for 1 hour. Cells were fixed in formalin and permeabilized with 0.5% triton X-100. PLA was performed using manufacturer protocol (Sigma) using ArPIKfyve (Santa cruz, 1:50 dilution) and COPB1 (Abcam, 1:100 dilution) antibodies. Images were captured on an LSM800 Zeiss confocal microscope as described above.

4.6 Acknowledgements

We would like to acknowledge technical support from the uOttawa CBIA core staff, Chloë van Oostende and Skye Green, as well as Alexander Pelletier for advice on data analysis. We acknowledge Lawrence Puente and the OHRI Proteomics Core Facility for performing mass spectrometry for our BioID screens.

Chapter 5: General Discussion and Future Directions

5.1 Summary of thesis findings and future directions

EBOV and other filoviruses undergo a complex entry sequence that is highly dependent on host cell trafficking pathways in order to gain passage to entry-conducive compartments deep within the LE/LY network. The overall goal of this thesis was to identify and dissect how EBOV regulates its transport to these compartments through co-opting host cell trafficking factors. Results from the studies presented in this thesis have demonstrated that the entry of EBOV and other filoviruses depends on cellular proteins that regulate multiple facets of endosomal trafficking, from metabolism of phosphoinositide signaling lipids required for endosome maturation to activation of tethering complexes required for endosome fusion. In addition to these findings that contribute to our knowledge of the mechanisms of filovirus entry, work in this thesis has also optimized and advanced a number of experimental tools and methodologies that can be applied not only to the field of viral entry but are broadly applicable to studying how fundamental cellular trafficking processes are regulated in the context of cellular homeostasis and dysregulated in the context of disease pathogenesis.

In **Chapter 2**, we examined the role of the LE/LY-associated HOPS tethering complex in EBOV entry using an optimized inducible dual gRNA CRISPR strategy. This approach allowed us to individually interrogate each subunit of the HOPS complex as well as those of the closely related EE-associated CORVET tethering complex. In doing so we were able to differentiate the importance of the HOPS and CORVET complexes in EBOV entry and validate the specific importance of the HOPS complex and its role in regulating LE/LY fusion. Furthermore, using the same CRISPR approach as well as microscopy to visualize EBOV trafficking in cells, we determined that efficient EBOV trafficking to NPC1 requires binding between the HOPS

complex and its positive regulator, UVRAG. Using site-directed mutagenesis, we were able to further define the mechanism of UVRAG–HOPS coordination by mapping the specific regions on UVRAG required for binding to the HOPS complex.

The HOPS complex was first identified as an EBOV entry factor in a genetic screen performed by Carette et al. in 2011, which also uncovered PIKfyve and Sac3 (171). As preliminary follow up in the same report, the authors validated that EBOV entry was impaired in cells deficient in the HOPS subunits Vps11 and Vps33a. However, as these subunits form part of the C-Vps core that is shared with the CORVET complex, we sought to delineate the role of the HOPS and CORVET complexes in EBOV entry by examining their shared and specific subunits. Using individual KO cells for each subunit, we determined that functionality of HOPS complex, but not the CORVET complex, is required for efficient EBOV entry.

These results further highlight the role of UVRAG in regulating HOPS activity and viral trafficking, which was first reported in a study by Pirooz et al. that found UVRAG to be important for IAV and VSV entry (308). A recent study has also reported that the SARS-CoV-2 ORF3a protein can subvert autophagy by directly binding to the HOPS subunit Vps39, preventing its association with the SNARE STX17, suggesting that the HOPS complex may be a shared target for multiple viruses (410).

A key remaining question is how EBOV regulates the activity of UVRAG and the HOPS complex, including whether EBOV can enhance their association to promote viral entry. Previous studies have shown that UVRAG activity can be modulated via post translational modifications including phosphorylation and ubiquitination (243,411,412). However, our understanding of the precise mechanisms underlying UVRAG regulation are complicated by its multifunctional roles in autophagosome induction and maturation, endocytic trafficking and

DNA repair. This multifunctionality is enabled in part by UVRAG's ability to associate in several distinct cellular complexes to regulate different processes (413,414). For instance, UVRAG associates in a complex with Beclin-1 and the PI3-kinase Vps34 to induce autophagosome formation, while it associates with Rab7 and the HOPS complex to promote both autophagosome and endosome maturation (307,314). Its overlapping roles in both endocytic trafficking and autophagy reflect the closely intertwined nature of these two processes, and how UVRAG is able to regulate multiple distinct trafficking steps remains poorly understood, with studies at times reporting conflicting results. For example, two groups have shown that UVRAG can be phosphorylated on multiple residues by mTORC1. Kim et al. found that mTORC1 mediated phosphorylation on UVRAG S498 negatively regulates UVRAG activity and endosome maturation by sequestering UVRAG with RUBICON, preventing its association with the HOPS complex and the activation of Vps34 (243). In contrast, Munson et al. reported that mTORC1 phosphorylates UVRAG on S550 and S571, which enhances Vps34 activity and regulates autophagosome and lysosome reformation in order to maintain lysosome integrity (412). It is unclear how mTORC1 is able to both positively and negatively regulate UVRAG functions, however, it would be of particular interest to explore further in the context of EBOV entry as it is known that EBOV can stimulate the PI3K/Akt pathway during entry, with mTORC1 being a major downstream effector of PI3K/Akt activation (350,415).

This study also presented a CRISPR strategy that has broad utility for the study of trafficking factors applicable beyond the field of viral entry. Genetic knockout of proteins involved in cellular trafficking can often have a deleterious effect on cell viability, as was observed in the case of UVRAG, which makes both generation of and experimentation with these KO cells technically challenging. The inducible CRISPR approach utilized in this study

enables the rapid induction of KO cells for experimentation, reducing the confounding effects of gene deletions on cell viability and potential off-target effects on other cell pathways. Furthermore, combining the inducible CRISPR approach with a dual gRNA strategy further enhances the efficiency of generating the desired gene knockout, particularly for larger genes (such as PIKfyve) or genes with multiple splicing variants.

In **Chapter 3**, we examined the role of the PIKfyve-ArPIKfyve-Sac3 phosphoinositide regulating complex in EBOV entry. Using complementary approaches incorporating CRISPR KO of each PAS subunit, small molecule PIKfyve inhibitors, site-directed mutagenesis of PIKfyve and Sac3, and a fluorescent PtdIns(3,5)P_2-binding probe as a proxy for PIKfyve activity, we were able to dissect the importance of each subunit for EBOV entry. We determined that PIKfyve kinase activity, but not Sac3 phosphatase activity, was required for EBOV entry. However, expression of both Sac3 and ArPIKfyve was still required for PAS complex integrity, which enables optimal PIKfyve kinase activity. Intriguingly, we also reported the first evidence that EBOV stimulates increased PtdIns(3,5)P_2 production during entry, suggesting that the virus is able to activate and/or enhance PIKfyve activity through a still unknown mechanism.

Following the above finding that EBOV could potentially stimulate PAS activity, we sought to further explore how the PAS complex could be regulated in **Chapter 4** using a BioID PPI screen to identify PAS interacting proteins. By running parallel screens using ArPIKfyve and Sac3 birA fusion proteins and comparing the resulting pools of candidate interactors for each protein, we were able to screen for high probability hits for interactors of the PAS complex as a whole. Among these hits were multiple members of the COPI complex, which was of interest to us as COPI has been increasingly implicated as a regulator of endosomal trafficking in addition

to its role as a golgi trafficking regulator. However, the mechanisms regulating COPI recruitment to and function on endosomes are largely unknown.

As preliminary follow-up on the COPI complex, we confirmed the interaction between the PAS and COPI complexes using a highly sensitive PLA assay. Using ArPIKfyve as a representative of the PAS complex and COPB1 as a representative of the COPI complex, we saw a specific interaction between both proteins that appeared to be diffusely localized throughout the cell. This suggests that the interaction between the PAS and COPI complexes could take place on endolysosomal membranes, signifying a possible functional relationship between the two complexes in regulating endosomal trafficking.

Whether COPI function on endosomes is required for EBOV entry is unknown, however, it has been implicated in the entry of other viruses. Endosomal COPI function was first implicated in viral entry by reports that injection of COPB1 antibodies block VSV and Simian virus 40 (SV40) entry (379,416). Similarly, VSV and SV40 entry are also impaired in ldlF CHO cells that are deficient in COPE (378). In the case of SV40, as well as Human Papillomavirus Type 16 (HPV16), COPI appears to be required for transport of newly internalized virions to the ER (417,418). An siRNA screen also identified COPD to be an entry factor for IAV (419). However, in the case of VSV and IAV, disruption of COPI function appears to indirectly affect entry by perturbing general membrane trafficking dynamics, as prolonged COPI inhibition using siRNA knockdown or prolonged Brefeldin A treatment impairs viral entry, while shorter incubations with Brefeldin A do not impact entry (420,421). Experiments incorporating genetic knockdown or knockout of COPI subunits as well as pharmacological inhibition using Arf1 inhibitors like Brefeldin A or Golgicide A will be useful in dissecting a potential role of the COPI complex in EBOV entry. Likewise, experiments using TurboID to assess the interaction between the PAS

complex and the COPI complex during EBOV entry will shed light on whether EBOV could stimulate or modulate PAS-COPI interactions.

With these studies taken together, we propose a model of EBOV entry as a regulated process involving the concerted activity of trafficking factors specifically required for shuttling of endocytosed cargo to the LE/LY compartment (Figure 5.1). Viral-induced activation of these trafficking factors likely occurs through activation of cell surface receptors through GP-dependent and/or GP-independent mechanisms. Activation of the PAS complex, potentially via the PI3K/Akt pathway, results in PtdIns(3,5)P_2 production and endosomal maturation, while activation of UVRAG and the HOPS complex, potentially via mTORC1, promotes fusion of LE/LYs, which together enhance delivery of EBOV virions to entry-conducive compartments.

5.2 Targeting viral entry in the development of therapeutics

Viral entry has long been an attractive target for antiviral therapies. As the first step of the viral life cycle, blocking entry could inhibit both viral spread within the host and reduce cytopathic effects associated with infection. Furthermore, viruses that share similar entry mechanisms may have conserved requirements for specific entry factors, which represent potential broad spectrum antiviral targets (422–424).

Despite these advantages, relatively few entry inhibitors have been approved by regulatory agencies such as the FDA and EMA for clinical use. These approved agents all target enveloped viruses, and either directly target viral envelope proteins (such as the HIV-1 inhibitor Enfuvirtide, a peptide that mimics the HR2 region of gp41 and inhibits viral fusion) or prevent viral receptor engagement by blocking cellular entry receptors (such as Bulevirtide, which binds to Na+-taurocholate cotransporting polypeptide (NTCP), the entry receptor used by hepatitis delta virus and hepatitis B virus) (425,426).

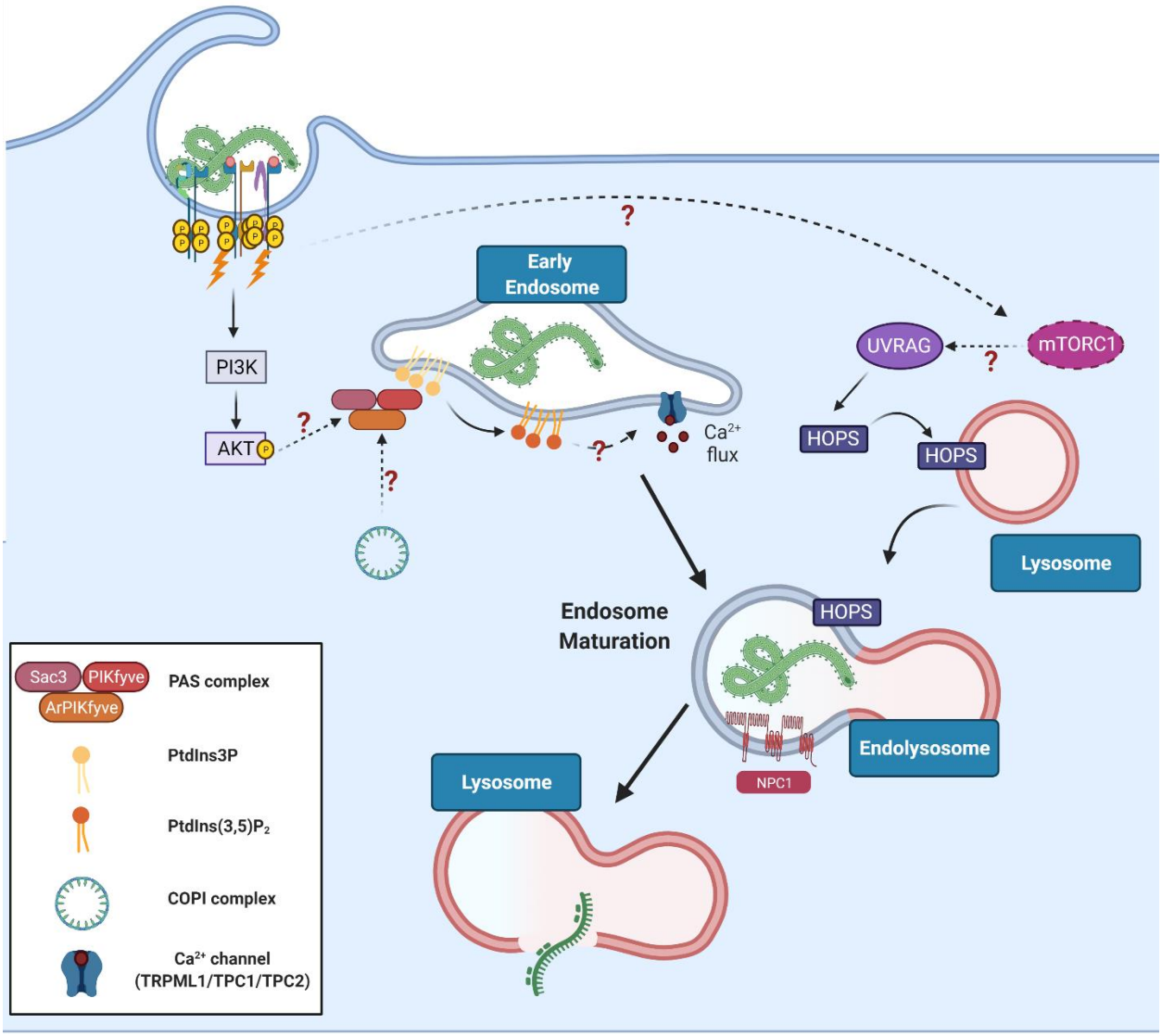

Figure 5.1 A model of Ebola virus trafficking with proposed roles for the PAS complex, the HOPS complex, and UVRAG

EBOV virions engage with cell surface receptors during attachment and internalization, including signalling receptors such as TIM/TAM family phosphatidylserine receptors and epidermal growth factor receptor tyrosine kinases. Through still ill-defined mechanisms, EBOV-induced activation of cell signalling pathways promotes viral internalization through macropinocytosis and potentially enhances trafficking of virions to the LE/LY compartment. Signalling through the PI3K/Akt axis may stimulate activity of the PAS complex, which is recruited to early endosomes and catalyzes PtdIns3P→PtdIns(3,5)P_2 conversion required for endosome maturation and activates PtdIns(3,5)P_2 effectors such as Ca^{2+} channels. Viral-induced activation of signalling, potentially through mTORC1, may also stimulate association of UVRAG with the HOPS complex, which stimulates tethering and fusion between LEs and LYs. The COPI complex may also participate in endosomal trafficking via association with the PAS complex through an unknown mechanism.

Targeting viral entry presents several challenges in the development of antivirals. Direct acting antivirals that target viral proteins risk selecting for viral escape mutants resistant to the drug, as has been observed in clinical trials for Enfuvirtide (426). Furthermore, fusion mimetic peptides are not easily administered as they cannot be taken orally and must be injected. Entry-specific indirect acting antivirals that target host cell proteins have thus far been restricted to cell surface entry receptors due to the difficulty of accessing intracellular receptors, thus hindering their use for viruses that enter through endosomal compartments such as filoviruses.

Thus far the avenue of targeting cell trafficking pathways to inhibit entry of such viruses has been largely unexplored. However, targeting viral trafficking has several advantages that warrant further investigation for the development of antiviral therapeutics. In addition to the potential to inhibit infection by viruses that use intracellular receptors, viruses that enter through endosomal compartments often share conserved requirements for trafficking factors that represent broad spectrum antiviral targets. As shown in this thesis, inhibiting trafficking factors such as PIKfyve or UVRAG was effective against multiple filoviruses, including MARV. Furthermore, inhibiting PIKfyve has been shown to be effective in blocking entry of SARS CoV-1 and SARS CoV-2 (168,427,428). In addition, many proteins involved in endosomal trafficking have identified small molecule inhibitors, including those approved for clinical use for other purposes. Screening libraries of these inhibitors for their effect on viral infection is a promising strategy for the accelerated development of antiviral therapeutics, and indeed trafficking inhibitors are routinely identified in small molecule screens for antiviral compounds (166,428–430).

Of course, we cannot overlook the potential cytotoxic effects of inhibiting essential trafficking mechanisms in cells, which is perhaps the primary argument against this strategy.

While cytotoxicity must be a primary consideration for any drug treatment, recent investigation into the use of apilimod for the treatment of COVID-19 offers an exciting opportunity to study the utility of targeting viral trafficking as an antiviral strategy. Apilimod (also known as STA-5326 and LAM-002A) was first uncovered in a small molecule inhibitor screen for IL-12/IL-23 inhibitors (431), and has been tested in phase I/II clinical trials for the treatment of Crohn's disease, rheumatoid arthritis, psoriasis and B-cell cancers (432–436). While these trials did not ultimately establish significant anti-inflammatory effects of apilimod treatment over placebo, they did find apilimod to be well tolerated with only minor side effects, despite the vacuolization and other cytopathologies observed with apilimod treatment *in vitro* by our lab and others. This favourable safety profile is encouraging for the potential repurposing of apilimod for other clinical therapies, and following two studies that independently found apilimod to be highly effective in blocking SARS-CoV-2 infection *in vitro*, apilimod is now being tested in a phase II clinical trial for the treatment of COVID-19 by AI Therapeutics, Inc in collaboration with Yale University (427,428,437). Results from this study will provide valuable insight into the effectiveness of viral trafficking inhibitors in a clinical setting, and have potential to be expanded to the treatment of filovirus associated diseases.

5.3 Concluding remarks

In many ways, viruses are both the first and the most proficient cell biologists, and by their ancientness and ubiquity are perhaps evolution's greatest success. Although they are seen as inert molecules with no conscious direction, they are nonetheless able to infiltrate, exploit and in many cases intricately manipulate the most fundamental cellular processes of their hosts to the benefit of their survival and replication.

Viral entry is no exception to this paradigm, and work in this thesis contributes to a century of research aimed at dissecting how viruses harness cellular pathways to enter cells and initiate infection. In particular, we provide evidence that EBOV is not just a benign passenger through the endosomal system but is able to activate cell trafficking factors to promote its entry. How EBOV and other filoviruses are able to precisely manipulate cellular signalling and trafficking pathways through a single envelope protein and its viral envelope lipids remains a tantalizing mystery waiting to be unravelled. In doing so, we can hope to gain insight not only into the molecular mechanisms underlying filovirus entry, but, as filoviruses have had millions of years of coevolution with their hosts to understand the intricacies of host cell biology, also insight into how these fundamental cellular processes are regulated.

References

1. Kuhn JH, Amarasinghe GK, Basler CF, Bavari S, Bukreyev A, Chandran K, et al. ICTV Virus Taxonomy Profile: Filoviridae. Journal of General Virology. 2019;100(6):911–2.

2. Years of Ebola Virus Disease Outbreaks. Centers for Disease Control and Prevention; 2020 Nov. Available from: https://www.cdc.gov/vhf/ebola/history/chronology.html?CDC_AA_refVal=https%3A%2F%2Fwww.cdc.gov%2Fvhf%2Febola%2Foutbreaks%2Fhistory%2Fchronology.html#anchor_1526565058132

3. Yang X-L, Tan CW, Anderson DE, Jiang R-D, Li B, Zhang W, et al. Characterization of a filovirus (Měnglà virus) from Rousettus bats in China. Nature Microbiology. 2019 Jan 7;1.

4. Negredo A, Palacios G, Vázquez-Morón S, González F, Dopazo H, Molero F, et al. Discovery of an Ebolavirus-Like Filovirus in Europe. PLoS Pathog. 2011 Oct 20;7(10):e1002304.

5. Shi M, Lin X-D, Chen X, Tian J-H, Chen L-J, Li K, et al. The evolutionary history of vertebrate RNA viruses. Nature. 2018 Apr;556(7700):197–202.

6. Goldstein T, Anthony SJ, Gbakima A, Bird BH, Bangura J, Tremeau-Bravard A, et al. The discovery of Bombali virus adds further support for bats as hosts of ebolaviruses. Nature Microbiology. 2018 Oct;3(10):1084–9.

7. Formenty P, Hatz C, Le Guenno B, Stoll A, Rogenmoser P, Widmer A. Human Infection Due to Ebola Virus, Subtype Côte d'Ivoire: Clinical and Biologic Presentation. The Journal of Infectious Diseases. 1999 Feb 1;179(Supplement_1):S48–53.

8. Cantoni D, Hamlet A, Michaelis M, Wass MN, Rossman JS. Risks Posed by Reston, the Forgotten Ebolavirus. mSphere. 2016 Dec 28;1(6):e00322-16.

9. Zehender G, Sorrentino C, Veo C, Fiaschi L, Gioffrè S, Ebranati E, et al. Distribution of Marburg virus in Africa: An evolutionary approach. Infection, Genetics and Evolution. 2016 Oct 1;44:8–16.

10. Taylor DJ, Dittmar K, Ballinger MJ, Bruenn JA. Evolutionary maintenance of filovirus-like genes in bat genomes. BMC Evol Biol. 2011 Nov 17;11:336.

11. Taylor DJ, Leach RW, Bruenn J. Filoviruses are ancient and integrated into mammalian genomes. BMC Evol Biol. 2010 Jun 22;10:193.

12. Belyi VA, Levine AJ, Skalka AM. Unexpected Inheritance: Multiple Integrations of Ancient Bornavirus and Ebolavirus/Marburgvirus Sequences in Vertebrate Genomes. PLoS Pathog. 2010 Jul 29;6(7).

13. Differentiation of filoviruses by electron microscopy. Virus Research. 1995 Dec 1;39(2–3):129–50.

14. Sanchez A, Kiley MP, Holloway BP, Auperin DD. Sequence analysis of the Ebola virus genome: organization, genetic elements, and comparison with the genome of Marburg virus. Virus Res. 1993 Sep;29(3):215–40.

15. Sanchez A, Rollin PE. Complete genome sequence of an Ebola virus (Sudan species) responsible for a 2000 outbreak of human disease in Uganda. Virus Research. 2005 Oct 1;113(1):16–25.

16. Feldmann H, Mühlberger E, Randolf A, Will C, Kiley MP, Sanchez A, et al. Marburg virus, a filovirus: messenger RNAs, gene order, and regulatory elements of the replication cycle. Virus Res. 1992 Jun;24(1):1–19.

17. Elliott LH, Kiley MP, McCormick JB. Descriptive analysis of Ebola virus proteins. Virology. 1985 Nov 1;147(1):169–76.

18. Noda T, Hagiwara K, Sagara H, Kawaoka Y. Characterization of the Ebola virus nucleoprotein–RNA complex. J Gen Virol. 2010 Jun;91(Pt 6):1478–83.

19. Watanabe S, Noda T, Kawaoka Y. Functional Mapping of the Nucleoprotein of Ebola Virus. Journal of Virology. 2006 Apr 15;80(8):3743–51.

20. Lee JE, Saphire EO. Ebolavirus glycoprotein structure and mechanism of entry. Future Virol. 2009;4(6):621–35.

21. Jasenosky LD, Kawaoka Y. Filovirus budding. Virus Research. 2004 Dec 1;106(2):181–8.

22. Madara JJ, Han Z, Ruthel G, Freedman BD, Harty RN. The multifunctional Ebola virus VP40 matrix protein is a promising therapeutic target. Future Virol. 2015 May;10(5):537–46.

23. Soni SP, Adu-Gyamfi E, Yong SS, Jee CS, Stahelin RV. The Ebola Virus Matrix Protein Deeply Penetrates the Plasma Membrane: An Important Step in Viral Egress. Biophysical Journal. 2013 May 7;104(9):1940–9.

24. Noda T, Sagara H, Suzuki E, Takada A, Kida H, Kawaoka Y. Ebola Virus VP40 Drives the Formation of Virus-Like Filamentous Particles Along with GP. J Virol. 2002 May 15;76(10):4855–65.

25. Jasenosky LD, Neumann G, Lukashevich I, Kawaoka Y. Ebola Virus VP40-Induced Particle Formation and Association with the Lipid Bilayer. Journal of Virology. 2001 Jun 1;75(11):5205–14.

26. Watanabe S, Watanabe T, Noda T, Takada A, Feldmann H, Jasenosky LD, et al. Production of Novel Ebola Virus-Like Particles from cDNAs: an Alternative to Ebola Virus Generation by Reverse Genetics. Journal of Virology. 2004 Jan 15;78(2):999–1005.

27. Manicassamy B, Rong L. Expression of Ebolavirus glycoprotein on the target cells enhances viral entry. Virology Journal. 2009 Jun 8;6(1):75.

28. Mehedi M, Falzarano D, Seebach J, Hu X, Carpenter MS, Schnittler H-J, et al. A New Ebola Virus Nonstructural Glycoprotein Expressed through RNA Editing. J Virol. 2011 Jun;85(11):5406–14.

29. Sanchez A, Trappier SG, Mahy BW, Peters CJ, Nichol ST. The virion glycoproteins of Ebola viruses are encoded in two reading frames and are expressed through transcriptional editing. Proc Natl Acad Sci U S A. 1996 Apr 16;93(8):3602–7.

30. Volchkova VA, Feldmann H, Klenk HD, Volchkov VE. The nonstructural small glycoprotein sGP of Ebola virus is secreted as an antiparallel-orientated homodimer. Virology. 1998 Oct 25;250(2):408–14.

31. Volchkova VA, Klenk HD, Volchkov VE. Delta-peptide is the carboxy-terminal cleavage fragment of the nonstructural small glycoprotein sGP of Ebola virus. Virology. 1999 Dec 5;265(1):164–71.

32. de La Vega M-A, Wong G, Kobinger GP, Qiu X. The Multiple Roles of sGP in Ebola Pathogenesis. Viral Immunol. 2015 Feb 1;28(1):3–9.

33. Zhu W, Banadyga L, Emeterio K, Wong G, Qiu X. The Roles of Ebola Virus Soluble Glycoprotein in Replication, Pathogenesis, and Countermeasure Development. Viruses. 2019 Oct 31;11(11).

34. Mohan GS, Li W, Ye L, Compans RW, Yang C. Antigenic subversion: a novel mechanism of host immune evasion by Ebola virus. PLoS Pathog. 2012;8(12):e1003065.

35. He J, Melnik LI, Komin A, Wiedman G, Fuselier T, Morris CF, et al. Ebola Virus Delta Peptide Is a Viroporin. J Virol. 2017 Jul 27;91(16).

36. Guha S, Melnik L, Garry RF, Wimley WC. Ebola Virus Delta-Peptide Acts as an Enterotoxic Viroporin In Vivo. Biophysical Journal. 2018 Feb 2;114(3):265a.

37. Pokhrel R, Pavadai E, Gerstman BS, Chapagain PP. Membrane pore formation and ion selectivity of the Ebola virus delta peptide. Phys Chem Chem Phys. 2019 Mar 6;21(10):5578–85.

38. Leroy EM, Kumulungui B, Pourrut X, Rouquet P, Hassanin A, Yaba P, et al. Fruit bats as reservoirs of Ebola virus. Nature. 2005 Dec 1;438(7068):575–6.

39. Han BA, Schmidt JP, Alexander LW, Bowden SE, Hayman DTS, Drake JM. Undiscovered Bat Hosts of Filoviruses. PLOS Negl Trop Dis. 2016 Jul 14;10(7):e0004815.

40. Olival KJ, Hayman DTS. Filoviruses in Bats: Current Knowledge and Future Directions. Viruses. 2014 Apr 17;6(4):1759–88.

41. Schuh AJ, Amman BR, Towner JS. Filoviruses and bats. Microbiology Australia. 2017 Mar;38(1):12–6.

42. Towner JS, Amman BR, Sealy TK, Carroll SAR, Comer JA, Kemp A, et al. Isolation of Genetically Diverse Marburg Viruses from Egyptian Fruit Bats. PLOS Pathog. 2009 Jul 31;5(7):e1000536.

43. Yuan J, Zhang Y, Li J, Zhang Y, Wang L-F, Shi Z. Serological evidence of ebolavirus infection in bats, China. Virol J. 2012 Oct 13;9:236.

44. He B, Feng Y, Zhang H, Xu L, Yang W, Zhang Y, et al. Filovirus RNA in Fruit Bats, China. Emerg Infect Dis. 2015 Sep;21(9):1675–7.

45. Ramírez de Arellano E, Sanchez-Lockhart M, Perteguer MJ, Bartlett M, Ortiz M, Campioli P, et al. First Evidence of Antibodies Against Lloviu Virus in Schreiber's Bent-Winged Insectivorous Bats Demonstrate a Wide Circulation of the Virus in Spain. Viruses. 2019 Apr 19;11(4).

46. Taniguchi S, Watanabe S, Masangkay JS, Omatsu T, Ikegami T, Alviola P, et al. Reston Ebolavirus antibodies in bats, the Philippines. Emerg Infect Dis. 2011 Aug;17(8):1559–60.

47. Pigott DM, Golding N, Mylne A, Huang Z, Weiss DJ, Brady OJ, et al. Mapping the zoonotic niche of Marburg virus disease in Africa. Trans R Soc Trop Med Hyg. 2015 Jun;109(6):366–78.

48. Peterson AT, Bauer JT, Mills JN. Ecologic and geographic distribution of filovirus disease. Emerg Infect Dis. 2004 Jan;10(1):40–7.

49. Glennon EE, Restif O, Sbarbaro SR, Garnier R, Cunningham AA, Suu-Ire RD, et al. Domesticated animals as hosts of henipaviruses and filoviruses: A systematic review. The Veterinary Journal. 2018 Mar 1;233:25–34.

50. Leroy EM, Rouquet P, Formenty P, Souquière S, Kilbourne A, Froment J-M, et al. Multiple Ebola Virus Transmission Events and Rapid Decline of Central African Wildlife. Science. 2004 Jan 16;303(5656):387–90.

51. Martini GA, Knauff HG, Schmidt HA, Mayer G, Baltzer G. A hitherto unknown infectious disease contracted from monkeys. “Marburg-virus” disease. Ger Med Mon. 1968 Oct;13(10):457–70.

52. Languon S, Quaye O. Filovirus Disease Outbreaks: A Chronological Overview. Virology(Auckl). 2019 Jan 1;10:1178122X19849927.

53. Towner JS, Khristova ML, Sealy TK, Vincent MJ, Erickson BR, Bawiec DA, et al. Marburgvirus genomics and association with a large hemorrhagic fever outbreak in Angola. J Virol. 2006 Jul;80(13):6497–516.

54. Burke, J, Declerq, R, Ghysebrechts, G. Ebola haemorrhagic fever in Zaire, 1976. Bull World Health Organ. 1978;56(2):271–93.

55. Coltart CEM, Lindsey B, Ghinai I, Johnson AM, Heymann DL. The Ebola outbreak, 2013–2016: old lessons for new epidemics. Philos Trans R Soc Lond B Biol Sci. 2017 May 26;372(1721).

56. Carroll MW, Matthews DA, Hiscox JA, Elmore MJ, Pollakis G, Rambaut A, et al. Temporal and spatial analysis of the 2014-2015 Ebola virus outbreak in West Africa. Nature. 2015 Aug 6;524(7563):97–101.

57. Gire SK, Goba A, Andersen KG, Sealfon RSG, Park DJ, Kanneh L, et al. Genomic surveillance elucidates Ebola virus origin and transmission during the 2014 outbreak. Science. 2014 Sep 12;345(6202):1369–72.

58. Henao-Restrepo AM, Camacho A, Longini IM, Watson CH, Edmunds WJ, Egger M, et al. Efficacy and effectiveness of an rVSV-vectored vaccine in preventing Ebola virus disease: final results from the Guinea ring vaccination, open-label, cluster-randomised trial (Ebola Ça Suffit!). The Lancet. 2017 Feb 4;389(10068):505–18.

59. First FDA-approved vaccine for the prevention of Ebola virus disease, marking a critical milestone in public health preparedness and response. FDA 2020. Available from: https://www.fda.gov/news-events/press-announcements/first-fda-approved-vaccine-prevention-ebola-virus-disease-marking-critical-milestone-public-health

60. Bache BE, Grobusch MP, Agnandji ST. Safety, immunogenicity and risk–benefit analysis of rVSV-ΔG-ZEBOV-GP (V920) Ebola vaccine in Phase I–III clinical trials across regions. Future Microbiology. 2020 Jan 1;15(2):85–106.

61. Ilunga Kalenga O, Moeti M, Sparrow A, Nguyen V-K, Lucey D, Ghebreyesus TA. The Ongoing Ebola Epidemic in the Democratic Republic of Congo, 2018-2019. N Engl J Med. 2019 Jul 25;381(4):373–83.

62. World Health Organization. Preliminary results on the efficacy of rVSV-ZEBOV-GP Ebola vaccine using the ring vaccination strategy in the control of an Ebola outbreak in the Democratic Republic of the Congo: an example of integration of research into epidemic response. 2019 Apr. Available from: https://www.who.int/csr/resources/publications/ebola/ebola-ring-vaccination-results-12-april-2019.pdf

63. Feldmann H, Geisbert TW. Ebola haemorrhagic fever. The Lancet. 2011 Mar 11;377(9768):849–62.

64. Bausch DG, Towner JS, Dowell SF, Kaducu F, Lukwiya M, Sanchez A, et al. Assessment of the Risk of Ebola Virus Transmission from Bodily Fluids and Fomites. J Infect Dis. 2007 Nov 15;196(Supplement_2):S142–7.

65. Dowell SF, Mukunu R, Ksiazek TG, Khan AS, Rollin PE, Peters CJ. Transmission of Ebola hemorrhagic fever: a study of risk factors in family members, Kikwit, Democratic Republic of the Congo, 1995. Commission de Lutte contre les Epidémies à Kikwit. J Infect Dis. 1999 Feb;179 Suppl 1:S87-91.

66. Gao X, Rong G, Lu Y, Duan X, Duan H. Symptoms closely associated with Ebola virus disease. The Lancet Infectious Diseases. 2016 Jan;16(1):18–9.

67. Chertow DS, Kleine C, Edwards JK, Scaini R, Giuliani R, Sprecher A. Ebola Virus Disease in West Africa — Clinical Manifestations and Management. New England Journal of Medicine. 2014 Nov 27;371(22):2054–7.

68. McElroy A. Understanding Bleeding in Ebola Virus Disease. Clin Adv Hematol Oncol. 2015 Jan;13(1):29–31.

69. Malvy D, McElroy AK, de Clerck H, Günther S, van Griensven J. Ebola virus disease. The Lancet. 2019 Mar 2;393(10174):936–48.

70. Carod-Artal FJ. Post-Ebolavirus disease syndrome: What do we know? Expert Rev Anti Infect Ther. 2015 Aug 13;1–3.

71. Scott JT, Sesay FR, Massaquoi TA, Idriss BR, Sahr F, Semple MG. Post-Ebola Syndrome, Sierra Leone. Emerg Infect Dis. 2016 Apr;22(4):641–6.

72. Wilson HW, Amo-Addae M, Kenu E, Ilesanmi OS, Ameme DK, Sackey SO. Post-Ebola Syndrome among Ebola Virus Disease Survivors in Montserrado County, Liberia 2016. Biomed Res Int. 2018 Jun 28.

73. Mate SE, Kugelman JR, Nyenswah TG, Ladner JT, Wiley MR, Cordier-Lassalle T, et al. Molecular Evidence of Sexual Transmission of Ebola Virus. New England Journal of Medicine. 2015 Dec 17;373(25): 2448-54.

74. Christie A, Davies-Wayne GJ, Cordier-Lasalle T, Blackley DJ, Laney AS, Williams DE, et al. Possible Sexual Transmission of Ebola Virus — Liberia, 2015. MMWR Morbidity and Mortality Weekly Report. 2015 May 8;64(17):479.

75. Boon SD, Marston BJ, Nyenswah TG, Jambai A, Barry M, Keita S, et al. Ebola Virus Infection Associated with Transmission from Survivors. Emerging Infectious Diseases. 2019 Feb;25(2):240.

76. Wool-Lewis RJ, Bates P. Characterization of Ebola Virus Entry by Using Pseudotyped Viruses: Identification of Receptor-Deficient Cell Lines. J Virol. 1998 Apr;72(4):3155–60.

77. Geisbert TW, Hensley LE, Gibb TR, Steele KE, Jaax NK, Jahrling PB. Apoptosis Induced In Vitro and In Vivo During Infection by Ebola and Marburg Viruses. Laboratory Investigation. 2000 Feb;80(2):171–86.

78. Geisbert TW, Hensley LE, Larsen T, Young HA, Reed DS, Geisbert JB, et al. Pathogenesis of Ebola Hemorrhagic Fever in Cynomolgus Macaques. Am J Pathol. 2003 Dec;163(6):2347–70.

79. Schnittler HJ, Feldmann H. Molecular pathogenesis of filovirus infections: role of macrophages and endothelial cells. Curr Top Microbiol Immunol. 1999;235:175–204.

80. Younan P, Iampietro M, Nishida A, Ramanathan P, Santos RI, Dutta M, et al. Ebola Virus Binding to Tim-1 on T Lymphocytes Induces a Cytokine Storm. mBio. 2017 Sep 26;8(5).

81. Okumura A, Pitha PM, Yoshimura A, Harty RN. Interaction between Ebola Virus Glycoprotein and Host Toll-Like Receptor 4 Leads to Induction of Proinflammatory Cytokines and SOCS1. J Virol. 2010 Jan 1;84(1):27–33.

82. Bradfute SB, Swanson PE, Smith MA, Watanabe E, McDunn JE, Hotchkiss RS, et al. Mechanisms and Consequences of Ebolavirus-Induced Lymphocyte Apoptosis. J Immunol. 2010 Jan 1;184(1):327–35.

83. Mahanty S, Hutchinson K, Agarwal S, Mcrae M, Rollin PE, Pulendran B. Cutting Edge: Impairment of Dendritic Cells and Adaptive Immunity by Ebola and Lassa Viruses. The Journal of Immunology. 2003 Mar 15;170(6):2797–801.

84. Falasca L, Agrati C, Petrosillo N, Di Caro A, Capobianchi MR, Ippolito G, et al. Molecular mechanisms of Ebola virus pathogenesis: focus on cell death. Cell Death Differ. 2015 Aug;22(8):1250–9.

85. Basler CF, Amarasinghe GK. Evasion of interferon responses by Ebola and Marburg viruses. J Interferon Cytokine Res. 2009 Sep;29(9):511–20.

86. Lubaki NM, Ilinykh P, Pietzsch C, Tigabu B, Freiberg AN, Koup RA, et al. The lack of maturation of Ebola virus-infected dendritic cells results from the cooperative effect of at least two viral domains. J Virol. 2013 Jul;87(13):7471–85.

87. Jin H, Yan Z, Prabhakar BS, Feng Z, Ma Y, Verpooten D, et al. The VP35 protein of Ebola virus impairs dendritic cell maturation induced by virus and lipopolysaccharide. J Gen Virol. 2010 Feb;91(Pt 2):352–61.

88. Iampietro M, Younan P, Nishida A, Dutta M, Lubaki NM, Santos RI, et al. Ebola virus glycoprotein directly triggers T lymphocyte death despite of the lack of infection. PLoS Pathog. 2017 May 22;13(5).

89. Hoenen T, Groseth A, Falzarano D, Feldmann H. Ebola virus: unravelling pathogenesis to combat a deadly disease. Trends in Molecular Medicine. 2006 May 1;12(5):206–15.

90. Basler CF, Wang X, Mühlberger E, Volchkov V, Paragas J, Klenk H-D, et al. The Ebola virus VP35 protein functions as a type I IFN antagonist. PNAS. 2000 Oct 24;97(22):12289–94.

91. Edwards MR, Liu G, Mire CE, Sureshchandra S, Luthra P, Yen B, et al. Differential Regulation of Interferon Responses by Ebola and Marburg Virus VP35 Proteins. Cell Reports. 2016 Feb 23;14(7):1632–40.

92. Leung DW, Shabman RS, Farahbakhsh M, Prins KC, Borek DM, Wang T, et al. Structural and functional characterization of Reston Ebola virus VP35 interferon inhibitory domain. J Mol Biol. 2010 Jun 11;399(3):347–57.

93. Yen B, Mulder LCF, Martinez O, Basler CF. Molecular basis for ebolavirus VP35 suppression of human dendritic cell maturation. J Virol. 2014 Nov;88(21):12500–10.

94. Leung DW, Ginder ND, Fulton DB, Nix J, Basler CF, Honzatko RB, et al. Structure of the Ebola VP35 interferon inhibitory domain. PNAS. 2009 Jan 13;106(2):411–6.

95. Leung DW, Prins KC, Borek DM, Farahbakhsh M, Tufariello JM, Ramanan P, et al. Structural basis for dsRNA recognition and interferon antagonism by Ebola VP35. Nat Struct Mol Biol. 2010 Feb;17(2):165–72.

96. Chang T-H, Kubota T, Matsuoka M, Jones S, Bradfute SB, Bray M, et al. Ebola Zaire virus blocks type I interferon production by exploiting the host SUMO modification machinery. PLoS Pathog. 2009 Jun;5(6):e1000493.

97. Prins KC, Cárdenas WB, Basler CF. Ebola Virus Protein VP35 Impairs the Function of Interferon Regulatory Factor-Activating Kinases IKKε and TBK-1. Journal of Virology. 2009 Apr 1;83(7):3069–77.

98. Cárdenas WB, Loo Y-M, Gale M, Hartman AL, Kimberlin CR, Martínez-Sobrido L, et al. Ebola virus VP35 protein binds double-stranded RNA and inhibits alpha/beta interferon production induced by RIG-I signaling. J Virol. 2006 Jun;80(11):5168–78.

99. Xu W, Edwards MR, Borek DM, Feagins AR, Mittal A, Alinger JB, et al. Ebola virus VP24 targets a unique NLS binding site on karyopherin alpha 5 to selectively compete with nuclear import of phosphorylated STAT1. Cell Host Microbe. 2014 Aug 13;16(2):187–200.

100. Zhang APP, Bornholdt ZA, Liu T, Abelson DM, Lee DE, Li S, et al. The ebola virus interferon antagonist VP24 directly binds STAT1 and has a novel, pyramidal fold. PLoS Pathog. 2012 Feb;8(2):e1002550.

101. Reid SP, Valmas C, Martinez O, Sanchez FM, Basler CF. Ebola virus VP24 proteins inhibit the interaction of NPI-1 subfamily karyopherin alpha proteins with activated STAT1. J Virol. 2007 Dec;81(24):13469–77.

102. Reid SP, Leung LW, Hartman AL, Martinez O, Shaw ML, Carbonnelle C, et al. Ebola virus VP24 binds karyopherin alpha1 and blocks STAT1 nuclear accumulation. J Virol. 2006 Jun;80(11):5156–67.

103. Mateo M, Reid SP, Leung LW, Basler CF, Volchkov VE. Ebolavirus VP24 binding to karyopherins is required for inhibition of interferon signaling. J Virol. 2010 Jan;84(2):1169–75.

104. Colavita F, Biava M, Castilletti C, Lanini S, Miccio R, Portella G, et al. Inflammatory and Humoral Immune Response during Ebola Virus Infection in Survivor and Fatal Cases Occurred in Sierra Leone during the 2014–2016 Outbreak in West Africa. Viruses. 2019 Apr 23;11(4).

105. Baize S, Leroy EM, Georges AJ, Georges-Courbot M-C, Capron M, Bedjabaga I, et al. Inflammatory responses in Ebola virus-infected patients. Clin Exp Immunol. 2002 Apr;128(1):163–8.

106. Baize S, Leroy EM, Georges-Courbot M-C, Capron M, Lansoud-Soukate J, Debré P, et al. Defective humoral responses and extensive intravascular apoptosis are associated with fatal outcome in Ebola virus-infected patients. Nature Medicine. 1999 Apr;5(4):423–6.

107. McElroy AK, Akondy RS, Davis CW, Ellebedy AH, Mehta AK, Kraft CS, et al. Human Ebola virus infection results in substantial immune activation. Proc Natl Acad Sci U S A. 2015 Apr 14;112(15):4719–24.

108. Leroy EM, Baize S, Volchkov VE, Fisher-Hoch SP, Georges-Courbot MC, Lansoud-Soukate J, et al. Human asymptomatic Ebola infection and strong inflammatory response. Lancet. 2000 Jun 24;355(9222):2210–5.

109. McElroy AK, Akondy RS, Mcllwain DR, Chen H, Bjornson-Hooper Z, Mukherjee N, et al. Immunologic timeline of Ebola virus disease and recovery in humans. JCI Insight. 2020 May 21;5(10).

110. Reynard S, Journeaux A, Gloaguen E, Schaeffer J, Varet H, Pietrosemoli N, et al. Immune parameters and outcomes during Ebola virus disease. JCI Insight. 2019 Jan 10;4(1).

111. Whelan SPJ, Barr JN, Wertz GW. Transcription and replication of nonsegmented negative-strand RNA viruses. Curr Top Microbiol Immunol. 2004;283:61–119.

112. Muhlberger E. Filovirus replication and transcription. Future Virology. 2007 Mar 1;2(2):205–16.

113. Licata JM, Johnson RF, Han Z, Harty RN. Contribution of Ebola Virus Glycoprotein, Nucleoprotein, and VP24 to Budding of VP40 Virus-Like Particles. Journal of Virology. 2004 Jul 15;78(14):7344–51.

114. Gc JB, Gerstman BS, Chapagain PP. Membrane association and localization dynamics of the Ebola virus matrix protein VP40. Biochimica et Biophysica Acta (BBA) - Biomembranes. 2017 Oct 1;1859(10):2012–20.

115. Ruigrok RW, Schoehn G, Dessen A, Forest E, Volchkov V, Dolnik O, et al. Structural characterization and membrane binding properties of the matrix protein VP40 of Ebola virus. J Mol Biol. 2000 Jun 30;300(1):103–12.

116. Timmins J, Schoehn G, Kohlhaas C, Klenk H-D, Ruigrok RWH, Weissenhorn W. Oligomerization and polymerization of the filovirus matrix protein VP40. Virology. 2003 Aug 1;312(2):359–68.

117. Hoenen T, Biedenkopf N, Zielecki F, Jung S, Groseth A, Feldmann H, et al. Oligomerization of Ebola Virus VP40 Is Essential for Particle Morphogenesis and Regulation of Viral Transcription. Journal of Virology. 2010 Jul 15;84(14):7053–63.

118. Scianimanico S, Schoehn G, Timmins J, Ruigrok RHW, Klenk H-D, Weissenhorn W. Membrane association induces a conformational change in the Ebola virus matrix protein. EMBO J. 2000 Dec 15;19(24):6732–41.

119. GC JB, Gerstman BS, Stahelin RV, Chapagain PP. The Ebola virus protein VP40 hexamer enhances the clustering of PI(4,5)P2 lipids in the plasma membrane. Phys Chem Chem Phys. 2016 Oct 19;18(41):28409–17.

120. Soni SP, Stahelin RV. The Ebola Virus Matrix Protein VP40 Selectively Induces Vesiculation from Phosphatidylserine-enriched Membranes. J Biol Chem. 2014 Nov 28;289(48):33590–7.

121. Adu-Gyamfi E, Johnson KA, Fraser ME, Scott JL, Soni SP, Jones KR, et al. Host Cell Plasma Membrane Phosphatidylserine Regulates the Assembly and Budding of Ebola Virus. J Virol. 2015 Aug 19;89(18):9440–53.

122. Johnson KA, Taghon GJF, Scott JL, Stahelin RV. The Ebola Virus matrix protein, VP40, requires phosphatidylinositol 4,5-bisphosphate (PI(4,5)P2) for extensive oligomerization at the plasma membrane and viral egress. Scientific Reports. 2016 Jan 12;6:19125.

123. Johnson KA, Budicini MR, Urata S, Bhattarai N, Gerstman BS, Chapagain PP, et al. PI(4,5)P2 Binding Sites in the Ebola Virus Matrix Protein Modulate Assembly and Budding. bioRxiv. 2018 Jun 7;341248.

124. Moller-Tank S, Maury W. Phosphatidylserine receptors: Enhancers of enveloped virus entry and infection. Virology. 2014 Nov;468–470:565–80.

125. Nanbo A, Maruyama J, Imai M, Ujie M, Fujioka Y, Nishide S, et al. Ebola virus requires a host scramblase for externalization of phosphatidylserine on the surface of viral particles. PLOS Pathogens. 2018 Jan 16;14(1):e1006848.

126. Harrison SC. Viral membrane fusion. Nat Struct Mol Biol. 2008 Jul;15(7):690–8.

127. Volchkov VE, Feldmann H, Volchkova VA, Klenk H-D. Processing of the Ebola virus glycoprotein by the proprotein convertase furin. Proc Natl Acad Sci U S A. 1998 May 12;95(10):5762–7.

128. Jeffers SA, Sanders DA, Sanchez A. Covalent Modifications of the Ebola Virus Glycoprotein. J Virol. 2002 Dec 15;76(24):12463–72.

129. Sanchez A, Yang Z-Y, Xu L, Nabel GJ, Crews T, Peters CJ. Biochemical Analysis of the Secreted and Virion Glycoproteins of Ebola Virus. J Virol. 1998 Aug;72(8):6442–7.

130. Moller-Tank S, Maury W. Ebola Virus Entry: A Curious and Complex Series of Events. PLoS Pathog. 2015 Apr 30;11(4):e1004731.

131. White JM, Delos SE, Brecher M, Schornberg K. Structures and Mechanisms of Viral Membrane Fusion Proteins: Multiple Variations on a Common Theme. Critical Reviews in Biochemistry and Molecular Biology. 2008 Jan 1;43(3):189–219.

132. Lee JE, Fusco ML, Hessell AJ, Oswald WB, Burton DR, Saphire EO. Structure of the Ebola virus glycoprotein bound to an antibody from a human survivor. Nature. 2008 Jul;454(7201):177–82.

133. Lennemann NJ, Rhein BA, Ndungo E, Chandran K, Qiu X, Maury W. Comprehensive Functional Analysis of N-Linked Glycans on Ebola Virus GP1. mBio. 2014 Feb 28;5(1).

134. Feldmann H, Will C, Schikore M, Slenczka W, Klenk HD. Glycosylation and oligomerization of the spike protein of Marburg virus. Virology. 1991 May;182(1):353–6.

135. Feldmann H, Nichol ST, Klenk HD, Peters CJ, Sanchez A. Characterization of filoviruses based on differences in structure and antigenicity of the virion glycoprotein. Virology. 1994 Mar;199(2):469–73.

136. Wang B, Wang Y, Frabutt DA, Zhang X, Yao X, Hu D, et al. Mechanistic Understanding of N-Glycosylation in Ebola Virus Glycoprotein Maturation and Function. J Biol Chem. 2017 Feb 14;jbc.M116.768168.

137. Durham ND, Howard AR, Govindan R, Senjobe F, Fels JM, Diehl WE, et al. Real-Time Analysis of Individual Ebola Virus Glycoproteins Reveals Pre-Fusion, Entry-Relevant Conformational Dynamics. Viruses. 2020 Jan 15;12(1).

138. Yang Z, Duckers HJ, Sullivan NJ, Sanchez A, Nabel EG, Nabel GJ. Identification of the Ebola virus glycoprotein as the main viral determinant of vascular cell cytotoxicity and injury. Nature Medicine. 2000 Aug;6(8):886–9.

139. Weissenhorn W, Carfí A, Lee K-H, Skehel JJ, Wiley DC. Crystal Structure of the Ebola Virus Membrane Fusion Subunit, GP2, from the Envelope Glycoprotein Ectodomain. Molecular Cell. 1998 Nov;2(5):605–16.

140. Malashkevich VN, Schneider BJ, McNally ML, Milhollen MA, Pang JX, Kim PS. Core structure of the envelope glycoprotein GP2 from Ebola virus at 1.9-Å resolution. PNAS. 1999 Mar 16;96(6):2662–7.

141. Gregory SM, Harada E, Liang B, Delos SE, White JM, Tamm LK. Structure and function of the complete internal fusion loop from Ebolavirus glycoprotein 2. PNAS. 2011 Jul 5;108(27):11211–6.

142. Marzi A, Möller P, Hanna SL, Harrer T, Eisemann J, Steinkasserer A, et al. Analysis of the Interaction of Ebola Virus Glycoprotein with DC-SIGN (Dendritic Cell—Specific Intercellular Adhesion Molecule 3—Grabbing Nonintegrin) and Its Homologue DC-SIGNR. J Infect Dis. 2007 Nov 15;196(Supplement 2):S237–46.

143. Alvarez CP, Lasala F, Carrillo J, Muñiz O, Corbí AL, Delgado R. C-type lectins DC-SIGN and L-SIGN mediate cellular entry by Ebola virus in cis and in trans. J Virol. 2002 Jul;76(13):6841–4.

144. Gramberg T, Hofmann H, Möller P, Lalor PF, Marzi A, Geier M, et al. LSECtin interacts with filovirus glycoproteins and the spike protein of SARS coronavirus. Virology. 2005 Sep 30;340(2):224–36.

145. Powlesland AS, Fisch T, Taylor ME, Smith DF, Tissot B, Dell A, et al. A novel mechanism for LSECtin binding to Ebola virus surface glycoprotein through truncated glycans. J Biol Chem. 2008 Jan 4;283(1):593–602.

146. Takada A, Fujioka K, Tsuiji M, Morikawa A, Higashi N, Ebihara H, et al. Human Macrophage C-Type Lectin Specific for Galactose and N-Acetylgalactosamine Promotes Filovirus Entry. Journal of Virology. 2004 Mar 15;78(6):2943–7.

147. Marzi A, Akhavan A, Simmons G, Gramberg T, Hofmann H, Bates P, et al. The Signal Peptide of the Ebolavirus Glycoprotein Influences Interaction with the Cellular Lectins DC-SIGN and DC-SIGNR. Journal of Virology. 2006 Jul 1;80(13):6305–17.

148. Lin G, Simmons G, Pöhlmann S, Baribaud F, Ni H, Leslie GJ, et al. Differential N-Linked Glycosylation of Human Immunodeficiency Virus and Ebola Virus Envelope Glycoproteins Modulates Interactions with DC-SIGN and DC-SIGNR. Journal of Virology. 2003 Jan 15;77(2):1337–46.

149. O'Hearn A, Wang M, Cheng H, Lear-Rooney CM, Koning K, Rumschlag-Booms E, et al. Role of EXT1 and Glycosaminoglycans in the Early Stage of Filovirus Entry. Journal of Virology. 2015 May 15;89(10):5441–9.

150. Fadok VA, Bratton DL, Frasch SC, Warner ML, Henson PM. The role of phosphatidylserine in recognition of apoptotic cells by phagocytes. Cell Death & Differentiation. 1998 Jul;5(7):551–62.

151. Amara A, Mercer J. Viral apoptotic mimicry. Nat Rev Micro. 2015 Aug;13(8):461–9.

152. Jemielity S, Wang JJ, Chan YK, Ahmed AA, Li W, Monahan S, et al. TIM-family Proteins Promote Infection of Multiple Enveloped Viruses through Virion-associated Phosphatidylserine. PLoS Pathog. 2013 Mar 28;9(3):e1003232.

153. Moller-Tank S, Kondratowicz AS, Davey RA, Rennert PD, Maury W. Role of the Phosphatidylserine Receptor TIM-1 in Enveloped-Virus Entry. J Virol. 2013 Aug 1;87(15):8327–41.

154. Kobayashi N, Karisola P, Peña-Cruz V, Dorfman DM, Jinushi M, Umetsu SE, et al. TIM-1 and TIM-4 Glycoproteins Bind Phosphatidylserine and Mediate Uptake of Apoptotic Cells. Immunity. 2007 Dec 21;27(6):927–40.

155. Kondratowicz AS, Lennemann NJ, Sinn PL, Davey RA, Hunt CL, Moller-Tank S, et al. T-cell immunoglobulin and mucin domain 1 (TIM-1) is a receptor for Zaire Ebolavirus and Lake Victoria Marburgvirus. PNAS. 2011 May 17;108(20):8426–31.

156. Shimojima M, Takada A, Ebihara H, Neumann G, Fujioka K, Irimura T, et al. Tyro3 Family-Mediated Cell Entry of Ebola and Marburg Viruses. Journal of Virology. 2006 Oct 15;80(20):10109–16.

157. Hunt CL, Kolokoltsov AA, Davey RA, Maury W. The Tyro3 Receptor Kinase Axl Enhances Macropinocytosis of Zaire Ebolavirus. J Virol. 2011 Jan 1;85(1):334–47.

158. Brindley MA, Hunt CL, Kondratowicz AS, Bowman J, Sinn PL, McCray PB, et al. Tyrosine kinase receptor Axl enhances entry of Zaire ebolavirus without direct interactions with the viral glycoprotein. Virology. 2011 Jul 5;415(2):83–94.

159. Mercer J, Helenius A. Gulping rather than sipping: macropinocytosis as a way of virus entry. Current Opinion in Microbiology. 2012 Aug;15(4):490–9.

160. Swanson JA, Watts C. Macropinocytosis. Trends Cell Biol. 1995 Nov;5(11):424–8.

161. Aleksandrowicz P, Marzi A, Biedenkopf N, Beimforde N, Becker S, Hoenen T, et al. Ebola virus enters host cells by macropinocytosis and clathrin-mediated endocytosis. J Infect Dis. 2011 Nov;204 Suppl 3:S957-967.

162. Nanbo A, Imai M, Watanabe S, Noda T, Takahashi K, Neumann G, et al. Ebolavirus Is Internalized into Host Cells via Macropinocytosis in a Viral Glycoprotein-Dependent Manner. PLoS Pathog. 2010 Sep;6(9).

163. Saeed MF, Kolokoltsov AA, Albrecht T, Davey RA. Cellular Entry of Ebola Virus Involves Uptake by a Macropinocytosis-Like Mechanism and Subsequent Trafficking through Early and Late Endosomes. PLoS Pathog. 2010 Sep 16;6(9):e1001110.

164. Kondratowicz AS, Hunt CL, Davey RA, Cherry S, Maury WJ. AMP-Activated Protein Kinase Is Required for the Macropinocytic Internalization of Ebolavirus. J Virol. 2013 Jan 15;87(2):746–55.

165. Mulherkar N, Raaben M, de la Torre JC, Whelan SP, Chandran K. The Ebola virus glycoprotein mediates entry via a non-classical dynamin-dependent macropinocytic pathway. Virology. 2011 Oct 25;419(2):72–83.

166. Kuroda M, Halfmann P, Kawaoka Y. HER2-mediated enhancement of Ebola virus entry. PLoS Pathog. 2020 Oct 14;16(10).

167. Stewart CM, Phan A, Bo Y, LeBlond ND, Smith TKT, Laroche G, et al. Ebola virus triggers receptor tyrosine kinase-dependent signaling to promote the delivery of viral particles to entry-conducive intracellular compartments. PLoS Pathog. 2021 Jan 29;17(1):e1009275.

168. Mingo RM, Simmons JA, Shoemaker CJ, Nelson EA, Schornberg KL, D'Souza RS, et al. Ebola and SARS Display Late Cell Entry Kinetics: Evidence that Transport to NPC1+ Endolysosomes is a Rate-Defining Step. J Virol. 2014 Dec 31;JVI.03398-14.

169. Spence JS, Krause TB, Mittler E, Jangra RK, Chandran K. Direct Visualization of Ebola Virus Fusion Triggering in the Endocytic Pathway. mBio. 2016 Mar 2;7(1):e01857-15.

170. Simmons JA, D'Souza RS, Ruas M, Galione A, Casanova JE, White JM. Ebolavirus Glycoprotein Directs Fusion through NPC1+ Endolysosomes. J Virol. 2016 Jan 1;90(1):605–10.

171. Carette JE, Raaben M, Wong AC, Herbert AS, Obernosterer G, Mulherkar N, et al. Ebola virus entry requires the cholesterol transporter Niemann-Pick C1. Nature. 2011 Sep 15;477(7364):340–3.

172. Brecher M, Schornberg KL, Delos SE, Fusco ML, Saphire EO, White JM. Cathepsin Cleavage Potentiates the Ebola Virus Glycoprotein To Undergo a Subsequent Fusion-Relevant Conformational Change. J Virol. 2012 Jan 1;86(1):364–72.

173. Schornberg K, Matsuyama S, Kabsch K, Delos S, Bouton A, White J. Role of Endosomal Cathepsins in Entry Mediated by the Ebola Virus Glycoprotein. J Virol. 2006 Apr 15;80(8):4174–8.

174. Chandran K, Sullivan NJ, Felbor U, Whelan SP, Cunningham JM. Endosomal Proteolysis of the Ebola Virus Glycoprotein Is Necessary for Infection. Science. 2005 Jun 10;308(5728):1643–5.

175. Zhao Y, Ren J, Harlos K, Stuart DI. Structure of glycosylated NPC1 luminal domain C reveals insights into NPC2 and Ebola virus interactions. FEBS Lett. 2016 Mar;590(5):605-12

176. Wang H, Shi Y, Song J, Qi J, Lu G, Yan J, et al. Ebola Viral Glycoprotein Bound to Its Endosomal Receptor Niemann-Pick C1. Cell. 2016 Jan 14;164(1):258–68.

177. Bortz RH, Wong AC, Grodus MG, Recht HS, Pulanco MC, Lasso G, et al. A Virion-Based Assay for Glycoprotein Thermostability Reveals Key Determinants of Filovirus Entry and Its Inhibition. Journal of Virology. 2020 Aug 31;94(18).

178. Harrison JS, Higgins CD, Chandran K, Lai JR. Designed protein mimics of the Ebola virus glycoprotein GP2 α-helical bundle: Stability and pH effects. Protein Sci. 2011 Sep;20(9):1587–96.

179. Harrison JS, Koellhoffer JF, Chandran K, Lai JR. Marburg Virus Glycoprotein GP2: pH-Dependent Stability of the Ectodomain α-Helical Bundle. Biochemistry. 2012 Mar 27;51(12):2515–25.

180. Misasi J, Chandran K, Yang J-Y, Considine B, Filone CM, Côté M, et al. Filoviruses Require Endosomal Cysteine Proteases for Entry but Exhibit Distinct Protease Preferences. J Virol. 2012 Mar 15;86(6):3284–92.

181. Ng M, Ndungo E, Jangra RK, Cai Y, Postnikova E, Radoshitzky SR, et al. Cell entry by a novel European filovirus requires host endosomal cysteine proteases and Niemann–Pick C1. Virology. 2014 Nov;468–470:637–46.

182. Martinez O, Johnson J, Manicassamy B, Rong L, Olinger GG, Hensley LE, et al. Zaire Ebola virus entry into human dendritic cells is insensitive to cathepsin L inhibition. Cellular Microbiology. 2010 Feb 1;12(2):148–57.

183. Wong AC, Sandesara RG, Mulherkar N, Whelan SP, Chandran K. A Forward Genetic Strategy Reveals Destabilizing Mutations in the Ebolavirus Glycoprotein That Alter Its Protease Dependence during Cell Entry. J Virol. 2010 Jan;84(1):163–75.

184. Côté M, Misasi J, Ren T, Bruchez A, Lee K, Filone CM, et al. Small molecule inhibitors reveal Niemann-Pick C1 is essential for Ebola virus infection. Nature. 2011 Sep 15;477(7364):344–8.

185. Miller EH, Obernosterer G, Raaben M, Herbert AS, Deffieu MS, Krishnan A, et al. Ebola virus entry requires the host-programmed recognition of an intracellular receptor. The EMBO Journal. 2012 Apr 18;31(8):1947–60.

186. Kondoh T, Letko M, Munster VJ, Manzoor R, Maruyama J, Furuyama W, et al. Single-Nucleotide Polymorphisms in Human NPC1 Influence Filovirus Entry Into Cells. The Journal of Infectious Diseases. 2018 Dec 15;218(Suppl 5):S397.

187. Hoffmann M, Hernández MG, Berger E, Marzi A, Pöhlmann S. The Glycoproteins of All Filovirus Species Use the Same Host Factors for Entry into Bat and Human Cells but Entry Efficiency Is Species Dependent. PLOS ONE. 2016 Feb 22;11(2):e0149651.

188. Herbert AS, Davidson C, Kuehne AI, Bakken R, Braigen SZ, Gunn KE, et al. Niemann-Pick C1 Is Essential for Ebolavirus Replication and Pathogenesis In Vivo. mBio. 2015 May 26;6(3).

189. Infante R, Brown M, Goldstein J. NPC2 facilitates bidirectional transfer of cholesterol between NPC1 and lipid bilayers, a potential step in cholesterol egress from lysosomes. The FASEB Journal. 2009;23(S1):521.5-521.5.

190. Vanier MT, Millat G. Niemann–Pick disease type C. Clinical Genetics. 2003;64(4):269–81.

191. Manicassamy B, Wang J, Jiang H, Rong L. Comprehensive Analysis of Ebola Virus GP1 in Viral Entry. Journal of Virology. 2005 Apr 15;79(8):4793–805.

192. Brindley MA, Hughes L, Ruiz A, McCray PB, Sanchez A, Sanders DA, et al. Ebola Virus Glycoprotein 1: Identification of Residues Important for Binding and Postbinding Events. Journal of Virology. 2007 Jul 15;81(14):7702–9.

193. Kuhn JH, Radoshitzky SR, Guth AC, Warfield KL, Li W, Vincent MJ, et al. Conserved Receptor-binding Domains of Lake Victoria Marburgvirus and Zaire Ebolavirus Bind a Common Receptor. J Biol Chem. 2006 Jun 9;281(23):15951–8.

194. Bornholdt ZA, Ndungo E, Fusco ML, Bale S, Flyak AI, Crowe JE, et al. Host-Primed Ebola Virus GP Exposes a Hydrophobic NPC1 Receptor-Binding Pocket, Revealing a Target for Broadly Neutralizing Antibodies. mBio. 2016 Mar 2;7(1):e02154-15.

195. Li X, Saha P, Li J, Blobel G, Pfeffer SR. Clues to the mechanism of cholesterol transfer from the structure of NPC1 middle lumenal domain bound to NPC2. PNAS. 2016 Sep 6;113(36):10079–84.

196. Gong X, Qian H, Zhou X, Wu J, Wan T, Cao P, et al. Structural Insights into the Niemann-Pick C1 (NPC1)-Mediated Cholesterol Transfer and Ebola Infection. Cell. 2016 Jun 2;165(6):1467–78.

197. Ndungo E, Herbert AS, Raaben M, Obernosterer G, Biswas R, Miller EH, et al. A Single Residue in Ebola Virus Receptor NPC1 Influences Cellular Host Range in Reptiles. mSphere. 2016 Apr;1(2).

198. Pontremoli C, Forni D, Cagliani R, Filippi G, De Gioia L, Pozzoli U, et al. Positive Selection Drives Evolution at the Host–Filovirus Interaction Surface. Mol Biol Evol. 2016 Nov 1;33(11):2836–47.

199. White JM, Whittaker GR. Fusion of Enveloped Viruses in Endosomes. Traffic. 2016 Jun;17(6):593–614.

200. Nathan L, Lai A, Millet J, Straus M, Whittaker GR, Freed JH, et al. Calcium ions directly interact with the Ebola virus fusion peptide to promote structure-function changes that enhance infection. ACS Infect Dis. 2020 Feb 14;6(2):250-260.

201. Das DK, Bulow U, Diehl WE, Durham ND, Senjobe F, Chandran K, et al. Conformational changes in the Ebola virus membrane fusion machine induced by pH, Ca2+, and receptor binding. PLOS Biology. 2020 Feb 10;18(2):e3000626.

202. Sakurai Y, Kolokoltsov AA, Chen C-C, Tidwell MW, Bauta WE, Klugbauer N, et al. Two-pore channels control Ebola virus host cell entry and are drug targets for disease treatment. Science. 2015 Feb 27;347(6225):995–8.

203. Penny CJ, Vassileva K, Jha A, Yuan Y, Chee X, Yates E, et al. Mining of Ebola virus entry inhibitors identifies approved drugs as two-pore channel pore blockers. Biochimica et Biophysica Acta (BBA) - Molecular Cell Research. 2019 Jul 1;1866(7):1151–61.

204. Huotari J, Helenius A. Endosome maturation. The EMBO Journal. 2011 Aug 31;30(17):3481–500.

205. Qiu S, Côté M. From hitchhiker to hijacker: pathogen exploitation of endosomal phosphoinositides. Biochemistry and Cell Biology. 2019 Feb;97(1):1-9.

206. Gruenberg J, van der Goot FG. Mechanisms of pathogen entry through the endosomal compartments. Nat Rev Mol Cell Biol. 2006 Jul;7(7):495–504.

207. Lozach P-Y, Huotari J, Helenius A. Late-penetrating viruses. Current Opinion in Virology. 2011 Jul;1(1):35–43.

208. Pizarro-Cerdá J, Kühbacher A, Cossart P. Phosphoinositides and host–pathogen interactions. Biochimica et Biophysica Acta (BBA) - Molecular and Cell Biology of Lipids. 2015 Jun;1851(6):911–8.

209. Mottola G. The complexity of Rab5 to Rab7 transition guarantees specificity of pathogen subversion mechanisms. Front Cell Infect Microbiol. 2014 Dec 22;4:180.

210. Rink J, Ghigo E, Kalaidzidis Y, Zerial M. Rab Conversion as a Mechanism of Progression from Early to Late Endosomes. Cell. 2005 Sep 9;122(5):735–49.

211. Zerial M, McBride H. Rab proteins as membrane organizers. Nature Reviews Molecular Cell Biology. 2001 Feb;2(2):107–17.

212. Poteryaev D, Datta S, Ackema K, Zerial M, Spang A. Identification of the Switch in Early-to-Late Endosome Transition. Cell. 2010 Apr 30;141(3):497–508.

213. Lippé R, Miaczynska M, Rybin V, Runge A, Zerial M. Functional Synergy between Rab5 Effector Rabaptin-5 and Exchange Factor Rabex-5 When Physically Associated in a Complex. Mol Biol Cell. 2001 Jul;12(7):2219–28.

214. Horiuchi H, Lippé R, McBride HM, Rubino M, Woodman P, Stenmark H, et al. A novel Rab5 GDP/GTP exchange factor complexed to Rabaptin-5 links nucleotide exchange to effector recruitment and function. Cell. 1997 Sep 19;90(6):1149–59.

215. Rybin V, Ullrich O, Rubino M, Alexandrov K, Simon I, Seabra MC, et al. GTPase activity of Rab5 acts as a timer for endocytic membrane fusion. Nature. 1996 Sep 19;383(6597):266–9.

216. Stenmark H, Vitale G, Ullrich O, Zerial M. Rabaptin-5 is a direct effector of the small GTPase Rab5 in endocytic membrane fusion. Cell. 1995 Nov 3;83(3):423–32.

217. Lippé R, Horiuchi H, Runge A, Zerial M. Expression, purification, and characterization of Rab5 effector complex, rabaptin-5/rabex-5. Methods Enzymol. 2001;329:132–45.

218. Schnatwinkel C, Christoforidis S, Lindsay MR, Uttenweiler-Joseph S, Wilm M, Parton RG, et al. The Rab5 Effector Rabankyrin-5 Regulates and Coordinates Different Endocytic Mechanisms. PLOS Biology. 2004 Aug 24;2(9):e261.

219. Christoforidis S, Miaczynska M, Ashman K, Wilm M, Zhao L, Yip S-C, et al. Phosphatidylinositol-3-OH kinases are Rab5 effectors. Nature Cell Biology. 1999 Aug;1(4):249–52.

220. Nielsen E, Christoforidis S, Uttenweiler-Joseph S, Miaczynska M, Dewitte F, Wilm M, et al. Rabenosyn-5, a Novel Rab5 Effector, Is Complexed with Hvps45 and Recruited to Endosomes through a Fyve Finger Domain. Journal of Cell Biology. 2000 Oct 30;151(3):601–12.

221. Christoforidis S, McBride HM, Burgoyne RD, Zerial M. The Rab5 effector EEA1 is a core component of endosome docking. Nature. 1999 Feb 18;397(6720):621–5.

222. Merithew E, Stone C, Eathiraj S, Lambright DG. Determinants of Rab5 Interaction with the N Terminus of Early Endosome Antigen 1. J Biol Chem. 2003 Mar 7;278(10):8494–500.

223. Lawe DC, Patki V, Heller-Harrison R, Lambright D, Corvera S. The FYVE Domain of Early Endosome Antigen 1 Is Required for Both Phosphatidylinositol 3-Phosphate and Rab5 Binding. J Biol Chem. 2000 Feb 4;275(5):3699–705.

224. Markgraf DF, Ahnert F, Arlt H, Mari M, Peplowska K, Epp N, et al. The CORVET subunit Vps8 cooperates with the Rab5 homolog Vps21 to induce clustering of late endosomal compartments. Mol Biol Cell. 2009 Dec;20(24):5276–89.

225. Balderhaar HJ kleine, Lachmann J, Yavavli E, Bröcker C, Lürick A, Ungermann C. The CORVET complex promotes tethering and fusion of Rab5/Vps21-positive membranes. PNAS. 2013 Mar 5;110(10):3823–8.

226. Peplowska K, Markgraf DF, Ostrowicz CW, Bange G, Ungermann C. The CORVET tethering complex interacts with the yeast Rab5 homolog Vps21 and is involved in endo-lysosomal biogenesis. Dev Cell. 2007 May;12(5):739–50.

227. Balderhaar HJ kleine, Ungermann C. CORVET and HOPS tethering complexes – coordinators of endosome and lysosome fusion. J Cell Sci. 2013 Mar 15;126(6):1307–16.

228. Del Conte-Zerial P, Brusch L, Rink JC, Collinet C, Kalaidzidis Y, Zerial M, et al. Membrane identity and GTPase cascades regulated by toggle and cut-out switches. Mol Syst Biol. 2008 Jul 15;4:206.

229. Haas AK, Fuchs E, Kopajtich R, Barr FA. A GTPase-activating protein controls Rab5 function in endocytic trafficking. Nature Cell Biology. 2005 Sep;7(9):887–93.

230. Chotard L, Mishra AK, Sylvain M-A, Tuck S, Lambright DG, Rocheleau CE. TBC-2 regulates RAB-5/RAB-7-mediated endosomal trafficking in Caenorhabditis elegans. Mol Biol Cell. 2010 Jul 1;21(13):2285–96.

231. Langemeyer L, Borchers A-C, Herrmann E, Füllbrunn N, Han Y, Perz A, et al. A conserved and regulated mechanism drives endosomal Rab transition. Pfeffer SR, Zerial M, editors. eLife. 2020 May 11;9:e56090.

232. Kinchen JM, Ravichandran KS. Identification of two evolutionarily conserved genes regulating processing of engulfed apoptotic cells. Nature. 2010 Apr;464(7289):778–82.

233. Nordmann M, Cabrera M, Perz A, Bröcker C, Ostrowicz C, Engelbrecht-Vandré S, et al. The Mon1-Ccz1 Complex Is the GEF of the Late Endosomal Rab7 Homolog Ypt7. Current Biology. 2010 Sep 28;20(18):1654–9.

234. Cabrera M, Engelbrecht-Vandré S, Ungermann C. Function of the Mon1-Ccz1 complex on endosomes. Small GTPases. 2014 Oct 31;5(3).

235. Cabrera M, Nordmann M, Perz A, Schmedt D, Gerondopoulos A, Barr F, et al. The Mon1–Ccz1 GEF activates the Rab7 GTPase Ypt7 via a longin-fold–Rab interface and association with PI3P-positive membranes. J Cell Sci. 2014 Mar 1;127(5):1043–51.

236. Marwaha R, Arya SB, Jagga D, Kaur H, Tuli A, Sharma M. The Rab7 effector PLEKHM1 binds Arl8b to promote cargo traffic to lysosomes. J Cell Biol. 2017 Apr 3;216(4):1051–70.

237. Rawet-Slobodkin M, Elazar Z. PLEKHM1: A Multiprotein Adaptor for the Endolysosomal System. Molecular Cell. 2015 Jan 8;57(1):1–3.

238. Kant R van der, Jonker CTH, Wijdeven RH, Bakker J, Janssen L, Klumperman J, et al. Characterization of the Mammalian CORVET and HOPS Complexes and Their Modular Restructuring for Endosome Specificity. J Biol Chem. 2015 Dec 18;290(51):30280–90.

239. Jordens I, Fernandez-Borja M, Marsman M, Dusseljee S, Janssen L, Calafat J, et al. The Rab7 effector protein RILP controls lysosomal transport by inducing the recruitment of dynein-dynactin motors. Curr Biol. 2001 Oct 30;11(21):1680–5.

240. Cantalupo G, Alifano P, Roberti V, Bruni CB, Bucci C. Rab-interacting lysosomal protein (RILP): the Rab7 effector required for transport to lysosomes. EMBO J. 2001 Feb 15;20(4):683–93.

241. Liu K, Xing R, Jian Y, Gao Z, Ma X, Sun X, et al. WDR91 is a Rab7 effector required for neuronal development. J Cell Biol. 2017 Oct 2;216(10):3307–21.

242. Sun Q, Westphal W, Wong KN, Tan I, Zhong Q. Rubicon controls endosome maturation as a Rab7 effector. PNAS. 2010 Nov 9;107(45):19338–43.

243. Kim Y-M, Jung CH, Seo M, Kim EK, Park J-M, Bae SS, et al. mTORC1 Phosphorylates UVRAG to Negatively Regulate Autophagosome and Endosome Maturation. Molecular Cell. 2015 Jan 22;57(2):207–18.

244. Balla T. Phosphoinositides: Tiny Lipids With Giant Impact on Cell Regulation. Physiological Reviews. 2013 Jul 1;93(3):1019–137.

245. Funderburk SF, Wang QJ, Yue Z. The Beclin 1-VPS34 complex--at the crossroads of autophagy and beyond. Trends Cell Biol. 2010 Jun;20(6):355–62.

246. Murray JT, Panaretou C, Stenmark H, Miaczynska M, Backer JM. Role of Rab5 in the Recruitment of hVps34/p150 to the Early Endosome. Traffic. 2002;3(6):416–27.

247. Gillooly DJ, Simonsen A, Stenmark H. Cellular functions of phosphatidylinositol 3-phosphate and FYVE domain proteins. Biochem J. 2001 Apr 15;355(Pt 2):249–58.

248. Lemmon MA. Membrane recognition by phospholipid-binding domains. Nat Rev Mol Cell Biol. 2008 Feb;9(2):99–111.

249. Henne WM, Buchkovich NJ, Emr SD. The ESCRT Pathway. Developmental Cell. 2011 Jul 19;21(1):77–91.

250. Babst M. MVB Vesicle Formation: ESCRT-Dependent, ESCRT-Independent and Everything in Between. Curr Opin Cell Biol. 2011 Aug;23(4):452–7.

251. Matsuo H, Chevallier J, Mayran N, Blanc IL, Ferguson C, Fauré J, et al. Role of LBPA and Alix in Multivesicular Liposome Formation and Endosome Organization. Science. 2004 Jan 23;303(5657):531–4.

252. Kajimoto T, Okada T, Miya S, Zhang L, Nakamura S. Ongoing activation of sphingosine 1-phosphate receptors mediates maturation of exosomal multivesicular endosomes. Nature Communications. 2013 Nov 15;4(1):2712.

253. Trajkovic K, Hsu C, Chiantia S, Rajendran L, Wenzel D, Wieland F, et al. Ceramide Triggers Budding of Exosome Vesicles into Multivesicular Endosomes. Science. 2008 Feb 29;319(5867):1244–7.

254. Hessvik NP, Llorente A. Current knowledge on exosome biogenesis and release. Cell Mol Life Sci. 2018 Jan 1;75(2):193–208.

255. Gruenberg J, Stenmark H. The biogenesis of multivesicular endosomes. Nature Reviews Molecular Cell Biology. 2004 Apr 1;5(4):nrm1360.

256. Sbrissa D, Ikonomov OC, Shisheva A. Phosphatidylinositol 3-Phosphate-interacting Domains in PIKfyve. J Biol Chem. 2002 Feb 22;277(8):6073–9.

257. McEwen RK, Dove SK, Cooke FT, Painter GF, Holmes AB, Shisheva A, et al. Complementation analysis in PtdInsP kinase-deficient yeast mutants demonstrates that Schizosaccharomyces pombe and murine Fab1p homologues are phosphatidylinositol 3-phosphate 5-kinases. J Biol Chem. 1999 Nov 26;274(48):33905–12.

258. Jefferies HBJ, Cooke FT, Jat P, Boucheron C, Koizumi T, Hayakawa M, et al. A selective PIKfyve inhibitor blocks PtdIns(3,5)P2 production and disrupts endomembrane transport and retroviral budding. EMBO Rep. 2008 Feb;9(2):164–70.

259. Sbrissa D, Ikonomov OC, Fenner H, Shisheva A. ArPIKfyve Homomeric and Heteromeric Interactions Scaffold PIKfyve and Sac3 in a Complex to Promote PIKfyve Activity and Functionality. Journal of Molecular Biology. 2008 Dec 26;384(4):766–79.

260. Sbrissa D, Ikonomov OC, Fu Z, Ijuin T, Gruenberg J, Takenawa T, et al. Core Protein Machinery for Mammalian Phosphatidylinositol 3,5-Bisphosphate Synthesis and Turnover That Regulates the Progression of Endosomal Transport. J Biol Chem. 2007 Aug 17;282(33):23878–91.

261. Ikonomov OC, Sbrissa D, Mlak K, Kanzaki M, Pessin J, Shisheva A. Functional Dissection of Lipid and Protein Kinase Signals of PIKfyve Reveals the Role of PtdIns 3,5-P2 Production for Endomembrane Integrity. J Biol Chem. 2002 Mar 15;277(11):9206–11.

262. Lees JA, Li P, Kumar N, Weisman LS, Reinisch KM. Insights into Lysosomal PI(3,5)P2 Homeostasis from a Structural-Biochemical Analysis of the PIKfyve Lipid Kinase Complex. Molecular Cell. 2020 Nov 19;80(4):736-743.

263. Ikonomov OC, Sbrissa D, Shisheva A. Mammalian Cell Morphology and Endocytic Membrane Homeostasis Require Enzymatically Active Phosphoinositide 5-Kinase PIKfyve. J Biol Chem. 2001 Jul 13;276(28):26141–7.

264. Ikonomov OC, Sbrissa D, Fenner H, Shisheva A. PIKfyve-ArPIKfyve-Sac3 Core Complex. J Biol Chem. 2009 Dec 18;284(51):35794–806.

265. Ikonomov OC, Sbrissa D, Delvecchio K, Xie Y, Jin J-P, Rappolee D, et al. The Phosphoinositide Kinase PIKfyve Is Vital in Early Embryonic Development. J Biol Chem. 2011 Apr 15;286(15):13404–13.

266. Jin N, Chow CY, Liu L, Zolov SN, Bronson R, Davisson M, et al. VAC14 nucleates a protein complex essential for the acute interconversion of PI3P and PI(3,5)P2 in yeast and mouse. EMBO J. 2008 Dec 17;27(24):3221–34.

267. Shisheva A. PIKfyve: Partners, Significance, Debates and Paradoxes. Cell Biol Int. 2008 Jun;32(6):591–604.

268. Shisheva A. PIKfyve and its Lipid Products in Health and in Sickness. Phosphoinositides and Disease Springer Netherlands; 2012. p. 127–62. Current Topics in Microbiology and Immunology.

269. Ikonomov OC, Sbrissa D, Fligger J, Delvecchio K, Shisheva A. ArPIKfyve Regulates Sac3 Protein Abundance and Turnover. J Biol Chem. 2010 Aug 27;285(35):26760–4.

270. Botelho RJ, Efe JA, Teis D, Emr SD. Assembly of a Fab1 Phosphoinositide Kinase Signaling Complex Requires the Fig4 Phosphoinositide Phosphatase. Mol Biol Cell. 2008 Oct;19(10):4273–86.

271. Bharadwaj R, Cunningham KM, Zhang K, Lloyd TE. FIG4 regulates lysosome membrane homeostasis independent of phosphatase function. Hum Mol Genet. 2015 Dec 11;ddv505.

272. Strunk BS, Steinfeld N, Lee S, Jin N, Muñoz-Rivera C, Meeks G, et al. Roles for a lipid phosphatase in the activation of its opposing lipid kinase. MBoC. 2020 Jun 17;31(17):1835–45.

273. Compton LM, Ikonomov OC, Sbrissa D, Garg P, Shisheva A. Active vacuolar H+ATPase and functional cycle of Rab5 are required for the vacuolation defect triggered by PtdIns(3,5)P2 loss under PIKfyve or Vps34 deficiency. American Journal of Physiology - Cell Physiology. 2016 Jun 22;ajpcell.00104.2016.

274. de Lartigue J, Polson H, Feldman M, Shokat K, Tooze SA, Urbé S, et al. PIKfyve Regulation of Endosome-Linked Pathways. Traffic. 2009 Jul 1;10(7):883–93.

275. Ikonomov OC, Sbrissa D, Shisheva A. Localized PtdIns 3,5-P2 synthesis to regulate early endosome dynamics and fusion. Am J Physiol, Cell Physiol. 2006 Aug;291(2):C393-404.

276. Min SH, Suzuki A, Stalker TJ, Zhao L, Wang Y, McKennan C, et al. Loss of PIKfyve in platelets causes a lysosomal disease leading to inflammation and thrombosis in mice. Nat Commun. 2014 Sep 2;5:4691.

277. Choy CH, Saffi G, Gray MA, Wallace C, Dayam RM, Ou Z-YA, et al. Lysosome enlargement during inhibition of the lipid kinase PIKfyve proceeds through lysosome coalescence. Journal of Cell Science. 2018 May 15;131(10).

278. Kim GHE, Dayam RM, Prashar A, Terebiznik M, Botelho RJ. PIKfyve Inhibition Interferes with Phagosome and Endosome Maturation in Macrophages. Traffic. 2014 Oct 1;15(10):1143–63.

279. Schulze U, Vollenbröker B, Kühnl A, Granado D, Bayraktar S, Rescher U, et al. Cellular vacuolization caused by overexpression of the PIKfyve-binding deficient Vac14L156R is rescued by starvation and inhibition of vacuolar-ATPase. Biochimica et Biophysica Acta (BBA) - Molecular Cell Research. 2017 May;1864(5):749-759

280. McCartney AJ, Zhang Y, Weisman LS. Phosphatidylinositol 3,5-bisphosphate: low abundance, high significance. Bioessays. 2014 Jan;36(1):52–64.

281. Whitley P, Reaves BJ, Hashimoto M, Riley AM, Potter BVL, Holman GD. Identification of Mammalian Vps24p as an Effector of Phosphatidylinositol 3,5-Bisphosphate-dependent Endosome Compartmentalization. J Biol Chem. 2003 Oct 3;278(40):38786–95.

282. Dong X, Shen D, Wang X, Dawson T, Li X, Zhang Q, et al. PI(3,5)P2 Controls Membrane Traffic by Direct Activation of Mucolipin Ca2+ Release Channels in the Endolysosome. Nat Commun. 2010 Jul 13;1(4).

283. Jha A, Ahuja M, Patel S, Brailoiu E, Muallem S. Convergent regulation of the lysosomal two-pore channel-2 by Mg2+, NAADP, PI(3,5)P2 and multiple protein kinases. EMBO J. 2014 Mar 3;33(5):501–11.

284. Li X, Wang X, Zhang X, Zhao M, Tsang WL, Zhang Y, et al. Genetically encoded fluorescent probe to visualize intracellular phosphatidylinositol 3,5-bisphosphate localization and dynamics. PNAS. 2013 Dec 24;110(52):21165–70.

285. Hay JC. Calcium: a fundamental regulator of intracellular membrane fusion? EMBO Rep. 2007 Mar;8(3):236–40.

286. Luzio JP, Bright NA, Pryor PR. The role of calcium and other ions in sorting and delivery in the late endocytic pathway. Biochemical Society Transactions. 2007 Nov 1;35(5):1088–91.

287. Grimm C, Butz E, Chen C-C, Wahl-Schott C, Biel M. From mucolipidosis type IV to Ebola: TRPML and two-pore channels at the crossroads of endo-lysosomal trafficking and disease. Cell Calcium. 2017 Nov;67:148-155

288. Venkatachalam K, Wong C-O, Zhu MX. The role of TRPMLs in endolysosomal trafficking and function. Cell Calcium. 2015 Jul 1;58(1):48–56.

289. Shen D, Wang X, Xu H. Pairing Phosphoinositides with Calcium Ions in Endolysosomal Dynamics. Bioessays. 2011 Jun;33(6):448–57.

290. Castonguay J, Orth JHC, Müller T, Sleman F, Grimm C, Wahl-Schott C, et al. The two-pore channel TPC1 is required for efficient protein processing through early and recycling endosomes. Sci Rep. 2017 Aug 30;7(1):10038.

291. Dayam RM, Saric A, Shilliday RE, Botelho RJ. The Phosphoinositide-Gated Lysosomal Ca2+ Channel, TRPML1, Is Required for Phagosome Maturation. Traffic. 2015 Sep 1;16(9):1010–26.

292. Dayam RM, Sun CX, Choy CH, Mancuso G, Glogauer M, Botelho RJ. The Lipid Kinase PIKfyve Coordinates the Neutrophil Immune Response through the Activation of the Rac GTPase. The Journal of Immunology. 2017 Sep 15;199(6):2096–105.

293. Krishna S, Palm W, Lee Y, Yang W, Bandyopadhyay U, Xu H, et al. PIKfyve regulates vacuole maturation and nutrient recovery following engulfment. Developmental cell. 2016 Sep 12;38(5):536.

294. Isobe Y, Nigorikawa K, Tsurumi G, Takemasu S, Takasuga S, Kofuji S, et al. PIKfyve accelerates phagosome acidification through activation of TRPML1 while arrests aberrant vacuolation independent of the Ca2+ channel. J Biochem. 2019 Jan 1;165(1):75–84.

295. Capurro MI, Greenfield LK, Prashar A, Xia S, Abdullah M, Wong H, et al. VacA generates a protective intracellular reservoir for Helicobacter pylori that is eliminated by activation of the lysosomal calcium channel TRPML1. Nat Microbiol. 2019 Aug;4(8):1411–23.

296. Qiu S, Leung A, Bo Y, Kozak RA, Anand SP, Warkentin C, et al. Ebola virus requires phosphatidylinositol (3,5) bisphosphate production for efficient viral entry. Virology. 2017 Oct 11;513:17–28.

297. Zou J, Hu B, Arpag S, Yan Q, Hamilton A, Zeng Y-S, et al. Reactivation of Lysosomal Ca2+ Efflux Rescues Abnormal Lysosomal Storage in FIG4-Deficient Cells. J Neurosci. 2015 Apr 29;35(17):6801–12.

298. Marshansky V, Futai M. The V-type H+-ATPase in vesicular trafficking: targeting, regulation and function. Curr Opin Cell Biol. 2008 Aug;20(4):415–26.

299. Scott CC, Gruenberg J. Ion flux and the function of endosomes and lysosomes: pH is just the start. BioEssays. 2011;33(2):103–10.

300. Bowman EJ, Siebers A, Altendorf K. Bafilomycins: a class of inhibitors of membrane ATPases from microorganisms, animal cells, and plant cells. Proc Natl Acad Sci U S A. 1988 Nov;85(21):7972–6.

301. Ohkuma S, Chudzik J, Poole B. The effects of basic substances and acidic ionophores on the digestion of exogenous and endogenous proteins in mouse peritoneal macrophages. Journal of Cell Biology. 1986 Mar 1;102(3):959–66.

302. Henao-Restrepo AM, Longini IM, Egger M, Dean NE, Edmunds WJ, Camacho A, et al. Efficacy and effectiveness of an rVSV-vectored vaccine expressing Ebola surface glycoprotein: interim results from the Guinea ring vaccination cluster-randomised trial. Lancet. 2015 Aug 29;386(9996):857–66.

303. Qiu X, Audet J, Lv M, He S, Wong G, Wei H, et al. Two-mAb cocktail protects macaques against the Makona variant of Ebola virus. Science Translational Medicine. 2016 Mar 9;8(329):329ra33-329ra33.

304. Qiu X, Wong G, Audet J, Bello A, Fernando L, Alimonti JB, et al. Reversion of advanced Ebola virus disease in nonhuman primates with ZMapp. Nature. 2014 Oct 2;514(7520):47-53.

305. Mendoza EJ, Qiu X, Kobinger GP. Progression of Ebola Therapeutics During the 2014–2015 Outbreak. Trends in Molecular Medicine. 2016 Feb 1;22(2):164–73.

306. Nelson EA, Dyall J, Hoenen T, Barnes AB, Zhou H, Liang JY, et al. The phosphatidylinositol-3-phosphate 5-kinase inhibitor apilimod blocks filoviral entry and infection. PLOS Neglected Tropical Diseases. 2017 Apr 12;11(4):e0005540.

307. Liang C, Lee J, Inn K-S, Gack MU, Li Q, Roberts EA, et al. Beclin1-binding UVRAG targets the class C Vps complex to coordinate autophagosome maturation and endocytic trafficking. Nat Cell Biol. 2008 Jul;10(7):776–87.

308. Pirooz SD, He S, Zhang T, Zhang X, Zhao Z, Oh S, et al. UVRAG is required for virus entry through combinatorial interaction with the class C-Vps complex and SNAREs. PNAS. 2014 Feb 18;111(7):2716–21.

309. Aoki Y, Manzano R, Lee Y, Dafinca R, Aoki M, Douglas AGL, et al. C9orf72 and RAB7L1 regulate vesicle trafficking in amyotrophic lateral sclerosis and frontotemporal dementia. Brain. 2017 Apr 1;140(4):887–97.

310. Stewart CM, Dorion SS, Ottenbrite MAF, LeBlond ND, Smith TKT, Qiu S, et al. A Diacylglycerol Kinase Inhibitor, R-59-022, Blocks Filovirus Internalization in Host Cells. Viruses. 2019 Mar;11(3).

311. Wang T, Wei JJ, Sabatini DM, Lander ES. Genetic Screens in Human Cells Using the CRISPR-Cas9 System. Science. 2014 Jan 3;343(6166):80–4.

312. Vidigal JA, Ventura A. Rapid and efficient one-step generation of paired gRNA CRISPR-Cas9 libraries. Nat Commun. 2015 Aug 17;6:8083.

313. Jinek M, Chylinski K, Fonfara I, Hauer M, Doudna JA, Charpentier E. A Programmable Dual-RNA–Guided DNA Endonuclease in Adaptive Bacterial Immunity. Science. 2012 Aug 17;337(6096):816–21.

314. Liang C, Feng P, Ku B, Dotan I, Canaani D, Oh B-H, et al. Autophagic and tumour suppressor activity of a novel Beclin1-binding protein UVRAG. Nature Cell Biology. 2006 Jul;8(7):688.

315. Jiang P, Mizushima N. LC3- and p62-based biochemical methods for the analysis of autophagy progression in mammalian cells. Methods. 2015 Mar 15;75:13–8.

316. Cherry S. What have RNAi screens taught us about viral-host interactions? Current opinion in microbiology. 2009 Aug;12(4):446.

317. Jae LT, Raaben M, Herbert AS, Kuehne AI, Wirchnianski AS, Soh T, et al. Lassa virus entry requires a trigger-induced receptor switch. Science. 2014 Jun 27;344(6191):1506–10.

318. Marceau CD, Puschnik AS, Majzoub K, Ooi YS, Brewer SM, Fuchs G, et al. Genetic dissection of Flaviviridae host factors through genome-scale CRISPR screens. Nature. 2016 Jul;535(7610):159–63.

319. Afzal S, Hao Z, Itsumi M, Abouelkheer Y, Brenner D, Gao Y, et al. Autophagy-independent functions of UVRAG are essential for peripheral naive T-cell homeostasis. PNAS. 2015 Jan 27;112(4):1119–24.

320. Perini ED, Schaefer R, Stöter M, Kalaidzidis Y, Zerial M. Mammalian CORVET Is Required for Fusion and Conversion of Distinct Early Endosome Subpopulations. Traffic. 2014;15(12):1366–89.

321. Miaczynska M, Christoforidis S, Giner A, Shevchenko A, Uttenweiler-Joseph S, Habermann B, et al. APPL Proteins Link Rab5 to Nuclear Signal Transduction via an Endosomal Compartment. Cell. 2004 Feb 6;116(3):445–56.

322. Desai TM, Marin M, Mason C, Melikyan GB. pH regulation in early endosomes and interferon-inducible transmembrane proteins control avian retrovirus fusion. The Journal of Biological Chemistry. 2017 May 12;292(19):7817.

323. Shtanko O, Reyes AN, Jackson WT, Davey RA. Autophagy-Associated Proteins Control Ebola Virus Internalization Into Host Cells. J Infect Dis. 2018 Dec 15;218(Suppl 5):S346–54.

324. Konermann S, Brigham MD, Trevino AE, Joung J, Abudayyeh OO, Barcena C, et al. Genome-scale transcriptional activation by an engineered CRISPR-Cas9 complex. Nature. 2015 Jan;517(7536):583–8.

325. Hayer A, Shao L, Chung M, Joubert L-M, Yang HW, Tsai F-C, et al. Engulfed cadherin fingers are polarized junctional structures between collectively migrating endothelial cells. Nature cell biology. 2016 Dec;18(12):1311.

326. Duex JE, Nau JJ, Kauffman EJ, Weisman LS. Phosphoinositide 5-phosphatase Fig 4p is required for both acute rise and subsequent fall in stress-induced phosphatidylinositol 3,5-bisphosphate levels. Eukaryotic Cell. 2006 Apr;5(4):723–31.

327. Morioka S, Nigorikawa K, Hazeki K, Ohmura M, Sakamoto H, Matsumura T, et al. Phosphoinositide phosphatase Sac3 regulates the cell surface expression of scavenger receptor A and formation of lipid droplets in macrophages. Experimental Cell Research. 2017 Aug 15;357(2):252-259.

328. Ho CY, Alghamdi TA, Botelho RJ. Phosphatidylinositol-3,5-bisphosphate: no longer the poor PIP2. Traffic. 2012 Jan;13(1):1–8.

329. Jin N, Lang MJ, Weisman LS. Phosphatidylinositol 3,5-bisphosphate: regulation of cellular events in space and time. Biochemical Society Transactions. 2016 Feb 15;44(1):177–84.

330. Er EE, Mendoza MC, Mackey AM, Rameh LE, Blenis J. AKT Facilitates EGFR Trafficking and Degradation by Phosphorylating and Activating PIKfyve. Sci Signal. 2013 Jun 11;6(279):ra45–ra45.

331. Ferguson CJ, Lenk GM, Meisler MH. Defective autophagy in neurons and astrocytes from mice deficient in PI(3,5)P2. Hum Mol Genet. 2009 Dec 15;18(24):4868–78.

332. Ikonomov OC, Fligger J, Sbrissa D, Dondapati R, Krzysztof M, Deeb R, Shisheva A. Kinesin adapter JLP links PIKfyve to microtubule-based endosome-to-trans-Golgi network traffic of furin., Kinesin Adapter JLP Links PIKfyve to Microtubule-based Endosome-to-Trans-Golgi Network Traffic of Furin. J Biol Chem. 2009 Feb 6;284, 284(6, 6):3750, 3750–61.

333. Martin S, Harper CB, May LM, Coulson EJ, Meunier FA, Osborne SL. Inhibition of PIKfyve by YM-201636 Dysregulates Autophagy and Leads to Apoptosis-Independent Neuronal Cell Death. PLoS ONE. 2013 Mar 27;8(3):e60152.

334. Chow CY, Landers JE, Bergren SK, Sapp PC, Grant AE, Jones JM, et al. Deleterious Variants of FIG4, a Phosphoinositide Phosphatase, in Patients with ALS. Am J Hum Genet. 2009 Jan 9;84(1):85–8.

335. Chow CY, Zhang Y, Dowling JJ, Jin N, Adamska M, Shiga K, et al. Mutation of FIG4 causes neurodegeneration in the pale tremor mouse and patients with CMT4J. Nature. 2007 Jul 5;448(7149):68–72.

336. Lenk GM, Ferguson CJ, Chow CY, Jin N, Jones JM, Grant AE, et al. Pathogenic Mechanism of the FIG4 Mutation Responsible for Charcot-Marie-Tooth Disease CMT4J. PLOS Genet. 2011 Jun 2;7(6):e1002104.

337. Osmanovic A, Rangnau I, Kosfeld A, Abdulla S, Janssen C, Auber B, et al. FIG4 variants in central European patients with amyotrophic lateral sclerosis: a whole-exome and targeted sequencing study. Eur J Hum Genet. 2017 Feb;25(3):324-331.

338. Zhang Y, Zolov SN, Chow CY, Slutsky SG, Richardson SC, Piper RC, et al. Loss of Vac14, a regulator of the signaling lipid phosphatidylinositol 3,5-bisphosphate, results in neurodegeneration in mice. PNAS. 2007 Oct 30;104(44):17518–23.

339. Shoemaker CJ, Schornberg KL, Delos SE, Scully C, Pajouhesh H, Olinger GG, et al. Multiple Cationic Amphiphiles Induce a Niemann-Pick C Phenotype and Inhibit Ebola Virus Entry and Infection. PLoS ONE. 2013 Feb 18;8(2):e56265.

340. Radoshitzky SR, Abraham J, Spiropoulou CF, Kuhn JH, Nguyen D, Li W, et al. Transferrin receptor 1 is a cellular receptor for New World haemorrhagic fever arenaviruses. Nature. 2007 Mar 1;446(7131):92–6.

341. York J, Nunberg JH. Role of the Stable Signal Peptide of Junín Arenavirus Envelope Glycoprotein in pH-Dependent Membrane Fusion. J Virol. 2006 Aug;80(15):7775–80.

342. Johannsdottir HK, Mancini R, Kartenbeck J, Amato L, Helenius A. Host Cell Factors and Functions Involved in Vesicular Stomatitis Virus Entry. Journal of Virology. 2009 Jan 1;83(1):440–53.

343. Martinez MG, Forlenza MB, Candurra NA. Involvement of cellular proteins in Junin arenavirus entry. Biotechnology Journal. 2009;4(6):866–70.

344. Ikonomov OC, Sbrissa D, Ijuin T, Takenawa T, Shisheva A. Sac3 Is an Insulin-regulated Phosphatidylinositol 3,5-Bisphosphate Phosphatase. J Biol Chem. 2009 Sep 4;284(36):23961–71.

345. Ikonomov OC, Sbrissa D, Compton LM, Kumar R, Tisdale EJ, Chen X, et al. The Protein Complex of Neurodegeneration-related Phosphoinositide Phosphatase Sac3 and ArPIKfyve Binds the Lewy Body-associated Synphilin-1, Preventing Its Aggregation. The Journal of Biological Chemistry. 2015 Nov 20;290(47):28515.

346. Shisheva A, Sbrissa D, Ikonomov O. Cloning, Characterization, and Expression of a Novel Zn2+-Binding FYVE Finger-Containing Phosphoinositide Kinase in Insulin-Sensitive Cells. Mol Cell Biol. 1999 Jan;19(1):623–34.

347. Alghamdi TA, Ho CY, Mrakovic A, Taylor D, Mao D, Botelho RJ. Vac14 Protein Multimerization Is a Prerequisite Step for Fab1 Protein Complex Assembly and Function. J Biol Chem. 2013 Mar 29;288(13):9363–72.

348. Cai X, Xu Y, Cheung AK, Tomlinson RC, Alcázar-Román A, Murphy L, et al. PIKfyve, a Class III PI Kinase, Is the Target of the Small Molecular IL-12/IL-23 Inhibitor Apilimod and a Player in Toll-like Receptor Signaling. Chemistry & Biology. 2013 Jul 25;20(7):912–21.

349. Bray M, Geisbert TW. Ebola virus: The role of macrophages and dendritic cells in the pathogenesis of Ebola hemorrhagic fever. The International Journal of Biochemistry & Cell Biology. 2005 Aug;37(8):1560–6.

350. Saeed MF, Kolokoltsov AA, Freiberg AN, Holbrook MR, Davey RA. Phosphoinositide-3 Kinase-Akt Pathway Controls Cellular Entry of Ebola Virus. PLoS Pathog. 2008 Aug;4(8).

351. Liu Y, Lai Y-C, Hill EV, Tyteca D, Carpentier S, Ingvaldsen A, et al. Phosphatidylinositol 3-phosphate 5-kinase (PIKfyve) is an AMPK target participating in contraction-stimulated glucose uptake in skeletal muscle. Biochem J. 2013 Oct 15;455(2):195–206.

352. Finkelshtein D, Werman A, Novick D, Barak S, Rubinstein M. LDL receptor and its family members serve as the cellular receptors for vesicular stomatitis virus. PNAS. 2013 Apr 30;110(18):7306–11.

353. Mire CE, White JM, Whitt MA. A Spatio-Temporal Analysis of Matrix Protein and Nucleocapsid Trafficking during Vesicular Stomatitis Virus Uncoating. PLOS Pathogens. 2010 Jul 15;6(7):e1000994.

354. Mayor S, Presley JF, Maxfield FR. Sorting of membrane components from endosomes and subsequent recycling to the cell surface occurs by a bulk flow process. J Cell Biol. 1993 Jun 15;121(6):1257–69.

355. Rizopoulos Z, Balistreri G, Kilcher S, Martin CK, Syedbasha M, Helenius A, et al. Vaccinia Virus Infection Requires Maturation of Macropinosomes. Traffic. 2015 Aug;16(8):814–31.

356. Hernandez LD, Hueffer K, Wenk MR, Galán JE. Salmonella Modulates Vesicular Traffic by Altering Phosphoinositide Metabolism. Science. 2004 Jun 18;304(5678):1805–7.

357. Kerr MC, Wang JTH, Castro NA, Hamilton NA, Town L, Brown DL, et al. Inhibition of the PtdIns(5) kinase PIKfyve disrupts intracellular replication of Salmonella. The EMBO Journal. 2010 Apr 21;29(8):1331–47.

358. Sanjana NE, Shalem O, Zhang F. Improved vectors and genome-wide libraries for CRISPR screening. Nat Methods. 2014 Aug;11(8):783–4.

359. Ariotti N, Hall TE, Rae J, Ferguson C, McMahon K-A, Martel N, et al. Modular Detection of GFP-Labeled Proteins for Rapid Screening by Electron Microscopy in Cells and Organisms. Developmental Cell. 2015 Nov 23;35(4):513–25.

360. De Craene J-O, Bertazzi DL, Bär S, Friant S. Phosphoinositides, Major Actors in Membrane Trafficking and Lipid Signaling Pathways. International Journal of Molecular Sciences. 2017 Mar 15;18(3):634.

361. Botelho RJ. Changing phosphoinositides “on the fly”: how trafficking vesicles avoid an identity crisis. Bioessays. 2009 Oct 1;31(10):1127–36.

362. Clague MJ, Urbé S, de Lartigue J. Phosphoinositides and the endocytic pathway. Exp Cell Res. 2009 May 15;315(9):1627–31.

363. Di Paolo G, De Camilli P. Phosphoinositides in cell regulation and membrane dynamics. Nature. 2006 Oct 12;443(7112):651–7.

364. Campeau PM, Lenk GM, Lu JT, Bae Y, Burrage L, Turnpenny P, et al. Yunis-Varón Syndrome Is Caused by Mutations in FIG4, Encoding a Phosphoinositide Phosphatase. Am J Hum Genet. 2013 May 2;92(5):781–91.

365. Rutherford AC, Traer C, Wassmer T, Pattni K, Bujny MV, Carlton JG, et al. The mammalian phosphatidylinositol 3-phosphate 5-kinase (PIKfyve) regulates endosome-to-TGN retrograde transport. J Cell Sci. 2006 Oct 1;119(Pt 19):3944–57.

366. Hessvik NP, Øverbye A, Brech A, Torgersen ML, Jakobsen IS, Sandvig K, et al. PIKfyve inhibition increases exosome release and induces secretory autophagy. Cell Mol Life Sci. 2016 Dec 1;73(24):4717–37.

367. Hou J-Z, Xi Z-Q, Niu J, Li W, Wang X, Liang C, et al. Inhibition of PIKfyve using YM201636 suppresses the growth of liver cancer via the induction of autophagy. Oncology Reports. 2019 Mar 1;41(3):1971–9.

368. Sharma G, Guardia CM, Roy A, Vassilev A, Saric A, Griner LN, et al. A family of PIKFYVE inhibitors with therapeutic potential against autophagy-dependent cancer cells disrupt multiple events in lysosome homeostasis. Autophagy. 2019 Mar 8;15(10):1694–718.

369. Hayashi K, Sasai M, Iwasaki A. Toll-like receptor 9 trafficking and signaling for type I interferons requires PIKfyve activity. Int Immunol. 2015 Sep 1;27(9):435–45.

370. Hazeki K, Uehara M, Nigorikawa K, Hazeki O. PIKfyve Regulates the Endosomal Localization of CpG Oligodeoxynucleotides to Elicit TLR9-Dependent Cellular Responses. PLOS ONE. 2013 Sep 9;8(9):e73894.

371. Balklava Z, Niehage C, Currinn H, Mellor L, Guscott B, Poulin G, et al. The Amyloid Precursor Protein Controls PIKfyve Function. PLOS ONE. 2015 Jun 30;10(6):e0130485.

372. Currinn H, Wassmer T. The amyloid precursor protein (APP) binds the PIKfyve complex and modulates its function. Biochemical Society Transactions. 2016 Feb 15;44(1):185–90.

373. Schulze U, Vollenbröker B, Braun DA, Le TV, Granado D, Kremerskothen J, et al. The Vac14-interaction Network Is Linked to Regulators of the Endolysosomal and Autophagic Pathway. Mol Cell Proteomics. 2014 Jun 1;13(6):1397–411.

374. Gingras A-C, Abe KT, Raught B. Getting to know the neighborhood: using proximity-dependent biotinylation to characterize protein complexes and map organelles. Current Opinion in Chemical Biology. 2019 Feb 1;48:44–54.

375. Roux KJ, Kim DI, Raida M, Burke B. A promiscuous biotin ligase fusion protein identifies proximal and interacting proteins in mammalian cells. J Cell Biol. 2012 Mar 19;196(6):801–10.

376. Varnaitė R, MacNeill SA. Meet the neighbors: Mapping local protein interactomes by proximity-dependent labeling with BioID. Proteomics. 2016 Oct;16(19):2503–18.

377. Catimel B, Schieber C, Condron M, Patsiouras H, Connolly L, Catimel J, et al. The PI(3,5)P2 and PI(4,5)P2 Interactomes. J Proteome Res. 2008 Dec 5;7(12):5295–313.

378. Daro E, Sheff D, Gomez M, Kreis T, Mellman I. Inhibition of Endosome Function in CHO Cells Bearing a Temperature-sensitive Defect in the Coatomer (COPI) Component ε-COP. J Cell Biol. 1997 Dec 29;139(7):1747–59.

379. Andrew Whitney J, Gomez M, Sheff D, Kreis TE, Mellman I. Cytoplasmic coat proteins involved in endosome function. Cell. 1995 Dec 1;83(5):703–13.

380. Hackam DJ, Botelho RJ, Sjolin C, Rotstein OD, Robinson JM, Schreiber AD, et al. Indirect Role for COPI in the Completion of Fcγ Receptor-mediated Phagocytosis. J Biol Chem. 2001 May 25;276(21):18200–8.

381. Gu F, Aniento F, Parton RG, Gruenberg J. Functional Dissection of COP-I Subunits in the Biogenesis of Multivesicular Endosomes. The Journal of Cell Biology. 1997 Dec 1;139(5):1183–95.

382. Gu F, Gruenberg J. ARF1 Regulates pH-dependent COP Functions in the Early Endocytic Pathway. J Biol Chem. 2000 Mar 17;275(11):8154–60.

383. Gabriely G, Kama R, Gerst JE. Involvement of Specific COPI Subunits in Protein Sorting from the Late Endosome to the Vacuole in Yeast. Mol Cell Biol. 2007 Jan;27(2):526–40.

384. Roux KJ, Kim DI, Burke B. BioID: a screen for protein-protein interactions. Curr Protoc Protein Sci. 2013 Nov 5;74:Unit 19.23.

385. Branon TC, Bosch JA, Sanchez AD, Udeshi ND, Svinkina T, Carr SA, et al. Efficient proximity labeling in living cells and organisms with TurboID. Nature Biotechnology. 2018 Sep;36(9):880–7.

386. Choi H, Larsen B, Lin Z-Y, Breitkreutz A, Mellacheruvu D, Fermin D, et al. SAINT: Probabilistic Scoring of Affinity Purification - Mass Spectrometry Data. Nat Methods. 2011 Jan;8(1):70–3.

387. Tuncbag N, Braunstein A, Pagnani A, Huang S-SC, Chayes J, Borgs C, et al. Simultaneous Reconstruction of Multiple Signaling Pathways via the Prize-Collecting Steiner Forest Problem. J Comput Biol. 2013 Feb;20(2):124–36.

388. Akhmedov M, Kedaigle A, Chong RE, Montemanni R, Bertoni F, Fraenkel E, et al. PCSF: An R-package for network-based interpretation of high-throughput data. PLOS Computational Biology. 2017 Jul 31;13(7):e1005694.

389. Mellacheruvu D, Wright Z, Couzens AL, Lambert J-P, St-Denis N, Li T, et al. The CRAPome: a Contaminant Repository for Affinity Purification Mass Spectrometry Data. Nat Methods. 2013 Aug;10(8):730–6.

390. Knight JD, Choi H, Gupta GD, Pelletier L, Raught B, Nesvizhskii AI, et al. ProHits-viz: a suite of web-tools for visualizing interaction proteomics data. Nat Methods. 2017 Jun 29;14(7):645–6.

391. Götz S, García-Gómez JM, Terol J, Williams TD, Nagaraj SH, Nueda MJ, et al. High-throughput functional annotation and data mining with the Blast2GO suite. Nucleic Acids Research. 2008 Jun 1;36(10):3420–35.

392. Heberle H, Meirelles GV, da Silva FR, Telles GP, Minghim R. InteractiVenn: a web-based tool for the analysis of sets through Venn diagrams. BMC Bioinformatics. 2015 May 22;16(1):169.

393. Tuncbag N, Gosline SJC, Kedaigle A, Soltis AR, Gitter A, Fraenkel E. Network-Based Interpretation of Diverse High-Throughput Datasets through the Omics Integrator Software Package. PLOS Computational Biology. 2016 Apr 20;12(4):e1004879.

394. Budak G, Ozsoy OE, Son YA, Can T, Tuncbag N. Reconstruction of the temporal signaling network in Salmonella-infected human cells. Frontiers in Microbiology. 2015 Jul 20;6:730.

395. Szklarczyk D, Franceschini A, Kuhn M, Simonovic M, Roth A, Minguez P, et al. The STRING database in 2011: functional interaction networks of proteins, globally integrated and scored. Nucleic Acids Res. 2011 Jan 1;39(suppl_1):D561–8.

396. Chen EY, Tan CM, Kou Y, Duan Q, Wang Z, Meirelles GV, et al. Enrichr: interactive and collaborative HTML5 gene list enrichment analysis tool. BMC Bioinformatics. 2013 Apr 15;14(1):128.

397. Chen K, Lu H, Gao T, Xue X, Wang C, Miao F. Synergic interaction between amyloid precursor protein and neural cell adhesion molecule promotes neurite outgrowth. Oncotarget. 2016 Feb 12;7(12):14199–206.

398. McCartney AJ, Zolov SN, Kauffman EJ, Zhang Y, Strunk BS, Weisman LS, et al. Activity-dependent PI(3,5)P2 synthesis controls AMPA receptor trafficking during synaptic depression. PNAS. 2014 Nov 11;111(45):E4896–905.

399. Ikonomov OC, Sbrissa D, Dondapati R, Shisheva A. ArPIKfyve-PIKfyve interaction and role in insulin-regulated GLUT4 translocation and glucose transport in 3T3-L1 adipocytes. Exp Cell Res. 2007 Jul 1;313(11):2404–16.

400. Ikonomov OC, Sbrissa D, Mlak K, Shisheva A. Requirement for PIKfyve Enzymatic Activity in Acute and Long-Term Insulin Cellular Effects. Endocrinology. 2002 Dec 1;143(12):4742–54.

401. Berwick DC, Dell GC, Welsh GI, Heesom KJ, Hers I, Fletcher LM, et al. Protein kinase B phosphorylation of PIKfyve regulates the trafficking of GLUT4 vesicles. J Cell Sci. 2004 Dec 1;117(25):5985–93.

402. Arakel EC, Schwappach B. Formation of COPI-coated vesicles at a glance. J Cell Sci. 2018 Mar 1;131(5):jcs209890.

403. Beck R, Ravet M, Wieland FT, Cassel D. The COPI system: Molecular mechanisms and function. FEBS Letters. 2009 Sep 3;583(17):2701–9.

404. Botelho RJ, Hackam DJ, Schreiber AD, Grinstein S. Role of COPI in Phagosome Maturation. J Biol Chem. 2000 May 26;275(21):15717–27.

405. Xu P, Hankins HM, MacDonald C, Erlinger SJ, Frazier MN, Diab NS, et al. COPI mediates recycling of an exocytic SNARE by recognition of a ubiquitin sorting signal. eLife. 2017 Oct 23;6:e28342.

406. Aniento F, Gu F, Parton RG, Gruenberg J. An endosomal beta COP is involved in the pH-dependent formation of transport vesicles destined for late endosomes. J Cell Biol. 1996 Apr;133(1):29–41.

407. Liggins MC, Flesher JL, Jahid S, Vasudeva P, Eby V, Takasuga S, et al. PIKfyve regulates melanosome biogenesis. PLOS Genetics. 2018 Mar 27;14(3):e1007290.

408. Bissig C, Croisé P, Heiligenstein X, Hurbain I, Lenk GM, Kaufman E, et al. The PIKfyve complex regulates the early melanosome homeostasis required for physiological amyloid formation. Journal of Cell Science. 2019 Mar 1;132(5).

409. Tsuruta F, Dolmetsch RE. PIKfyve mediates the motility of late endosomes and lysosomes in neuronal dendrites. Neuroscience Letters. 2015 Sep 25;605:18–23.

410. Miao G, Zhao H, Li Y, Ji M, Chen Y, Shi Y, et al. ORF3a of the COVID-19 virus SARS-CoV-2 blocks HOPS complex-mediated assembly of the SNARE complex required for autolysosome formation. Developmental Cell. 2020 Dec 16;S1534-5807(20)31016-9.

411. Feng X, Jia Y, Zhang Y, Ma F, Zhu Y, Hong X, et al. Ubiquitination of UVRAG by SMURF1 promotes autophagosome maturation and inhibits hepatocellular carcinoma growth. Autophagy. 2019 Jul 3;15(7):1130–49.

412. Munson MJ, Allen GF, Toth R, Campbell DG, Lucocq JM, Ganley IG. mTOR activates the VPS34–UVRAG complex to regulate autolysosomal tubulation and cell survival. The EMBO Journal. 2015 Sep 2;34(17):2272–90.

413. Funderburk. SF, Wang QJ, Yue Z. Beclin 1-VPS34 complex – At the Crossroads of Autophagy and Beyond. Trends Cell Biol. 2010 Jun;20(6):355–62.

414. Zhao Z, Ni D, Ghozalli I, Pirooz SD, Ma B, Liang C. UVRAG: At the crossroad of autophagy and genomic stability. Autophagy. 2012 Sep 1;8(9):1392–3.

415. Condon KJ, Sabatini DM. Nutrient regulation of mTORC1 at a glance. J Cell Sci. 2019 Nov 1;132(21).

416. Richards AA, Stang E, Pepperkok R, Parton RG. Inhibitors of COP-mediated Transport and Cholera Toxin Action Inhibit Simian Virus 40 Infection. Mol Biol Cell. 2002 May;13(5):1750–64.

417. Norkin LC, Anderson HA, Wolfrom SA, Oppenheim A. Caveolar Endocytosis of Simian Virus 40 Is Followed by Brefeldin A-Sensitive Transport to the Endoplasmic Reticulum, Where the Virus Disassembles. J Virol. 2002 May;76(10):5156–66.

418. Laniosz V, Dabydeen SA, Havens MA, Meneses PI. Human Papillomavirus Type 16 Infection of Human Keratinocytes Requires Clathrin and Caveolin-1 and Is Brefeldin A Sensitive. J Virol. 2009 Aug;83(16):8221–32.

419. König R, Stertz S, Zhou Y, Inoue A, Hoffmann H-H, Bhattacharyya S, et al. Human host factors required for influenza virus replication. Nature. 2010 Feb;463(7282):813–7.

420. Cureton DK, Burdeinick-Kerr R, Whelan SPJ. Genetic Inactivation of COPI Coatomer Separately Inhibits Vesicular Stomatitis Virus Entry and Gene Expression. Journal of Virology. 2012 Jan 15;86(2):655–66.

421. Sun E, He J, Zhuang X. Dissecting the Role of COPI Complexes in Influenza Virus Infection. J Virol. 2013 Mar;87(5):2673–85.

422. Pattnaik GP, Chakraborty H. Entry Inhibitors: Efficient Means to Block Viral Infection. J Membrane Biol. 2020 Oct 1;253(5):425–44.

423. Dimitrov DS. Virus entry: molecular mechanisms and biomedical applications. Nat Rev Microbiol. 2004 Feb;2(2):109–22.

424. Mazzon M, Marsh M. Targeting viral entry as a strategy for broad-spectrum antivirals. F1000Res. 2019 Sep 12;8:F1000.

425. Kang C, Syed YY. Bulevirtide: First Approval. Drugs. 2020 Oct 1;80(15):1601–5.

426. Hardy H, Skolnik PR. Enfuvirtide, a new fusion inhibitor for therapy of human immunodeficiency virus infection. Pharmacotherapy. 2004 Feb;24(2):198–211.

427. Kang Y-L, Chou Y, Rothlauf PW, Liu Z, Soh TK, Cureton D, et al. Inhibition of PIKfyve kinase prevents infection by Zaire ebolavirus and SARS-CoV-2. PNAS. 2020 Aug 25;117(34):20803–13.

428. Riva L, Yuan S, Yin X, Martin-Sancho L, Matsunaga N, Pache L, et al. Discovery of SARS-CoV-2 antiviral drugs through large-scale compound repurposing. Nature. 2020 Oct;586(7827):113–9.

429. Anantpadma M, Kouznetsova J, Wang H, Huang R, Kolokoltsov A, Guha R, et al. Large-Scale Screening and Identification of Novel Ebola Virus and Marburg Virus Entry Inhibitors. Antimicrob Agents Chemother. 2016 Jul 22;60(8):4471–81.

430. Mohr EL, McMullan LK, Lo MK, Spengler JR, Bergeron É, Albariño CG, et al. Inhibitors of cellular kinases with broad-spectrum antiviral activity for hemorrhagic fever viruses. Antiviral Research. 2015 Aug 1;120:40–7.

431. Wada Y, Lu R, Zhou D, Chu J, Przewloka T, Zhang S, et al. Selective abrogation of Th1 response by STA-5326, a potent IL-12/IL-23 inhibitor. Blood. 2007 Feb 1;109(3):1156–64.

432. Wada Y, Cardinale I, Khatcherian A, Chu J, Kantor AB, Gottlieb AB, et al. Apilimod inhibits the production of IL-12 and IL-23 and reduces dendritic cell infiltration in psoriasis. PLoS One. 2012;7(4):e35069.

433. Krausz S, Boumans MJH, Gerlag DM, Lufkin J, van Kuijk AWR, Bakker A, et al. Brief report: a phase IIa, randomized, double-blind, placebo-controlled trial of apilimod mesylate, an interleukin-12/interleukin-23 inhibitor, in patients with rheumatoid arthritis. Arthritis Rheum. 2012 Jun;64(6):1750–5.

434. Burakoff R, Barish CF, Riff D, Pruitt R, Chey WY, Farraye FA, et al. A phase 1/2A trial of STA 5326, an oral interleukin-12/23 inhibitor, in patients with active moderate to severe Crohn's disease. Inflamm Bowel Dis. 2006 Jul;12(7):558–65.

435. Sands BE, Jacobson EW, Sylwestrowicz T, Younes Z, Dryden G, Fedorak R, et al. Randomized, double-blind, placebo-controlled trial of the oral interleukin-12/23 inhibitor apilimod mesylate for treatment of active Crohn's disease. Inflamm Bowel Dis. 2010 Jul;16(7):1209–18.

436. Harb WA, Diefenbach CS, Lakhani N, Rutherford SC, Schreeder MT, Ansell SM, et al. Phase 1 Clinical Safety, Pharmacokinetics (PK), and Activity of Apilimod Dimesylate (LAM-002A), a First-in-Class Inhibitor of Phosphatidylinositol-3-Phosphate 5-Kinase (PIKfyve), in Patients with Relapsed or Refractory B-Cell Malignancies. Blood. 2017 Dec 7;130(Supplement 1):4119–4119.

437. AI Therapeutics, Inc. A Phase II Randomized, Double-Blind, Placebo-Controlled Study of LAM-002A for the Prevention of Progression of COVID-19. clinicaltrials.gov; 2020 Nov. Report No.: NCT04446377. Available from: https://clinicaltrials.gov/ct2/show/NCT04446377

Appendix

6.1 Permissions

Figures adapted from International Committee on Taxonomy of Viruses (ICTV) (Fig. 1.1):

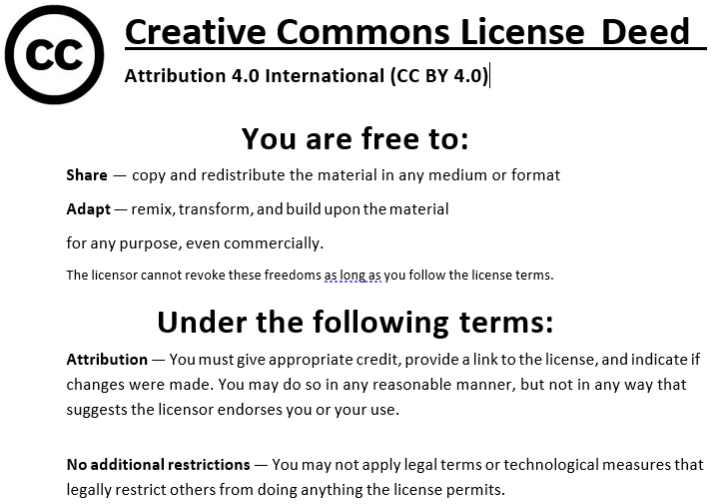

Creative Commons License Deed

Attribution 4.0 International (CC BY 4.0)

You are free to:

Share — copy and redistribute the material in any medium or format

Adapt — remix, transform, and build upon the material

for any purpose, even commercially.

The licensor cannot revoke these freedoms as long as you follow the license terms.

Under the following terms:

Attribution — You must give appropriate credit, provide a link to the license, and indicate if changes were made. You may do so in any reasonable manner, but not in any way that suggests the licensor endorses you or your use.

No additional restrictions — You may not apply legal terms or technological measures that legally restrict others from doing anything the license permits.

Figures adapted from PLOS journals (Fig. 1.2B, Fig 1.4):

Licenses and Copyright

The following policy applies to all PLOS journals, unless otherwise noted.

Reuse of PLOS Article Content

PLOS applies the Creative Commons Attribution (CC BY) license to articles and other works we publish. If you submit your paper for publication by PLOS, you agree to have the CC BY license applied to your work. Under this Open Access license, you as the author agree that anyone can reuse your article in whole or part for any purpose, for free, even for commercial purposes. Anyone may copy, distribute, or reuse the content as long as the author and original source are properly cited. This facilitates freedom in re-use and also ensures that PLOS content can be mined without barriers for the needs of research.

Figures reprinted from Traffic (Fig. 1.5):

This Agreement between Ms. Shirley Qiu ("You") and John Wiley and Sons ("John Wiley and Sons") consists of your license details and the terms and conditions provided by John Wiley and Sons and Copyright Clearance Center.

License Number	5000950339102
License date	Feb 02, 2021
Licensed Content Publisher	John Wiley and Sons
Licensed Content Publication	Traffic
Licensed Content Title	Fusion of Enveloped Viruses in Endosomes
Licensed Content Author	Judith M. White, Gary R. Whittaker
Licensed Content Date	Apr 7, 2016
Licensed Content Volume	17
Licensed Content Issue	6
Licensed Content Pages	22
Type of use	Dissertation/Thesis
Requestor type	University/Academic
Format	Electronic
Portion	Figure/table
Number of figures/tables	1
Will you be translating?	No
Title	Trafficking factors involved in Ebola virus entry
Institution name	University of Ottawa
Expected presentation date	Feb 2021
Portions	Figure 2
Requestor Location	Ms. Shirley Qiu 451 Smyth Road Room 4105Q Ottawa, ON K1H8M5 Canada Attn: Ms. Shirley Qiu
Publisher Tax ID	EU826007151
Total	0.00 CAD

Figures created using BioRender* (Fig. 1.2A, Fig. 1.6, Fig. 1.7, Fig. 5.1):

bio RENDER

Licensing and Usage

	Basic (Free) Account*	Academic Subscription	Industry Subscription
Educational Uses:			
Academic poster	✓	✓	✓
Thesis/dissertation (unpublished)	✓	✓	✓
Internal meetings (lab or team)	✓	✓	✓
Conference presentation	✓	✓	✓
Assignment/Exam	✓	✓	✓
Teaching slides	✓	✓	✓
Personal blog/website posts	✓	✓	✓
Personal social media posts	✓	✓	✓
Publishing Uses:			
Journal publication		✓	✓
Textbook publication (< 5 figures)		✓	✓
Published thesis		✓	✓
Commercial Uses:			
Any uses that generate profit			✓
Textbook publication (5+ figures)			✓
Trade show materials (ie. brochures)			✓
Information packages/User guides			✓

*Watermark must be included in exported figure
*Free trial on a premium plan recommended for print uses
For use cases not listed here, please go to **biorender.com/contact**

*Figures exported under an academic subscription

Figures adapted from the Centers for Disease Control and Prevention (CDC) (Fig 1.3):

CDC Centers for Disease Control and Prevention

Using CDC.gov

Use of Agency Materials

Most of the information on the CDC and ATSDR websites is not subject to copyright, is in the public domain, and may be freely used or reproduced without obtaining copyright permission.

There are, however, a few exceptions. A federal government website may have a mix of public domain and copyright-protected materials. First, some resources, as well as images, on the CDC and ATSDR websites are restricted in their use because they were developed by government contractors or grantees, or have been licensed by a third party. Second, the U.S. government work designation does not apply to works of state and local governments; works of state and local governments may be protected by copyright. Third, copyright laws also differ internationally. While U.S. federal copyright laws may not protect U.S. government works outside the United States, the work may still be protected under the copyright laws of other countries when used in these jurisdictions. Copyright-protected materials featured on the CDC and ATSDR websites should include a copyright statement. However, if in doubt, please write to the contact point for that site.

The following requirements must be followed to utilize CDC's public domain content:

1) Attribution to the agency that developed the material must be provided in your use of the materials. Such attribution should clearly state the materials were developed by CDC ATSDR and/or HHS (e.g., "Source: CDC"; "Materials developed by CDC");

2) You must utilize a disclaimer which clearly indicates that your use of the material, including any links to the materials on the CDC, ATSDR or HHS websites, does not imply endorsement by CDC, ATSDR, HHS or the United States Government of you, your company, product, facility, service or enterprise. All such disclaimers must be prominently and unambiguously displayed (e.g., "Reference to specific commercial products, manufacturers, companies, or trademarks does not constitute its endorsement or recommendation by the U.S. Government, Department of Health and Human Services, or Centers for Disease Control and Prevention;

3) You may not change the substantive content of the materials; and

4) You must state that the material is otherwise available on the agency website for no charge.

6.2 BioID screen data

	Total spectral count			SAINT probability score		Fold change B score*	
Gene	**birA**	**ArPIKfyve**	**Sac3**	**ArPIKfyve**	**Sac3**	**ArPIKfyve**	**Sac3**
AAK1	6	4	11	0.01	0.78	1.09	2.23
AARS	5	0	4	0	0.05	0	1.1
AARS2	3	1	2	0	0.08	0.72	0.96
ABCE1	6	3	5	0	0.01	0.79	1.04
ABCF1	5	4	11	0	0	0.56	1.16
ABCF2	4	6	6	0	0	1	0.87
ABI1	9	6	5	0	0	1.09	0.82
ABRAXAS2	4	10	9	0.89	0.87	3.21	2.52
ACACA	117	55	87	0	0	0.33	0.44
ACADSB	1	4	3	0.96	0.87	3.09	2.19
ACBD3	1	6	2	0.97	0.24	3.39	1.31
ACIN1	26	13	18	0	0	0.36	0.42
ACLY	15	30	25	0.84	0.55	3.09	2.21
ACO2	2	3	3	0.53	0.56	1.81	1.6
ACTL6A	5	0	0	0	0	0	0
ACTN4	0	0	8	0	0	0	0.78
ACTR1A	22	20	15	0	0	1.48	0.96
ADD1	3	2	4	0.07	0.48	1.07	1.56
ADRM1	12	16	16	0.05	0.05	1.96	1.68
ADSL	3	8	4	0.89	0.48	3.19	1.56
AFDN	27	44	75	0.17	0.97	2.61	3.74
AFG3L2	0	6	0	1	0	6.85	0
AGK	0	8	1	1	0	8.8	1.83
AGPS	3	5	1	0.64	0	2.13	0.66
AHCY	5	3	6	0.01	0.31	1	1.52
AHNAK	1	0	4	0	0	0	0.02
AHSA1	0	5	4	0.01	0	1.45	1.06
AIFM1	13	23	30	0.68	0.93	2.72	2.99
AIMP1	11	15	8	0.2	0	2.1	1.02
AIMP2	4	6	6	0.24	0.27	1.81	1.58
AKAP1	5	2	4	0	0	0.36	0.52
AKAP8L	0	0	4	0	1	0	4.3
ALB	62	19	18	0	0	0.52	0.43
ALDH18A1	3	5	5	0.64	0.68	2.13	1.86
ALDH1B1	4	5	4	0.36	0.2	1.76	1.29
ALDH3A2	0	5	3	0.36	0.07	2.14	1.27
ALDOA	14	11	23	0	0.53	1.27	2.17

ALYREF	21	14	8	0	0	1.1	0.57
AMOT	12	1	1	0	0	0.25	0.23
ANKFY1	0	3	0	0.99	0	3.92	0
ANKHD1	4	6	17	0	0.05	0.89	1.95
ANKRD17	3	5	18	0	0	0.42	1.13
ANXA2	19	6	8	0	0	0.3	0.33
AP1M1	0	0	3	0	1	0	3.48
AP3B1	1	4	8	0.96	1	3.09	4.8
AP3D1	0	3	0	0.53	0	2.1	0
APC	2	2	4	0	0	0.68	0.99
APOD	1	0	3	0	0.87	0	2.19
APOL2	4	3	6	0.06	0.59	1.17	1.78
ARCN1	10	11	15	0.01	0.21	1.61	1.84
ARHGAP21	1	5	9	0.99	1	3.7	5.32
ARHGEF12	1	3	2	0.85	0.63	2.47	1.67
ARHGEF7	3	7	7	0.84	0.86	2.84	2.46
ARID3A	4	0	0	0	0	0	0
ARMCX3	2	7	6	0.95	0.92	3.6	2.74
ARPIN	2	2	5	0.27	0.85	1.36	2.36
ATAD3B	4	23	17	1	0.99	7	4.5
ATP1A1	23	39	34	0.38	0.07	2.7	2.01
ATP2A2	1	8	5	0.99	0.74	3.58	2.09
ATP5F1A	26	41	36	0.12	0.01	2.52	1.89
ATP5F1B	31	43	34	0	0	2.24	1.52
ATP5F1C	10	11	10	0.04	0.02	1.71	1.35
ATP6V1A	4	4	3	0.03	0.01	1.3	0.92
ATP6V1B2	0	3	0	0.99	0	3.92	0
ATP6V1E1	4	3	2	0.06	0	1.17	0.79
ATXN2	2	1	3	0	0.01	0.57	1
ATXN2L	19	27	24	0	0	1.19	0.9
AURKB	3	3	5	0.23	0.68	1.42	1.86
B3GAT3	0	2	0	0.97	0	2.95	0
BAG6	0	0	4	0	1	0	4.3
BCAP31	0	0	2	0	0.97	0.09	2.65
BCLAF1	8	1	7	0	0	0	0.32
BPTF	3	0	0	0	0	0	0
BRCC3	1	3	1	0.85	0	2.47	1.15
BSG	3	23	5	1	0.68	8.49	1.86
BUB3	7	4	6	0	0	0.76	0.93
BYSL	4	6	4	0.56	0.2	2.05	1.29
C1QBP	3	5	7	0.64	0.86	2.13	2.46
C2CD5	0	3	0	0.99	0	3.92	0
CACYBP	5	3	6	0	0.08	0.9	1.36

CAD	6	6	8	0.09	0.4	1.52	1.69
CALD1	3	3	13	0	0	0.11	0.34
CALML5	6	2	1	0	0	0.65	0.4
CAMLG	0	4	2	1	0.97	4.9	2.65
CAMSAP1	0	0	3	0	0.87	0	2.42
CAND1	3	7	2	0.84	0.08	2.84	0.96
CANX	0	8	5	1	0.99	6.12	3.57
CAP1	6	10	4	0.2	0	1.99	0.8
CAPRIN1	14	6	14	0	0	0.58	1.06
CAPZA1	11	25	15	0.84	0.02	3.05	1.61
CAPZA2	7	14	11	0.73	0.34	2.65	1.82
CAPZB	9	10	5	0.02	0	1.6	0.76
CBR1	0	0	6	0	1	0	5.96
CBSL	9	5	9	0	0.03	0.94	1.35
CBX3	5	16	0	0.87	0	2.53	0
CBX5	0	3	0	0.85	0	2.73	0
CCAR2	17	3	5	0	0	0.3	0.39
CCDC124	2	4	7	0.42	0.97	1.88	2.6
CCDC43	3	11	7	0.99	0.6	3.23	1.87
CCDC6	0	0	5	0	1	0	5.13
CCDC8	0	2	3	0.97	1	2.95	3.48
CCDC85C	1	6	6	1	1	4.32	3.76
CCDC88A	1	3	2	0.85	0.63	2.47	1.67
CCT2	58	68	127	0	0.9	1.9	2.99
CCT3	57	62	156	0	0.98	1.79	3.78
CCT4	76	71	167	0	0.86	1.51	3
CCT5	21	25	72	0	0.99	1.79	4.27
CCT6A	26	45	90	0.06	0.99	2.56	4.3
CCT7	45	58	131	0	0.98	2.1	3.99
CCT8	86	107	215	0	0	1.54	2.61
CD2AP	2	5	17	0	0	0.37	0.96
CD2BP2	3	3	2	0.03	0	1.23	0.83
CDC37	0	8	2	0.97	0.29	4.7	1.42
CDC5L	8	1	2	0	0	0.14	0.19
CDC73	5	0	0	0	0	0	0
CDK1	5	5	11	0.13	0.88	1.49	2.57
CDK12	6	0	3	0	0	0	0.43
CDK9	8	0	3	0	0	0	0.57
CENPV	2	5	1	0.83	0	2.7	0.84
CEP131	9	3	6	0	0	0.63	0.95
CEP170	11	45	52	1	1	3.02	2.96
CEP170B	0	4	3	1	1	4.9	3.48
CEP97	0	7	13	1	1	7.82	11.74

CFAP410	0	9	2	1	0.97	9.77	2.65
CGN	11	0	1	0	0	0	0.25
CHAF1B	5	1	4	0	0.05	0.5	1.1
CHD4	33	4	11	0	0	0.07	0.15
CHMP2B	3	2	3	0	0.04	0.92	1.09
CHMP4B	4	3	2	0	0	0.93	0.63
CHTOP	10	15	10	0.41	0.02	2.28	1.35
CIP2A	2	9	20	0.99	1	4.5	8.07
CKAP4	10	33	27	0.97	0.95	4.84	3.4
CKAP5	35	58	82	0	0.01	1.62	1.94
CKB	5	7	9	0.46	0.76	1.99	2.15
CLNS1A	0	5	2	1	0.97	5.87	2.65
CLPB	0	0	2	0	0.97	0	2.65
CLTC	28	25	36	0	0	1.39	1.68
CLUH	1	0	4	0	0.96	0	2.71
CNN3	4	18	19	1	1	4.4	3.96
CNOT1	6	25	20	0.98	0.97	5.62	3.88
CNOT2	11	11	6	0.01	0	1.57	0.8
CNOT9	3	5	2	0.64	0.08	2.13	0.96
COG4	0	3	1	0.99	0	3.92	1.83
COPA	13	27	19	0.81	0.12	3.02	1.84
COPB1	4	36	24	1	1	7.09	4.09
COPB2	6	11	13	0.39	0.8	2.18	2.18
COPG1	0	17	11	1	1	9.38	5.39
COPG2	14	41	34	0	0	1.64	1.17
COPS3	4	3	3	0.06	0.07	1.17	1.04
COPS4	2	4	1	0.72	0	2.26	0.84
CORO1B	0	2	8	0	0	0.15	0.38
CORO1C	4	5	12	0	0	0.68	1.27
CPSF1	7	0	2	0	0	0	0.52
CPSF7	9	3	5	0	0	0.63	0.82
CPVL	2	3	2	0.53	0.29	1.81	1.22
CRK	12	15	22	0	0	1.1	1.36
CRKL	8	16	13	0.73	0.39	2.71	1.92
CS	1	0	5	0	0.74	0	2.09
CSDE1	18	12	22	0	0	0.63	0.95
CSE1L	6	6	10	0.09	0.69	1.52	2.05
CSNK1E	0	3	1	0.99	0	3.92	1.83
CSNK1G3	3	0	0	0	0	0	0
CSTF1	4	0	1	0	0	0	0.55
CSTF2	7	4	7	0	0	0.67	0.93
CTNNA1	7	4	3	0	0	0.82	0.58
CTNNB1	7	5	4	0.01	0	1.15	0.84

CTNND1	9	1	0	0	0	0.19	0
CTPS1	0	6	4	0	0	0.65	0.41
CTTN	3	17	35	0	0	0.77	1.31
CWC15	6	3	0	0	0	0.59	0
CXXC1	3	0	0	0	0	0	0
CYFIP1	9	13	20	0.37	0.91	2.18	2.79
DAP3	1	2	4	0.6	0.96	1.86	2.71
DARS	25	28	26	0	0	1.76	1.4
DBNL	4	10	17	0.69	1	2.31	3.23
DBT	21	17	27	0	0.01	1.32	1.75
DCTN1	31	46	42	0	0	2.19	1.71
DCTN2	4	13	6	0.95	0.59	4.09	1.78
DCTN4	3	0	0	0	0	0	0
DDOST	2	11	5	0.87	0	2.69	1.18
DDX1	0	0	7	0	1	0	4.72
DDX17	48	26	56	0	0	0.87	1.55
DDX21	7	2	8	0	0	0.21	0.55
DDX39B	11	4	10	0	0	0.43	0.81
DDX3X	32	24	39	0	0	0.88	1.2
DDX42	5	0	0	0	0	0	0
DDX46	13	0	2	0	0	0	0.09
DDX5	27	16	30	0	0	0.75	1.17
DDX6	8	4	5	0	0	0.8	0.84
DEK	7	2	4	0	0	0.58	0.84
DHX15	8	1	9	0	0	0.21	0.88
DHX29	3	3	8	0	0.17	0.87	1.69
DHX30	19	8	18	0	0	0.73	1.31
DHX9	29	10	37	0	0	0.32	0.94
DIAPH3	0	2	1	0	0	0.73	0.45
DIDO1	9	1	0	0	0	0.06	0
DLD	4	4	7	0.18	0.73	1.47	2.03
DLGAP5	0	0	3	0	0	0	0.96
DLST	8	14	9	0.71	0.11	2.58	1.48
DNAJA1	13	23	31	0.68	0.94	2.72	3.09
DNAJA2	4	7	10	0.7	0.9	2.34	2.77
DNAJA3	1	10	2	1	0.63	6.78	1.67
DNAJB1	10	10	13	0	0	1.25	1.36
DNAJB11	2	3	6	0.53	0.92	1.81	2.74
DNAJB12	0	8	7	1	1	8.8	6.78
DNAJB6	1	5	5	0.99	0.99	3.7	3.24
DNAJC13	5	21	25	0.98	0.99	5.46	5.51
DNAJC7	6	5	13	0.03	0.88	1.3	2.6
DNTTIP2	0	0	3	0	0	0	0.71

DOCK7	5	12	12	0.89	0.9	3.23	2.78
DPYSL2	2	6	13	0.91	1	3.15	5.41
DPYSL4	0	9	8	1	1	9.77	7.61
DPYSL5	3	4	7	0.45	0.86	1.78	2.46
DRG1	6	17	13	0.95	0.83	3.55	2.37
DSG1	34	18	21	0	0	0.89	0.88
DSG2	15	0	0	0	0	0	0
DSN1	3	4	3	0.45	0.25	1.78	1.26
DSP	83	39	9	0	0	0.78	0.17
DTD1	0	2	3	0.97	1	2.95	3.48
DVL2	3	14	27	0	0.19	1.57	2.51
DYNC1H1	29	47	41	0.13	0.01	2.6	1.94
DYNC1I2	10	15	15	0.41	0.45	2.28	1.95
DYNC1LI1	9	10	10	0.07	0.08	1.71	1.48
DYNC1LI2	2	5	5	0.72	0.74	2.25	1.97
EBNA1BP2	0	2	0	0.27	0	1.57	0
ECH1	2	8	2	0.97	0.29	4.05	1.22
ECPAS	5	1	2	0	0	0.5	0.68
EDC3	2	5	5	0.83	0.85	2.7	2.36
EDC4	4	13	25	0.03	1	2	3.17
EEF1A1	9	26	34	0	0	0.92	1.02
EEF1B2	2	1	3	0	0.04	0.65	1.14
EEF1D	8	14	12	0	0	1.34	1
BLOC1S5	3	2	1	0.07	0	1.07	0.66
EEF1G	55	57	49	0	0	1.64	1.2
EEF2	40	52	75	0	0	1.6	1.95
EFHD2	2	6	6	0	0	1.21	1.05
EFTUD2	3	5	6	0.34	0.68	1.84	1.87
EHBP1	0	4	6	0.72	0.92	2.62	3.18
EIF2B4	0	5	3	1	1	5.87	3.48
EIF2S1	10	7	4	0	0	1.01	0.56
EIF2S3	9	7	9	0	0	0.84	0.9
EIF3A	35	51	41	0	0	2.27	1.56
EIF3B	14	15	14	0.01	0	1.7	1.37
EIF3C	21	34	45	0.01	0.63	2.27	2.54
EIF3D	3	5	4	0.34	0.14	1.84	1.35
EIF3E	19	18	12	0	0	1.53	0.9
EIF3F	6	9	8	0.25	0.14	1.97	1.54
EIF3G	2	6	11	0.06	0.97	1.75	2.58
EIF3H	5	4	7	0.05	0.5	1.25	1.73
EIF3I	5	8	9	0.62	0.76	2.24	2.15
EIF3J	0	3	0	0.99	0	3.92	0
EIF3L	7	7	10	0.07	0.46	1.53	1.82

EIF3M	13	12	13	0	0.01	1.47	1.36
EIF4A1	26	21	23	0	0	1.17	1.09
EIF4A3	15	13	14	0	0	1.34	1.23
EIF4B	9	11	26	0	0	0.51	0.98
EIF4G1	67	42	60	0	0	0.7	0.84
EIF4G2	15	17	31	0	0	1	1.51
EIF4G3	24	15	17	0	0	0.95	0.92
EIF5	1	2	2	0	0	0.2	0.18
EIF5B	2	0	3	0	0	0	0.61
ELAVL1	7	10	4	0.05	0	1.8	0.72
ELP5	0	4	1	0.18	0	1.78	0.67
EMC2	2	4	2	0.72	0.29	2.26	1.22
EMD	23	22	22	0	0	1.28	1.09
ENAH	4	13	12	0.99	0.98	3.62	2.89
ENO1	18	12	40	0	0.81	0.99	2.65
ENTR1	0	0	5	0	1	0	5.13
EPB41	2	5	13	0	0	0.71	1.42
EPB41L2	7	7	6	0	0	0.34	0.26
EPB41L3	3	3	9	0.01	0.94	1.08	2.32
EPRS	83	103	96	0	0	1.74	1.38
EPS15	0	2	4	0.6	0.96	2.05	3
EPS15L1	0	4	7	0	0	0.41	0.57
ERC1	3	9	20	0.39	1	2.17	3.89
ERH	3	2	0	0	0	0.81	0
ERLIN2	10	9	7	0.01	0	1.42	0.99
ESYT2	5	5	6	0	0	1.04	1.05
ETFA	2	7	6	0.96	0.9	3	2.28
EWSR1	16	15	13	0	0	1.51	1.13
EXOC2	0	0	4	0	1	0	4.3
EXOC4	17	17	20	0	0	1.54	1.54
EXOSC6	4	2	2	0	0	0.88	0.79
FAF2	6	8	9	0.36	0.56	1.95	1.87
FAM120A	2	3	7	0.16	0.97	1.5	2.6
FAR1	5	2	1	0	0	0.75	0.46
FARSA	28	18	27	0	0	1.07	1.34
FASN	126	202	267	0	0	1.92	2.15
FH	0	0	7	0	1	0	6.78
FHL1	5	3	3	0.01	0.01	1	0.89
FIG4	0	348	480	1	1	340.1	397.48
FIP1L1	17	2	8	0	0	0.24	0.62
FKBP15	4	1	3	0	0.01	0.52	0.92
FKBP4	0	3	12	0.99	1	3.92	10.91
FKBP8	0	7	2	1	0.97	7.82	2.65

FLG2	37	16	23	0	0	0.73	0.88
FLII	5	7	10	0.46	0.83	1.99	2.36
FLNB	28	43	81	0	0	0.32	0.51
FLNC	21	35	43	0	0	0.66	0.69
FLOT1	5	0	0	0	0	0	0
FMR1	6	2	9	0	0.56	0.65	1.87
FUBP1	5	1	5	0	0	0.38	0.98
FXR2	6	0	3	0	0	0	0.77
FYN	3	0	0	0	0	0	0
G3BP1	14	3	11	0	0	0.31	0.79
G3BP2	6	4	6	0	0	0.91	1.11
GALK1	1	3	4	0.85	0.96	2.47	2.71
GANAB	3	9	20	0.93	1	3.54	6.36
GAPDH	14	17	17	0.03	0.04	1.91	1.64
GAPVD1	2	15	20	0.19	0.82	2.56	2.87
GART	0	0	2	0	0.97	0	2.65
GATAD2A	27	6	11	0	0	0.36	0.53
GATAD2B	26	4	6	0	0	0.22	0.27
GCC2	6	5	5	0.03	0.04	1.3	1.14
GCDH	2	3	2	0.53	0.29	1.81	1.22
GCN1	10	28	26	0.95	0.94	4.13	3.28
GEMIN4	6	0	1	0	0	0	0.4
GEMIN5	8	16	17	0	0	0.68	0.62
GFPT1	2	0	6	0	0.92	0	2.74
GIGYF2	55	83	136	0	0	1.25	1.73
GLG1	8	4	0	0	0	0.86	0
GLIPR2	6	0	0	0	0	0	0
GLUD1	3	5	3	0.64	0.25	2.13	1.26
GNAI2	4	1	0	0	0	0.59	0
GNAI3	4	3	2	0.06	0	1.17	0.79
GNB1	6	3	0	0	0	0.79	0
GNB2	3	0	0	0	0	0	0
GOLGA3	0	3	2	0.85	0.63	2.73	1.85
GOLGA4	0	3	0	0.99	0	3.92	0
GOLGA5	2	0	2	0	0.29	0	1.22
GOT2	5	3	13	0.01	0.92	1	2.99
GPC4	6	0	0	0	0	0	0
GPHN	7	6	8	0.02	0.17	1.34	1.49
GPN1	0	4	3	1	1	4.9	3.48
GPS1	0	3	3	0.99	1	3.92	3.48
GRSF1	5	2	2	0	0	0.68	0.61
GSTP1	0	0	4	0	1	0	4.3
GTF2F1	9	0	2	0	0	0	0.42

GTF2I	50	20	45	0	0	0.52	0.97
GTPBP4	3	0	0	0	0	0	0
H1F0	3	6	2	0.77	0.08	2.48	0.96
H1FX	16	14	7	0	0	1.41	0.65
H2AFY	2	5	5	0.34	0.37	1.93	1.69
H3F3B	2	7	0	0.05	0	1.8	0
HACD3	4	7	2	0.7	0	2.34	0.79
HADHA	12	13	13	0.02	0.02	1.7	1.46
HADHB	7	10	6	0.43	0.03	2.11	1.17
HAT1	4	12	8	0.98	0.72	3.36	2.01
HAUS1	1	0	3	0	0.87	0	2.19
HAUS3	1	1	4	0	0.96	1.25	2.71
HAUS4	0	8	5	1	1	8.8	5.13
HAUS5	6	9	18	0.53	0.95	2.16	3.52
HAUS6	4	4	18	0	0.92	0.72	2.32
HAUS7	2	6	6	0.91	0.92	3.15	2.74
HAX1	2	5	2	0.83	0.29	2.7	1.22
HCFC1	10	0	4	0	0	0	0.15
HDAC2	8	0	2	0	0	0	0.36
HDDC2	2	8	2	0.97	0.29	4.05	1.22
HDHD5	1	0	2	0	0.63	0	1.67
HDLBP	27	39	40	0	0	1.36	1.19
HEATR5B	7	7	8	0.07	0.17	1.53	1.49
HGS	3	5	7	0.64	0.86	2.13	2.46
HIST1H1E	78	87	53	0	0	1.7	0.88
HIST1H2BO	34	79	9	0.04	0	2.84	0.31
HIST1H4A	19	62	22	1	0	3.83	1.19
HLA-B	5	11	13	0.86	0.92	2.98	2.99
HMGA1	5	4	0	0	0	1.02	0
HMGA2	14	16	1	0.02	0	1.8	0.2
HMGN1	2	7	0	0.95	0	3.6	0
HMGN2	3	7	4	0.84	0.48	2.84	1.56
HMGN4	1	4	0	0.96	0	3.09	0
HNRNPA0	5	1	2	0	0	0.35	0.47
HNRNPA1	33	57	39	0	0	2.25	1.32
HNRNPA2B1	75	101	59	0	0	1.93	0.97
HNRNPAB	20	22	14	0	0	1.65	0.92
HNRNPC	18	30	11	0.01	0	2.2	0.74
HNRNPD	10	14	6	0	0	1.48	0.6
HNRNPDL	4	11	0	0.88	0	2.52	0
HNRNPF	12	11	15	0	0	1.02	1.16
HNRNPH1	47	42	26	0	0	1.39	0.74
HNRNPH3	4	12	4	0.93	0.2	3.8	1.29

HNRNPK	16	7	24	0	0	0.34	0.9
HNRNPL	3	0	3	0	0	0	0.28
HNRNPM	74	58	105	0	0	1.12	1.71
HNRNPR	20	4	16	0	0	0.32	0.93
HNRNPU	23	35	50	0	0	1.51	1.82
HNRNPUL2	0	0	2	0	0.63	0	1.85
HP1BP3	6	3	8	0	0	0.59	1.14
HPRT1	4	2	5	0	0.4	0.88	1.53
HRNR	15	7	8	0	0	0.8	0.78
HS2ST1	0	5	0	1	0	5.87	0
HSD17B10	1	6	6	0.97	0.98	3.39	2.95
HSP90AB1	109	136	220	0	0	1.7	2.33
HSP90B1	12	18	19	0.06	0.12	2.08	1.88
HSPA1B	185	149	273	0	0	1.21	1.88
HSPA4	16	10	24	0	0.04	0.96	1.85
HSPA4L	9	2	11	0	0.15	0.47	1.61
HSPA5	80	63	76	0	0	1.14	1.16
HSPA8	140	114	195	0	0	1.04	1.51
HSPA9	45	36	73	0	0	1.17	1.99
HSPBP1	0	2	1	0.97	0	2.95	1.83
HSPD1	68	63	77	0	0	1.39	1.44
HSPH1	18	14	25	0	0	1.1	1.63
HTATSF1	2	0	2	0	0	0	0.47
HUWE1	6	16	12	0.92	0.84	3.68	2.42
IARS	37	32	33	0	0	1.39	1.22
IFT74	0	1	3	0	1	1.97	3.48
IFT81	2	1	5	0	0.85	0.91	2.36
IGBP1	0	2	3	0.6	0.87	2.05	2.42
IGF2BP1	45	25	45	0	0	0.93	1.4
IGF2BP2	14	6	13	0	0	0.74	1.28
IGF2BP3	26	11	16	0	0	0.72	0.88
IGF2R	2	4	6	0.72	0.92	2.26	2.74
ILF3	7	9	29	0	1	1.14	2.91
IMMT	6	26	14	0.99	0.9	5.83	2.78
IMPDH2	9	3	6	0	0	0.58	0.89
INA	52	38	50	0	0	1.19	1.33
IQGAP1	2	5	6	0.83	0.92	2.7	2.74
IRAK1	4	10	9	0.89	0.87	3.21	2.52
IRS4	51	11	15	0	0	0.38	0.43
ITSN1	0	3	3	0.99	1	3.92	3.48
JPT2	3	3	4	0.23	0.48	1.42	1.56
JUP	36	20	7	0	0	0.86	0.28
KARS	24	18	17	0	0	1.23	1

KDM3B	5	0	1	0	0	0	0.16
KEAP1	0	1	5	0	0.68	0.86	2.22
KHSRP	38	14	36	0	0	0.51	1.08
KIF11	14	15	30	0	0.34	1.27	2.1
KIF13A	0	3	3	0.99	1	3.92	3.48
KIF14	12	7	9	0	0	0.97	1.05
KIF23	8	0	0	0	0	0	0
KIF2A	3	8	7	0.89	0.86	3.19	2.46
KIF4A	8	0	3	0	0	0	0.31
KIF5B	69	85	103	0	0	1.72	1.76
KIF7	2	0	6	0	0.92	0	2.74
KLC2	16	10	21	0	0	0.92	1.57
KLC4	2	3	10	0.53	0.99	1.81	4.26
KPNA2	10	8	14	0	0.31	1.28	1.83
KPNB1	9	18	22	0.84	0.93	2.96	3.06
KPRP	28	1	1	0	0	0.11	0.1
KTN1	15	15	14	0	0	0.96	0.77
LAP3	1	3	3	0.85	0.87	2.47	2.19
LARP1	16	11	13	0	0	0.4	0.4
LARP4	2	3	3	0.01	0.01	1.13	1
LARP7	6	0	2	0	0	0	0.54
LARS	8	15	11	0.28	0.01	2.23	1.44
LDHA	19	34	27	0.07	0	2.46	1.68
LDHB	25	26	29	0	0	1.55	1.47
LIMA1	4	0	0	0	0	0	0
LMAN2	2	6	2	0.91	0.29	3.15	1.22
LMNA	3	2	2	0	0	0.55	0.49
LMNB1	4	2	6	0	0	0.43	0.87
LMNB2	2	3	5	0.16	0.74	1.5	1.97
LRPPRC	26	20	37	0	0	1.2	1.85
LRRC47	3	2	8	0.07	0.9	1.07	2.76
LRRC59	1	4	5	0.78	0.92	2.42	2.54
LRRFIP1	9	8	12	0	0.01	1.16	1.44
LSM12	12	4	2	0	0	0.61	0.33
LUZP1	8	2	11	0	0	0.16	0.56
LYN	15	0	0	0	0	0	0
MAGED1	6	10	11	0.41	0.61	2.17	2.04
MAGED2	11	20	21	0.05	0.13	2.13	1.91
MAP1B	2	9	7	0.99	0.96	4.5	3.12
MAP3K7	2	4	8	0.72	0.98	2.26	3.5
MAP4	40	43	54	0	0	0.73	0.77
MAP7D3	24	28	28	0	0	1.36	1.16
MAPRE1	4	7	5	0.47	0.11	2.07	1.36

MAPRE2	2	4	0	0.42	0	1.88	0
MARCKSL1	9	11	14	0.14	0.54	1.87	2
MARS	11	18	11	0.56	0.01	2.49	1.36
MATR3	17	3	11	0	0	0.24	0.61
MCCC1	48	28	43	0	0	0.49	0.63
MCCC2	100	82	112	0	0	1.36	1.57
MCM3	4	1	9	0	0.86	0.52	2.23
MCM4	3	0	1	0	0	0	0.41
MCM6	5	4	6	0	0	0.94	1.14
MCM7	12	4	9	0	0	0.61	1.05
MDC1	0	0	4	0	0	0	0.26
MDH2	4	3	10	0.06	0.9	1.17	2.77
MED24	4	0	0	0	0	0	0
MFAP1	0	0	2	0	0	0	0.54
MKI67	0	0	4	0	0	0	0.05
MKLN1	3	0	0	0	0	0	0
MOV10	2	0	2	0	0.29	0	1.22
MPRIP	1	1	9	0	1	0.98	4.17
MRE11	5	7	13	0.46	0.92	1.99	2.99
MRPL18	0	3	0	0.99	0	3.92	0
MRPS22	3	3	6	0.23	0.79	1.42	2.16
MRPS31	0	5	3	1	1	5.87	3.48
MRTFB	9	3	26	0	0.96	0.63	3.58
MTA1	3	0	0	0	0	0	0
MTA2	8	0	2	0	0	0	0.36
MTDH	21	9	13	0	0	0.48	0.58
MTHFD1	13	15	15	0.03	0.03	1.81	1.55
MTX1	0	3	2	0.99	0.97	3.92	2.65
MYBBP1A	9	2	5	0	0	0.3	0.53
MYCBP2	1	0	2	0	0.63	0	1.67
MYO1C	4	0	1	0	0	0	0.48
MYO1D	2	0	0	0	0	0	0
MYO6	7	6	9	0.02	0.3	1.34	1.65
NAA15	3	1	17	0	1	0.72	5.46
NACA	10	13	32	0	1	1.59	3.19
NAP1L4	19	16	29	0	0	1.2	1.8
NAPA	2	4	1	0.72	0	2.26	0.84
NASP	5	0	0	0	0	0	0
NBR1	0	0	3	0	0.56	0	1.86
NCAPD2	7	20	20	0.94	0.95	4.02	3.44
NCAPG	3	14	14	1	1	3.6	3.09
NCAPH	5	5	7	0	0	0.64	0.74
NCK1	0	3	3	0.53	0.56	2.1	1.86

NCKAP1	14	15	16	0	0	1.49	1.35
NCL	47	41	60	0	0	0.86	1.06
NCOR1	7	0	2	0	0	0	0.39
NDUFS1	4	4	7	0.18	0.73	1.47	2.03
NDUFS7	0	2	0	0.97	0	2.95	0
NEFL	12	8	14	0	0.05	1.1	1.57
NEFM	37	30	20	0	0	1.31	0.76
NEK1	0	5	3	1	1	5.87	3.48
NEK9	1	13	18	1	1	8.62	10.01
NELFE	3	0	1	0	0	0	0.26
NFRKB	2	0	0	0	0	0	0
NIFK	2	6	1	0.91	0	3.15	0.84
NME2	0	3	1	0.99	0	3.92	1.83
NMT1	0	4	17	0.72	1	2.62	8.03
NOLC1	3	1	5	0	0	0.21	0.55
NOM1	5	1	7	0	0.5	0.5	1.73
NONO	51	6	17	0	0	0.16	0.35
NOP16	0	4	0	1	0	4.9	0
NOP2	7	1	9	0	0	0.27	1.16
NOP56	0	0	6	0	0.01	0	1.33
NOP58	0	0	5	0	0	0	0.96
NPM1	50	37	26	0	0	0.39	0.24
NSDHL	2	3	2	0.53	0.29	1.81	1.22
NSF	6	8	12	0.36	0.84	1.95	2.42
NSUN2	5	4	2	0	0	1.02	0.55
NUDC	6	13	41	0	1	1.71	4.36
NUDT5	0	4	3	0.96	0.87	3.41	2.42
NUF2	3	1	3	0	0.25	0.72	1.26
NUFIP2	13	4	10	0	0	0.22	0.42
NUMA1	18	0	7	0	0	0	0.11
NUP107	4	2	7	0	0.73	0.88	2.03
NUP153	14	0	1	0	0	0	0.07
NUP214	9	8	16	0	0	0.34	0.55
NUP88	3	3	5	0.01	0.1	1.08	1.41
NUP93	3	2	5	0.07	0.68	1.07	1.86
OAT	0	2	4	0.97	1	2.95	4.3
OCIAD1	2	4	4	0.72	0.75	2.26	1.98
OCLN	3	0	0	0	0	0	0
OGA	6	3	0	0	0	0.87	0
OGT	21	6	15	0	0	0.51	1.01
OSBPL9	8	4	8	0	0.05	0.86	1.34
PA2G4	5	7	14	0	0.12	1.12	1.8
PABPC1	58	39	53	0	0	1.04	1.19

PABPC4	35	26	39	0	0	1.15	1.46
PABPN1	12	6	5	0	0	0.85	0.64
PACSIN3	2	0	0	0	0	0	0
PAICS	21	35	28	0	0	1.85	1.27
PARP1	40	40	58	0	0	1.41	1.73
PC	103	137	115	0	0	0.36	0.26
PCBP1	39	41	38	0	0	1.5	1.19
PCBP2	32	35	36	0	0	1.46	1.28
PCCA	61	39	68	0	0	0.53	0.77
PCCB	78	71	82	0	0	1.14	1.12
PCM1	13	6	18	0	0	0.49	1.15
PCNA	6	16	15	0.92	0.92	3.68	2.97
PDCD6IP	2	4	5	0.72	0.85	2.26	2.36
PDCL3	0	3	4	0.99	1	3.92	4.3
PDHA1	0	3	3	0.99	1	3.92	3.48
PDHB	6	10	8	0.66	0.4	2.38	1.69
PDIA3	13	7	17	0	0.11	0.91	1.75
PDIA4	5	0	10	0	0.83	0	2.36
PDLIM1	5	13	11	0.95	0.65	2.61	1.93
PDS5A	3	2	5	0	0.02	0.73	1.26
PEAK1	0	0	2	0	0.63	0	1.85
PELO	3	7	4	0.84	0.48	2.84	1.56
PES1	5	2	4	0	0	0.24	0.35
PEX14	5	9	8	0.11	0.04	1.87	1.45
PFAS	5	0	5	0	0	0	0.98
PFDN2	1	4	1	0.96	0	3.09	1.15
PFKL	3	5	3	0.64	0.25	2.13	1.26
PGAM5	13	17	11	0.1	0	2.04	1.17
PGRMC1	0	3	2	0.99	0.97	3.92	2.65
PHB	7	10	14	0.43	0.85	2.11	2.46
PHB2	31	34	34	0	0	1.78	1.52
PHF5A	3	2	0	0.07	0	1.07	0
PHF8	3	0	0	0	0	0	0
PHGDH	47	44	52	0	0	1.54	1.54
PHKA1	0	0	2	0	0.97	0	2.65
PIH1D1	5	5	5	0.02	0.03	1.35	1.18
PIK3C3	0	1	3	0	1	1.97	3.48
PIKFYVE	0	203	278	1	1	198.81	230.63
PKM	19	9	27	0	0	0.44	1.05
PKP1	8	8	2	0.04	0	1.55	0.47
PKP4	7	0	0	0	0	0	0
PLEC	55	28	27	0	0	0.78	0.64
PLIN3	6	16	6	0	0	1.56	0.56

PNN	14	7	10	0	0	0.28	0.34
POLDIP3	7	6	5	0	0	1.15	0.86
POLR2A	2	3	3	0.03	0.04	1.29	1.14
POLR2B	7	6	6	0.02	0.03	1.34	1.17
POLR3C	3	0	0	0	0	0	0
PPAT	0	5	2	1	0.97	5.87	2.65
PPFIA1	1	0	6	0	1	0	3.76
PPP1CB	20	16	4	0	0	1.26	0.33
PPP1R10	14	6	6	0	0	0.36	0.32
PPP1R12A	1	5	6	0.01	0.02	1.4	1.42
PPP2R1A	2	4	6	0.72	0.92	2.26	2.74
PPP2R2A	0	3	4	0.99	1	3.92	4.3
PRDX1	4	2	3	0	0	0.36	0.43
PRDX6	1	2	3	0	0	0.7	0.83
PRKAR1A	21	24	21	0	0	1.83	1.38
PRKAR2A	5	5	5	0.02	0.03	1.35	1.18
PRKCSH	7	1	5	0	0.01	0.39	1.01
PRKDC	59	67	61	0	0	1.86	1.45
PRPF19	6	1	2	0	0	0.44	0.59
PRPF31	3	0	0	0	0	0	0
PRPF40A	7	0	1	0	0	0	0.33
PRPF6	6	2	5	0	0.04	0.65	1.14
PRPF8	7	3	3	0	0	0.4	0.35
PRPS1	0	4	4	1	1	4.9	4.3
PRPSAP2	0	4	2	1	0.97	4.9	2.65
PRRC2A	2	3	3	0	0	0.69	0.61
PRRC2B	6	4	8	0	0.14	0.99	1.54
PRRC2C	26	18	34	0	0	0.77	1.21
PSMA1	4	1	1	0	0	0.59	0.55
PSMA4	0	2	5	0.97	1	2.95	5.13
PSMC1	7	5	11	0.01	0.61	1.15	1.98
PSMC2	16	13	16	0	0	1.02	1.06
PSMC3	10	5	4	0	0	0.86	0.63
PSMC4	4	2	2	0	0	0.88	0.79
PSMC5	8	20	19	0.92	0.92	3.6	2.94
PSMC6	8	8	12	0.04	0.51	1.55	1.92
PSMD1	1	6	10	1	1	4.32	5.84
PSMD11	19	12	15	0	0	1.05	1.1
PSMD12	1	8	7	1	0.99	4.35	3.35
PSMD13	3	4	3	0.45	0.25	1.78	1.26
PSMD2	8	18	20	0.86	0.93	3.03	2.86
PSMD3	6	4	13	0.01	0.88	1.09	2.6
PSMD4	9	7	4	0	0	1.17	0.64

PSMD7	5	7	4	0.46	0.05	1.99	1.1
PSME3	12	3	1	0	0	0.34	0.16
PTBP1	7	2	7	0	0	0.29	0.66
PTMA	2	3	12	0.53	1	1.81	5.03
PUM1	2	0	3	0	0.56	0	1.6
PYCR2	2	8	9	0.97	0.99	4.05	3.88
PYCR3	1	6	6	1	1	4.32	3.76
PYGL	3	2	8	0.07	0.9	1.07	2.76
PYM1	5	4	7	0.05	0.5	1.25	1.73
QARS	19	21	33	0	0.22	1.65	2.17
QKI	3	2	5	0.07	0.68	1.07	1.86
RAB11FIP5	1	3	3	0.51	0.54	1.94	1.72
RAB3GAP2	0	3	6	0.85	1	2.73	4.15
RAB5C	4	7	4	0.7	0.2	2.34	1.29
RACGAP1	17	0	8	0	0	0	0.69
RACK1	5	12	6	0.89	0.31	3.23	1.52
RAD50	1	6	8	1	1	4.32	4.8
RADX	3	0	0	0	0	0	0
RAE1	1	4	3	0.78	0.54	2.42	1.72
RAN	4	7	9	0	0	0.96	1.04
RANBP2	13	15	17	0	0	0.25	0.24
RANBP3	10	11	9	0	0	0.9	0.65
RANBP9	6	0	1	0	0	0	0.4
RANGAP1	8	17	20	0	0	0.89	0.89
RARS	41	29	42	0	0	0.87	1.06
RASAL2	1	2	3	0.6	0.87	1.86	2.19
RBBP4	14	7	5	0	0	0.85	0.56
RBBP7	12	5	5	0	0	0.69	0.61
RBM10	2	0	0	0	0	0	0
RBM14	12	7	10	0	0	0.97	1.15
RBM17	6	0	1	0	0	0	0.22
RBM25	7	4	2	0	0	0.54	0.29
RBM26	9	2	0	0	0	0.23	0
RBM39	5	0	9	0	0.13	0	1.61
RBM4	6	6	6	0.09	0.11	1.52	1.32
RBM7	4	1	2	0	0	0.59	0.79
RBMX	12	17	3	0.09	0	2.08	0.41
RCOR1	3	0	0	0	0	0	0
RDX	2	7	4	0.01	0	1.63	0.9
RELA	1	3	4	0.85	0.96	2.47	2.71
REPS1	0	3	7	0.85	1	2.73	4.72
RFC1	6	0	12	0	0	0	0.99
RFC2	2	5	1	0.83	0	2.7	0.84

RFC3	9	18	8	0.84	0.01	2.96	1.21
RFC5	2	6	3	0.91	0.56	3.15	1.6
RFX5	2	0	0	0	0	0	0
RNF20	4	1	4	0	0.03	0.52	1.14
RNH1	0	2	5	0.97	1	2.95	5.13
ROCK1	0	2	6	0.97	1	2.95	5.96
RPAP3	4	4	27	0	1	0.77	3.64
RPL10	7	4	5	0	0	0.82	0.86
RPL10A	4	7	9	0.7	0.87	2.34	2.52
RPL11	12	8	9	0	0	0.9	0.86
RPL12	6	6	2	0	0	1.09	0.42
RPL13	36	22	19	0	0	0.96	0.71
RPL13A	7	7	5	0	0	1.31	0.86
RPL14	9	6	8	0	0	1.02	1.13
RPL15	4	1	2	0	0	0.31	0.41
RPL17	3	2	0	0	0	0.92	0
RPL18	15	8	9	0	0	0.86	0.83
RPL18A	11	5	8	0	0	0.64	0.83
RPL19	3	3	10	0.01	0.98	1.08	2.55
RPL21	4	5	1	0.09	0	1.55	0.48
RPL22	2	5	2	0.02	0	1.5	0.68
RPL23	1	3	1	0.03	0	1.36	0.63
RPL23A	9	0	2	0	0	0	0.42
RPL24	6	7	3	0	0	1.17	0.52
RPL26	15	1	0	0	0	0.2	0
RPL27	3	1	0	0	0	0.72	0
RPL28	12	8	0	0	0	0.86	0
RPL3	16	10	15	0	0	0.89	1.11
RPL30	2	1	1	0	0	0.91	0.84
RPL4	48	54	49	0	0	1.76	1.36
RPL5	7	7	15	0	0	0.91	1.56
RPL6	17	14	13	0	0	0.71	0.57
RPL7	8	9	15	0.1	0.81	1.72	2.36
RPL7A	20	19	22	0	0	1.48	1.46
RPL8	16	8	11	0	0	0.85	0.97
RPL9	6	4	5	0	0	0.61	0.64
RPLP0	37	18	30	0	0	0.79	1.1
RPLP2	2	0	0	0	0	0	0
RPN1	4	9	5	0.39	0	2.1	1.1
RPRD1B	5	2	0	0	0	0.75	0
RPS11	6	3	0	0	0	0.67	0
RPS12	2	5	1	0.83	0	2.7	0.84
RPS13	2	2	1	0.27	0	1.36	0.84

RPS14	10	7	2	0	0	0.96	0.32
RPS16	7	5	0	0	0	0.92	0
RPS18	10	5	4	0	0	0.86	0.63
RPS19	10	5	5	0	0	0.86	0.75
RPS2	13	11	9	0	0	1.18	0.85
RPS23	4	0	0	0	0	0	0
RPS25	3	6	2	0.77	0.08	2.48	0.96
RPS26	5	6	2	0.07	0	1.57	0.61
RPS27	9	10	3	0	0	1.42	0.46
RPS27A	46	56	42	0	0	1.99	1.28
RPS3	33	39	38	0	0	1.7	1.41
RPS3A	47	49	47	0	0	1.59	1.3
RPS4X	13	8	14	0	0.01	1.02	1.46
RPS5	3	6	4	0.77	0.48	2.48	1.56
RPS6	16	11	13	0	0	0.97	0.97
RPS7	1	4	0	0	0	1.17	0
RPS8	28	21	24	0	0	1.1	1.06
RPS9	9	4	2	0	0	0.73	0.4
RPSA	25	28	24	0	0	1.76	1.3
RRBP1	48	19	28	0	0	0.66	0.82
RRP1	5	4	4	0.05	0.05	1.25	1.1
RRP1B	0	0	8	0	1	0	5.3
RTCB	7	6	11	0	0.14	1.15	1.69
RUFY1	0	1	8	0	1	1.97	7.61
RUVBL1	26	28	31	0	0	0.92	0.87
RUVBL2	67	60	77	0	0	1.48	1.61
SAMHD1	4	4	4	0.18	0.2	1.47	1.29
SART1	13	2	4	0	0	0.13	0.19
SART3	16	2	5	0	0	0.16	0.27
SCAMP3	0	3	4	0.85	0.96	2.73	3
SCFD1	4	6	5	0.56	0.4	2.05	1.53
SCRIB	7	0	0	0	0	0	0
SDHA	4	4	3	0.03	0.01	1.3	0.92
SEC13	4	2	4	0	0.2	0.88	1.29
SEC16A	7	9	13	0	0.04	1.34	1.61
SEC22B	3	4	4	0.45	0.48	1.78	1.56
SEC23IP	3	2	4	0.07	0.48	1.07	1.56
SEC62	2	10	2	0.99	0.29	4.95	1.22
SELENBP1	0	4	0	1	0	4.9	0
SEPTIN11	10	17	17	0.65	0.68	2.56	2.19
SEPTIN2	10	18	10	0.73	0.02	2.7	1.35
SEPTIN7	7	9	9	0.27	0.3	1.92	1.65
SEPTIN9	11	15	20	0.2	0.77	2.1	2.35

SERBP1	45	53	70	0	0	1.22	1.37
SERPINH1	5	5	7	0	0	0.52	0.6
SETD1A	14	3	2	0	0	0.43	0.29
SF1	8	2	4	0	0	0.23	0.34
SF3A1	44	37	44	0	0	1	1
SF3A3	16	5	5	0	0	0.57	0.49
SF3B1	46	8	19	0	0	0.16	0.29
SF3B2	14	0	4	0	0	0	0.16
SF3B3	19	3	17	0	0	0.31	1.2
SFPQ	39	10	20	0	0	0.35	0.58
SFXN1	8	11	13	0.33	0.64	2.06	2.06
SH3GL1	8	12	7	0.22	0	2.07	1.11
SH3GLB1	0	2	2	0.97	0.97	2.95	2.65
SHMT2	7	3	7	0	0.07	0.77	1.33
SHTN1	0	2	6	0.97	1	2.95	5.96
SIN3A	3	0	0	0	0	0	0
SKA3	0	4	1	1	0	4.9	1.83
SLC16A1	2	5	0	0.02	0	1.5	0
SLC25A10	2	7	1	0.95	0	3.6	0.84
SLC25A11	10	9	9	0.01	0.01	1.42	1.23
SLC25A13	2	8	10	0.97	0.99	4.05	4.26
SLC25A3	23	19	15	0	0	1.27	0.87
SLC25A5	14	37	21	1	0	2.92	1.45
SLK	23	32	39	0	0	1.44	1.49
SMARCA4	7	1	2	0	0	0.2	0.27
SMARCA5	10	1	4	0	0	0.1	0.21
SMARCC1	3	0	0	0	0	0	0
SMARCC2	3	0	0	0	0	0	0
SMC1A	9	5	11	0	0.15	0.94	1.61
SMC2	23	31	18	0.01	0	2.16	1.1
SMC3	23	11	31	0	0.02	0.81	1.84
SMC4	4	33	18	1	1	7.87	3.76
SMG7	0	3	6	0.99	1	3.92	5.96
SMN2	1	2	3	0.22	0.54	1.46	1.72
SNAP23	8	3	0	0	0	0.69	0
SND1	7	7	23	0	1	1.01	2.59
SNRNP200	7	0	1	0	0	0	0.16
SNRNP70	0	0	5	0	1	0	5.13
SNRPA	2	0	4	0	0.46	0	1.65
SNRPA1	6	3	3	0	0	0.35	0.31
SNRPD2	4	1	2	0	0	0.42	0.57
SNRPD3	0	4	0	0.72	0	2.62	0
SNW1	8	0	6	0	0	0	0.43

SNX1	9	16	28	0	0.99	1.56	2.27
SNX2	8	10	13	0.01	0.18	1.64	1.79
SNX5	3	6	5	0.77	0.68	2.48	1.86
SNX6	2	4	5	0.72	0.85	2.26	2.36
SNX9	2	2	8	0.27	0.98	1.36	3.5
SORT1	0	6	0	1	0	6.85	0
SPAG9	1	8	9	0.99	1	3.58	3.43
SPART	3	9	11	0.93	0.97	3.54	3.66
SPTAN1	13	1	5	0	0	0.17	0.44
SPTBN1	10	0	1	0	0	0	0.24
SPTBN2	5	2	2	0	0	0.75	0.68
SPTLC1	1	6	1	1	0	4.32	1.15
SRGAP2	1	0	3	0	0.87	0	2.19
SRP14	5	4	0	0	0	1.02	0
SRP19	1	1	5	0	0.99	1.25	3.24
SRP54	2	6	11	0.91	1	3.15	4.65
SRP68	17	17	22	0	0	0.96	1.04
SRP72	13	19	34	0.04	0.95	2.06	3.07
SRPK2	4	0	0	0	0	0	0
SRPRB	1	3	7	0.85	1	2.47	4.28
SRRM2	5	2	2	0	0	0.16	0.14
SRRT	4	0	3	0	0.07	0	1.04
SRSF1	4	11	4	0.91	0.2	3.51	1.29
SRSF3	4	15	0	1	0	3.36	0
SRSF9	3	7	0	0.84	0	2.84	0
SSB	17	8	9	0	0	0.8	0.77
SSR1	0	5	2	1	0.97	5.87	2.65
SSRP1	4	0	9	0	0.86	0	2.23
STAU1	6	2	8	0	0.14	0.6	1.54
STAU2	4	2	8	0	0.72	0.78	2.01
STIP1	6	4	30	0	1	0.99	5.21
STMN1	4	3	3	0.01	0.01	1.04	0.92
STOML2	3	6	0	0.77	0	2.48	0
STRAP	16	20	17	0.03	0	1.98	1.45
STRIP1	0	4	3	1	1	4.9	3.48
STRN	6	15	14	0.91	0.9	3.46	2.78
STRN3	7	14	14	0.73	0.75	2.65	2.27
STRN4	1	5	3	0.91	0.54	2.9	1.72
STUB1	0	2	2	0.97	0.97	2.95	2.65
STX12	0	3	1	0.99	0	3.92	1.83
STX4	1	2	0	0.6	0	1.86	0
STX7	3	7	1	0.84	0	2.84	0.66
SUGT1	6	9	12	0.25	0.74	1.97	2.2

SUPT16H	1	0	2	0	0	0	0.8
SYNCRIP	24	7	23	0	0	0.45	1.16
TACC3	2	1	9	0	0.99	0.65	2.77
TAF15	8	7	12	0	0.09	1.19	1.66
TAF4	9	0	2	0	0	0	0.42
TAGLN2	8	11	11	0	0	0.84	0.72
TARDBP	12	15	13	0	0	1.6	1.2
TARS	0	0	2	0	0.97	0	2.65
TBC1D15	1	2	8	0	0.72	0.89	2.28
TCOF1	31	0	1	0	0	0	0.04
TCP1	51	80	181	0	0.99	2.56	4.88
TFAM	7	7	4	0.07	0	1.53	0.84
TFRC	2	3	6	0.03	0.68	1.29	1.96
THOC2	4	0	0	0	0	0	0
THRAP3	18	0	9	0	0	0	0.32
TIMM23	1	5	2	0.99	0.63	3.7	1.67
TIMM44	0	3	3	0.99	1	3.92	3.48
TIMM50	8	23	8	0.95	0.01	3.82	1.24
TJP1	11	6	15	0	0	0.3	0.58
TJP2	14	23	39	0.29	0.96	2.43	3.45
TKT	1	0	4	0	0.8	0	2.13
TLN1	61	70	81	0	0	1.49	1.47
TMEM43	0	3	2	0.99	0.97	3.92	2.65
TMF1	0	3	7	0.99	1	3.92	6.78
TMPO	18	10	9	0	0	0.33	0.26
TNIP1	2	5	9	0.72	1	2.25	3.23
TNKS1BP1	5	7	7	0	0	0.9	0.78
TNRC6B	7	6	17	0	0.85	0.94	2.07
TOMM22	5	9	7	0.53	0.19	2.24	1.55
TOP1	12	1	7	0	0	0.2	0.69
TOR1AIP1	3	6	6	0.06	0.07	1.68	1.47
TOX4	11	1	3	0	0	0.11	0.19
TP53	28	8	1	0	0	0.51	0.1
TP53BP2	5	10	9	0.7	0.57	2.46	1.93
TPD52L2	2	6	5	0.91	0.85	3.15	2.36
TPI1	11	4	9	0	0	0.66	1.13
TPR	117	61	82	0	0	0.59	0.68
TRAP1	15	10	14	0	0	1.05	1.23
TRIM28	67	14	25	0	0	0.27	0.4
TRIP12	9	6	5	0	0	0.96	0.72
TTC1	1	2	3	0.6	0.87	1.86	2.19
TTC28	3	16	26	1	1	5.2	7.04
TTC4	1	2	4	0.6	0.96	1.86	2.71

TUBG1	2	14	6	1	0.92	6.74	2.74
TUBGCP2	2	3	4	0.53	0.75	1.81	1.98
TUBGCP3	4	1	4	0	0.03	0.52	1.14
TUFM	14	20	18	0	0	1.87	1.45
TXNDC5	3	2	6	0.07	0.79	1.07	2.16
U2SURP	3	0	0	0	0	0	0
UBA1	15	3	23	0	0.33	0.4	2.04
UBAP2	8	3	11	0	0	0.39	1
UBAP2L	13	10	16	0	0	0.52	0.68
UBE2O	2	12	6	1	0.92	5.85	2.74
UGGT1	0	0	3	0	1	0	3.48
UNC45A	7	21	28	1	1	3.14	3.53
UPF1	0	0	4	0	1	0	4.3
UQCRC1	6	10	6	0.66	0.11	2.38	1.32
UQCRC2	22	13	20	0	0	0.98	1.26
URI1	0	0	6	0	1	0	5.96
USO1	10	15	11	0.07	0	2.02	1.31
USP15	4	14	3	0	0	1.13	0.27
USP9X	2	23	20	1	1	10.78	8.07
UTRN	4	15	13	0.97	0.96	4.67	3.51
VAC14	10	1695	1059	1	1	241.05	127.73
VARS	4	1	1	0	0	0.42	0.39
VCL	3	12	6	0.98	0.79	4.6	2.16
VCP	25	12	22	0	0	0.81	1.23
VCPIP1	4	4	13	0	0.49	0.82	1.97
VDAC1	1	10	6	0.92	0.27	3.23	1.79
VDAC2	5	23	8	0.41	0	2.68	0.87
VDAC3	2	3	2	0.01	0	1.13	0.76
VPS52	4	0	1	0	0	0	0.55
VTA1	3	7	3	0.84	0.25	2.84	1.26
WARS	5	9	13	0	0	0.93	1.12
WASF2	3	6	3	0.77	0.25	2.48	1.26
WASH6P	8	3	8	0	0.05	0.69	1.34
WASHC2A	2	4	5	0.72	0.85	2.26	2.36
WDHD1	6	0	0	0	0	0	0
WDR26	7	2	4	0	0	0.58	0.84
WDR5	7	3	4	0	0	0.77	0.84
WNK1	3	8	8	0.89	0.9	3.19	2.76
XIAP	3	7	1	0.01	0	1.58	0.37
XPO1	2	5	6	0.83	0.92	2.7	2.74
XPO5	4	0	2	0	0	0	0.79
XRCC5	7	7	14	0	0	0.87	1.39
XRCC6	17	1	13	0	0	0.12	0.71

YBX1	63	61	79	0	0	1.59	1.75
YBX3	23	20	37	0	0.24	1.42	2.18
YLPM1	7	2	2	0	0	0.27	0.25
YME1L1	2	4	8	0.72	0.98	2.26	3.5
YTHDF2	8	6	11	0.01	0.36	1.2	1.77
YTHDF3	3	2	9	0.07	0.93	1.07	3.06
YWHAB	0	0	6	0	1	0	5.96
YWHAE	15	15	14	0	0	1.6	1.28
YWHAG	3	2	3	0.07	0.25	1.07	1.26
YWHAH	2	2	5	0.27	0.85	1.36	2.36
YWHAQ	11	11	13	0.01	0.07	1.57	1.58
YWHAZ	12	14	17	0.04	0.26	1.82	1.87
ZC3H11A	7	0	0	0	0	0	0
ZC3H14	10	2	1	0	0	0.21	0.13
ZC3H4	7	1	2	0	0	0.22	0.29
ZC3HAV1	25	14	36	0	0	0.64	1.33
ZFR	9	0	6	0	0	0	0.38
ZNF428	0	2	0	0.97	0	2.95	0
ZNF598	4	3	10	0.06	0.9	1.17	2.77
ZNF638	2	0	0	0	0	0	0
ZW10	2	4	7	0.72	0.96	2.26	3.12
ZYX	12	20	30	0	0.97	1.92	2.42

* The fold change score B (FC-B) is a more stringent fold change metric that takes the average of the top 3 highest spectral counts for the abundance estimate

6.3 From hitchhiker to hijacker: pathogen exploitation of endosomal phosphoinositides (Review)

From hitchhiker to hijacker: pathogen exploitation of endosomal phosphoinositides

Shirley Qiu[1,2,3] and Marceline Côté[1,2,3]

[1]Department of Biochemistry, Microbiology, and Immunology, University of Ottawa, Ottawa, Canada

[2]Ottawa Institute of Systems Biology, University of Ottawa, Ottawa, Canada

[3]University of Ottawa Center for Infection, Immunity and Inflammation, Ottawa, Canada

This review has previously been published in Biochemistry and Cell Biology as one of a selection of papers from the 2017 CSMB Conference:

Qiu S, Côté M. From hitchhiker to hijacker: pathogen exploitation of endosomal phosphoinositides. Biochemistry and Cell Biology. 2019 Feb;97(1):1-9.

Abstract

Signalling through phosphoinositide lipids is essential for regulating many cellular processes, including endosomal trafficking. A number of intracellular pathogens have found ways to subvert host trafficking pathways via exploitation of endosomal phosphoinositides. This review will discuss how pathogens such as bacteria, viruses, and eukaryotic parasites depend on endosomal phosphoinositides for infection, as well as the mechanisms through which some are able to actively manipulate these signalling lipids to facilitate invasion, survival, replication, and immune evasion.

Key words: Endosomal trafficking, phosphoinositides, lipid signalling, host-pathogen interactions

Introduction

Vesicular trafficking is a defining characteristic of eukaryotic cells. The sorting and transport of macromolecules between cellular compartments is a dynamically regulated process involving precise spatiotemporal signalling events on membranes. The highly regulated nature of endosomal trafficking is essential not only for proper transport of cargos throughout the cell, but also for maintaining organelle and endosome identity and function. Central to this regulation is the turnover of a repertoire of signalling lipids known as phosphoinositides (PIs) on the cytosolic leaflet of cell membranes. Generated by the reversible phosphorylation of the glycerophospholipid phosphatidylinositol (PtdIns), these lipids are responsible for recruiting and activating effector proteins on cellular membranes. These proteins in turn carry out various downstream effector functions as enzymes, ion channels, recruiters of other proteins, and more. Together with these effectors, PIs help define the identity of cellular compartments (Balla 2013, Di Paolo and De Camilli 2006, Mayinger 2012).

Seven PIs are found in mammals in vivo, generated by the reversible phosphorylation of the D3, D4, and/or D5 positions on the myo-inositol head group of PtdIns. The turnover and interconversion between the different PIs is controlled by lipid kinases and phosphatases, which serve as the master regulators of PI localization, and in turn, membrane identity (Sasaki et al. 2009). The location of PIs is essential to their function. For example, PtdIns(4,5)P2 is found primarily on the plasma membrane (PM), where it is involved in regulating endocytosis and exocytosis, cytoskeleton remodelling, and generating secondary messengers for signal transduction (Bout and Divecha 2009). In contrast, PtdIns3P, PtdIns(3,5)P2, and (as recently determined), a pool of PtdIns5P, are mainly localized to endosomal membranes and have

important roles in regulating endosomal maturation, sorting, and trafficking (McCartney et al. 2014, Schink et al. 2013, Viaud et al. 2014a). This minireview will focus primarily on these endosomal PIs (Table 1).

PIs regulate vesicular trafficking by recruiting and activating proteins with PI-binding domains. One important class of PI effectors are the Rab GTPases, which in their active GTP-bound form further recruit cytosolic proteins with important effector functions for endosomal trafficking. PIs and Rabs may also regulate each other in a feedback loop, as certain Rab effectors are PI kinases and phosphatases that act to quench PI-induced signalling. PIs themselves may also recruit Rab guanine nucleotide exchange factors (GEFs) and GTPase activating proteins (GAPs) that activate and arrest Rab activity, respectively (Di Paolo and De Camilli 2006).

PtdIns3P is generated primarily from PtdIns by the Class III PI3 kinase (PI3K) vacuolar protein sorting 34 (Vps34), and is enriched on early endosomes (EEs) and multivesicular bodies (MVBs). Rab5 has been shown to be important for PtdIns3P production on EEs, as Vps34 is a Rab5 effector (Christoforidis et al. 1999). PtdIns3P effectors include early endosome antigen 1 (EEA1), the PtdIns-3 kinase PIKfyve, several members of the sorting nexin (SXN) family, and Hrs, a component of the endosomal sorting complexes required for transport (ESCRT), all of which contain PtdIns3P binding domains such as FYVE (Fab1, YOTB, Vac1, EEA1) or PX (phox homology) (Lemmon 2008). These effectors are responsible for a number of functions downstream of EEs, such as sorting into MVBs, homotypic fusion between EEs as well as heterotypic fusion with other endosomes, and maturation of EE into late endosomes (LEs) and lysosomes (LYs) (Schink et al. 2013).

PtdIns(3,5)P2, which is generated from PtdIns3P by the lipid kinase PIKfyve in mammalian cells, is enriched in LE/LY compartments. Conversion between PtdIns3P and PtdIns(3,5)P2 is a hallmark of endosomal maturation and progression through the degradative endocytic pathway. Regeneration of PtdIns3P from PtdIns(3,5)P2 is catalyzed by the PtdIns-5 phosphatase Sac3 (Sbrissa et al. 2007), which exists in a ternary complex with PIKfyve and adaptor protein ArPIKfyve (associated regulator of PIKfyve) (Ikonomov et al. 2009). PtdIns(3,5)P2 can also be dephosphorylated by the 3-phosphatases of the myotubularin/myotubularin-related (MTM/MTMR) family (Begley and Dixon 2005). Although PtdIns(3,5)P2 accounts for less than 1% of all cellular PIs, it is critical for endosomal membrane homeostasis. This is most strikingly demonstrated by the appearance of enlarged cytoplasmic vacuoles of late endocytic origin when PtdIns(3,5)P2 levels are reduced (Ikonomov et al. 2001). Bona fide PtdIns(3,5)P2 effectors are scarce compared to PtdIns3P effectors; however, those identified to date include the transient receptor cation channel mucolipin-1 (TRPML-1) as well as the two pore channels TPC1 and TPC2 (Dong et al. 2010, Jha et al. 2014), all of which are permeable to Ca2+, an important signalling messenger for membrane fusion. How exactly these and other effectors are modulated by PtdIns(3,5)P2 still remains largely unexplained.

Finally, PtdIns5P, the most recently identified PI, has also been revealed to play a role in endosomal membrane dynamics. PtdIns5P is generated primarily from phosphorylation of PtdIns by PIKfyve, and potentially via dephosphorylation PtdIns(3,5)P2 by the MTM/MTMR 3-phosphatases (Shisheva et al. 2015). Previously thought to be primarily nuclear in localization, where it is involved in regulating transcriptional activity (Shisheva 2013, Viaud et al. 2014b), a cytoplasmic pool of PtdIns5P was recently identified, primarily on the PM, but also on endosomes, autophagosomes, the endoplasmic reticulum and the golgi (Sarkes and Rameh 2010,

Vicinanza et al. 2015). Recent characterization of PtdIns5P has revealed that it may be involved in actin cytoskeleton rearrangement as well as degradation of some PM receptors such as EGFR (Ramel et al. 2011, Viaud et al. 2014a). Under basal conditions, levels of PtdIns5P are low in cells, though PtdIns5P levels can increase transiently upon stress conditions such as UV irradiation and osmotic shock (Hill et al. 2010, Jones et al. 2006). Currently, the only known direct PtdIns5P effector is the nuclear protein inhibitor of growth 2 (ING2) through its plant homeodomain (PHD) (Gozani et al. 2003).

Because the maintenance of endosomal homeostasis is critical for nearly all facets of cell function, it is not surprising that dysregulation of the intricate signalling network that governs trafficking events has been implicated in several diseases and disorders. In particular, mutations in the enzymes that catalyze the interconversion between PtdIns3P and PtdIns(3,5)P2 have been implicated in several neuron and motor diseases, including Charcot Marie Tooth Disease Type 4J and ALS (Sac3) (Lenk et al. 2011), X-linked myotubular myopathy (MTM1) (Pierson et al. 2005) and Charcot Marie Tooth Disease Type 4B (MTMR13) (Azzedine et al. 2003).

Endosomal PIs have also been shown to play an important role in host-pathogen interactions (Table 2). Intracellular pathogens rely on host trafficking machinery for invasion, replication, and immune evasion. Interestingly, it is becoming increasingly clear that these pathogens not only rely on host trafficking machinery, but are often able to manipulate and exploit host lipids to facilitate infection. For example, bacteria can manipulate endosomal PIs to generate an intracellular niche favourable to growth and replication, while viruses may modulate PIs in order to facilitate trafficking to viral receptors. Understanding how pathogens are able to

exploit host PIs, their effectors, and their metabolizing enzymes will provide crucial insight into host-pathogen interactions and may facilitate the development of antimicrobial therapeutics.

Bacteria

Many bacteria have been found to both require and manipulate endosomal PIs via the secretion of bacterial effectors into host cells, which modulate PI metabolism to promote invasion, replication, and immune evasion.

Salmonella

Modulation of host PIs has been well documented in the enteropathic bacterium Salmonella enterica, which causes gastroenteritis and typhoid in humans (Figure 1A). Upon initial invasion of host cells, this intracellular pathogen establishes a specialized niche within the host cell's endosomal system known as the Salmonella containing vacuole (SCV). Biogenesis of the SCV depends upon bacterial effector proteins, which are secreted into the host cytosol by a type III secretion system (T3SS) during invasion. These effectors are responsible for inducing actin cytoskeletal rearrangement to facilitate engulfment of bacteria into nonphagocytic cells (McGhie et al. 2009) . The Salmonella-containing macropinosome then undergoes a process similar to classic endosomal maturation, acquiring early endosome markers such as Rab5 and EEA1, followed by late endosome markers such as LAMP1 and Rab7. However, unlike typical late endosomes, the SCV avoids fusion with lysosomes, thereby avoiding degradation and establishing a specialized endosomal niche for replication (Knodler and Steele-Mortimer 2003).

Though the molecular mechanisms by which S. enterica induces and maintains the formation of the SCV are not completely understood, it is clear that modulation of host PIs is

important for SCV biogenesis and bacterial survival. This is achieved in part by a T3SS effector, the lipid phosphatase SopB (SigD). Expression of SopB appears to be important for generation of SCVs after invasion, as isogenic S. enterica with deleted or phosphatase-deficient SopB are capable of invading cells but show reduction in SCV retention and size (Hernandez et al. 2004). Furthermore, expression of SopB alone in cells can induce formation of macropinosomes from the PM that migrate to the perinuclear region (Hernandez et al. 2004). SopB expression is required for multiple stages of SCV maturation, including initial PtdIns3P enrichment and subsequent recruitment of endosomal markers such as EEA1 and Rab7 (Mallo et al. 2008, Scott et al. 2002), as well as inhibition of fusion between SCVs and lysosomes (Bakowski et al. 2010, Dukes et al. 2006). Most intriguing is its ability to directly metabolize PIs through its phosphatidylinositol-5-phosphatase activity. In vitro SopB is able to hydrolyze PtdIns(3,4)P2, PtdIns(3,5)P2, and PtdIns(3,4,5)P3 ; however, Mallo et al. have demonstrated that infection by S. enterica results in an increase in PtdIns4P and PtdIns5P, concomitant with a decrease in PtdIns(4,5)P2, suggesting that the primary lipid substrate of SopB is PtdIns(4,5)P2 on the PM (Hernandez et al. 2004, Mallo et al. 2008). Though the reason(s) that PtdIns(4,5)P2 is the primary target of SopB remains to be elucidated, one possibility is that it reduces the electrostatically unfavourable interaction between the PM and Rab5, thereby promoting Rab5 recruitment. Indeed, Rab5 recruitment to the SCV has been shown to be critical for recruitment of the PI3 kinase Vps34, which is responsible for generating PtndIns3P on EEs, as well as on SCVs (Mallo et al. 2008). This enrichment of PtdIns3P is in turn essential for recruitment of host PtdIns3P effectors such as EEA1, Hrs, and PIKfyve, which together facilitate maturation of EEs and sorting towards either recycling endosomes or late endosomes. Dai et al. have also demonstrated that SopB-dependent PtdIns3P production is required for recruitment of VAMP8

to Salmonella-induced PM ruffles (Dai et al. 2007). VAMP8 is a v-SNARE important for homotypic fusion between EEs and LEs, and is important for Salmonella invasion.

Maturation of the SCV into a more LE-like compartment involves acquisition of LE markers such as Rab7 and LAMP1, as well as acidification of the lumen (Knodler and Steele-Mortimer 2003). This maturation is important for induction of expression of Salmonella pathogenicity island 2 (SPI2) genes, which are important for bacterial survival and replication, and is dependent on PtdIns3P conversion to PtdIns(3,5)P2 by PIKfyve (Kerr et al. 2010). Kerr et al. have demonstrated that inhibition of PIKfyve kinase activity results in impaired S. enterica replication. Furthermore, when PIKfyve activity is inhibited, the SCV fails to colocalize with LAMP1, indicating that establishment of productive SCVs requires PtdIns(3,5)P2 generation (Kerr et al. 2010).

It is unclear how S. enterica effectors prevent the fusion of SCV with endolysosomes, as would normally occur to endosomes in the degradative pathway. Work by Bakowski et al. has demonstrated that the reduction of surface charge on the SCV may play a role in inhibiting recruitment of effectors with polycationic motifs. They found that reduction of PtdIns(4,5)P2 on SCV, a negatively charged phospholipid, reduced the recruitment of Rab23 and Rab35, which are both known to facilitate fusion of LEs with LYs (Bakowski et al. 2010).

Shigella

Like S. enterica, Shigella, the cause of bacillary dysentery, is an intracellular bacterium that secretes effector proteins into the host cytosol via a T3SS. Similar to S. enterica, S. flexneri invasion into gastrointestinal epithelial cells requires massive but localized actin cytoskeleton

rearrangements in order to facilitate phagocytic uptake (Cossart 1997) into a bacteria-containing vacuole. However, unlike Salmonella, Shigella is able to rupture this vacuole to escape into the cytosol, where replication and eventually invasion into neighboring cells takes place (Ray et al. 2009). Cell-to-cell spread of cytosolic bacteria also requires massive host membrane rearrangements, resulting in actin-induced protrusions into neighboring cells, and the generation of new bacteria-containing vacuoles in adjacent cells (Mellouk et al. 2014, Stevens et al. 2006).

This dependence on significant but transient changes in host membrane dynamics suggests that modulation of host PIs is important for Shigella infection. Indeed, one T3SS effector secreted by Shigella early during infection is the phosphatidylinisotol-4-kinase IpgD, a SopB homologue capable of hydrolyzing PtdIns(4,5)P2 into PtdIns5P. One of the first pieces of evidence supporting the importance of IpgD for modulating membrane dynamics was the demonstration by Niebuhr et al. that IpgD expression alters cell morphology by uncoupling the PM from the actin cytoskeleton, resulting in membrane blebbing (Niebuhr et al. 2002). Using a fluorescent PtdIns5P probe, Pendaries et al. showed an accumulation of PtdIns5P at S. flexneri entry foci (Pendaries et al. 2006). This transient and localized increase in PtdIns5P appears to have several significant downstream signalling consequences. First, PtdIns5P production can activate a number of GTPases important for actin cytoskeleton rearrangement, including Cdc42 and Rac1 (Niebuhr et al. 2002, Viaud et al. 2014b). Viaud et al. have shown that PtdIns5P can bind to and activate Tiam1, a Rac1 GEF which binds PtdIns5P through a C-terminal PH domain (Viaud et al. 2014b).

Furthermore, IpgD and PtdIns5P induce activation of the PI3K/Akt pathway through phosphorylation of Akt. This appears to occur rapidly upon invasion, with colocalization of a

PtdIns5P probe and phosphorylated Akt on the PM apparent within 10 minutes of infection (Pendaries et al. 2006). Furthermore, this activation of Akt appears to require epidermal growth factor receptor (EGFR), as treatment with EGFR inhibitors or knockdown of EGFR expression reduces Akt activation upon infection (Ramel et al. 2011). The PI3K/Akt pathway and EGFR signalling are both involved in cell survival and proliferation, and indeed, infection by S. flexneri renders cells more resistant to inducers of apoptosis (Pendaries et al. 2006). Evidence suggests that PtdIns5P not only triggers activation of EGFR and the PI3K/Akt pathway, but prolongs EGFR signalling by impairing its degradation. Upon activation, EGFR is typically rapidly internalized and degraded in the lysosome. Upon IpgD expression and PtdIns5P production, however, activated EGFR and Akt is still detectable for as long as 24–48 hours post expression (Ramel et al. 2011). Further characterization of EGFR trafficking revealed accumulation in earlier endocytic compartments as opposed to late endosomes and lysosomes.

Besides enhancing cell survival and proliferation (both favourable for bacterial survival and replication), PtdIns5P production has been shown to be involved in immune evasion through multiple mechanisms. These include inhibiting the release of extracellular “danger signals” such as extracellular ATP (Puhar et al. 2013) and inducing the degradation of cell surface receptors such as ICAM-1, which are involved in recruitment of immune cells (Boal et al. 2016). Interestingly, Boal et al. demonstrated that PtdIns5P production results in internalization of both EGFR and ICAM-1 in the same cell. However, while ICAM-1 is targeted to the lysosome for degradation, EGFR is sequestered in EEs and spared from this fate, suggesting that PtdIns5P has dual roles in modulating surface receptors, protecting some from degradation while shuttling others to the lysosome. How it is able to fine tune internalization and trafficking in a ligand-

dependent manner still requires elucidation, although one possibility is that it does so through the differential recruitment of specific PtdIns5P effectors (Boal et al. 2015).

Finally, PtdIns5, PtdIns3P and PI3-kinases have been shown to be involved in vacuole rupture of S. flexneri, which allows bacteria to access the cytosolic site of replication prior to invading neighboring cells. Specifically, PtdIns5P production by IpgD was shown to be required to recruit Rab11, a recycling endosome marker, to Shigella entry sites, which appears to be involved in vacuole rupture (Mellouk et al. 2014) through an unknown mechanism.

Bacterial invasion of neighboring cells involves actin-based protrusions through the PM of both cells, leading to the formation of vacuoles in the neighboring cell. Formation of vacuoles requires the class II PI3-kinase PIK3C2A, which generates PtdIns3P. Vacuoles also display an accumulation of phospho-tyrosine residues. Both require a functional T3SS, suggesting that a yet-to-be identified secreted effector is responsible for activating PIK3C2A (Dragoi and Agaisse 2015).

Mycobacteria

Mycobacterium is a genus of intracellular bacteria which includes Mycobacterium tuberculosis, the cause of tuberculosis in humans. Like Salmonella and Shigella, mycobacteria are able to establish a specialized endosomal niche within their target cells, alveolar macrophages. This mycobacterial phagosomal compartment (MPC) is defined by specialized characteristics, such as reduced acidification, and the absence of several LE/LY associated markers and enzymes including mannose-6-phosphate receptor (M6PR) and mature cathepsin D (Deretic and Fratti 1999). Interestingly, the MPC also lacks some classical EE-associated

markers, such as EEA1 (Fratti et al. 2001). Vergne et al. furthermore have shown that while MPCs containing dead mycobacteria harbour PtdIns3P, MPCs with live bacteria actively exclude this PI (Vergne et al. 2005).

Since PtdIns3P is required for recruitment of effectors that promote maturation into late endosomes, by excluding this PI from bacteria-containing phagosomes, M. tuberculosis may be able to shield itself from progressing down the degradative endocytic pathway. Similar to SopB and IpgD in Salmonella and Shigella, M. tuberculosis encodes a lipid phosphatase, SapM, which hydrolyzes PtdIns3P to PtdIns (Puri et al. 2013, Saleh and Belisle 2000, Vergne et al. 2005). While the mechanism of action of this phosphatase still requires characterization, in vitro assays have demonstrated that it can block phagosome-lysosome fusion (Vergne et al. 2005). In addition to the 3-phosphatase activity of SapM, mycobacteria also express PI analogs, including lipid lipoarabinomannan (ManLAM) and its precursor phosphatidylinositol mannoside (PIM), which are able to intercalate into host endosomal membranes (Beatty et al. 2000). Studies by Fratti et al. have shown in vitro that phagosomes coated with ManLAM show less accumulation of the PtdIns3P effector EEA1 and its effector Syntaxin 6 (Fratti et al. 2001, 2003) compared to control phagosomes, while those coated with PIM showed no change in Syntaxin6 recruitment. Syntaxin 6 is particularly important for retrograde trafficking of proteins between the trans golgi network (TGN) and endosomes, including that of the late endosomal proteins M6PR, LAMP1 and vacuolar H+-ATPases. Therefore, by interfering with recruitment of host effectors necessary for lysosomal biogenesis, mycobacterial ManLAM could facilitate the creation of a protective niche for replication.

Legionella

The intracellular pathogen Legionella pneumophila, the causative agent of Legionnaire's disease, also replicates in a specialized intracellular niche, the Legionella containing vacuole (LCV) within protozoans and human alveolar macrophages. The formation and maturation of the LCV is driven by a number of Legionella effectors secreted by the bacterial Icm/Dot type IV secretion system (T4SS). Live cell imaging of Legionella-infected amoeba has demonstrated that dynamic recruitment, enrichment, and elimination of host cell PIs on the LCV membrane are important for formation and maturation of this specialized compartment (Weber et al. 2014). Maturation of the LCV is characterized by a gradual enrichment in PtdIns4P concomitant with the shedding of PtdIns3P. The enrichment of PtdIns4P on the LCV is important for recruiting PtdIns4P-binding Legionella effectors, such as SidC and SidM. These play important roles in shaping the LCV, including recruitment of the ER and modulation of Rab GTP signalling (Steiner et al. 2017). It appears Legionella has also evolved effectors that modulate PtdIns3P levels on the LCV, as Toulabi et al. have also identified a Legionella 3-phosphatase, SidP, which is able to hydrolyze PtdIns3P and PtdIns(3,5)P2 (Toulabi et al. 2013). Though the role of SidP during Legionella infection is still under investigation, similar to M. tuberculosis, restricting PtdIns3P production may inhibit progression of the LCV to the host degradative pathway.

Eukaryotic parasites

Intracellular eukaryotic parasites rely on their own PI metabolism to regulate signalling and trafficking (McIntosh et al. 2007, Tawk et al. 2011, Vaid et al. 2010), as well as host cell PI metabolism to establish and maintain infection. Some parasite-derived PI-binding proteins have been identified, including Toxoplasma gondii TgPH1 (PtdIns(3,5)P2) (Daher et al. 2016) and

Phytophthora sojae Avr1b, Avh5 and Avh331 (PtdIns3P) (Lu et al. 2013); however, the roles of these proteins during infection remain largely unknown.

Malaria parasites, protozoans belonging to the genus Plasmodium, go through several distinct life cycle stages in both their mosquito and vertebrate hosts. Upon inoculation by mosquito bite, parasites travel to the host liver and infect hepatocytes, where they replicate in a specialized parasitophorous vacuole (PV) into exo-eythrocytic forms (EEFs) that are capable of infecting erythrocytes (Mota et al. 2001). Thieleke-Matos et al. investigated interaction of the PV with the host cell endosomal PI system and found that parasite replication was dependent on PtdIns(3,5)P2 and its effector TRPML (Thieleke-Matos et al. 2014). Inhibition of either PIKfyve or TRPML pharmacologically or with genetic knock-down delayed parasite growth. The authors did not directly monitor PtdIns(3,5)P2 dynamics, but did find rapid accumulation and clearance of PtdIns3P on the PV at the onset of replication, suggesting it is rapidly converted to PtdIns(3,5)P2 by PIKfyve.

Another intriguing way in which eukaryotic parasites can alter host cell PI dynamics is to produce exogenous PIs that are secreted into target cells. This is particularly important if endogenous levels of specific PIs are low in host cells. For instance, in plants, PtdIns3P expressed on the outer surface of the PM can be used by pathogen effectors, including virulence factors, with PtdIns3P-binding RXLR motifs to gain entry into the cell (Kale et al. 2010). PtdIns3P levels may be transiently increased by secretion of exogenous parasite-derived PtdIns3P. For example, Lu et al. have detected PtdIns3P in hyphae of the plant pathogen Phytophthora (Lu et al. 2013). Silencing parasite PI3K genes or pre-treating hyphae with the PI3K inhibitor LY294002 reduced virulence, and overexpression of PtdIns3P-binding proteins or

the plant homolog of PIKfyve in plant cells increased resistance to infection, presumably by reducing levels of PtdIns3P accessible to the parasite (Figure 1B).

As the repertoire of identified bacterial and parasite effectors continues to grow, it is becoming clear that host PIs are an important target. However, few of these effectors have been characterized in detail, and much remains to be done to understand how they interact with cellular machinery. In particular, PtdIns5P, the last PI to be identified and previously thought to be exclusively nuclear in localization, has now been revealed to play an important role at the PM and in endosomes during bacterial infection, in at least two bacterial species. Whether other bacteria utilize or modify this lipid, and through which effectors, are important questions as we continue to identify and characterize bacterial effector proteins.

Viruses

Compared to bacteria and eukaryotic pathogens, where numerous pathogen-encoded PI-modulating effectors have been characterized, viruses possess a limited coding capacity which restricts the number of viral effector proteins capable of directly modifying host processes. Nonetheless, multiple aspects of the viral life cycle, including entry, replication, and budding are intimately tied to host endosomal trafficking, suggesting a reliance on PI metabolism and signalling. The characterization of viral interaction with the host cell PI system is just beginning, and acquiring more tools to study PI dynamics in cells will better enable us to dissect the molecular mechanisms underlying these interactions.

PI-binding viral proteins have been identified in select viruses, such as H7 in vaccinia virus (Kolli et al. 2015), the gag polyprotein in equine infectious anemia virus (EIAV)

(Fernandes et al. 2011), and the VP5 polyprotein in infectious bursal disease virus (IBDV) (Méndez et al. 2015), all of which have demonstrated PtdIns3P-binding capability in vitro. The roles these PI-binding viral proteins play during infection are still largely uncharacterized; however, initial studies indicate that EIAV gag may use binding to PtdIns3P to direct its trafficking through specific cellular compartments during viral morphogenesis (Fernandes et al. 2011), and IBDV VP5 may be involved in facilitating cell-to-cell spread (Méndez et al. 2015).

While evidence of viral proteins directly binding endosomal PIs remains limited, it is increasingly evident that viruses are able to alter host trafficking factors, including those that govern endosomal PI metabolism. This has been studied mainly in the field of viral entry, since many viruses rely on intracellular trafficking pathways for delivery of virions to appropriate intracellular compartments containing triggering factors for viral escape from endosomes. These factors, which include low pH, host proteases, and/or viral receptors, are found throughout the endosomal trafficking system, in EEs, MVBs and/or in LEs/LYs. Biogenesis, maturation, and fusion between these compartments is controlled in part by PtdIns3P, PtdIns(3,5)P2 and their various effectors.

Viruses which enter cells in EE and MVBs rely primarily on PtdIns3P and its effectors. For example, vesicular stomatitis virus (VSV) has been shown to depend on the PtdIns3P effector Hrs, part of the ESCRT-0 complex that is involved in MVB formation. Furthermore, PtdIns3P is also involved in VSV nucleocapsid release, in part through is effector Sorting Nexin 6 (Le Blanc et al. 2005).

PtdIns3P production depends on PI3 kinases, of which there are three classes. The majority of endosomal PtdIns3P is synthesized by the class III PI3K Vps34, whose recruitment

to nascent endosomes is dependent on Rab5 (Gillooly et al. 2001). The role of PI3Ks in viral entry can be assessed by examining the effect of the PI3K inhibitors wortmannin and LY294002 on infection. Unsurprisingly, inhibition of PI3Ks inhibits entry by a number of viruses, including Kaposi's sarcoma-associated herpesvirus (KSHV) (Naranatt et al. 2003), human rhinovirus (Brabec et al. 2006), lassa fever virus and lymphocytic choriomeningitis virus (LCMV) (Pasqual et al. 2011), Ebola virus (Saeed et al. 2008), and African swine fever virus (Cuesta-Geijo et al. 2012). What remains largely uncharacterized is whether these viruses can activate PI3Ks during entry, or if they are able to rely on basal PI3K activity. Naranatt et al. have shown that the KSHV glycoprotein can interact with cell surface integrin receptors, which can activate PI3Ks downstream (Naranatt et al. 2003). Upon entry, Ebola virus has also been shown to activate Akt, which is a downstream effector of class I PI3Ks (Saeed et al. 2008).

Viruses which require deeper trafficking in the endocytic pathway to LEs and LYs also rely on PtdIns(3,5)P2, which is primarily localized on LE compartments and is produced solely by the lipid kinase PIKfyve (Shisheva 2008) in mammalian cells. PIKfyve is recruited to PtdIns3P-enriched membranes via a FYVE domain, thus allowing sequential conversion of PtdIns3P to PtdIns(3,5)P2 (Ikonomov et al. 2001). Inhibition of PIKfyve and PtdIns(3,5)P2 production has been shown to inhibit entry by viruses which fuse in LE/LYs, such as vaccinia virus (Rizopoulos et al. 2015), African swine fever virus (Cuesta-Geijo et al. 2012) and filoviruses (Nelson et al. 2017, Qiu et al. 2018). Furthermore, work from our lab using fluorescent PI probes and live cell imaging has demonstrated that Ebola virus (EBOV) not only depends on PIKfyve activity for entry, but is able to upregulate PtdIns(3,5)P2 production on vesicular membranes during infection. How EBOV modulates PtdIns(3,5)P2 production is still unknown. However, since previous reports have indicated that EBOV can activate Akt upon

entry (Saeed et al. 2010), and that Akt is able to directly activate PIKfyve (Er et al. 2013), this raises the intriguing possibility that EBOV could exploit the PI3K/Akt pathway to activate PIKfyve and facilitate its trafficking (Figure 1C).

In addition to viral entry, endosomal PIs also play a role in viral morphogenesis, budding, and immune evasion. For instance, PtdIns(3,5)P2 has been shown to be important for post-entry steps of the viral life cycle. Jefferies et al. demonstrated that inhibition of PIKfyve reduces retroviral budding (Jefferies et al. 2008), and Murray et al. have also demonstrated that siRNA-mediated knockdown of PIKfyve impairs HIV replication (Murray et al. 2005).

Finally, viruses may manipulate host PIs in order to evade recognition by the host immune system. Niazy et al. have shown that herpes simplex virus-1 (HSV-1), which is able to persist in host cells and establish a latent infection, evades the immune system in part by interfering with antigen presentation by the major histocompatibility complex (MHC) (Niazy et al. 2017). Expression of the HSV glycoprotein B (gB) causes formation of PtdIns3P+ vacuoles in host cells, which contain substantial amounts of the MHC molecules HLA-DR and HLA-DM colocalized with EEA1. This suggests that gB is able to interfere with antigen presentation by trapping MHC molecules in early endosomal compartments, potentially via increased PtdIns3P production on these compartments.

We are just beginning to understand how viruses interact with the host cell PI system, and much work remains to be done to unravel the mechanisms through which viruses regulate host lipids to achieve infection. It is clear that endosomal PIs play an important role in many aspects of the viral life cycle; however, few viral proteins that directly bind PIs have been identified, and their roles are largely unknown. This raises the important question of how viruses modulate host

lipids, whether through direct binding; or, more likely, indirectly through the activation of signalling pathways with downstream effects on PI metabolism and activity. It also remains to be determined whether viruses that use similar entry/budding pathways share the same requirements for host PIs, and have evolved similar mechanisms to regulate these lipids.

Conclusions and perspectives

Through millions of years of coevolution, pathogens have evolved to not only to adapt to their hosts, but also to actively manipulate their hosts to adapt to them. Hijacking of the intricately regulated host endosomal trafficking system is another way that parasites, bacteria, and viruses shape their environments to establish specialized replicative niches, facilitate endosomal transport to target compartments, and evade detection by the immune system. Whether through secretion of PI-metabolizing enzymes, manipulation of host PI regulators, or direct secretion of exogenous PIs into host cells, intracellular pathogens are able to actively manipulate host lipid dynamics in order to ensure invasion and survival.

The intimate dependence of pathogens upon host cell PIs for multiple aspects of infection reveals novel targets for antimicrobial therapeutics. These could involve targeting pathogen-encoded proteins which modulate host PIs, or the host proteins themselves that pathogens rely on. The involvement of PIs in multiple aspects of infection, including initial invasion, establishment of replicative niches, as well as cell egress and cell-to-cell spread, indicate that targeting PIs may inhibit infection at multiple steps. Finally, evidence that many pathogens rely on the same endosomal lipids reveals common pathways and targets for antimicrobial development.

Despite their limited genome size and repertoire of effector proteins compared to their mammalian hosts, pathogens have been fine-tuned by evolution to precisely and effectively target and regulate the highly dynamic and complex host PI system. This raises the exciting possibility of using pathogens as tools to probe and dissect how PI dynamics are regulated. This includes using pathogen effectors as PI probes, uncovering new roles for previously poorly understood lipids like PtdIns5P, and identifying new signalling pathways, protein-protein interactions, and novel functions for known proteins.

Understanding the complex interplay between pathogens and the host cell processes they manipulate will give us a clearer picture of the pathogen life cycle as well as the fundamental mechanisms governing host cell biology.

Acknowledgements

S.Q. is supported by a scholarship from the Natural Sciences and Engineering Research Council of Canada (NSERC). M.C. is a Canada Research Chair in Molecular Virology and Antiviral Therapeutics. This work was supported by a grant to M.C. by NSERC.

References

Azzedine, H., Bolino, A., Taïeb, T., Birouk, N., Di Duca, M., Bouhouche, A., Benamou, S., Mrabet, A., Hammadouche, T., Chkili, T., et al. 2003. Mutations in MTMR13, a New Pseudophosphatase Homologue of MTMR2 and Sbf1, in Two Families with an Autosomal Recessive Demyelinating Form of Charcot-Marie-Tooth Disease Associated with Early-Onset Glaucoma. Am. J. Hum. Genet. 72, 1141–1153.

Bakowski, M.A., Braun, V., Lam, G.Y., Yeung, T., Do Heo, W., Meyer, T., Finlay, B.B., Grinstein, S., and Brumell, J.H. 2010. The Phosphoinositide Phosphatase SopB Manipulates Membrane Surface Charge and Trafficking of the Salmonella-Containing Vacuole. Cell Host Microbe 7, 453–462.

Balla, T. 2013. Phosphoinositides: Tiny Lipids With Giant Impact on Cell Regulation. Physiol. Rev. 93, 1019–1137.

Beatty, W.L., Rhoades, E.R., Ullrich, H.-J., Chatterjee, D., Heuser, J.E., and Russell, D.G. 2000. Trafficking and Release of Mycobacterial Lipids from Infected Macrophages. Traffic 1, 235–247.

Begley, M.J., and Dixon, J.E. 2005. The structure and regulation of myotubularin phosphatases. Curr. Opin. Struct. Biol. 15, 614–620.

Boal, F., Mansour, R., Gayral, M., Saland, E., Chicanne, G., Xuereb, J.-M., Marcellin, M., Burlet-Schiltz, O., Sansonetti, P.J., Payrastre, B., et al. 2015. TOM1 is a PI5P effector involved in the regulation of endosomal maturation. J Cell Sci 128, 815–827.

Boal, F., Puhar, A., Xuereb, J.-M., Kunduzova, O., Sansonetti, P.J., Payrastre, B., and Tronchère, H. 2016. PI5P Triggers ICAM-1 Degradation in Shigella Infected Cells, Thus Dampening Immune Cell Recruitment. Cell Rep. 14, 750–759.

Bout, I. van den, and Divecha, N. 2009. PIP5K-driven PtdIns(4,5)P2 synthesis: regulation and cellular functions. J Cell Sci 122, 3837–3850.

Brabec, M., Blaas, D., and Fuchs, R. 2006. Wortmannin delays transfer of human rhinovirus serotype 2 to late endocytic compartments. Biochem. Biophys. Res. Commun. 348, 741–749.

Cai, X., Xu, Y., Cheung, A.K., Tomlinson, R.C., Alcázar-Román, A., Murphy, L., Billich, A., Zhang, B., Feng, Y., Klumpp, M., et al. 2013. PIKfyve, a Class III PI Kinase, Is the Target of the Small Molecular IL-12/IL-23 Inhibitor Apilimod and a Player in Toll-like Receptor Signaling. Chem. Biol. 20, 912–921.

Christoforidis, S., Miaczynska, M., Ashman, K., Wilm, M., Zhao, L., Yip, S.C., Waterfield, M.D., Backer, J.M., and Zerial, M. 1999. Phosphatidylinositol-3-OH kinases are Rab5 effectors. Nat. Cell Biol. 1, 249–252.

Cossart, P. 1997. Host/pathogen interactions. Subversion of the mammalian cell cytoskeleton by invasive bacteria. J. Clin. Invest. 99, 2307–2311.

Cuesta-Geijo, M.A., Galindo, I., Hernáez, B., Quetglas, J.I., Dalmau-Mena, I., and Alonso, C. 2012. Endosomal maturation, Rab7 GTPase and phosphoinositides in African swine fever virus entry. PloS One 7, e48853.

Daher, W., Morlon-Guyot, J., Alayi, T.D., Tomavo, S., Wengelnik, K., and Lebrun, M. 2016. Identification of Toxoplasma TgPH1, a pleckstrin homology domain-containing protein that binds to the phosphoinositide PI(3,5)P2. Mol. Biochem. Parasitol.

Dai, S., Zhang, Y., Weimbs, T., Yaffe, M.B., and Zhou, D. 2007. Bacteria-generated PtdIns(3)P Recruits VAMP8 to Facilitate Phagocytosis. Traffic 8, 1365–1374.

Deretic, V., and Fratti, R.A. 1999. Mycobacterium tuberculosis phagosome. Mol. Microbiol. 31, 1603–1609.

Di Paolo, G., and De Camilli, P. 2006. Phosphoinositides in cell regulation and membrane dynamics. Nature 443, 651–657.

Dong, X., Shen, D., Wang, X., Dawson, T., Li, X., Zhang, Q., Cheng, X., Zhang, Y., Weisman, L.S., Delling, M., et al. 2010. PI(3,5)P2 Controls Membrane Traffic by Direct Activation of Mucolipin Ca2+ Release Channels in the Endolysosome. Nat. Commun. 1.

Dragoi, A.-M., and Agaisse, H. 2015. The Class II Phosphatidylinositol 3-Phosphate Kinase PIK3C2A Promotes Shigella flexneri Dissemination through Formation of Vacuole-Like Protrusions. Infect. Immun. 83, 1695–1704.

Dukes, J.D., Lee, H., Hagen, R., Reaves, B.J., Layton, A.N., Galyov, E.E., and Whitley, P. 2006. The secreted Salmonella dublin phosphoinositide phosphatase, SopB, localizes to PtdIns(3)P-containing endosomes and perturbs normal endosome to lysosome trafficking. Biochem. J. 395, 239–247.

Er, E.E., Mendoza, M.C., Mackey, A.M., Rameh, L.E., and Blenis, J. 2013. AKT Facilitates EGFR Trafficking and Degradation by Phosphorylating and Activating PIKfyve. Sci Signal 6, ra45–ra45.

Fernandes, F., Chen, K., Ehrlich, L.S., Jin, J., Chen, M.H., Medina, G.N., Symons, M., Montelaro, R., Donaldson, J., Tjandra, N., et al. 2011. Phosphoinositides Direct Equine Infectious Anemia Virus Gag Trafficking and Release. Traffic 12, 438–451.

Fratti, R.A., Backer, J.M., Gruenberg, J., Corvera, S., and Deretic, V. 2001. Role of phosphatidylinositol 3-kinase and Rab5 effectors in phagosomal biogenesis and mycobacterial phagosome maturation arrest. J. Cell Biol. 154, 631–644.

Fratti, R.A., Chua, J., Vergne, I., and Deretic, V. 2003. Mycobacterium tuberculosis glycosylated phosphatidylinositol causes phagosome maturation arrest. Proc. Natl. Acad. Sci. U. S. A. 100, 5437–5442.

Gillooly, D.J., Morrow, I.C., Lindsay, M., Gould, R., Bryant, N.J., Gaullier, J.-M., Parton, R.G., and Stenmark, H. 2000. Localization of phosphatidylinositol 3-phosphate in yeast and mammalian cells. EMBO J. 19, 4577–4588.

Gillooly, D.J., Simonsen, A., and Stenmark, H. 2001. Cellular functions of phosphatidylinositol 3-phosphate and FYVE domain proteins. Biochem. J. 355, 249–258.

Gozani, O., Karuman, P., Jones, D.R., Ivanov, D., Cha, J., Lugovskoy, A.A., Baird, C.L., Zhu, H., Field, S.J., Lessnick, S.L., et al. 2003. The PHD Finger of the Chromatin-Associated Protein ING2 Functions as a Nuclear Phosphoinositide Receptor. Cell 114, 99–111.

Hernandez, L.D., Hueffer, K., Wenk, M.R., and Galán, J.E. 2004. Salmonella Modulates Vesicular Traffic by Altering Phosphoinositide Metabolism. Science 304, 1805–1807.

Hill, E.V., Hudson, C.A., Vertommen, D., Rider, M.H., and Tavaré, J.M. 2010. Regulation of PIKfyve phosphorylation by insulin and osmotic stress. Biochem. Biophys. Res. Commun. 397, 650–655.

Ikonomov, O.C., Sbrissa, D., and Shisheva, A. 2001. Mammalian Cell Morphology and Endocytic Membrane Homeostasis Require Enzymatically Active Phosphoinositide 5-Kinase PIKfyve. J. Biol. Chem. 276, 26141–26147.

Ikonomov, O.C., Sbrissa, D., Fenner, H., and Shisheva, A. 2009. PIKfyve-ArPIKfyve-Sac3 Core Complex Contact sites and their consequences for Sac3 phosphatase activity and endocytic membrane homeostasis. J. Biol. Chem. 284, 35794–35806.

Jefferies, H.B.J., Cooke, F.T., Jat, P., Boucheron, C., Koizumi, T., Hayakawa, M., Kaizawa, H., Ohishi, T., Workman, P., Waterfield, M.D., et al. 2008. A selective PIKfyve inhibitor blocks PtdIns(3,5)P2 production and disrupts endomembrane transport and retroviral budding. EMBO Rep. 9, 164–170.

Jha, A., Ahuja, M., Patel, S., Brailoiu, E., and Muallem, S. 2014. Convergent regulation of the lysosomal two-pore channel-2 by Mg2+, NAADP, PI(3,5)P2 and multiple protein kinases. EMBO J. 33, 501–511.

Jones, D.R., Bultsma, Y., Keune, W.-J., Halstead, J.R., Elouarrat, D., Mohammed, S., Heck, A.J., D'Santos, C.S., and Divecha, N. 2006. Nuclear PtdIns5P as a Transducer of Stress Signaling: An In Vivo Role for PIP4Kbeta. Mol. Cell 23, 685–695.

Kale, S.D., Gu, B., Capelluto, D.G.S., Dou, D., Feldman, E., Rumore, A., Arredondo, F.D., Hanlon, R., Fudal, I., Rouxel, T., et al. 2010. External Lipid PI3P Mediates Entry of Eukaryotic Pathogen Effectors into Plant and Animal Host Cells. Cell 142, 284–295.

Kerr, M.C., Wang, J.T.H., Castro, N.A., Hamilton, N.A., Town, L., Brown, D.L., Meunier, F.A., Brown, N.F., Stow, J.L., and Teasdale, R.D. 2010. Inhibition of the PtdIns(5) kinase PIKfyve disrupts intracellular replication of Salmonella. EMBO J. 29, 1331–1347.

Knodler, L.A., and Steele-Mortimer, O. 2003. Taking Possession: Biogenesis of the Salmonella-Containing Vacuole. Traffic 4, 587–599.

Kolli, S., Meng, X., Wu, X., Shengjuler, D., Cameron, C.E., Xiang, Y., and Deng, J. 2015. Structure-function analysis of vaccinia virus H7 protein reveals a novel phosphoinositide binding fold essential for poxvirus replication. J. Virol. 89, 2209–2219.

Lawe, D.C., Patki, V., Heller-Harrison, R., Lambright, D., and Corvera, S. 2000. The FYVE Domain of Early Endosome Antigen 1 Is Required for Both Phosphatidylinositol 3-Phosphate and Rab5 Binding. J. Biol. Chem. 275, 3699–3705.

Le Blanc, I., Luyet, P.-P., Pons, V., Ferguson, C., Emans, N., Petiot, A., Mayran, N., Demaurex, N., Fauré, J., Sadoul, R., et al. 2005. Endosome-to-cytosol transport of viral nucleocapsids. Nat. Cell Biol. 7, 653–664.

Lemmon, M.A. 2008. Membrane recognition by phospholipid-binding domains. Nat. Rev. Mol. Cell Biol. 9, 99–111.

Lenk, G.M., Ferguson, C.J., Chow, C.Y., Jin, N., Jones, J.M., Grant, A.E., Zolov, S.N., Winters, J.J., Giger, R.J., Dowling, J.J., et al. 2011. Pathogenic Mechanism of the FIG4 Mutation Responsible for Charcot-Marie-Tooth Disease CMT4J. PLOS Genet 7, e1002104.

Li, X., Wang, X., Zhang, X., Zhao, M., Tsang, W.L., Zhang, Y., Yau, R.G.W., Weisman, L.S., and Xu, H. 2013. Genetically encoded fluorescent probe to visualize intracellular phosphatidylinositol 3,5-bisphosphate localization and dynamics. Proc. Natl. Acad. Sci. U. S. A. 110, 21165–21170.

Lu, S., Chen, L., Tao, K., Sun, N., Wu, Y., Lu, X., Wang, Y., and Dou, D. 2013. Intracellular and Extracellular Phosphatidylinositol 3-Phosphate Produced by Phytophthora Species Is Important for Infection. Mol. Plant 6, 1592–1604.

Mallo, G.V., Espina, M., Smith, A.C., Terebiznik, M.R., Alemán, A., Finlay, B.B., Rameh, L.E., Grinstein, S., and Brumell, J.H. 2008. SopB promotes phosphatidylinositol 3-phosphate formation on Salmonella vacuoles by recruiting Rab5 and Vps34. J. Cell Biol. 182, 741–752.

Mayinger, P. 2012. Phosphoinositides and vesicular membrane traffic. Biochim. Biophys. Acta 1821, 1104–1113.

McCartney, A.J., Zhang, Y., and Weisman, L.S. 2014. Phosphatidylinositol 3,5-bisphosphate: low abundance, high significance. BioEssays News Rev. Mol. Cell. Dev. Biol. 36, 52–64.

McGhie, E.J., Brawn, L.C., Hume, P.J., Humphreys, D., and Koronakis, V. 2009. Salmonella takes control: effector-driven manipulation of the host. Curr. Opin. Microbiol. 12, 117–124.

McIntosh, M.T., Vaid, A., Hosgood, H.D., Vijay, J., Bhattacharya, A., Sahani, M.H., Baevova, P., Joiner, K.A., and Sharma, P. 2007. Traffic to the Malaria Parasite Food Vacuole. A novel pathway involving a phosphatidylinositol-3-phosphate-binding protein. J. Biol. Chem. 282, 11499–11508.

Mellouk, N., Weiner, A., Aulner, N., Schmitt, C., Elbaum, M., Shorte, S.L., Danckaert, A., and Enninga, J. 2014. Shigella Subverts the Host Recycling Compartment to Rupture Its Vacuole. Cell Host Microbe 16, 517–530.

Méndez, F., Garay, T. de, Rodríguez, D., and Rodríguez, J.F. 2015. Infectious Bursal Disease Virus VP5 Polypeptide: A Phosphoinositide-Binding Protein Required for Efficient Cell-to-Cell Virus Dissemination. PLOS ONE 10, e0123470.

Méresse, S., Steele-Mortimer, O., Finlay, B.B., and Gorvel, J.P. 1999. The rab7 GTPase controls the maturation of Salmonella typhimurium-containing vacuoles in HeLa cells. EMBO J. 18, 4394–4403.

Mota, M.M., Pradel, G., Vanderberg, J.P., Hafalla, J.C.R., Frevert, U., Nussenzweig, R.S., Nussenzweig, V., and Rodríguez, A. 2001. Migration of Plasmodium Sporozoites Through Cells Before Infection. Science 291, 141–144.

Murray, J.L., Mavrakis, M., McDonald, N.J., Yilla, M., Sheng, J., Bellini, W.J., Zhao, L., Le Doux, J.M., Shaw, M.W., Luo, C.-C., et al. 2005. Rab9 GTPase Is Required for Replication of Human Immunodeficiency Virus Type 1, Filoviruses, and Measles Virus. J. Virol. 79, 11742–11751.

Naranatt, P.P., Akula, S.M., Zien, C.A., Krishnan, H.H., and Chandran, B. 2003. Kaposi's Sarcoma-Associated Herpesvirus Induces the Phosphatidylinositol 3-Kinase-PKC-ζ-MEK-ERK Signaling Pathway in Target Cells Early during Infection: Implications for Infectivity. J. Virol. 77, 1524–1539.

Nelson, E.A., Dyall, J., Hoenen, T., Barnes, A.B., Zhou, H., Liang, J.Y., Michelotti, J., Dewey, W.H., DeWald, L.E., Bennett, R.S., et al. 2017. The phosphatidylinositol-3-phosphate 5-kinase inhibitor apilimod blocks filoviral entry and infection. PLoS Negl. Trop. Dis. 11, e0005540.

Niazy, N., Temme, S., Bocuk, D., Giesen, C., König, A., Temme, N., Ziegfeld, A., Gregers, T.F., Bakke, O., Lang, T., et al. 2017. Misdirection of endosomal trafficking mediated by herpes simplex virus–encoded glycoprotein B. FASEB J. 31, 1650–1667.

Niebuhr, K., Giuriato, S., Pedron, T., Philpott, D.J., Gaits, F., Sable, J., Sheetz, M.P., Parsot, C., Sansonetti, P.J., and Payrastre, B. 2002. Conversion of PtdIns(4,5)P2 into PtdIns(5)P by the S.flexneri effector IpgD reorganizes host cell morphology. EMBO J. 21, 5069–5078.

Pasqual, G., Rojek, J.M., Masin, M., Chatton, J.-Y., and Kunz, S. 2011. Old World Arenaviruses Enter the Host Cell via the Multivesicular Body and Depend on the Endosomal Sorting Complex Required for Transport. PLOS Pathog. 7, e1002232.

Pendaries, C., Tronchère, H., Arbibe, L., Mounier, J., Gozani, O., Cantley, L., Fry, M.J., Gaits-Iacovoni, F., Sansonetti, P.J., and Payrastre, B. 2006. PtdIns(5)P activates the host cell PI3-kinase/Akt pathway during Shigella flexneri infection. EMBO J. 25, 1024–1034.

Pierson, C.R., Tomczak, K., Agrawal, P., Moghadaszadeh, B., and Beggs, A.H. 2005. X-Linked Myotubular and Centronuclear Myopathies. J. Neuropathol. Exp. Neurol. 64, 555–564.

Puhar, A., Tronchère, H., Payrastre, B., Tran Van Nhieu, G., and Sansonetti, P.J. 2013. A Shigella Effector Dampens Inflammation by Regulating Epithelial Release of Danger Signal ATP through Production of the Lipid Mediator PtdIns5P. Immunity 39, 1121–1131.

Puri, R.V., Reddy, P.V., and Tyagi, A.K. 2013. Secreted Acid Phosphatase (SapM) of Mycobacterium tuberculosis Is Indispensable for Arresting Phagosomal Maturation and Growth of the Pathogen in Guinea Pig Tissues. PLoS ONE 8.

Qiu, S., Leung, A., Bo, Y., Kozak, R.A., Anand, S.P., Warkentin, C., Salambanga, F.D.R., Cui, J., Kobinger, G., Kobasa, D., et al. 2018. Ebola virus requires phosphatidylinositol (3,5) bisphosphate production for efficient viral entry. Virology 513, 17–28.

Raiborg, C., Bremnes, B., Mehlum, A., Gillooly, D.J., D'Arrigo, A., Stang, E., and Stenmark, H. 2001. FYVE and coiled-coil domains determine the specific localisation of Hrs to early endosomes. J. Cell Sci. 114, 2255–2263.

Ramel, D., Lagarrigue, F., Pons, V., Mounier, J., Dupuis-Coronas, S., Chicanne, G., Sansonetti, P.J., Gaits-Iacovoni, F., Tronchère, H., and Payrastre, B. 2011. Shigella flexneri Infection Generates the Lipid PI5P to Alter Endocytosis and Prevent Termination of EGFR Signaling. Sci Signal 4, ra61–ra61.

Ray, K., Marteyn, B., Sansonetti, P.J., and Tang, C.M. 2009. Life on the inside: the intracellular lifestyle of cytosolic bacteria. Nat. Rev. Microbiol. 7, 333–340.

Rizopoulos, Z., Balistreri, G., Kilcher, S., Martin, C.K., Syedbasha, M., Helenius, A., and Mercer, J. 2015. Vaccinia Virus Infection Requires Maturation of Macropinosomes. Traffic Cph. Den. 16, 814–831.

Saeed, M.F., Kolokoltsov, A.A., Freiberg, A.N., Holbrook, M.R., and Davey, R.A. 2008. Phosphoinositide-3 Kinase-Akt Pathway Controls Cellular Entry of Ebola Virus. PLoS Pathog. 4.

Saeed, M.F., Kolokoltsov, A.A., Albrecht, T., and Davey, R.A. 2010. Cellular Entry of Ebola Virus Involves Uptake by a Macropinocytosis-Like Mechanism and Subsequent Trafficking through Early and Late Endosomes. PLoS Pathog 6, e1001110.

Saleh, M.T., and Belisle, J.T. 2000. Secretion of an Acid Phosphatase (SapM) by Mycobacterium tuberculosis That Is Similar to Eukaryotic Acid Phosphatases. J. Bacteriol. 182, 6850–6853.

Sarkes, D., and Rameh, L.E. 2010. A Novel HPLC-Based Approach Makes Possible the Spatial Characterization of Cellular PtdIns5P and Other Phosphoinositides. Biochem. J. 428, 375–384.

Sasaki, T., Takasuga, S., Sasaki, J., Kofuji, S., Eguchi, S., Yamazaki, M., and Suzuki, A. 2009. Mammalian phosphoinositide kinases and phosphatases. Prog. Lipid Res. 48, 307–343.

Sbrissa, D., Ikonomov, O.C., and Shisheva, A. 2002. Phosphatidylinositol 3-Phosphate-interacting Domains in PIKfyve binding specificity and role in PIKfyve endomembrane localization. J. Biol. Chem. 277, 6073–6079.

Sbrissa, D., Ikonomov, O.C., Fu, Z., Ijuin, T., Gruenberg, J., Takenawa, T., and Shisheva, A. 2007. Core Protein Machinery for Mammalian Phosphatidylinositol 3,5-Bisphosphate Synthesis and Turnover That Regulates the Progression of Endosomal Transport. J. Biol. Chem. 282, 23878–23891.

Sbrissa, D., Ikonomov, O.C., Filios, C., Delvecchio, K., and Shisheva, A. 2012. Functional dissociation between PIKfyve-synthesized PtdIns5P and PtdIns(3,5)P2 by means of the PIKfyve inhibitor YM201636. Am. J. Physiol. - Cell Physiol. 303, C436–C446.

Schink, K.O., Raiborg, C., and Stenmark, H. 2013. Phosphatidylinositol 3-phosphate, a lipid that regulates membrane dynamics, protein sorting and cell signalling. BioEssays 35, 900–912.

Scott, C.C., Cuellar-Mata, P., Matsuo, T., Davidson, H.W., and Grinstein, S. 2002. Role of 3-Phosphoinositides in the Maturation ofSalmonella-containing Vacuoles within Host Cells. J. Biol. Chem. 277, 12770–12776.

Shisheva, A. 2008. PIKfyve: Partners, Significance, Debates and Paradoxes. Cell Biol. Int. 32, 591–604.

Shisheva, A. 2013. PtdIns5P: News and views of its appearance, disappearance and deeds. Arch. Biochem. Biophys. 538, 171–180.

Shisheva, A., Sbrissa, D., and Ikonomov, O. 2015. Plentiful PtdIns5P from scanty PtdIns(3,5)P2 or from ample PtdIns? PIKfyve-dependent models: Evidence and speculation. BioEssays News Rev. Mol. Cell. Dev. Biol. 37, 267–277.

Steiner, B., Weber, S., and Hilbi, H. 2017. Formation of the Legionella-containing vacuole: phosphoinositide conversion, GTPase modulation and ER dynamics. Int. J. Med. Microbiol.

Stenmark, H., Aasland, R., Toh, B.-H., and D'Arrigo, A. 1996. Endosomal Localization of the Autoantigen EEA1 Is Mediated by a Zinc-binding FYVE Finger. J. Biol. Chem. 271, 24048–24054.

Stevens, J.M., Galyov, E.E., and Stevens, M.P. 2006. Actin-dependent movement of bacterial pathogens. Nat. Rev. Microbiol. 4, 91–101.

Tawk, L., Dubremetz, J.-F., Montcourrier, P., Chicanne, G., Merezegue, F., Richard, V., Payrastre, B., Meissner, M., Vial, H.J., Roy, C., et al. 2011. Phosphatidylinositol 3-Monophosphate Is Involved in Toxoplasma Apicoplast Biogenesis. PLOS Pathog. 7, e1001286.

Teasdale, R.D., and Collins, B.M. 2012. Insights into the PX (phox-homology) domain and SNX (sorting nexin) protein families: structures, functions and roles in disease. Biochem. J. 441, 39–59.

Thieleke-Matos, C., da Silva, M.L., Cabrita-Santos, L., Pires, C.F., Ramalho, J.S., Ikonomov, O., Seixas, E., Shisheva, A., Seabra, M.C., and Barral, D.C. 2014. Host PI(3,5)P2 activity is required for Plasmodium berghei growth during liver stage infection. Traffic Cph. Den. 15, 1066–1082.

Toulabi, L., Wu, X., Cheng, Y., and Mao, Y. 2013. Identification and Structural Characterization of a Legionella Phosphoinositide Phosphatase. J. Biol. Chem. 288, 24518–24527.

Vaid, A., Ranjan, R., Smythe, W.A., Hoppe, H.C., and Sharma, P. 2010. PfPI3K, a phosphatidylinositol-3 kinase from Plasmodium falciparum, is exported to the host erythrocyte and is involved in hemoglobin trafficking. Blood 115, 2500–2507.

Vergne, I., Chua, J., Lee, H.-H., Lucas, M., Belisle, J., and Deretic, V. 2005. Mechanism of phagolysosome biogenesis block by viable Mycobacterium tuberculosis. Proc. Natl. Acad. Sci. U. S. A. 102, 4033–4038.

Viaud, J., Boal, F., Tronchère, H., Gaits-Iacovoni, F., and Payrastre, B. 2014a. Phosphatidylinositol 5-phosphate: A nuclear stress lipid and a tuner of membranes and cytoskeleton dynamics. BioEssays 36, 260–272.

Viaud, J., Lagarrigue, F., Ramel, D., Allart, S., Chicanne, G., Ceccato, L., Courilleau, D., Xuereb, J.-M., Pertz, O., Payrastre, B., et al. 2014b. Phosphatidylinositol 5-phosphate regulates invasion through binding and activation of Tiam1. Nat. Commun. 5, ncomms5080.

Vicinanza, M., Korolchuk, V.I., Ashkenazi, A., Puri, C., Menzies, F.M., Clarke, J.H., and Rubinsztein, D.C. 2015. PI(5)P Regulates Autophagosome Biogenesis. Mol. Cell 57, 219–234.

Weber, S., Wagner, M., and Hilbi, H. 2014. Live-Cell Imaging of Phosphoinositide Dynamics and Membrane Architecture during Legionella Infection. mBio 5, e00839–13.

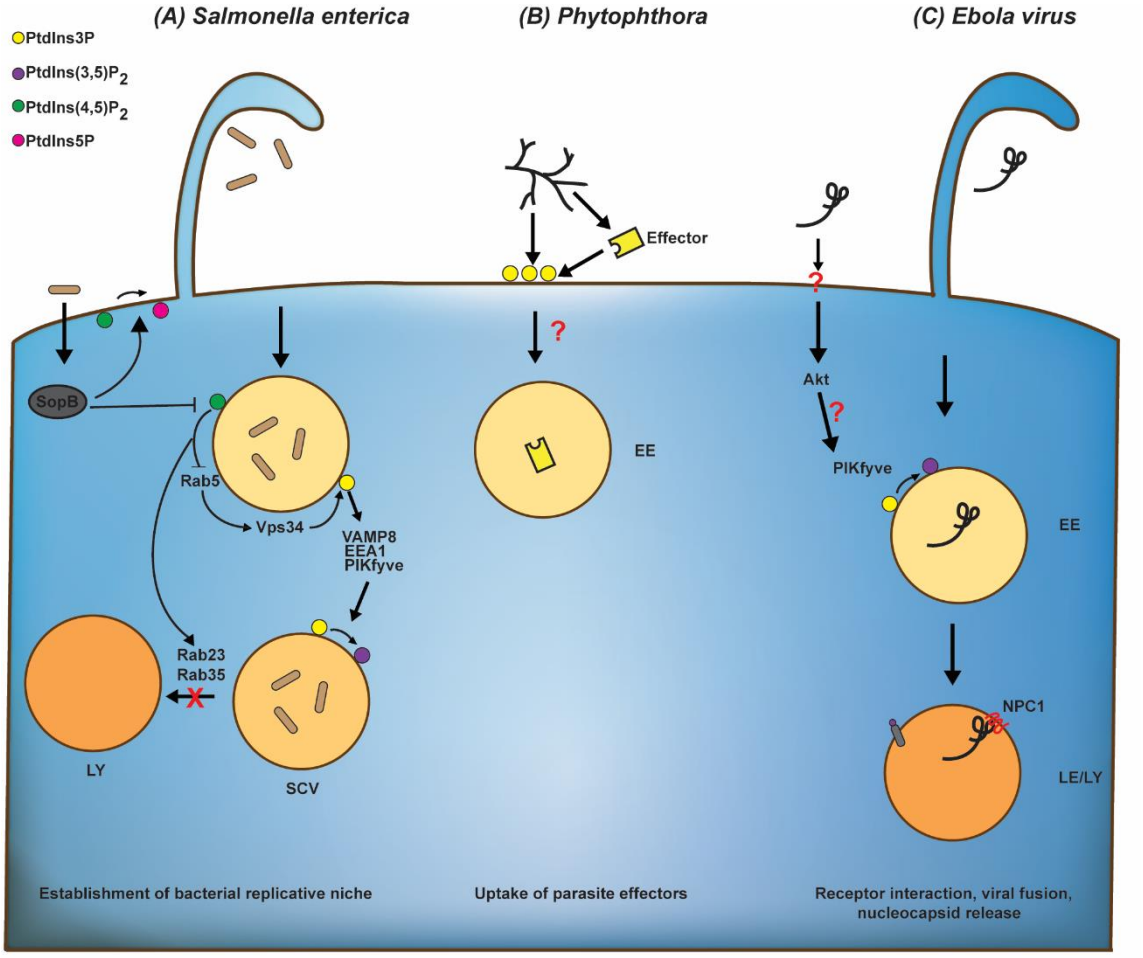

Figure 1. Manipulation of endosomal phosphoinositides by a bacterial, eukaryotic, and viral pathogen. (A) *Salmonella enterica* effector SopB is secreted into the host cell cytosol, where it dephosphorylates PtdIns(4,5)P_2 to PtdIns5P on the plasma membrane and nascent *Salmonella*-containing vacuole (SCV). Reduction of PtdIns(4,5)P_2 facilitates recruitment of Rab5 and Vps34. Generation of PtdIns3P on the SCV by Vps34 recruits PtdIns3P effectors VAMP8, EEA1, and PIKfyve, which facilitate SCV maturation and trafficking. PIKfyve generates PtdIns(3,5)P_2 which is required for SCV maturation and bacterial replication. Reduction of PtdIns(4,5)P_2 also inhibits recruitment of Rab23 and Rab34, which promote fusion with lysosomes, thus inhibiting bacterial degradation. (B) *Phytophthora* secretes extracellular PtdIns3P, facilitating uptake of parasite effectors with PtdIns3P binding domains through an unknown mechanism. (C) Ebola virus is internalized into host cells and trafficked through early endosomes to late endosomes/lysosomes, where its receptor, Niemann Pick-C1 (NPC1) is localized, a process which depends on the conversion of PtdIns3P to PtdIns(3,5)P_2 by PIKfyve. Whether and how Ebola activates PIKfyve is unknown; however, it may do so by activating the PI3K/Akt pathway. EE = early endosome, LE = late endosome, LY = lysosome.

Table 1. Endosomal PIs: Cellular localization, effector proteins, and tools for study. * For PtdIns3P effector proteins, only those mentioned in this review are listed.

PI	Localization	Host effector proteins	Inhibitors	Probes	Reference
PtdIns3P	Early endosomes, multivesicular bodies, autophagosomes	EEA1, Hrs, PIKfyve, SXNs, VAMP8*	Wortmannin LY294002	2XFYVE	(Dai et al., 2007; Gillooly et al., 2000; Lawe et al., 2000; Raiborg et al., 2001; Sbrissa et al., 2002; Stenmark et al., 1996; Teasdale and Collins, 2012)
PtdIns(3,5)P_2	Multivesicular bodies, late endosomes, lysosomes	TRPML1, TPC1, TPC2	YM201636 Apilimod	2XML1N	(Cai et al., 2013; Dong et al., 2010; Jefferies et al., 2008; Jha et al., 2014; Li et al., 2013)
PtdIns5P	Nuclear membranes, plasma membrane, ER, golgi, autophagosomes, endosomes?	ING2	YM201636 (low concentration)	PHD Finger	(Gozani et al., 2003; Sbrissa et al., 2012; Shisheva, 2013)

Table 2. Role of endosomal and plasma membrane phosphoinositides for infection by pathogens.

Pathogen	*PIs required*	*Effector(s)*	*Function(s)*	*Reference*
Bacteria				
Salmonella enterica	PtdIns(4,5)P_2 ↓	SopB/SigD	Biogenesis of Salmonella containing vacuole, bacterial survival	Bakowski et al., 2010; Dai et al., 2007; Dukes et al., 2006; Hernandez et al., 2004; Kerr et al., 2010; Mallo et al., 2008; Méresse et al., 1999; Scott et al., 2002)
Shigella flexneri	PtdIns(4,5)P_2 ↓ PtdIns5P↑	IpgD	Host cell survival, bacterial engulfment, immune evasion, vacuole rupture	(Boal et al., 2016; Dragoi and Agaisse, 2015; Mellouk et al., 2014; Niebuhr et al., 2002; Pendaries et al., 2006; Puhar et al., 2013; Ramel et al., 2011; Viaud et al., 2014b)
Legionella pneumophila	PtdIns3P↓ PtdIns(3,5)P_2↓ PtdIns4P↑	SidP SidC, SidM	Bacterial survival?	(Toulabi et al., 2013)
Mycobacterium tuberculosis	PtdIns3P↓	SapM, ManLAM,	Biogenesis of Mycobacterium phagosomal compartment, bacterial survival	(Beatty et al., 2000; Fratti et al., 2001, 2003; Puri et al., 2013; Saleh and Belisle, 2000; Vergne et al., 2005)
Eukaryotic Parasites				
Plasmodium berghei	PtdIns3P PtdIns(3,5)P_2		Parasitophorous vacuole formation, parasite growth and survival	(Thieleke-Matos et al., 2014)
Phytophthora sojae	PtdIns3P↑	Phytophthora PI3 kinases	Translocation of parasite effectors	(Kale et al., 2010; Lu et al., 2013)
Viruses				
Equine anemia infectious virus	PtdIns3P	Gag polyprotein	Viral morphogenesis	(Fernandes et al., 2011)
Vaccinia virus	PtdIns3P PtdIns(3,5)P_2	H7	Viral membrane morphogenesis, viral entry	(Kolli et al., 2015; Rizopoulos et al., 2015)
Infectious bursal disease virus	PtdIns3P	VP5	Cell-to-cell spread?	(Méndez et al., 2015)
Vesicular stomatitis virus	PtdIns3P		Viral entry, nucleocapsid release	(Le Blanc et al., 2005)
Herpes simplex virus	PtdIns3P	Glycoprotein B	Block MHC presentation	(Niazy et al., 2017)
Murine leukemia virus	PtdIns(3,5)P_2		Viral budding	(Jefferies et al., 2008)
Human immunodeficiency virus	PtdIns3P		Viral replication	(Murray et al., 2005)
Ebola virus	PtdIns3P PtdIns(3,5)P_2↑		Viral entry	(Nelson et al., 2017; Qiu et al., 2017)
African swine fever virus,	PtdIns3P PtdIns(3,5)P_2		Viral entry	(Cuesta-Geijo et al., 2012)
Kaposi's sarcoma-associated herpesvirus, lymphocytic choriomeningitis virus, Lassa fever virus, human rhinovirus	PtdIns3P		Viral entry?	(Brabec et al., 2006; Naranatt et al., 2003; Pasqual et al., 2011; Saeed et al., 2008)

6.4 Curriculum vitae

SHIRLEY QIU

EDUCATION

PhD University of Ottawa 2015-2021
Microbiology and Immunology
Supervisor: Dr. Marceline Côté

BSc University of Toronto 2011-2015
Evolutionary Biology and Human Physiology
Minor in Philosophy

RESEARCH EXPERIENCE

PhD Dissertation, University of Ottawa 2015-2021
Advisor: Dr. Marceline Côté
Thesis title: "Characterization of host trafficking factors involved in Ebola virus entry"

Research Internship, Paraza Pharma Inc., Montreal Oct 2019
Biological Sciences Group

BSc Research Project, University of Toronto 2014-2015
Advisor: Dr. David Guttman
Thesis title: "Evolution of antibiotic resistance during de-esclation therapy in Pseudomonas aeruginosa"

BSc Research Project, University of Toronto 2014-2015
Advisor: Dr. Nicola Jones
Thesis title: "The effect of miR-142-3p on ATG16L1 and induced autophagy in Crohn's disease"

Research Assistant, University of Toronto May 2013-Sept 2013
Spencer Barrett Lab

PUBLICATIONS

Filoviruses use the HOPS complex and UVRAG to traffic to Niemann-Pick C1 compartments during viral entry
Yuxia Bo*, **Shirley Qiu***, Rory Mulloy, Marceline Côté. Journal of Virology (2020) 94(16) e01002-20
*Contributed equally

- Selected as a spotlight article

A Diacylglycerol Kinase Inhibitor, R-59-022, Blocks Filovirus Internalization in Host Cells
Corina Stewart, Stephanie Dorion, Marie Ottenbrite, Nicholas LeBlond, Tyler Smith, **Shirley Qiu**, Morgan Fullerton, Darwyn Kobasa, Marceline Côté. Viruses (2019) 11(3) 206

From hitchhiker to hijacker: pathogen exploitation of endosomal phosphoinositides
Shirley Qiu and Marceline Côté. Biochemistry and Cell Biology (2019) 97(1) 1-9

Ebola virus requires phosphatidylinositol (3,5) bisphosphate production for efficient viral entry
Shirley Qiu, Anders Leung, Yuxia Bo, Robert Kozak, Sai Priya Anand, Corina Warkentin, Fabiola D.R. Salambanga, Jennifer Cui, Gary Kobinger, Darwyn Kobasa, Marceline Côté
Virology 513 (2018) 17-28

- Selected as a highlighted article
- Selected for issue cover photo

CONFERENCE PRESENTATIONS

American Society for Virology Annual Meeting June 2020
Abstract accepted for oral presentation, Fort Collins CO
Travel award (meeting cancelled due to COVID-19)

Canadian Society for Virology Annual Meeting June 2020
Abstract accepted for oral presentation, Guelph ON
Travel award (meeting cancelled due to COVID-19)

Canadian Society for Virology Annual Meeting June 2018
Poster presentation, Halifax NS

American Society for Virology Annual Meeting July 2017
Oral presentation, Madison WI

Canadian Society for Molecular Biosciences Annual Meeting May 2017
Oral presentation, Ottawa ON

American Society for Virology Annual Meeting June 2016
Oral presentation, Blacksburg VA

TEACHING EXPERIENCE

Teaching Assistant, University of Ottawa 2019
MIC4126 (Virology)

SCHOLARSHIPS AND AWARDS

NSERC PGS D Scholarship – Doctoral 2017-2020

University of Ottawa Excellence Scholarship 2016-2020

Biochemistry, Microbiology and Immunology Seminar Day Award 1st place	2019
NSERC CGS Scholarship - Master's	2016-2017
Faculty of Graduate and Postdoctoral Studies Travel Award	2016, 2017
University of Ottawa Admission Scholarship	2015
Isabel Warne Fellowship	2015
University of Toronto Dean's List	2012-2015
University of Toronto Undergraduate Research Award	2014
Dr. James A. & Connie P. Dickson Scholarship in Science and Math	2014
Howard Ferguson Scholarship	2011
Cargill Scholarship	2011
University of Toronto Entrance Scholarship	2011
Governor General's Academic Medal	2011

PROFESSIONAL AFFILIATIONS

American Society for Virology
Canadian Society for Virology
Canadian Society for Molecular Biosciences
Ottawa Institute of Systems Biology
Ottawa Centre for Infection, Immunity, and Inflammation

GRADUATE COURSEWORK

Advanced Topics in Virology, Grade: A
Advanced Topics in Immunology, Grade: A
Imaging in Cell Biology, Grade: A
Host-Pathogen Interactions, Grade: A

VOLUNTEER AND LEADERSHIP EXPERIENCE

Undergraduate students supervised

Kathy Fu (2018-2019) Thesis title: "Investigation into the regulating mechanisms underlying the association of the PIKfyve-ArPIKfyve-Sac3 cellular trafficking complex"

Fabiola Salambanga (2016-2017) Thesis title: "Études des voies signalétiques de l'hôte impliquées dans le transport du virus Ébola lors de l'entrée virale"

University of Ottawa Microbiology and Immunology Program Review Committee
Student representative (2020)

Biochemistry, Microbiology and Immunology Graduate Student Council
Vice President of Wellness (2019-2020)

Let's Talk Science
Educator (2016-2019)

LANGUAGES

English: Native Language
French: Intermediate